DIAGENESIS AND AQUIFER CHARACTERISTICS OF THE SHERWOOD SANDSTONE GROUP IN NORTH NOTTINGHAMSHIRE

BY

Safaa Abd el-Bar Seif el-Dein

Thesis Submitted for the Degree of

Doctor of Philosophy

at the

University of Aston in Birmingham

1983

To

Reham and Mohsen

The University of Aston in Birmingham

DIAGENESIS AND AQUIFER CHARACTERISTICS OF THE SHERWOOD SANDSTONE GROUP IN NORTH NOTTINGHAMSHIRE

Safaa A. Seif-el-Dein

Doctor of Philosophy 1983

SUMMARY

The Sherwood Sandstone Group forms an important aquifer in Eastern England, which in North Nottinghamshire comprises the Nottingham Castle and Lenton Sandstone Formations. The aquifer is formed by an alluvial red-bed sequence dominated by medium-coarse grained sandstones which are texturally immature to submature and have only been subjected to shallow burial diagenesis.

These sandstones reached the mature stage of the meso diagenetic regime, and four stages are recognized in their diagenetic history depending upon the physical/chemical processes prevailing and the subsequent effect on porosity and permeability. Stage "One" represents changes including dissolution of unstable silicates, clay replacement, red colouration and precipitation of authigenic minerals (quartz, feldspar, illite, I/S, kaolinite, dolomite, ferroan calcite, calcite). The net result of these changes was porosity reduction. Stage "Two" included changes due to mechanical compaction which resulted in minor porosity reduction. Stage "Three" was the main phase of secondary porosity enhancement. Stage "Four" represents changes taking place in the present groundwater where porosity and permeability may have been increased by dissolution and partly reduced by kaolinite precipitation.

Porosity measured by water-resaturation and Hg-injection gave average values of 25.63% and 24.85% respectively. The results are comparable and showed marked correlation especially in highly porous/permeable rocks. Porosity measurements from photomicrographs were markedly off-set from laboratory results. Horizontal K_w ranged between 1.43×10^{-5} and 1.13×10^{-1} mm/sec, with an average of 1.68×10^{-2} mm/sec. The estimated K_{Hg} ranged between 7.29×10^{-6} and 6.99×10^{-2} mm/sec with an average of 1.47×10^{-2} mm/sec. Both results are significantly correlated for highly porous/permeable rocks. The hydraulic properties are highly dependent upon the diagenetic properties (as most of the pores present are of secondary origin) as well as the pore size distribution.

The chemistry of these groundwaters indicates that they are under-saturated with respect to dolomite, calcite, K-feldspar, I/S clay, and montmorillonite. The precipitation of kaolinite, and to a lesser extent illite, is favoured in the present groundwater regime.

Triassic, Diagenesis, Aquifer, Nottinghamshire, Hydrogeology.

LIST OF CONTENTS

	Page
CHAPTER 1 INTRODUCTION	1
1.1 SCOPE AND OUTLINE OF THE INVESTIGATION	1
1.2 PREVIOUS WORK	3
1.3 METHODOLOGY	5
CHAPTER 2 STRATIGRAPHY AND AQUIFER PROPERTIES	9
2.1 TRIASSIC AQUIFER OF EASTERN ENGLAND	9
2.2 GEOLOGY OF THE INVESTIGATED AREA	12
2.3 LITHOLOGICAL VARIATION OF BOREHOLES A3, A11, A14, A18	16
2.3.1 Borehole A11	20
2.3.2 Borehole A14	23
2.3.3 Borehole A18	25
2.3.4 Borehole A3	28
2.4 GROUNDWATER CONDITIONS	31
2.4.1 Definitions	31
2.4.2 Triassic Groundwater Level	33
CHAPTER 3 PETROGRAPHY, DIAGENESIS AND SECONDARY POROSITY DEVELOPMENT	40
3.1 INTRODUCTION	40
3.2 METHODS AND TECHNIQUES	40
3.3 GRAIN SIZE AND PACKING CHARACTERISTICS	43
3.3.1 Grain Size Analyses	43
3.3.2 Analysis of Grain Contacts	47
3.3.3 Packing	50
3.4 SANDSTONE MINERALOGY AND PETOGRAPHY	51
3.4.1 Quartz	52
3.4.2 Rock Fragments	55
3.4.3 Feldspars	56
3.4.4 Micas and Other Detrital Constituents	58
3.5 DIAGENESIS	58
3.5.1 Reddening: Source, Origin and Duration	59
3.5.2 Dissolution	63
3.5.3 Clay Replacement	66
3.5.4 Authigenic Minerals	67
3.5.4.1 Quartz	67
3.5.4.2 K-feldspar	70
3.5.4.3 Authigenic clays	72

Page

3.5.4.4 Carbonate 76

3.5.5 Authigenic Minerals : Paragenetic Sequence Relationships 78

3.6 POROSITY AS A FUNCTION OF DIAGENETIC PROCESSES 79

3.7 DISCUSSION 84

CHAPTER 4 POROSITY AND HYDRAULIC CONDUCTIVITY 90

4.1 INTRODUCTION 90

4.2 POROSITY 92

4.2.1 Porosity Measurements and Results 93

4.2.1.1 Liquid resaturation method 94

4.2.1.2 Mercury porosimeter method 100

4.2.1.3 Comparison of water resaturation and mercury penetration methods 109

4.2.1.4 Petrographic determination of porosity : estimation from photomicrographs 114

4.2.2 Relation between Porosity and Deviation Percent from Average Porosity 117

4.2.3 Density-Porosity Relationship 117

4.3 HYDRAULIC CONDUCTIVITY 118

4.3.1 Hydraulic Conductivity Determination 120

4.3.2 Laboratory Measurements of Hydraulic Conductivity 122

4.3.2.1 Apparatus, procedure and results 123

4.3.3 Indirect Determination of Hydraulic Conductivity : Calculation from Pore-Size Distribution 124

4.3.4 Hydraulic Conductivity Results : Comparison between K_w and K_{Hg} 125

4.4 RELATIONSHIP BETWEEN HYDRAULIC CONDUCTIVITY-POROSITY AND PORE-SIZE DISTRIBUTION 128

4.5 RELATIONSHIP BETWEEN HYDRAULIC CONDUCTIVITY AND LITHOLOGY 136

CHAPTER 5 GROUNDWATER CHEMISTRY 146

5.1 INTRODUCTION 146

5.2 METHODOLOGY 148

5.2.1 Sampling and Field Work 148

5.2.2 Sample Analysis 149

5.3 ANALYTICAL DATA 151

5.3.1 Specific Electrical Conductance 151

5.3.2 pH Values 153

5.3.3 Major Elements 155

Page

5.3.3.1 Calcium and magnesium 155

5.3.3.2 Potassium and sodium 156

5.3.4 Trace Elements 161

5.4 MINERAL ANALYSIS OF THE FINE RESIDUE 164

5.5 WATER CHEMISTRY AND MINERAL STABILITY 165

5.6 DISCUSSION 170

CHAPTER 6 DISCUSSION 174

CHAPTER 7 CONCLUSIONS 185

APPENDICES 195

Appendix 1 Formula for calculating porosity from water resaturation method 195

Appendix 2 Derivation of Washburn Equation 196

Appendix 3 Pore size distribution data and porosity calculation 197

Appendix 4 Chemical analyses of fine residues (< 0.38 μm) 198

REFERENCES 199

LIST OF FIGURES

Figure		Page
2.1	Distribution of British Triassic deposits	10
2.2	Triassic stratigraphy of Eastern England	13
2.3	Regional geology and location map of studied areas	15
2.4	Geology and Location map of BH A11, A14, A18	17
2.5	Geology and Location map of borehole A3	18
2.6	Lithological, Gamma and Resistivity Logs of borehole A11	21
2.7	Lithological, Gamma and Resistivity Logs of borehole A14	24
2.8	Lithological, Gamma and Resistivity Logs of borehole A18	27
2.9	Lithological Log of borehole A3	29
2.10	Triassic groundwater table at Dover Beck Valley (1974)	35
2.11	Triassic groundwater table at Dover Beck Valley (1975)	36
2.12	Triassic groundwater table at Dover Beck Valley (1976)	37
2.13	Seasonal fluctuation in water level of BH A11, A14 and A18 during 1975, 1976, 1977	39
3.1	Relationship between sample depth and matrix content	46
3.2	Relationship between sample depth and mean grain size (Mz ϕ)	46
3.3	Relationship between packing density (Pd) and consolidation factor (C_f)	51
3.4	X-ray diffraction patterns of the clay fractions in the Sherwood Sandstone Group	74
3.5	Schematic diagram of the diagenetic changes in the Sherwood Sandstone Group of north Nottinghamshire	89
4.1	Pore-size distribution curves representing the Sherwood Sandstone Group of borehole A11	104
4.2	Pore-size distribution curves representing the Sherwood Sandstone Group of borehole A14	105
4.3	Pore-size distribution curves representing the Sherwood Sandstone Group of borehole A18	106
4.4	Pore-size distribution curves representing the Sherwood Sandstone Group of borehole A3	107
4.5	Comparison of porosity measured by water-resaturation (ϕ_{sat}) and Hg injection (ϕ_{Hg})	110
4.6	Relationship between porosity (ϕ_{av}) and deviation per cent from average porosity (Dev %)	110
4.7	Relationship between porisity (ϕ_{sat}) and wet density (ρ_s)	119
4.8	Falling head permeameter	119
4.9	Comparison of measured hydraulic conductivity (K_w) with estimated values from pore-size distribution (K_{Hg})	127

Figure		Page
4.10	Relationship between porosity (ϕ_{av}) and hydraulic conductivity (K_w)	127
4.11	Relationship between calculated hydraulic conductivity (K_{Hg}) and median pore radius (Mr)	130
4.12	Relationship between measured hydraulic conductivity (K_w) and median pore radius (Mr)	130
4.13	Relationships among porosity, hydraulic conductivity (K_w) and pore size distribution of samples 3/4 (dashed line) and 3/6 (solid line)	131
4.14	Pore-size distribution curves and thin section photomicrographs for samples 14/23 and 14/33	133
4.15	Pore-size distribution curves, porosity and hydraulic conductivity of samples 14/26 and 14/40	134
4.16	Comparison among porosity, hydraulic conductivity, pore-size distribution and thin section photomicrographs of samples 14/23 and 14/27	137
4.17	Relationships between porosity, hydraulic conductivity and pore-size distribution of samples 14/26 and 14/43	138
4.18	Caliper log, lithological and hydraulic conductivity variations with depth within Sherwood Sandstone Group at BH A14	141
4.19	Caliper log, lithological and hydraulic conductivity variations with depth among the Sherwood Sandstone Group at BH A11	142
4.20	Caliper Log, lithological and hydraulic conductivity variations with depth among the Sherwood Sandstone Group at BH A18	144
4.21	Lithological and hydraulic conductivity variations with depth among the Sherwood Sandstone Group at BH A3	145
5.1	Specific electric conductance in μS/cm (at 25°C) for Triassic groundwater of the Sherwood Sandstone Group	152
5.2	Concentration of calcium, magnesium, sodium, potassium and silicon in the Triassic groundwater from borehole A11	158
5.3	Distribution of calcium, magnesium, sodium, potassium and silicon in the Triassic groundwater from borehole A14	159
5.4	Concentrations of calcium, magnesium, sodium, potassium and silicon in the Triassic groundwater from borehole A18	160
5.5	Plot of K/Na ratio against Na^+ concentration in the groundwater of the Sherwood Sandstone Group	162
5.6	X-ray diffraction patterns of the fine fraction suspended in Triassic groundwater of the Sherwood Sandstone Group	166
5.7 & 8	Plot of chemical composition of Triassic groundwater (from Sherwood Sandstone Group) on the stability field diagrams of Na and Ca silicate at 25°C and 1 atm.	168

Figure Page

5.9 Plot of chemical composition of Triassic groundwater on the activity diagram for alumino silicate system showing the fields of clay minerals 169

5.10 Plot of chemical composition of Triassic groundwater on the stability field diagram of the system K_2O-Na_2O-Al_2O_3-SiO_2-H_2O at 25°C and 1 atm. 169

6.1 Relationship between average porosity (ϕ_{av}) and mean grain size (Mz ϕ) 178

6.2 Relationship between average porosity (ϕ_{av}) and packing proximity (Pp) 178

6.3 Relationship between average porosity (ϕ_{av}) and carbonate cement content 180

6.4 Relationship between measured hydraulic conductivity (K_w) and mean grain size (Mz ϕ) 180

6.5 Relationship between measured hydraulic conductivity (K_w) and packing density (Pd) 182

6.6 Relationship between median pore radius (Mr) and mean grain size (Mz) 182

LIST OF TABLES

Table		Page
3.1	Sand, clay, carbonate fractions and grain size parameters for borehole A14	44
3.2	Grain contact and packing measurements	48
4.1	Porosity, density and hydraulic conductivity measurements of Sherwood Sandstone Group	98
4.2	Replication of porosity measurements by the water resaturation method	100
4.3	Advantage and disadvantage of water-resaturation and Hg-penetration methods	111
4.4	Comparison between average laboratory porosity (ϕ_{av}) with that measured from photomicrographs	115
5.1	Chemical composition of Triassic groundwater from the Sherwood Sandstone Group in Nottinghamshire	173
6.1	Matrix and cement content, grain size parameters, packing, grain contact, porosity and hydraulic conductivity measurements of Sherwood Sandstone Group from BH A14	175

LIST OF PLATES

Chapter Three

Plate 3.1 Detrital quartz types

Plate 3.2 Detrital quartz types

Plate 3.3 Rock fragments

Plate 3.4 Rock fragments and detrital feldspars

Plate 3.5 Detrital feldspars

Plate 3.6 Haematitic clay coatings

Plate 3.7 Haematitic clay coatings and mechanically infiltrated clay

Plate 3.8 Dissolution features

Plate 3.9 Dissolution features

Plate 3.10 Dissolution and clay replacement features

Plate 3.11 Clay replacement of silicate minerals

Plate 3.12 Clay replacement and dissolution

Plate 3.13 Authigenic quartz

Plate 3.14 Authigenic quartz and K-feldspar

Plate 3.15 Authigenic K-feldspar

Plate 3.16 Authigenic K-feldspar and authigenic clay

Plate 3.17 Authigenic kaolinite

Plate 3.18 Authigenic clay

Plate 3.19 Authigenic clay

Plate 3.20 Authigenic clay

Plate 3.21 Carbonate cement

Plate 3.22 Carbonate cement and authigenic minerals, sequence

Plate 3.23 Paragenetic sequence of authigeni minerals

Plate 3.24 Different types of pores

Chapter 4

Plate 4.1 Fractures and dissolution porosity

Acknowledgements

The author would like to thank the Egyptian Government and Tanta University, who provided the grant without which this work could not have been done. Thanks are also due to the Severn Trent Water Authority for providing the cores, help in the collection of water samples and permission to use some of the borehole data herein.

I would like to thank Dr. P. Turner for his assistance, kind supervision, and for reading and discussing the thesis. Special thanks are also due to Mr. C.J. Thompson for his technical assistance especially with SEM and porosimeter work.

Special thanks are due to the following for their help at different stages of the development of this work: Mr. J. Coundon for thin section preparation, Mrs. M. Whitehouse-Yeo, for helping with X-ray and chemical analyses, Miss G. Thompson for her assistance in the digitizing work, Dr. J.R. Ashworth for his help in the computer work, Dr. C. Page for his help and permission in the use of the Hg-porosimeter, Mr. P. Cox for photographic work.

Many thanks are due to the technical staff in the Departments of Geological Sciences and Metallurgy. Special thanks go to Mrs J. Davis for typing the thesis.

I am very grateful to my husband Mr. M. Kassem for accompanying me during my study, encouraging and helping me in the different ways only he could. Special thanks are due to my daughter Reham for being so busy whilst I was spending most of the time I should have been with her on the study. Thanks are due to Dr. R.A. Almusawi and all my friends and neighbours who helped in many different ways.

CHAPTER ONE

INTRODUCTION

1.1 SCOPE AND OUTLINE OF THE INVESTIGATION

The objectives of this study of the Sherwood Sandstone aquifer in northern Nottinghamshire are slightly different from routine hydrogeological and hydrochemical investigations. Particular emphasis has been placed on the effect of sedimentological and diagenetic parameters on the aquifer properties, and also the origin of porosity as well as the role of diagenesis in porosity creation and destruction. Water chemistry has been studied in order to provide a better understanding of the interaction between the aquifer rocks and groundwater and in particular to see how the aquifer rocks have been modified by the present-day groundwater regime.

The study is based on the analysis of four boreholes drilled in the Sherwood Sandstone Group of north Nottinghamshire. For each of the boreholes a detailed lithological log was made and particular attention paid to mineralogy, petrography and textural analyses. These studies were undertaken in order to establish the burial history and diagenetic environment of the aquifer. The results, particularly from textural studies and clay mineral analysis indicate that the rocks have only been subjected to shallow burial diagenesis. A detailed diagenetic study was carried out and has revealed that these sediments have undergone different diagenetic changes and reached the mature stage of the mesodiagenetic regime of Schmidt and McDonald (1979a). Also stress has been placed on the role of diagenesis on the hydrogeological characteristics of the aquifer. Destruction of the primary

porosity by authigenesis and cementation was important in the early history of the aquifer, and the creation of secondary porosity by dissolution was important later in its history.

The hydrogeological properties of these sandstone aquifers were studied by calculating porosity, density and hydraulic conductivity. The laboratory data were compared with the field data which reflect the effects of the secondary fissures and fractures on the hydraulic characters of these aquifers. Also the relationships between the hydraulic characters and some of the physical properties of the rocks have also been studied. A trial has been made for the measurement of porosity from thin section photographs but the results were obviously different from the laboratory measurements and are considered suitable for a limited range of lithologies.

The chemistry of groundwater samples from three boreholes was also investigated. The aim of this study was to see if pore water composition was affected by diagenetic changes within the aquifer. The precipitation of new minerals, dissolution of others, creation of new pores and destruction of others, and the transformation of one mineral to another, have all affected the chemistry of the groundwater during the history of the aquifer. The study indicates that the present groundwater is undersaturated with respect to dolomite, calcite, K-feldspar, montmorillonite and mixed layer (I/S) clay, which means their dissolution or replacement contributes to the origin of secondary porosity. At the same time this water is saturated with respect to kaolinite and the precipitation of this mineral may have occurred recently and been significant in the destruction of secondary porosity.

1.2 PREVIOUS WORK

Triassic rocks have a wide distribution over the British Isles both on the surface and in the subsurface, where their importance includes not only their groundwater potential but also hydrocarbon and gas. However, little attention has been given to these deposits before the last decade. These Triassic deposits have been considered among the principal sources of underground water, especially in the Midlands and northern England for over one hundred years. Although in some places, e.g. South Lancashire, these aquifers have recently been over-exploited as a result of excessive pumping (Howell, 1965; Bow et al., 1969).

Most of the studies done on these continental red beds have concerned their stratigraphy, depositional environments, source area, mineralogy and diagenesis (Taylor, 1968; Thompson, 1970; Waugh, 1970a, 1970b and 1978; Turner, 1980; Ali, 1982). However, little investigation of the hydrogeological characteristics of these water aquifers were done before 1965 although a limited amount of porosity data were published by De Rance (1882), Moore (1904) and Kendal (1921). No studies on hydraulic conductivity were done during this early period.

The hydrology and groundwater chemistry of lower Triassic sandstone aquifers in Nottinghamshire were studied by Land (1966). Important contributions were made by Howell (1965) and Bow et al. (1969) who documented the serious decline in the water table and the migration of brines into the Permo-Triassic aquifer of South Lancashire as a result of overpumping.

Regarding the hydrogeological properties of these Triassic water aquifers Bow et al. (1970) studied the porosity and permeability of unfissured

samples from South Lancashire and North Cheshire, representing "Bunter" and "Keuper" Sandstones. This laboratory study showed the anisotropic nature of these sandstones, with higher permeability values being parallel to the bedding plane. Also the upper limit of permeability values indicates the ability of the groundwater to permeate through these rocks in the field, even in the absence of secondary fissures.

The aquifer properties of the Sherwood Sandstone Group in Nottinghamshire were studied by Williams et al. (1972) who made a detailed laboratory investigation of the physical and hydrogeological characters of sandstone core samples from a site at Edwinstowe. The relationships between these properties were studied and a comparison between laboratory and field data was made. This study indicates a poor correlation between the physical properties of these sandstones and the intergranular hydraulic conductivity and also demonstrated the great importance of fissures systems on the field values of vertical and horizontal hydraulic conductivity. Comparison of field and laboratory data indicates that groundwater movement through fissures is four times greater than flow through intergranular pores. Another investigation on the aquifer properties of the Sherwood Sandstone, in Northwest England, and their relationships to some hydrogeophysical properties was carried out by Barker and Worthington (1973). A comprehensive analysis of the aquifer properties (porosity, intergranular permeability, specific yield and transmisivity) of Permo-Triassic sandstones from numerous localities in the United Kingdom was carried out by Lovelock (1977).

Chemical data for groundwater in general and for that of the Triassic in particular is scarce. However, previously available information

indicates that the groundwater of the Sherwood Sandstones in Nottinghamshire is dominated by calcium, magnesium and bicarbonate ions with total dissolved solids between 105 to 300 mg/l (Land, 1966).

A pioneer study of the processes operating in Triassic aquifer groundwaters including the role of natural abundance of elements and the interaction between groundwater and the surrounding geological environment was undertaken by Edmunds and Morgan-Jones (1976) in the Wolverhampton - East Shropshire area. Their study revealed that groundwater from the Wildmoor Sandstone Formation ("Bunter Pebble Beds" and "Upper Mottled Sandstones") are significantly undersaturated with respect to calcite and dolomite although the waters in the formations above and below (Lower Keuper Sandstone and Upper Mottled Sandstone) are saturated. Also Mg/Ca ratios in groundwaters from the Lower Keuper Sandstones and to less extent the Upper Mottled Sandstones are higher than the other underlying units, which may reflect the dominance of dolomitic cement in these sandstones. The high positive Eh values in the groundwater ensure the low concentration of natural trace metals, which generally ranged between 1-10 µg/l. Also the amount and nature of impurities in the sandstone control the chemistry of trace elements of the Triassic groundwater and the cation exchange reactions with clay minerals probably controlled the occurrence of certain elements including lithium.

1.3 METHODOLOGY

The investigation reported in this work is based on the study of the Sherwood Sandstone Group (Triassic) aquifer in North Nottinghamshire. The material used for the study included four borehole cores, drilled

in 1975 as part of the investigation programme for phase I of the Nottinghamshire Triassic Sandstone Conjunctive Use Investigation. These boreholes (BH A11, A14, A18 and A3) were subjected to detailed lithological logging and representative core samples were chosen for laboratory analysis using a variety of analytical techniques. Also groundwater samples were collected from three boreholes (A11, A14 and A18) for geochemical studies.

Impregnated thin sections were prepared for each core sample using green dyed araldite resin (araldite CY 212 and hardner HY 951). The green dye enables the easier identification of different types of pores and dissolution features and also allows visual estimates of porosity per cent in thin sections. For carbonate identification, some thin sections were stained using the combined stain technique of alizarin red-S and potassium ferricyanide in dilute HCl (Dickson, 1965). These thin sections were used for routine mineralogical and petrographic studies with some stress on the diagenetic features, in particular dissolution, clay replacement and mineral paragenesis. Also photo-micrographs were prepared for a number of representative thin sections and used for packing, grain contact analyses as well as porosity measurements.

The scanning electron microscope (SEM) with the energy dispersive analyser of X-rays (EDAX) was used to identify authigenic minerals and establish their temporal and textural relationships. SEM was used for the study of dissolution textures as well as pore-shape and geometry as seen in resin pore casts. These pore casts were prepared from impregnated rock chips by dissolving the rock using HCl and HF. The samples were mounted onto aluminium stubs then coated under vacuum by

carbon for EDAX analysis or gold for better resolution.

X-ray diffraction was used for the identification of clay minerals. Oriented clay samples (< 2 μm fraction) were prepared either by sedimentation onto glass slides or suction onto ceramic discs. The diffraction patterns for dry untreated, glycolated and heated (up to 550°C) samples were prepared using CO Kα or Cu Kα radiation. Also XRD was carried out on the fine fraction obtained from the filtration of groundwater samples through 0.45 μm pore size filters.

One inch (2.54 cm) diameter cores were cut parallel to the bedding planes of the large core samples. These cores were used for porosity measurements by means of the water resaturation method. Also, the same cores were used for hydraulic conductivity measurements using the falling head permeameter.

The Hg-injection method using Hg-penetration porosimeter model 900/901 series of 351 N/mm^2 pressure capacity was used for studying the pore-size distribution and porosity calculations. Estimates of permeability from the pore-size distribution were also made.

Grain size analysis was done on selected sandstone samples representing the Sherwood Sandstone Group of borehole A14. The samples were sieved through a set of $\frac{1}{2}$ ϕ intervals, after their disaggregation and HCl treatment. The data obtained in this way were used to calculate grain size statistics.

Trials were made assessing the value of the petrographic determination of porosity using representative photomicrographs. Porosity was determined manually by means of measuring the intersection lengths of the pores along equally spaced linear traverses and converting

to volume. Pore area was also measured directly for the same photomicrographs using "Hewlett-Packard 9825A Desktop Computer and 9874A Digitizer". This apparatus consists simply of a platen where the photo was fixed onto its active area by means of a magnet at each corner and pore spaces were traced by moving a cursor around the edges of the pore. While digitizing X and Y coordinates were recorded by means of a computer connected to the digitizer. This enabled pore area and perimeter to be computed for the photomicrographs and the results compared with those obtained using the other techniques.

Static groundwater samples were collected from boreholes A11, A14 and A18 for chemical analyses. The pH and electrical conductance were measured on the same day of collection both in the field and laboratory. The water samples were filtered through 0.45 μm pore-size filter and the fine residues obtained were used for XRD and chemical analyses. Then the water was analysed for the elements Ca, Mg, K, Na, Fe, Al, Si, Cd, Co, Cr, Cu, Mn, Ni, Pb, Zn and V, using atomic absorption spectrophotometry.

CHAPTER TWO

STRATIGRAPHY AND AQUIFER PROPERTIES

2.1 TRIASSIC AQUIFER OF EASTERN ENGLAND

Triassic successions have a wide distribution in the British Isles as either surface exposures or concealed beneath younger deposits (Figure 2.1). The successions include representatives of formations assigned to the Sherwood Sandstone, Mercia Mudstone and Penarth Groups. The Sherwood Sandstone Group (named after the ancient Sherwood Forest in Nottinghamshire) is the only group to be dealt with in detail in this work because of its importance as an aquifer. The Sherwood Sandstone Group is the arenaceous sequence which includes the formations previously known as the "Bunter" and the arenaceous (Lower) part of the "Keuper" in Britain (Warrington et al., 1980).

In Eastern England the Sherwood Sandstone Group comprises the Lenton Sandstone Formation (formerly "Lower Mottled Sandstone") overlain by the Nottingham Castle Formation (previously "Bunter Pebble Beds"). Both formations are unfossiliferous throughout the region. The Lenton Sandstone Formation consists of medium-dark red, fine-medium grained sandstone, frequently mottled yellow and green in patches and seams. The sandstone is poorly cemented, friable and easy to break down, with only a significant clay fraction (up to 10%) as binding material (Taylor, 1968). The maximum thickness of this formation is up to 30 m (100 ft) and is reasonably constant through much of Nottinghamshire as suggested by Swinnerton (1948). Hard and firm beds cemented with dolomite are recorded within the generally friable sequence particularly at the base of the old quarry faces

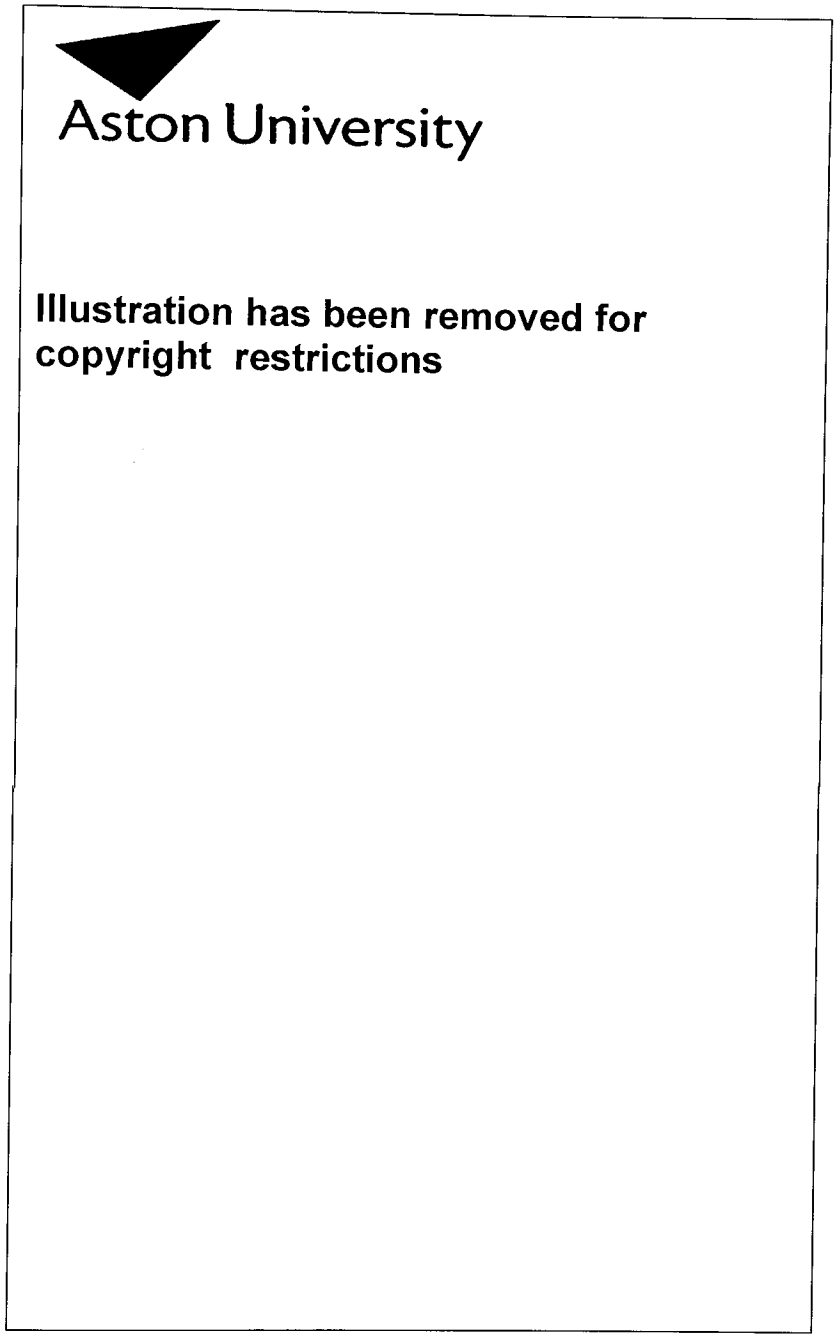

Figure 2.1 Distribution of British Triassic deposits (Warrington et al., 1980)

bordering Clifton Boulevard, Nottingham (Swinnerton, 1948). To the north of Mansfield there is an increase in grain size which is accompanied by a reduction in the clay content and this causes difficulty in distinguishing the formations comprising the Sherwood Sandstone Group (Taylor, 1968). There is no palaeontological evidence of the position of the Permian-Triassic boundary in Eastern England. The lower part of the Sherwood Sandstone Group in the Nottingham area, as around Chester, is probably Permian in age, while elsewhere this boundary may lay below the base of the Group (Warrington et al., 1980).

The Nottingham Castle Formation of Eastern England is a thick succession of light-medium red, sometimes yellow or buff coloured (at Nottingham Castle, University and Sandiacre) coarse friable sandstone, strongly current bedded, with pebbles arranged parallel to the true or current bedding. Thin mudstone beds up to 1 m thick are seen throughout the formation (Swinnerton, 1948; Taylor, 1968). The thickness of the Nottingham Castle Formation varies widely with recorded thickness of up to about 300 m in northern Nottinghamshire (Land, 1966), 200 m at Mansfield, 60 m at Nottingham University and 16 m at Dale (this thickness may or may not include the Lenton Sandstone Formation). The pebbles recorded in Eastern England are up to 8 cm diameter and mainly of local origin; Carboniferous Limestone, sandstones, cherts and Permian dolomite, together with a variety of older sedimentary, igneous and metamorphic rocks.

The boundary between this arenaceous fluviatile sequence and the overlying Mercia Mudstone Group is sharp throughout much of Eastern England with evidence of unconformity characterized by a thin pebble bed. This is up to 1 m thick at Nottingham University and is calcite-cemented (Swinnerton, 1948).

The Mercia Mudstone Group comprises mainly argillaceous units which overlie the Sherwood Sandstone Group and underlie the Penarth Group. It corresponds essentially to the former 'Keuper Marl' and consists of red, green and grey mudstone and siltstone with red and green sandstone intercalations. The base of this group is usually sharp but in gradational sequences the dominance of mudstone and siltstone over sandstone indicates the transition. This group consists of nine formations, three of them are arenaceous and all of them represented in north Leicestershire and south Nottinghamshire (Warrington et al., 1980). The lowest formation (Woodthorpe) passes rapidly towards Central Nottinghamshire into the following Retford Formation (mainly argillaceous). While both Redford Formation (formerly "Green Beds") and the Colwick Formation (formerly "Keuper Waterstone") are most distinguishable in Central and Northern Nottinghamshire (Figure 2.2).

The Penarth Group (formerly the Rhaetic) comprises dark grey shale at the base forming the Westbury Formation passing upwards to the grey-green calcareous mudstones of the Lilstock Formation. This lithology passes upwards into chocolate brown mudstones widespread over much of Eastern England. This group is poorly exposed in this region.

2.2 GEOLOGY OF THE INVESTIGATED AREA

The geological formations outcropping in the area under investigation in Central Nottinghamshire, are exclusively Triassic (Figure 2.3). The western limit of these Triassic rocks is bounded by the older Permian rocks followed further to the west by the Carboniferous limestones and coal measures. As these Triassic exposures dip gently to the south-east, they are conformably overlain to the east by younger Jurassic and Cretanceous rocks.

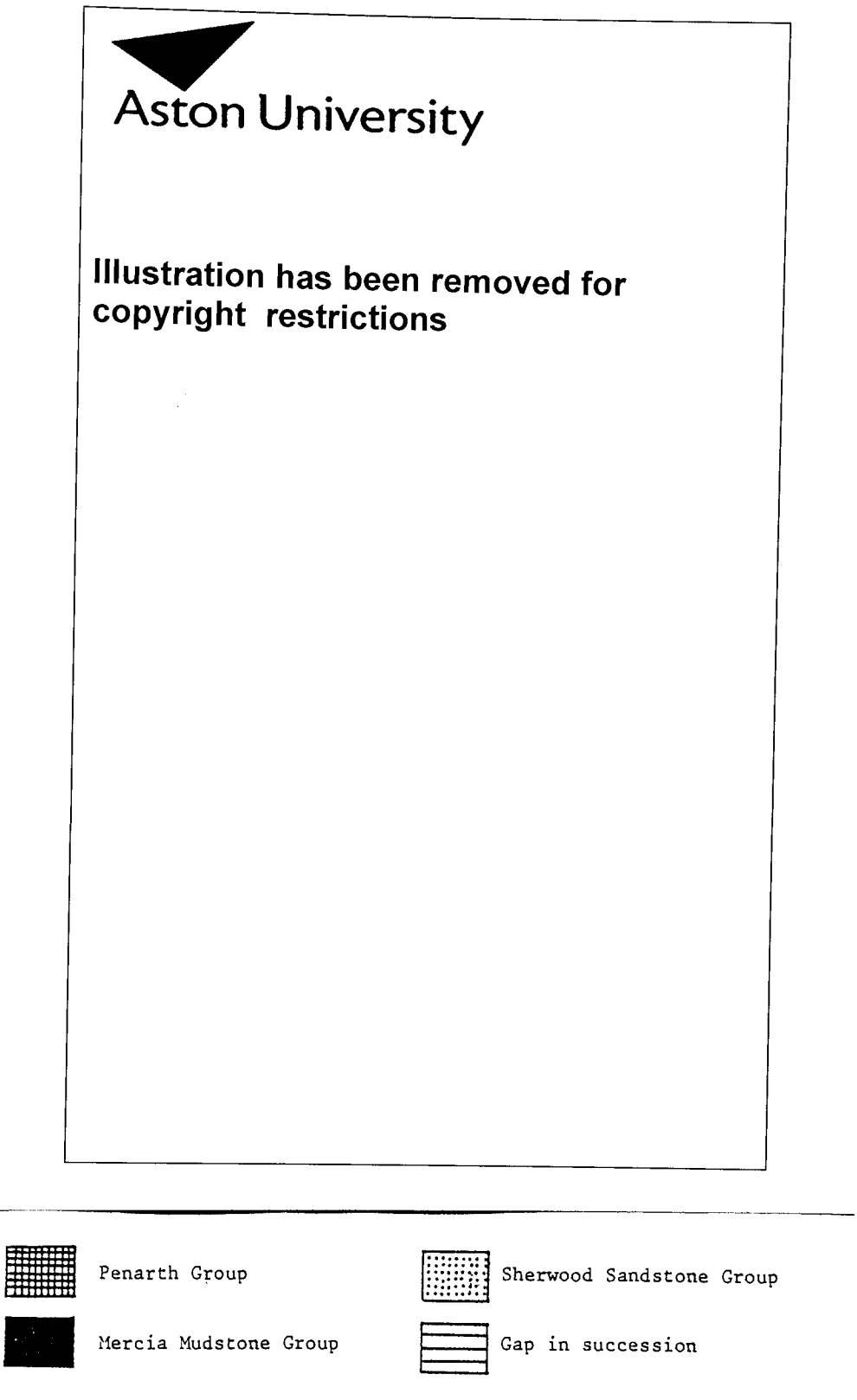

Figure 2.2 Triassic Stratigraphy of Eastern England (after Warrington et al., 1980)

These Triassic deposits which are the most extensively outcropping rocks in the area as shown from Figures 2.4 and 2.5, includes the Sherwood Sandstone Group, Mercia Mudstone Group and Colwick Formation (formerly "Keuper Waterstone"). The rocks dip gently to the south-east ($\sim 5^{o}$) where the Sherwood Sandstone Group is overlain and sealed by the Mercia Mudstone Group. This gives rise to confined conditions of the Lower Triassic water aquifer represented here by BH A14 and A18 (Figure 2.4). Some superficial Recent alluvial deposits, recorded along the Dover Beck Valley as well as a few disseminated patches of Pleistocene deposits have no effect upon the unconfined part of the underlying Sherwood Sandstone aquifer. This unconfined part of the aquifer is represented here by BH A3 and A11.

The Sherwood Sandstone Group in the investigated area includes both the Nottingham Castle and Lenten Sandstone Formations. Further to the north, those two formations cannot be distinguished from each other as represented here by BH A3 (Figure 2.5). In this area the Sherwood Sandstone Group is predominantly sandy and the thick conglomeratic units ('Bunter Pebble Beds') seen further south and west are absent. Nevertheless many of the sandstones are pebbly and the overall aspect is of coarsening upwards.

The junction of the Sherwood Sandstone Group and the overlying Mercia Mudstone Group is generally sharp with evidence of erosion of the lower Triassic rocks (Warrington et al., 1980). This unconformity or gap in the stratigraphic succession (Figure 2.2) was detected in the confined BH A18, where a one meter thick carbonate-cemented conglomerate bed was recorded. Unfortunately, the extent of this period of non-deposition or erosion cannot be detected from the available information. Even the actual thickness of the conglomeratic bed

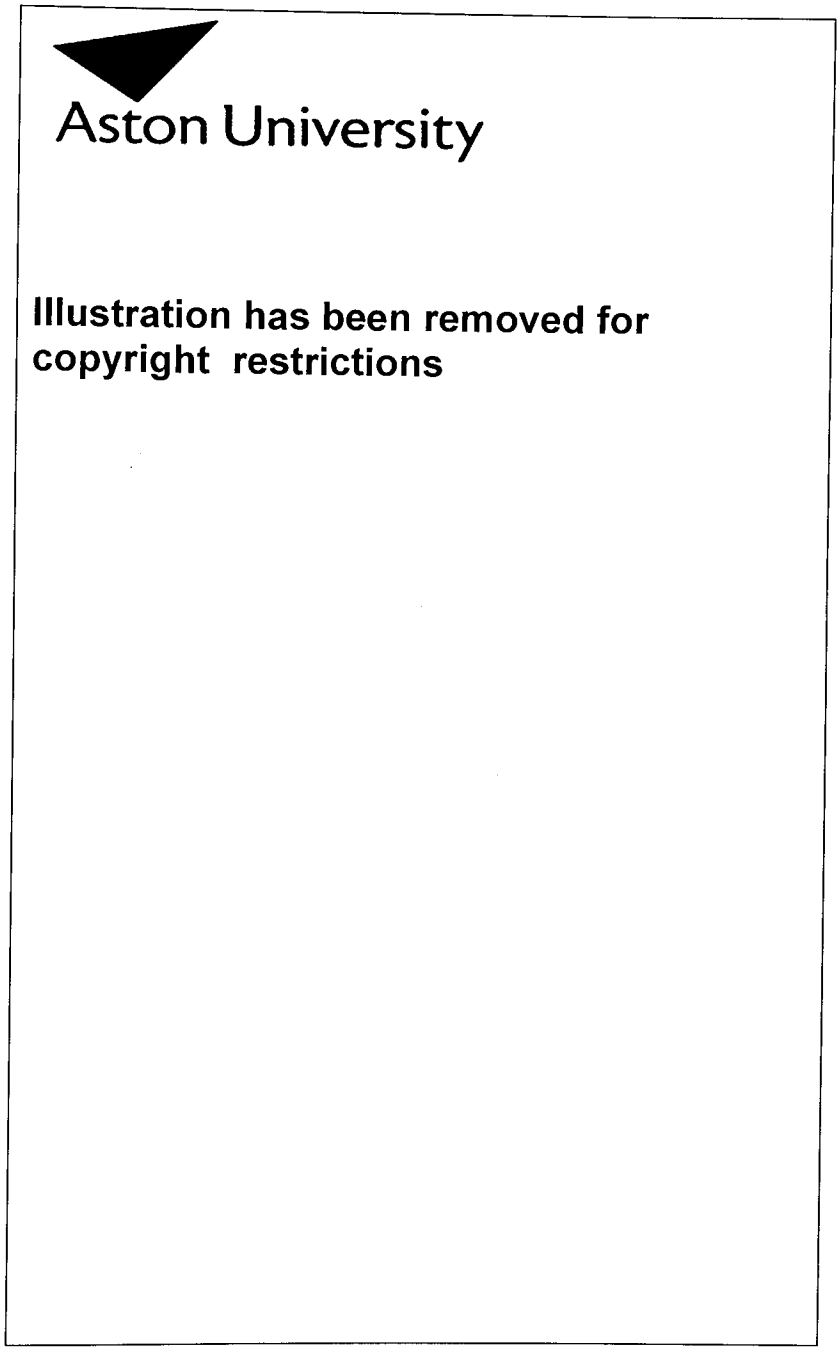

Fig. 2.3 Regional geology and location map of studied areas (Geological Survey of Great Britain, Sheet 2, 1957)

could not be known as a result of the core missing (low percentage core recovery). On the other hand, in the other confined condition, BH A14, no sign of unconformity was detected and this could either be due to the loss of conglomerate during coring processes or non-deposition at this area. The first idea of the loss of conglomerate during coring could be more reliable as only 79% of the core interval was recovered. The presence of a significant time gap between the Sherwood Sandstone and Mercia Mudstone Groups suggests that some diagenetic processes may have been completed at this stage. In particular, authigenesis and cementation which took place soon after deposition may have occurred prior to the deposition of the Mercia Mudstone Group.

In this area under study only Sherwood Sandstone Group and some members of the Mercia Mudstone Group (mainly Colwick Formation) are represented. The Penarth Group of the Late Triassic age is not represented at all in all the studied boreholes. The detailed lithology of these formations will be dealt with in the following section.

2.3 LITHOLOGICAL VARIATION OF BOREHOLES A3, A11, A14, A18

The work dealt with here is based on the detailed study of four boreholes, which formed part of the investigation program for phase I of the Nottinghamshrie Triassic Sandstone Conjunctive Use Investigation. The investigation included the drilling of 29 boreholes in all. The four boreholes studied are represented in Figures 2.4 and 2.5 and are:

BH A11 Dairy Farm (GR 575500)
BH A14 Low Field Farm (GR 668443)
BH A18 Mill Farm (GR 630500)
BH A3 Chequer House Farm (GR 64498126)

Figure 2.4 Geology and Location map of BH A11, A14, A18
(Geological Survey of Great Britain, Solid and Drift, Sheet 126, 1972)

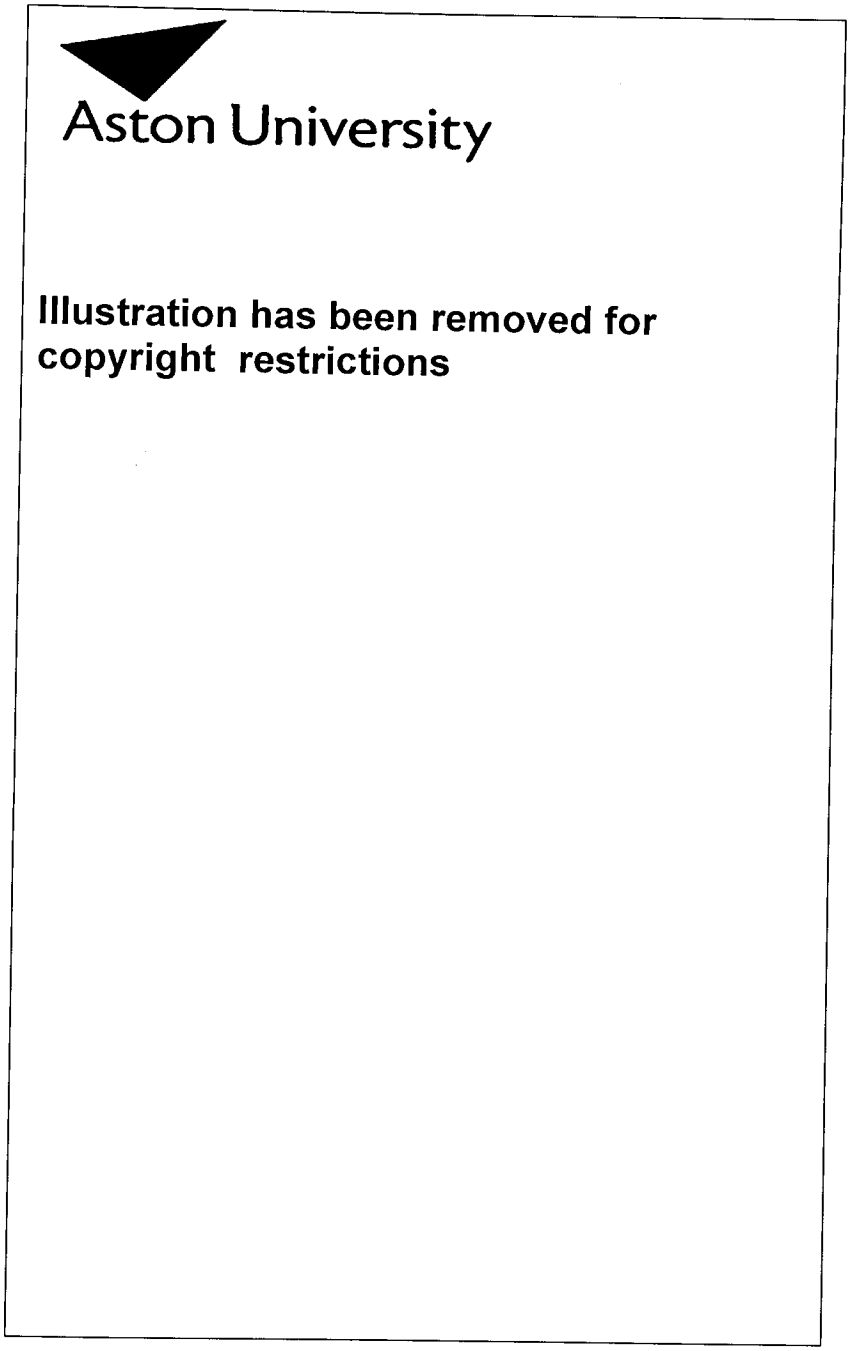

Figure 2.5 Geology and Location map of borehole A3 (Geological Survey of Great Britain, Solid and Drift, Sheet 101, 1967)

These four boreholes were cored or partially cored to their total depth to the base of the Triassic sandstones, with four inch nominal diameter for BH A11, A14 and A18, while A3 is of six inch diameter. Geophysical logging carried out on BH A11, A14 and A18 by the Water Research Centre Logging Unit, included Gamma, Resistivity, Caliper, Temperature and Differential Temperature, Heat Pulse Flowmeter and Conductivity. Television logging for BH A18 was also carried out.

The general lithology of the Sherwood Sandstone Group dealt with in this work, indicates the presence of the Nottingham Castle Formation and Lenton Sandstone Formation although the boundary between them is usually not easy to define. The Nottingham Castle Formation is represented by pebbly coarse-medium grained sandstones of pale red and sometimes yellowish grey or greyish yellow colour. The sandstones vary from friable to well-cemented. The Lenton Sandstone Formation is represented by moderate-dark reddish brown, medium-fine grained sandstones, pebble-free and characterized by abundant fractures and sedimentary textures. The Sherwood Sandstone Group shows thickness variation between 67 m and 120 m and is thinnest in BH A11 (67 m) and A3 (88 m). The maximum thickness (120 m) is recorded in BH A14 and A18. This is consistent with our knowledge of the regional variation. The Lower Mottled Sandstone and Bunter Pebble Beds (equivalent to Sherwood Sandstone Group) have a recorded thickness of about 300 m to the northern end of Nottinghamshire (Land, 1966) which thins southward to about 60 m at Nottingham and dies out about 8 miles south of Nottingham.

The two formations comprising the Sherwood Sandstone Group, show a general coarsening-upwards sedimentary cycle. A unit of 2 to 14 m thick has been identified towards the bottom end of the Nottingham

Castle Formation. This unit which is represented in all the boreholes studied comprises intercalation of sandstones, mudstone, siltstone and intraformational conglomerate.

The following is a detailed description of the four boreholes.

2.3.1 Borehole All

Borehole All at Dairy Farm (GR 575500) was drilled to a depth of 84 m with a core interval of 52 m and core recovery of 49.8 m (95.8%). This borehole, which was drilled in 1975, has 15 meter lining and the water level at that time was 16.06 m depth. The core samples studied from this borehole represent the interval between 12 m and 72 m depth.

The lithology of BH All (Figure 2.6) shows an overall uniform character from 12 to about 45 m depth, where the sandstone is of coarse to medium grain size. Occasionally pebbles with 6 cm diameter maximum size are seen and tend to be concentrated in the upper 20 m. The Gamma and Resistivity logs (Figure 2.6) confirm the uniform characters of these rocks.

From 12 to about 22 m depth the sandstone is yellowish grey (5Y 8/1), friable and poorly cemented. In this zone green mudstone pellets up to 4 cm diameter are common and the rocks are characterized by yellowish limonite-rich spots.

Between 22 m and 30 m depth, the sandstone is very similar but changes to greyish yellow (5Y 8/4) and there is an increase in the pebble content to about 10% (extra- and intraformational type). Between 30-32 m depth, the sandstone is pale red (10R 6/2) medium in grain size and with abundant reddish-brown mudstone flakes. The rocks are

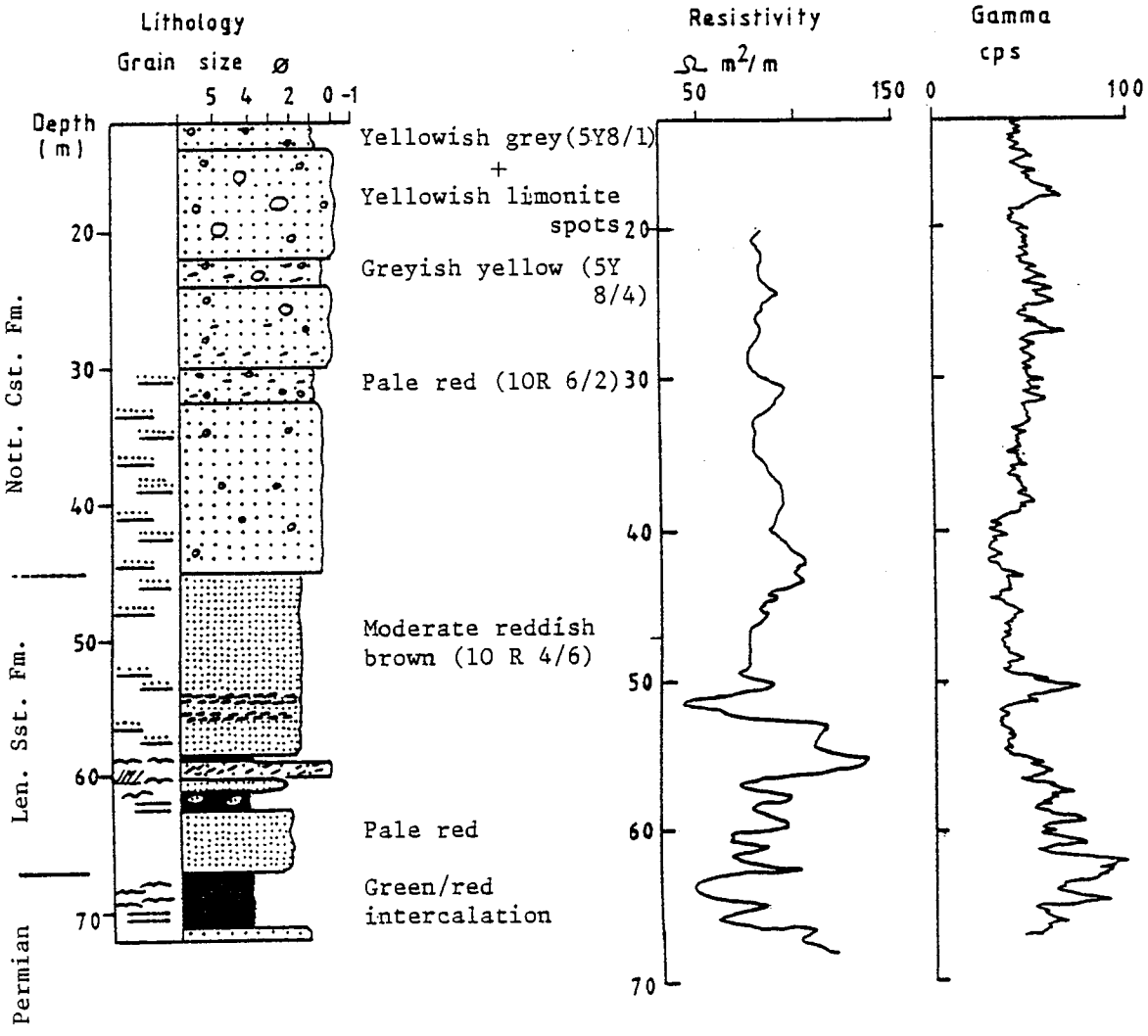

Figure 2.6 Lithological, Gamma and Resistivity Logs of borehole A11

less friable and show horizontal bedding between 2 cm and 14 cm thick.

Between 32 and about 45 m depth the sandstone is uniformly pale red (10R 6/2), medium-coarse grain size, with less than 10% pebbles and with horizontal bedding. The sandstones in this zone are well cemented.

Below 45 m depth and down to 58.6 m the sandstone tends to be finer in grain size and darker in colour and probably represents the top of the Lenton Sandstone Formation. The sandstone in this zone is medium-fine grain, moderate reddish brown (10R 4/6), firm and well cemented with an abundance of horizontal bedding or lamination 1 mm to 12 mm thick. These sandstones are almost pebble-free except for a concentration of mudflakes in thin laminae ($\sim$ 20-40 cm thick) at about 55 m depth, forming a distinctive mud-flake conglomerate.

Between 58.6 and 62.5 m depth is a 4 m thick unit comprising intercalations of mudstone, siltstone, sandstone and mud-flake conglomerate. Different sedimentary structures were present including cross-lamination and ripple marks.

Below this unit and down to about 67 m depth the sandstone is fine-very fine grained, massive, pebble-free and pale red. These rocks are hard and well-cemented and probably represent the lower end of the Lenton Sandstone Formation.

Below this sandstone and down to about 71 m depth, intercalation of green and red mudstone beds predominate and are characterized by cross-lamination and ripple marks. These beds are considered to be Permian in age. Beneath this Permian Marl is a sandstone

bed of medium grain size, pale red-green and well-cemented.

2.3.2 Borehole A14

Borehole A14 drilled at Low Field Farm (GR 668443) to its total depth (∿198 m) with core interval equal to 133.5 m and core recovered of 106 m (79%). The borehole, which was cored in 1975, has casing to a depth of 74 m and the water level recorded at that time was 2.70 m in depth. The core available in this study represents the interval between 63 and 198 m in depth.

The Nottingham Castle Formation in the Low Field Farm borehole is uniform medium-coarse pebbly sandstone. The conformable boundary with the mudstones of the Mercia Mudstone Group is seen at a depth of 68 m (Figure 2.7). There was no conglomeratic bed detected at the top of the Sherwood Sandstone Group, this could either be due to the loss of conglomerate during coring or to non-deposition. This conglomerate bed has also not been detected in BH A11, but is present in BH A18.

Between 68 m and 172 m depth the sandstones of the Nottingham Castle Formation are uniform as indicated by the Gamma and Resistivity logs (Figure 2.7)(Nottingham Triassic Conjunctive Use Investigations, Report No. 4,5), although the core is missing between 102.5-129 m and 135-171 m depths. The sandstone is generally pale red (5R 6/2 to 10R 6/2) with sometimes greyish red (10R 4/2) and pale yellowish brown (10YR 6/2) colours. The sandstone is medium-coarse grained, pebbly, with extra- and intraformational pebbles up to 72 mm in diameter. The pebble content (around 10%) decreases toward the top and bottom end of the formation. The rocks are normally massive and friable to well-cemented.

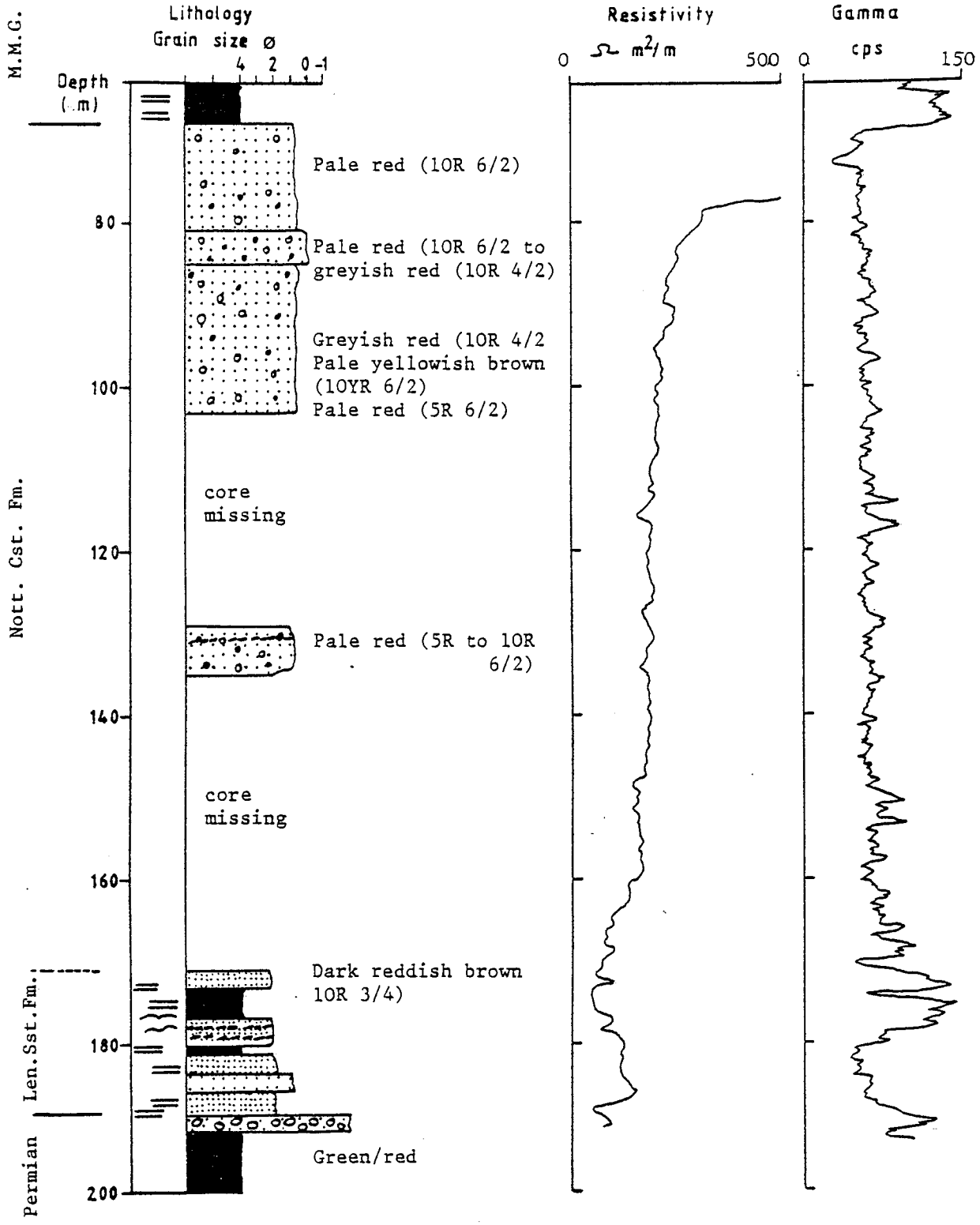

Figure 2.7 Lithological, Gamma and Resistivity Logs of borehole A14

At about 171 m depth the sandstones become darker in colour (dark reddish brown) and are intercalated with mudstones and siltstones. Sandstones have concentrations of mud-flakes in laminae forming thin mud-flake conglomerates. The sandstone is laminated, while the finer grained rocks are sometimes fissile. A variety of sedimentary structures including lenticular, wavy and convolute bedding are present as well as syn-depositional deformation structures. This particular unit is about 10 m thick and can be defined in boreholes A11 and A18.

Between 181-188.5 m depth the sandstone is dark reddish brown (10R 3/4), medium-fine grained, massive and sometimes laminated. Medium-coarse sandstone laminae were also detected. These pebble-free sandstones are fractured and fissured, indicating the importance of secondary permeability in this bed which probably represents the Lenton Sandstone Formation (previously Lower Mottled Sandstone).

Below this sandstone is a thin conglomeratic bed overlying green-red intercalations of mudstone and siltstone which are considered to be Permian in age.

2.3.3 Borehole A18

Borehole A18 at Mill Farm (GR 630500) was drilled to a depth of 147 m, with 67 m core interval and 49.6 m (74%) core recovery. The borehole was lined to a depth of 15 m and the water level recorded at 8.22 m depth in 1975.

This borehole starts with a thin laminated mudstone greenish grey (5GY 6/1) to pale red (5R 6/2) in colour, underlain by a one metre thick conglomeratic bed which is firm and well-cemented by carbonate.

This top bed represents the lowest beds of the Mercia Mudstone Group. Between 4.7 and 13 m depth there was no core recovery.

Between 13 and 19.5 m depth, the core recovered reveals a coarse grained sandstone of yellowish grey colour (5Y 7/2) changing to pale red (10R 6/2) between 13.5-15 m depth and to yellowish grey between 15-19.5 m depth. The sandstone shows abundant (up to 10%) extra- and intraformational pebbles. The core is missing between 19.5-33 m depth.

Between 33 and 51.5 m depth the sandstones are pale red (10R 6/2) and occasionally yellowish grey (5Y 8/1) medium-coarse grained and slightly pebbly ($\sim$ 5%). The rocks show lamination as well as oblique fractures. The samples are very friable between 35-51.5 m depth.

Although there was no recovery between 51.5 m and 100 m depth, the Gamma and Resistivity logs indicate a uniform nature of the sandstone to about 105 m depth (Figure 2.8).

Between 100 and 105 m depth the sandstone is medium-coarse grained, pale red (5R 6/2 to 10R 6/2) and occasionally pebbly, showing an increase of mud-flakes in the lower two metres. Cross bedding and small scale lamination (4-10 cm) are detected together with abundant fractures between 103-105 m depth.

From 105 m depth downwards the sandstones change to medium-fine grained, laminated (2-4 mm thick) and well-cemented. The amount and kind of pebbles present is very restricted, being predominantly intra-formational. This change could represent the transition to the Lenton Sandstone Formation (previously the Lower Mottled Sandstone).

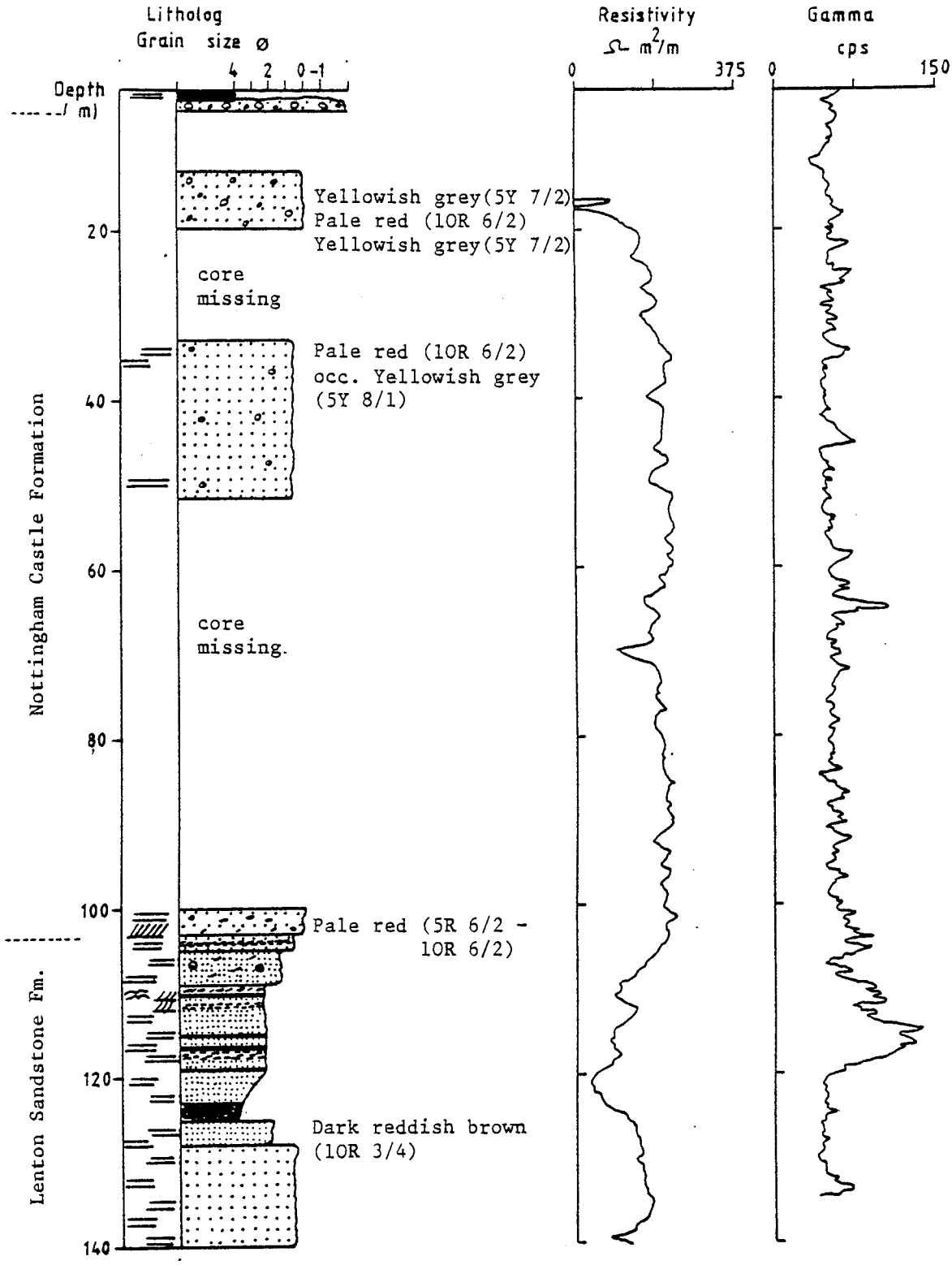

Figure 2.8 Lithological, Gamma and Resistivity Logs of borehole A18

Between 109 m and 123 m depth is a 14 m thick unit comprising a variety of sandstones (medium, fine and very fine grained) intercalated with siltstone and mudstone. Lamination, cross-bedding and ripple marks are present especially in the finer lithologies. Mudstone flakes, slabs and balls are abundant which are sometimes concentrated into laminae causing a noticeable decrease in the intergranular permeability of the rock. To about 125 m depth a two metre thick siltstone bed of reddish brown colour (10R 3/4), occasionally yellowish grey (5Y 8/1) is present (Figure 2.8).

Between 125 and 137 m depth sandstones are dark reddish brown, fine grained in the top three metres, followed by coarse grained laminated sandstone with horizontal fractures. To a depth of 140 m the sandstone becomes medium grained of pale red (10R 6/2) to grey (5YR 6/1), well-cemented, fractured and occasional pebbles were recorded.

2.3.4 Borehole A3

The only available information for borehole A3 at Chequer House Farm (GR 6449 8126) is the lithology, which was cored through the Sherwood Sandstone Group to a depth of about 89 m (the only available in this study). The sequence generally shows a coarsening upwards succession in which fine-medium grained sandstones in the lower 16 m changes upwards into a succession of predominantly medium-coarse grained sandstone. The medium-coarse grained sandstone is mostly pebbly to slightly pebbly. The pebbles disappear towards the base which could indicate the transition from the Nottingham Castle Formation to the finer grained, pebble-free Lenton Sandstone Formation (Figure 2.9).

The sandstone in general shows very clear evidence of abundant secondary pores in the form of dissolution vugs or over-sized pores,

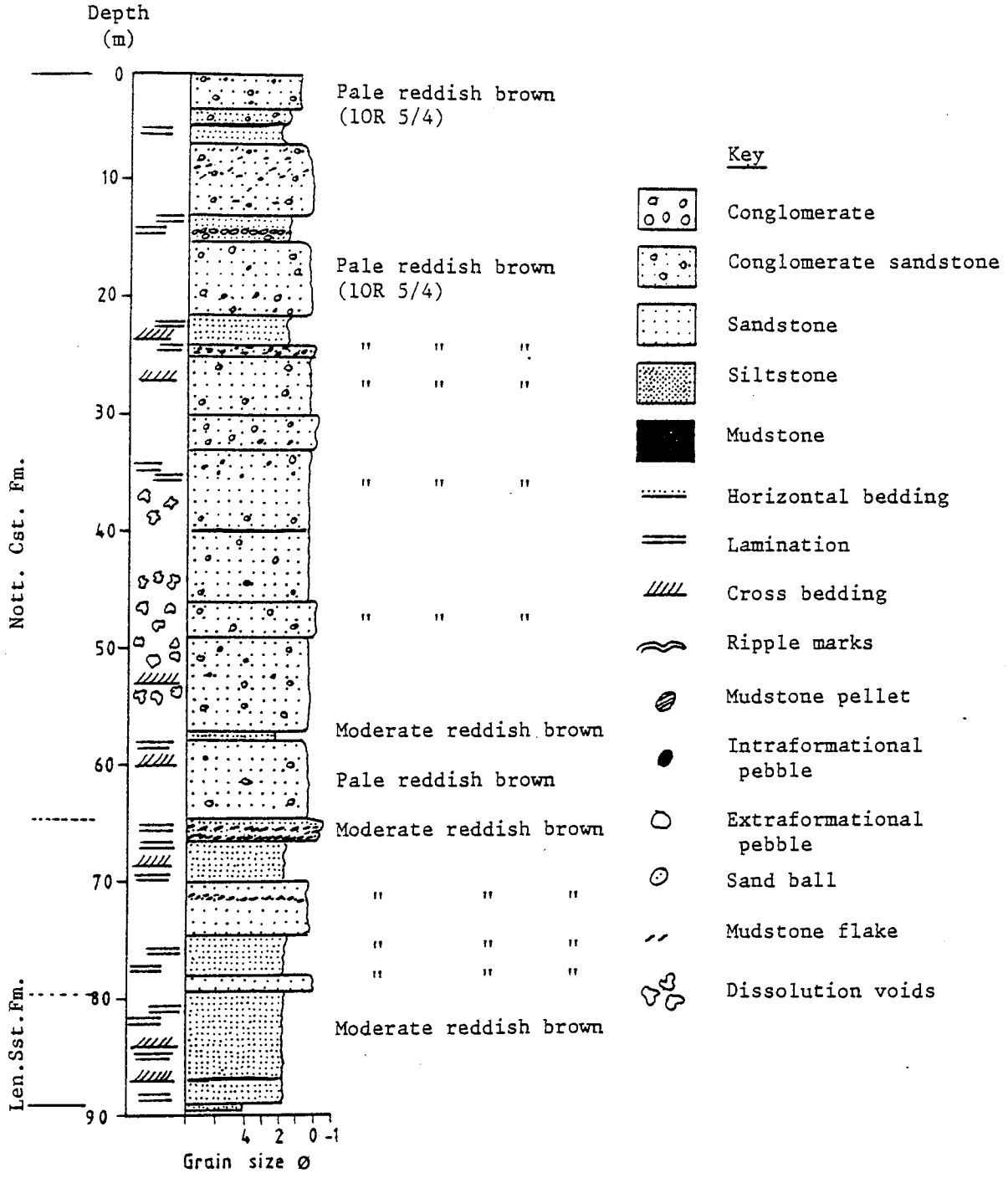

Figure 2.9 Lithological Log of Borehole A3

on a micro- and macro-scale. Fractures are also very abundant and either horizontal or irregular, giving rise to crumbly or brecciated rocks.

From 1-6 m depth the sandstone is generally pale reddish brown (10R 5/4) whilst intercalated mudstone horizons are dark reddish brown (10R 3/4). The sandstone shows coarsening-upwards sequence, from pebbly medium-fine grained at about 5.3 m depth to pebbly medium grained sandstone at about 4 m depth. Below this is a fine-very fine grained laminated sandstone alternating with thin pebbly mudstone lamina ($\sim$ 20 cm thick). The pebbles range between 8-75 mm in size.

Between 6 and 15.3 m depth the sandstones are pale reddish brown (10R 3/4) and show a coarsening-upwards microcycle. Pebbly medium-coarse grained sandstone predominate to about 13.2 m depth and are followed by medium-fine grained laminated and flaggy sandstones which are pebble free and interrupted by thin ($\sim$ 7 cm thick) conglomeratic bed. The pebbles are between 4-74 mm diameter, of extra- and intra-formational type with an abundance of dark reddish brown mudstone slabs, discs, pebbles and flakes. The finer variety is more consolidated and well-cemented.

From 15.3 to about 24 m depth is another microcycle similar to the above one. The main difference is in the amount and kind of pebbles present which are less abundant (slightly pebbly) but with a lower range of size (3 mm - 12 cm). Also the fine-medium grained sandstone is pebble-free, laminated and cross-bedded. Following this microcycle is a one metre thick bed of friable coarse grained sandstone with abundant intraformational pebbles up to 64 mm across.

From 25 m depth downwards to about 64.5 m depth the sandstone is generally medium-coarse grained, slightly pebbly with extraformational

pebbles dominate, up to 80 mm diameter. Lamination and cross-bedding are also recorded. The sandstone varies between very friable to well-cemented. From 33.4 m depth the sandstone is very friable, fractured (irregular) with an abundance of secondary dissolution vugs. Between the following depths 46-49 m, 49.7-52 m and 58.4-64.4 m the rock is characterised by horizontal fractures. Also fine-very fine grained sandstone bed ($\sim$ 50 cm thick) well-cemented and fractured interrupting the core at about 57 m depth.

Between 64.5 and 66.4 m depth is a two metre thick intercalation of fine-medium grained sandstone with mud-flake conglomerate. This horizon is recognized in all the studied boreholes and probably represents the transition between the two formations of the Sherwood Sandstone Group.

Below 66.4 m depth downwards the sandstones differ markedly from the upper beds. They are fine-medium grained, moderate reddish brown colour, pebble-free and well-cemented. Lamination and cross-bedding are quite common. Medium-coarse grained sandstone beds are present at 70-74.5 m and 78-79.5 m. The lower bed is typical of the Lenton Sandstone Formation. The abundance of fine grained sandstone beds intercalated with the medium-coarse grained sandstone strata in the upper part of the core and the presence of medium-coarse grained beds within the lower fine grained sandstone strata, make it difficult to distinguish clearly the two formations.

2.4 GROUNDWATER CONDITIONS

2.4.1 Definitions

An aquifer is a geological formation which is permeable enough to

store, transmit and yield significant quantities of water to wells or springs. The terms ground water reservoir and water-bearing formation are considered synonymous. The aquifer generally extends over a large area and may be overlain or underlain by a confining bed or layer which has no or little intergranular permeability and acts as a seal. These confining beds can be classified into: aquifuge, aquitard and aquiclude (Todd, 1980).

Aquifuge is a relatively impermeable bed that neither contains nor transmits water through it. Aquitard is a low permeability formation that can store ground water and transmit it to or from adjacent aquifers but does not yield water freely to wells (e.g. sandy clay). Aquiclude is a relatively impermeable bed that although saturated with ground water does not yield appreciable quantities of water to wells (e.g. clay).

Depending upon the presence or absence of the water table, and the position of the highly permeable unit with respect to the land surface, aquifers can be classified into: unconfined, confined and leaky or semiconfined (Todd, 1980; Fetter, 1980).

Unconfined aquifer (or water table aquifer) is one with highly permeable materials extending from land surface to the bottom of the aquifer. The water table in this case is present below the ground surface, fluctuating up and down depending upon the recharge, discharge, pumping rates (storage volume) as well as permeability. Confined aquifer, also known as an artesian or pressure aquifer has a permeable bed overlain by a relatively impermeable layer, so that ground water is confined under pressure. In this case the water level is above the bottom of the confining bed in wells penetrating

the aquifer. Unlike the unconfined aquifer, the water level in a well penetrating this aquifer depends mainly on the change in pressure rather than the storage volume of water. Leaky or semiconfined aquifer occurs when the permeable stratum is overlain or underlain by a semiconfined layer (aquitard).

2.4.2 Triassic Groundwater Level

The Sherwood Sandstone Group in the area under investigation shown to be outcropped toward the north and west directions giving rise to (apparently) unconfined aquifer which is represented here by BH A11 and A3 (Figures 2.4 and 2.5). As these Lower Triassic rocks gently dip south-east, they are overlain by the impermeable seal of Mercia Mudstone Group, where they are nearly saturated through their full thickness creating a confined condition represented here by BH A14, A18.

The water table of BH A11 and the potentiometric surface for the confined ones (BH A14 and A18) recorded in 1975 by the Nottinghamshire Triassic Conjunctive Use Investigation monitoring and in 1981 by the writer during the collection of water samples for chemical purposes are as follows:

	W.L. (1975) (metres)	W.L. (1981) (metres)
BH A11	16.06	14.25
BH A14	2.70	5.74
BH A18	8.22	8.26

which show slight change in the water table of the unconfined condition (BH A11) as well as the confined one (BH A14). BH A18

shows a fairly stable water level for this confined borehole. While in BH A14 a slight recession noticed in the ground water level could be due to the continuous pumping in the nearby pumping station. This could result in the development of a cone of depression of size and depth stabilized for a certain rate of pumping, as there is no evidence in the Nottinghamshire of a regional fall in the water table due to over-pumping (Land, 1966).

In order to give an idea about the picture of the water table condition on a regional scale, ground water contour maps constructed for the period between 1974-1976 at Dover Beck Catchment (Nottinghamshire Triassic Conjunctive Use Investigation, Report No. 6) have been used. These contour maps (Figures 2.10-2.12) show overall fairly stable conditions of the ground water level in which the confined area around Lambly and Woodborough record the highest water levels. A general south easterly sloping trend can be recognised with a gradient of 2.5 to 3.0 m/km in the northwest falling to less than half this value in the confined basin (Nottinghamshire Triassic Conjunctive Use Investigation).

Due to the high permeability of the Sherwood Sandstone Group fluctuations in ground water levels are relatively small. The seasonal change measurements for BH A11, A14 and A18 were shown by the monthly measurements of the water level during 1975, 1976 and 1977 (Figure 2.13). The water levels show fluctuations with a recession by the end of 1976 followed by recovery as a result of the summer drought due to heavy rain. This recovery was noticed in the unconfined condition (BH A11) and the confined borehole A18, where the Sherwood Sandstone aquifer at this borehole overlain by only four metres of

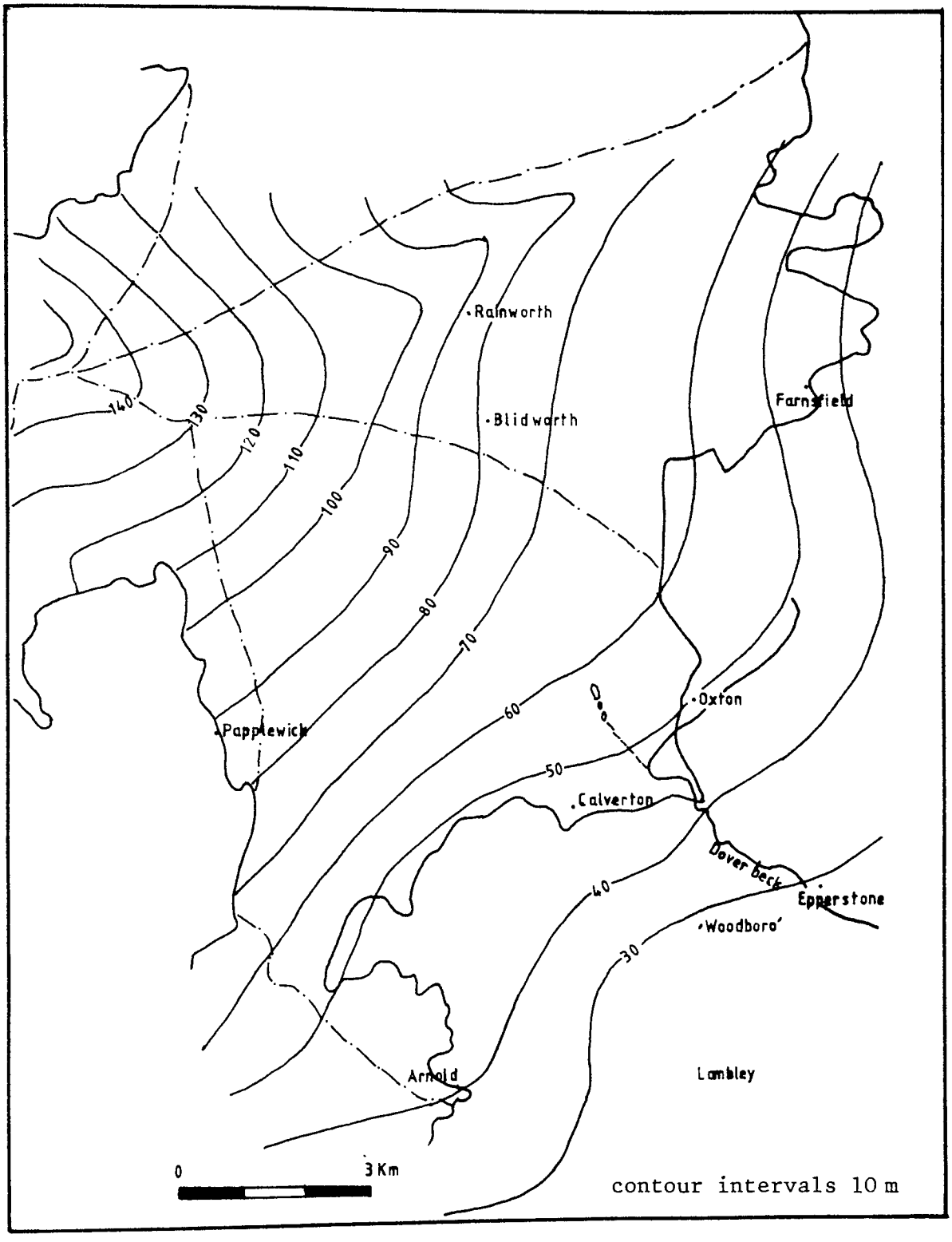

Figure 2.10 Triassic Groundwater table at Dover Beck Valley (1974)

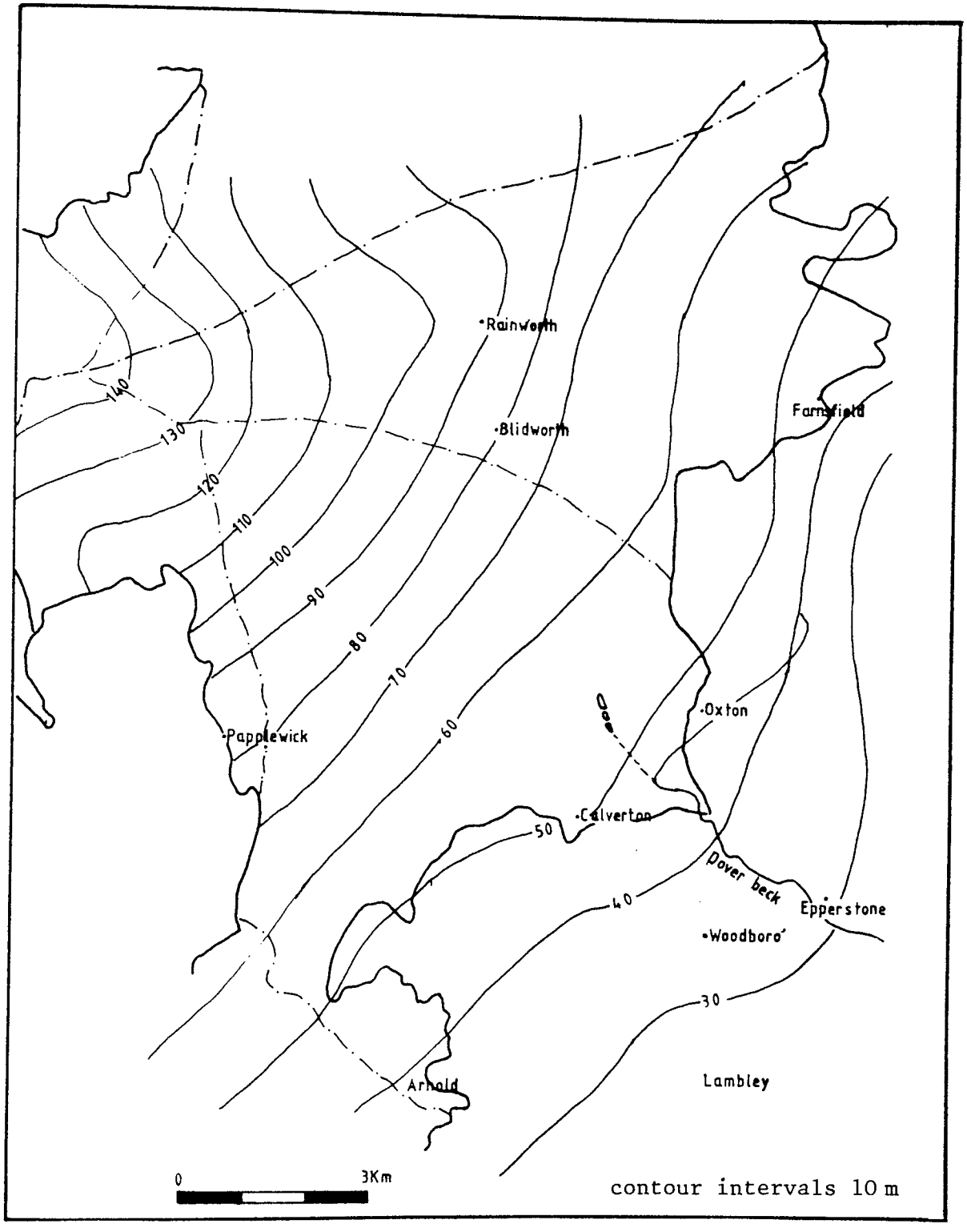

Figure 2.11 Triassic Groundwater table at Dover Beck Valley (1975)

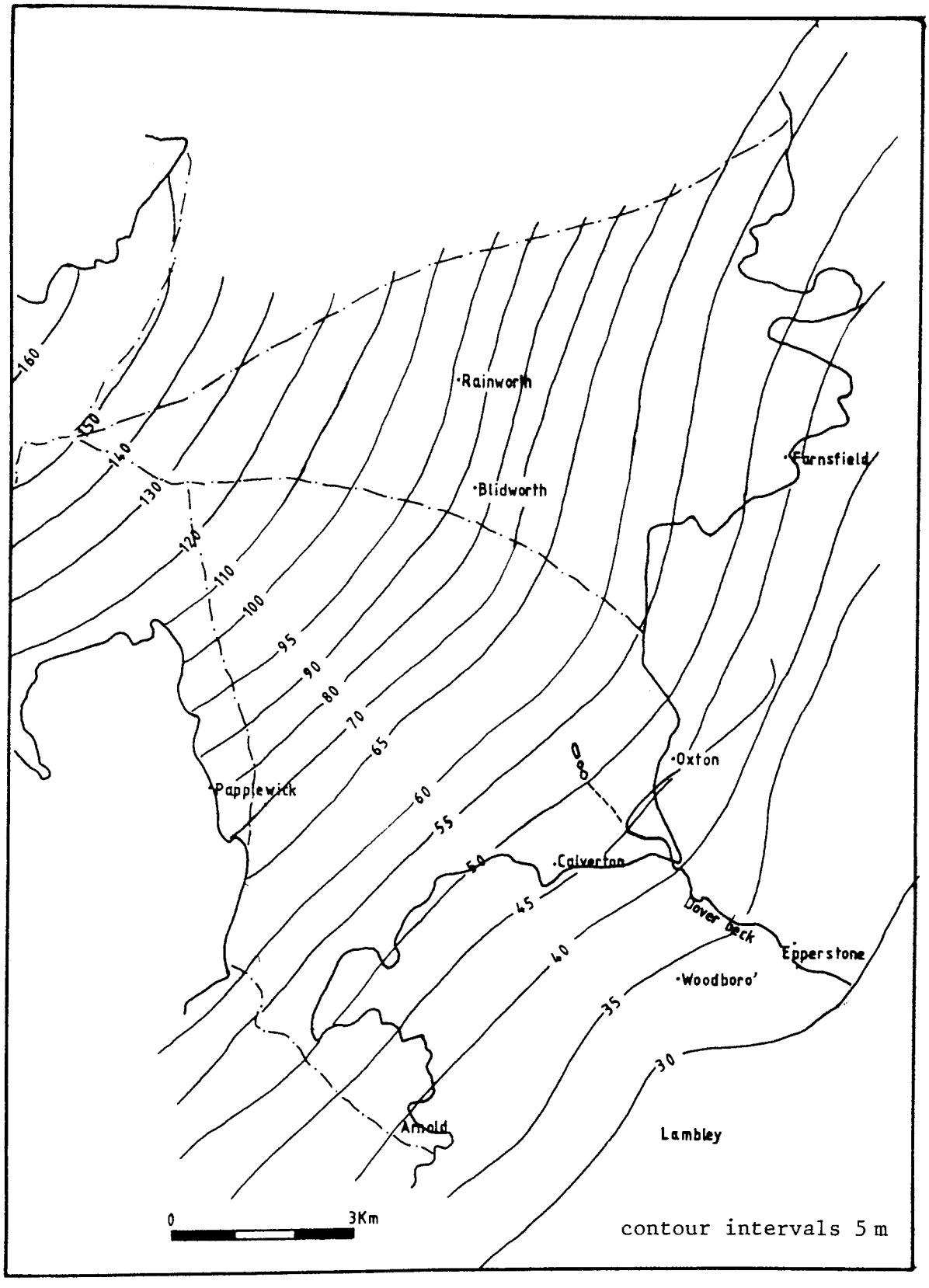

Figure 2.12 Triassic Groundwater table at Dover Beck Valley (1976)

impermeable mudstone. The recovery in this confined borehole is due to the fact that the Triassic outcrop lies only fifty metres to the west, in the Dover Beck stream channel, where any recharge through the unconfined part during high rainfall periods is obviously reflected in this borehole.

The two formations comprising the Sherwood Sandstone Group, and considered to form a single aquifer which is generally classified to confined and unconfined. However, the unconfined aquifer is actually not truly unconfined due to the presence of mudstone horizons which separate the permeable beds and give rise to partial confining horizons (Nottinghamshire Triassic Conjunctive Use Investigation, Report No. 6).

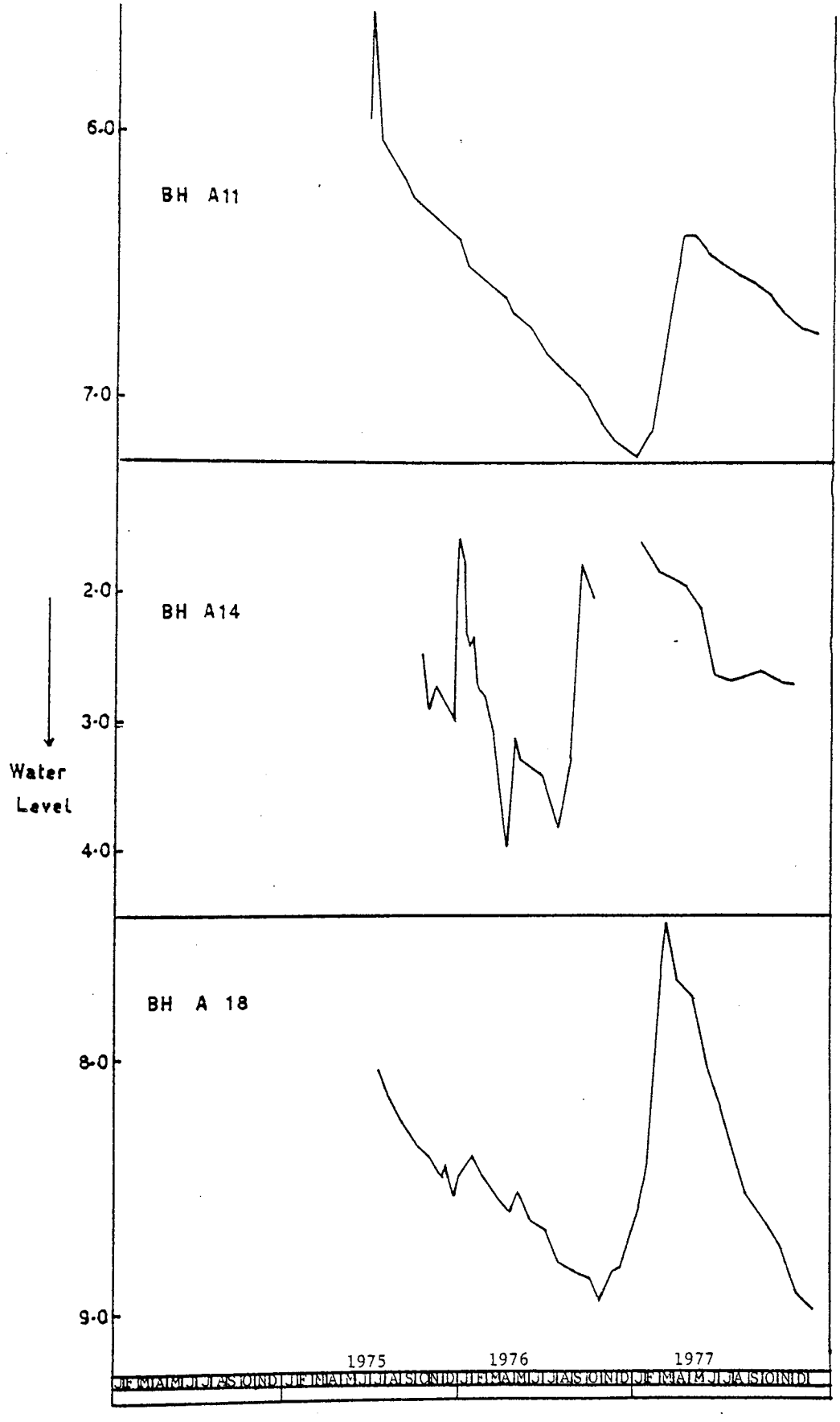

Figure 2.13 Seasonal fluctuation in water level of BH A11, A14 and A18 during 1975, 1976, 1977 (after Nottingham Triassic Conjunctive Use Investigation, Report No. 6)

CHAPTER THREE

PETROGRAPHY, DIAGENESIS AND SECONDARY POROSITY DEVELOPMENT

3.1 INTRODUCTION

This chapter deals mainly with the diagenesis of the sandstone from the Sherwood Sandstone Group of north Nottinghamshire and includes studies of their mineralogy, petrography and texture. The relation between diagenesis and different hydrological aspects such as porosity and the different types of pore spaces present has also been investigated. Generally, the sandstones studied may be classified according to Folk et al. (1970) as sublitharenite and subfeldsarenite.

3.2 METHODS AND TECHNIQUES

The core samples were subjected to the following techniques:

1. Impregnated thin sections preparation
2. Scanning electron microscope (SEM)
3. X-ray diffraction
4. Resin pore cast preparation
5. Textural analysis

Impregnated thin sections preparation

Thin slices of the core samples were impregnated with green dyed araldite resin, to provide contrast between the void spaces and the framework components, ready for thin section preparation. The resin used was araldite CY 212 and HY 951 hardner together with green dye. Two thin sections were prepared for each sample, one parallel to the

core axis and the other perpendicular to it. These thin sections (160 in all) were subjected to the study of the detrital and authigenic mineralogy, the different diagenetic features such as dissolution, clay replacement, compaction and the different textural relationships between the authigenic minerals to help in building up the picture of the diagenetic events. Some of these thin sections were stained using the combined stain (alizarin red-S and potassium ferricyanide) of Dickson (1965) in order to differentiate the carbonate phases present (calcite, ferroan calcite, dolomite and ferroan dolomite).

Scanning electron microscope

The scanning electron microscope (Cambridge Stereoscan 150) was used especially to study the authigenic minerals, dissolution features, time and texture relationships between the authigenic phases as well as the pore geometry. Twelve selected sandstone samples were prepared for SEM study. Samples with fresh surfaces were fixed onto stubs and coated with carbon. Alternatively gold coating was sometimes used for better resolution especially in the case of the pore cast study. The associated energy dispersive analysis of x-rays (Kevex-Ray System 5000) was used for mineral identification by means of semi-quantitative chemical analysis.

X-ray diffraction

Thirty three oriented clay samples (2 μm - by decantation) were prepared by the dispersion of gently disaggregated sandstone samples followed by sedimentation onto glass slides or suction onto ceramic discs. The oriented samples were dried at room temperature and analysed by X-ray diffraction (XRD) using Co Kα or Cu Kα radiation.

The samples were then glycolated using ethylene glycol for about 12-14 hours by a vaporization method (Kunze, 1955) for the glass slides. The ceramic discs were glycolated by standing them in a shallow pool of ethylene glycol for 2-4 hours at 80° C. The samples were then re-run under the same diffractometer conditions in order to identify the presence of expandable clay minerals.

In order to differentiate kaolinite from chlorite the samples were subsequently heated up to 550° C for two hours (Carrol, 1970). At this temperature kaolinite decomposes to amorphous meta-kaolin.

Resin pore cast preparation

The study of pore shape and geometry was done on a few selected samples by means of producing epoxy resin pore casts (Pittman and Duschatko, 1970). Rock chips of about 0.5 cm thickness were impregnated under vacuum using araldite CY 212 and hardner HY 951 (as in thin section preparation) and then treated in dilute HCl for about one hour to dissolve any carbonates present, followed by treatment with HF to dissolve the silicates. The remaining resin pore casts were then rinsed and oven dried. Small pieces were fixed onto stubs and coated with gold ready for SEM study.

Textural analysis

Grain size analysis of selected samples representing the Sherwood Sandstone Group from borehole A14 was carried out with $\frac{1}{2}\phi$ interval where first of all the weighed samples were disaggregated, treated with diluted HCl with gentle heating to dissolve the carbonates, and then sieved. The detrital constituents were re-weighed after

dissolving the carbonate (after HCl treatment) to calculate the weight of the carbonate present.

Shape of contact and number of contacts per grain together with the different type of packing were also measured on selected sandstone samples representing borehole A14, using photomicrographs (the same used for estimating porosity in Chapter Four).

3.3 GRAIN SIZE AND PACKING CHARACTERISTICS

3.3.1 Grain Size Analyses

From the mechanical analysis of the eleven sandstone samples representing borehole A14, cumulative curves with probability ordinate were plotted, from which the statistical parameters of Folk and Ward (1957) were calculated. These parameters: mean size (M_Z), inclusive graphic standard deviation (σ_I), inclusive graphic skewness (SK_I) and transformed graphic kurtosis (K_G') are presented in Table 3.1. Also the percentage of the sand and gravel (if present) fraction, clay fraction and carbonate were calculated (Table 3.1) as the following: the carbonate weights were calculated from weighing the sandstone samples before and after the HCl treatment, and the sand and gravel fraction calculated from the addition of the weight of both resulted from the sieving analysis, while the matrix or clays calculated from the weight of silt and mud fractions resulted from sieving analysis. The weight of the three fractions were recalculated into percentages.

Grain size values ranged between 1.65 ϕ to 3.23 ϕ (medium to very fine sand size). The sorting measured by the inclusive graphic standard deviation have values ranging from 0.68 ϕ to 1.1 ϕ (moderately well sorted to poorly sorted), while the moderately sorted one is the

Table 3.1 Sand, clay, carbonate fractions and grain size parameters for borehole A14

Sample No	Sand and coarser fraction(%)	Clay matrix (%)	Carbonate (%)	Mean Size Mz(ø)	σI (ø)	SK_I	K_G
43	79.74	5.08	14.34	1.72	0.99	+0.33	0.75
40	88.28	5.52	5.39	2.00	0.98	+0.26	0.68
39	86.39	6.58	6.36	2.26	1.1	+0.35	0.70
37	87.92	5.56	7.05	1.65	0.67	+0.32	0.69
35	81.58	4.88	13.19	1.95	0.68	+0.45	0.69
31	88.38	6.10	5.01	2.06	0.90	+0.56	0.74
27	85.66	7.69	6.11	2.29	1.05	+0.51	0.67
26	83.92	2.31	13.31	1.59	0.68	+0.29	0.63
25	91.57	2.75	5.23	1.99	0.70	+0.31	0.56
23	84.25	10.09	5.25	3.23	0.76	+0.32	0.71
16	76.82	10.73	12.46	3.01	0.94	+0.30	0.65

most common. The results of the examined samples show that they have skewness values ranging between +0.26 to +0.56 (fine skewed to strongly fine skewed). While the values of kurtosis fall in the field of the very leptokurtic class. According to Folk (1974) these rocks can be classified as texturally immature to submature.

No significant relationship was detected between the carbonate cement content and the sample depth as they have very low negative correlation ($r = -0.05$). On the other hand a positive relationship was found between matrix percentage and depth, the deeper the sample, the higher the fine fraction, with correlation coefficient $r = 0.53$ which is significant at the 90% confidence level (Figure 3.1). No relationship could be detected between the matrix and cement present.

The statistical characters of the grain size parameters ($Mz\phi$, σ_I, SK_I and KG) indicate that no significant correlation was found between these parameters and the depth except the mean size ($Mz\phi$) where a positive correlation was detected ($r = 0.748$, significant at 99% confidence level (Figure 3.2). This relationship is a function of the coarsening upward cycle within the Sherwood Sandstone Group. The Lenten Sandstone Formation is relatively finer in grain size than the Nottingham Castle Formation as indicated from the lithological logs (Chapter Two).

But one cannot rely on these analyses to give a fairly true picture of the exact grain size distribution of the original sediments deposited or predicting the ancient environment of deposition. This may be as a result of the post depositional changes which happened either by enlargement of the original constituents due to the authigenic mineral overgrowth or decreasing the actual size, either by the incomplete dissolution of the framework silicate or clay replacement

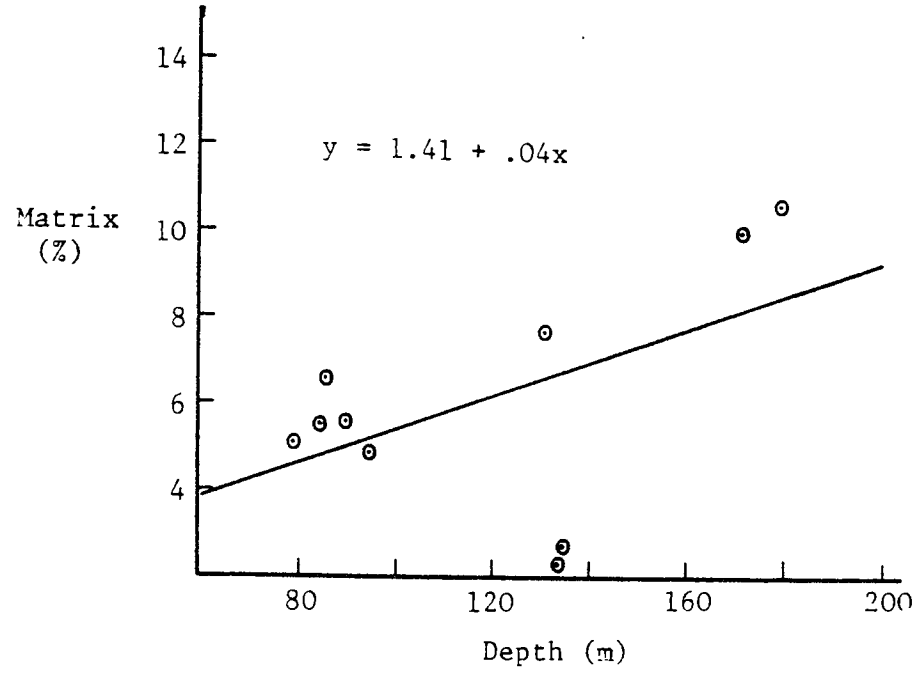

Fig 3.1 Relationship between sample depth and matrix content

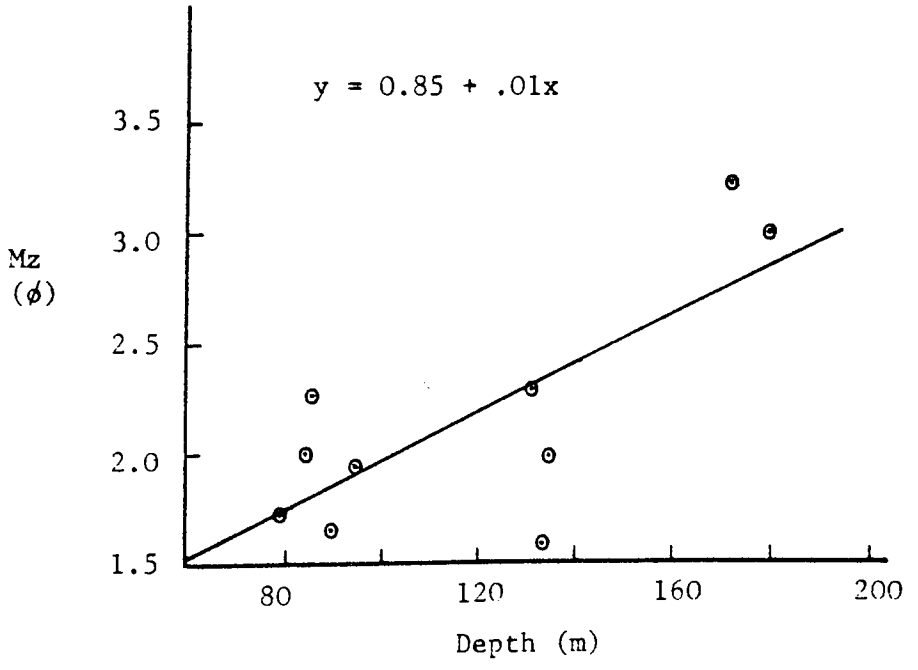

Fig 3.2 Relationship between sample depth and mean grain size (Mzϕ)

processing clay fraction decreasing the texture maturity of the original sediments. So these results have been mainly used for comparison with other parameters and are going to be dealt with in Chapter Four.

3.3.2 Analysis of Grain Contacts

The shape of contact (grain to grain contact) and the number of contacts per grain is considered to be one of the factors affecting the degree of consolidation and porosity of sandstones. Taylor (1950) points out that increasing degree of consolidation is shown in the form of grain contact; floating contacts are the simplest and are common in newly deposited sands, whereas sutured contacts are indicative of grains which have undergone stress and deep burial. Tangential, long and concave-convex contacts represent intermediate stages. Rittenhouse (1973, in Kharaka and Berry, 1976) found that the porosity of Gulf Coast Tertiary Sandstones decreased by an average of 1% for each 1000 ft of burial, though the porosity at any given depth varied widely and the porosity decrease was not uniform. The measurements of all types of contact present (floating, tangent or point, long, concave-convex and sutured) together with the number of contacts per grain were determined for seven samples representing borehole A14. The same samples were used in estimating porosity (ϕ photo) from photomicrographs. Approximately 400-500 grains were used in the calculation for each sample and the results recalculated into percentages (Table 3.2).

From Table 3.2 it can be shown that grains with only one contact are the most common with an average of 34.08%. Grains with two contacts are slightly less abundant followed by grains with no to three contacts with average values of 30.06, 17.66 and 14.51% respectively.

Table 3.2 Grain contact and packing measurements

Variables / Sample No (Depth m)	Number of contacts per grain (%)							Types of contact (%)					Packing (%)		Consolidation factor
	0	1	2	3	4	5	6&>6	Floating	Tangent	Long	Concavo-convex	Sutured	Pd(%)	Pp(%)	Cf(%)
44 (75.7)	17.10	31.83	30.88	15.68	4.04	0.24	0.24	9.66	31.68	43.89	8.99	5.77	63.36	36.05	53.9
43 (78.8)	27.70	34.56	26.47	9.80	1.23	0.24	0.0	18.77	31.39	32.69	7.93	9.22	53.58	14.29	51.49
36 (92.2)	13.08	35.26	32.82	15.08	3.10	0.44	0.22	7.51	31.17	46.18	8.65	6.49	53.75	29.53	55.09
33 (98.4)	15.55	38.46	30.35	13.51	2.70	0.42	0.0	8.74	43.07	25.97	13.48	8.74	63.01	29.25	54.08
27(130.8)	15.32	32.22	31.82	15.52	3.73	0.98	0.39	8.52	41.05	37.66	7.53	5.24	66.09	33.99	50.98
26(133.2)	25.60	40.82	22.95	9.90	0.73	0.0	0.0	17.27	34.05	34.70	10.69	3.29	71.82	22.32	49.74
23(171.8)	9.27	25.44	35.11	21.89	6.51	1.38	0.39	4.51	41.23	43.43	7.57	3.26	54.93	23.53	52.77
Arithmetic mean	17.66	34.08	30.06	14.51	3.51	0.53	0.18	10.71	36.23	37.79	9.22	6.00	60.93	26.99	52.58

Grains with four, five or more grain contents are rare. There is no direct relation between the number of contacts and depth as seen from Table 3.2

The consolidation factor (C_f), which is a weighting system based on the percentage of individual contacts has been calculated as an easy numerical way of giving an idea about the frequency of the different types of contacts. The values of 5, 4, 3, 2 and 1 are multiplied by the percentage of sutured (S), concave-convex (C), long (L), tangential (T) and floating (F) contacts respectively. The consolidation factor is given by the following equation:

$$C_f = \left(\frac{S \times 5 + C \times 4 + L \times 3 + T \times 2 + F}{500}\right) \times 100$$

where S, C, L, T and F are the percentage of the different type of contact mentioned above.

The values of C_f which are given in Table 3.2 show a rather limited variation from 49.74% to 55.09% with an arithmatic mean value of 52.58 and 3.69 variance. There is no definite relationship between C_f% and the sample depth. This could be due either to the limited number of samples that have been studied or the small range of depth covered by this study.

The low values of C_f in these sandstones indicates that sutured and concave-convex contacts are not abundant, while long and tangential contacts are the most abundant types with an average of 37.79 and 36.23% (Table 3.2). This reflects the fact that these sandstones have not been affected by great stress or deep burial.

3.3.3 Packing

Packing in sand-size sediments is the mutual spatial relationship between the grains as defined by Kahn (1958). He concluded that the concept of packing could be divided into two aspects, the unit properties and the aggregate properties. The first includes grain-to-grain contacts and is called packing proximity (Pp) and the latter deals with the closeness or spread of particles and is termed packing density (Pd). The Pp is expressed as the percentage of grain-to-grain contacts in a traverse of n contacts.

$$Pp = \frac{q}{n} \times 100 \quad (0 \leqslant q \leqslant n)$$

where q = number of grain-to-grain contacts

n = total number of contacts

while Pd is expressed mathematically as

$$Pd = \frac{m \sum_{i=1}^{i=n} g_i}{t} \times 100 \quad (0 \leqslant g_i \leqslant t/m)$$

where n is the total number of grain in a given traverse, m is the magnification, t is the length of the traverse and g_i is the grain intercept size.

The individual values of packing density and proximity are set out in Table 3.2 where both show rather a small range of variation between 14.29 and 36.05% for Pp and 53.58 and 71.82% for Pd. The arithmatic mean values and variance respectively equal 26.99 and 56.29 for Pp and 60.93 and 49.50 for Pd.

No significant relation could be detected between the sample depth and Pp or Pd. Only negative relationships were found between grain contacts (C_f%) and Pd% with r = -0.54 which is significant at only

80% confidence level using t-test (Figure 3.3). On the other hand positive correlation between C_f and Pp is also defined (r = +0.428) but is not very significant, (< 70% confidence level).

From the mechanical and textural analyses of these selective samples, it can be concluded that these texturally submature sandstones have undergone some compaction indicated by the presence of bent mineral grains (especially mica) and welded fractures, but have not suffered deep burial (Taylor, 1950). This is consistent with the results of clay mineral analysis (Section 3.5.2).

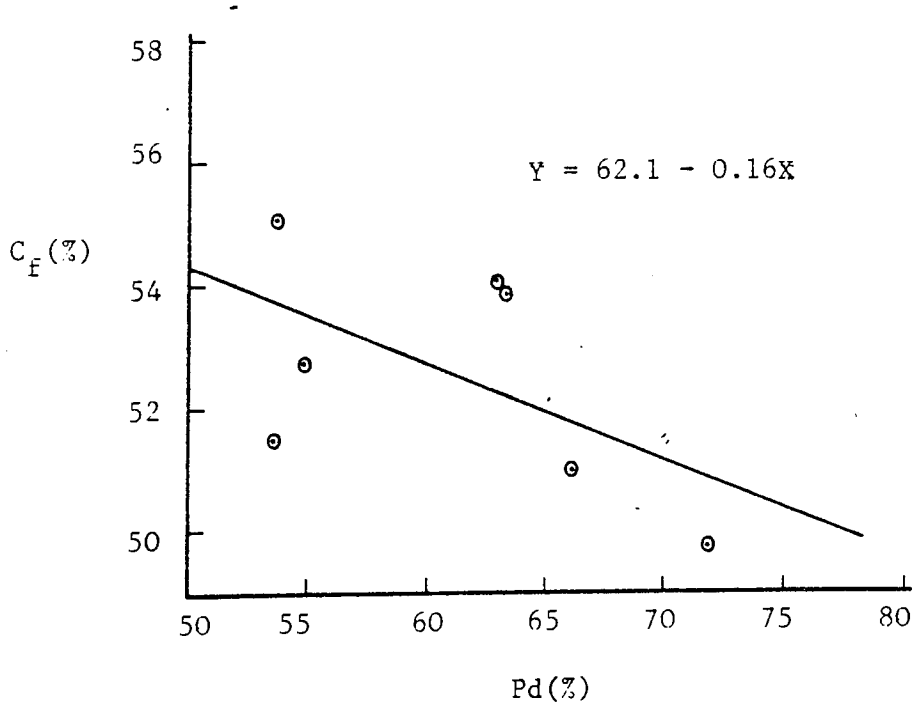

Fig 3.3 Relationship between packing density (Pd) and consolidation factor (C_f)

3.4 SANDSTONE MINERALOGY AND PETROGRAPHY

The Sherwood Sandstone Group comprises different rock types (as discussed in Chapter Two), including sandstones, pebbly sandstones,

thin conglomerates and intraformational conglomerate as well as mudstones and siltstones. Sandstones are by far the most abundant and the following is a description of the detrital framework components present in sandstones of the Lenton Sandstone and Nottingham Castle Formations.

The sandstones of the Nottingham Castle Formation are generally coarse to medium grain size, with less than 10% pebbles occasionally present and may be classified as grain size sandstones and slightly pebbly sandstone (Folk, 1954). The grain size of the sandstone tends to decrease toward the Lenton Sandstone Formation where it becomes medium to very fine grained sandstone, with mudstone intercalation which form the transitional beds between the two formations.

The sandstone under consideration is composed mainly of quartz which forms more than 75% of the whole detrital constituents. Both rock fragments and feldspars come in the second rank after quartz. According to Folk et al. (1970) these sandstones could be classified as sublitharenite to subfeldsarenite. The following is a brief description of the main detrital components.

3.4.1 Quartz

Quartz is the most predominant mineral as it is the most stable mineral under sedimentary environments. It forms more than 75% of the detrital constituents, and reaches up to about 95% especially in the fine grained sandstone varieties. The grains have subangular to subrounded outline with equant to subequant shape, and sometimes show elongation along long axis parallel to the bedding plane.

The detrital quartz present can be classified as non-undulatory monocrystalline, undulatory monocrystalline and polycrystalline according to Blatt and Christie (1963). In the fine and very fine sandstone varieties, the monocrystalline non-undulatory type forms most of the detritals. As the strained quartz (undulose and polycrystalline) is less stable than the unstrained type, and tends to disaggregate into its smaller components. The medium and coarse grained sandstones contain a high percentage of the monocrystalline quartz of both types. However, considerable amounts of polycrystalline quartz have been detected which may help to some extent, together with the different kinds of inclusion or other diagnostic features, in identifying the source rocks.

Monocrystalline quartz grains which have straight extension, no inclusions and water clear colour are very common in these sandstones under consideration (Plate 3.1A). According to Folk (1974) this quartz may be of volcanic origin. Monocrystalline quartz with slightly to strongly undulose extension are not uncommon (Plate 3.1B). But it is not possible to assign its origin (Folk, 1974), unless they have got some other diagnostic features inherited from its common source rocks.

Another type of monocrystalline quartz which is not abundant in the rocks under study is the one including abundant vacuoles (Plate 3.1C). This abundance of vacuoles gives rise to the milky appearance characterising the hydrothermal origin (Folk, 1974). Also the presence of vermicular chlorite inclusions in some quartz grains (Plate 3.1D) is a diagnostic feature of this hydrothermal provenance (Blatt et al., 1980; Folk, 1974).

Some of the quartz shown to be in intergrowth with K-feldspar forming myrmekitic and graphic texture (Plate 3.1A,E), which suggest an igneous (granitic) origin. Also some of these monocrystalline quartz grains show deformational lamellae, which may indicate metamorphic source (Young, 1976). Very rarely detected, reworked sedimentary quartz which may be characterized by rounded overgrowth. This kind of quartz is limited either because of the lack of the clayey film separating the original grain from its overgrowth, which makes it difficult to be distinguished under the ordinary microscope, or it is uncommon source rock.

Polycrystalline quartz is a grain which forms of two or more than two crystal units of different optical orientation. This type of quartz is more common in the medium and coarse sandstone and the pebbly varieties. Different polycrystalline quartz types were recorded in the rocks under consideration (Plate 3.1F and Plate 3.2A-D) including grains with two to more than ten crystals, with different crystal-crystal boundaries; straight, sutured and polygonal.

The granitic polycrystalline quartz which have between 2 and 5 crystals, where the crystals' shapes are subsequent to moderately elongated and no clear cyrstallographic orientation is noticed (Blatt et al., 1980), are also met with but are not common (Plate 3.1F). Sometimes the zones of different undulatory extinction are separated by well-defined dust lines (Plate 3.2A,B). This type of quartz may indicate a plutonic source but as it also could be derived from other sources, Folk (1974) gives the name "common" quartz to this type.

The polycrystalline quartz grain with more than 5 crystals, where the crystals are more elongated and show parallel crystallographic

orientation is considered to be of gneissic origin according to Blatt et al. (1980). This type of quartz is quite common more than the granitic ones, showing different crystal-crystal boundaries including sutured and polygonal (Plate 3.2C-F). Also gneissic polycrystalline quartz grains having a bimodal size distribution have also been recorded (Plate 3.2C). The schistose polycrystalline quartz having elongated, crystallographically oriented cyrstals with straight crystal boundaries, which include inclusions of oriented mica, are not uncommon have also been identified (Plate 3.2E,F).

3.4.2 Rock Fragments

These are one of the most important detrital components in the sediments as they give definitive information about the nature of the source rocks. In these rocks under consideration the rock fragments as well as feldspars come in the second rank after quartz, with ratio sometimes equal to each other or in most cases the rock fragments are more abundant. Both rock fragments and feldspar together form less than 25% of the detritals. The volcanic rock fragments are the most predominant type represented in the Sherwood Sandstone Group. Although the correct identification of most of these fine crystalline extrusive rocks is difficult, the following different types were recorded: Crypto- and microcrystalline volcanic (Plate 3.3A), others with porphyritic texture where phenocrysts of quartz and feldspar embedded in a microcrystalline felsitic matrix (Plate 3.3B). Trachyte, in which small feldspar laths are oriented parallel to each other and embedded in a fine crystalline matrix (Plate 3.3A). Fine cyrstalline rock fragments with fluidal texture, as well as rock fragments of pyroclastics were also recorded (Plate

3.2C). Most of the volcanic rock fragments are stained red.

The igneous plutonic rock fragments are very restricted in these rocks, and represented here by graphic andmyrmekitic granite (Plate 3.1A,E). The scarcity of these plutonic rock fragments is expected to be in these sand-size sediments (Blatt et al., 1980).

Sedimentary rock fragments represented by sandstone, hematitic mudstone, chert and dolomite. Different kinds of sandstone fragments were recorded including quartz-sandstone and hematitic sandstone (Plate 3.3 D,E) which represent reworked Triassic rocks. The hematitic mudstone is one of the most predominant rock types represented both under the microscope and in the hand specimen as mud balls, slabs and sometimes as discontinuous lamenae intercalated with the sandstone. These mudstone fragments are very commonly represented in the transitional bed between Nottingham Castle Formation and Lenton Sandstone Formation. Chert fragments which are represented by chalcedony (Plate 3.3F and 3.4A) characterized by its alternative dark and light fibrous texture. Also dolomite rock fragments were also detected especially in borehole A18.

Metamorphic rock fragments are quite common, where it is represented here by mica schist (Plate 3.2E,F). The other coarser grained metamorphic types (gneiss) are too coarse to be represented as a whole in these sand-sized sediments where they are represented mostly by their different types of polycrystalline quartz described before.

3.4.3 Feldspars

Feldspars are present in not more than 10% or less of the detritals, and are not as common as quartz and rock fragments. Feldspar present

is mainly potash type, together with a very restricted amount of plagioclase. The K-feldspar present in these sandstones under consideration is represented by orthoclase, microperthite and microcline in decreasing order of their abundance, together with antiperthite occasionally present.

The feldspars undergo different degrees of alteration as well as dissolution. The majority of the grains shown to have a brownish appearance (Plate 3.4B,C) due to bubble formation or vacuolization (Folk, 1974). Even for the microcline which is the most stable K-feldspar and commonly found fresh (Plate 3.4D), shown to be altered into mica and affected by dissolution as well (Plate 3.4E,F). Kaolinitization (Plate 3.5A), is sometimes met with as well as sericitization as it will be dealt with in the clay replacement section.

Most of the grains are covered by an authigenic overgrowth (Plate 3.5B), which is always shown to be dissoluted giving rise to the hacksaw termination. While the boundary of the internal detrital cores are mostly rounded (Plate 3.4D), which could be as a result of dissolution (Thein, 1966).

The dissolution of feldspar is a very common feature affecting both detrital and authigenic phase, as noticed from both thin section and SEM studies. Where the evidence of the extensive dissolution indicated from the presence of hollow grains with the relicts of the authigenic rim. The evidence of extensive feldspar dissolution could be one of the reasons of its restricted abundance. Also feldspars show partial and sometimes complete replacement by the diagenetic replacive minerals; dolomite, ferroan calcite and calcite (Plate 3.5C-E).

3.4.4 Micas and Other Detrital Constituents

The sheet silicates are represented here by biotite and muscovite both being more common in the finer grained sandstone. Biotite is quite common where it is sometimes shown to be bent due to compaction and most commonly oxidized where the iron oxide leached from the biotite and concentrated along the cleavage and more frequently it is completely replaced by hematite (Plate 3.6A,B). The abundance of biotite could have either metamorphic or volcanic origin, while the muscovite recommends the pegmatite origin.

Other constituents such as phlogopite and tourmaline of yellow, brown and occasionally blue ones, rutile, zircon, epidote, as well as considerable amounts of opaque iron oxide present and sometimes concentrated in certain lamina (Plate 3.5F).

3.5 DIAGENESIS

Diagenesis includes the process involving chemical, physical and physicochemical changes which take place after deposition and before metamorphism and which result in secondary porosity. This secondary sandstone porosity includes: fracturing of macro and micro type, shrinkage, and dissolution of detrital components and authigenic minerals or cement. The formation, preservation, alteration and destruction of these secondary sandstone porosity is dependent upon the specific diagenetic environment and burial depth. Accordingly diagenetic systems have been classified into three main stages (or regimes): Eodiagenesis, Mesodiagenesis and Telodiagenesis (Schmidt and McDonald, 1979a). Eodiagenesis includes all the changes which take place before any effective burial in the environment of deposition

and where the interstitial water chemistry is governed by the surface environment. Mesodiagenesis includes the changes which arise at any depth of burial above the metamorphic zone. Telodiagenetic changes occur during the exposure of the rocks after burial.

The Sherwood Sandstones dealt with in this work have undergone different diagenetic changes and reached the mature stage of the mesodiagenetic regime. These changes which result in alteration of pore systems by destroying primary porosity and developing different types of secondary porosity include:

(1) the reddening of the sediments

(2) dissolution features (main process in creating secondary porosity)

(3) clay-replacement of the unstable detritals especially feldspar

(4) development of an authigenic mineral suite which includes in paragenetic sequence: quartz, K-feldspar, kaolinite, dolomite, ferroan calcite, calcite and kaolinite. Authigenic illite, montmorillonite and mixed layer illite-smecite also occur but have no definite position in the sequence. They can, however, be shown to be post-dating quartz and feldspar and pre-dating calcite.

3.5.1 Reddening: Source, Origin and Duration

Red iron oxide (haematite) is one of the most important features of red beds because it imparts the characteristic colour of these rocks. However, only very small quantities of iron (0.1% Fe_2O_3) are sufficient to produce a bright red colour (Walker *et al.*, 1967). In

the rocks under consideration, pigmentary haematite is present in a variety of forms including coating of detrital grains often filling pits on the grain surface, as a pore-lining on detrital and authigenic grain surfaces and as interstitial matrix where it is closely associated with clay minerals (Plate 3.6 C-F and 3.7A).

The iron oxide pigments are more abundant in the fine grained sandstones toward the Lenton Sandstone Formation where mudstone and siltstone layers serve as impermeable barriers. Also there is an abundance of mica here which acts as an important source of post-depositional iron oxide. The impermeable mudstone beds distributed within the Sherwood Sandstone Group are darker in colour than the associated sandstone and contain more iron oxide than associated sandstones. However, the origin of colouration in these fine grained sediments may be quite different than the sandstones (Turner, 1980) and is not dealt with here.

In the medium to coarse grained sandstones which form the main part of the Triassic water aquifer, this haematitic iron oxide coating is not very abundant (Plate 3.6E) and often disappears completely especially in very porous and permeable rocks. It occurs as a film surrounding detrital grains and sometimes their authigenic overgrowths (Plate 3.1F) which indicates the persistence of reddening over a long period of time. Sometimes grain coatings are absent at the grain contact (Plate 3.6F) which indicates their post-depositional origin. The haematitic grain coatings are sometimes present as interstitial pore filling (Plate 3.7A) which have a great effect on the permeability of the rock. Haematite and other oxides also usually stain the interstitial matrix (Plate 3.6C), whatever its origin. In some cases, the iron oxide fills pits on the surface of the detrital grain (Plate

3.6E). Iron oxide of this type could be detrital (Folk, 1976; Turner, 1980).

The thin section study reveals that the iron oxide stain is nearly always red in colour (haematite) but sometimes is yellowish brown colour (goethite) especially towards the top end of Nottingham Castle Formation. However, the X-ray diffraction of the fine clay fraction separated from some of the studied sandstones, shows no evidence of haematite peaks despite their red colour. This indicates that the amount of haematite present is below the XRD detection limits.

The source of iron in these red pigments is commonly assumed to be iron-bearing silicates, especially amphibole, pyroxene, biotite, chlorite and epidote (Walker, 1967). The diagenetic alteration of these unstable detritals by hydrolysis releases iron, which converts to haematite on ageing (Walker, 1976). In the sandstones under consideration, the absence of amphibole and pyroxene may be the result of intensive hydrolysis or dissolution but they are unlikely to have ever been abundant in view of the fact that sedimentary and low grade metamorphic rocks dominated Triassic source areas. Phyllosilicates were, however, more abundant and evidence that biotite was a crucial source of haematite (Turner and Archer, 1977) is very common in these rocks. In the present study the biotite persists in various stages of alteration; from fresh ones, to those partially leached with the haematite concentrated along cleavage planes (Plate 3.6B and 3.7B), and also those completely replaced by haematite (Plate 3.6A and 3.7C). Sometimes completely altered biotites with the distribution of haematite all over the grain evenly, including the compacted parts (Plate 3.6B). This could be an indication of the early stage of oxidation before the mechanical compaction.

Another source of haematite could be the replacement of the iron-bearing minerals by dolomite (Hubert and Reed, 1978) where the early diagenetic dolomite replaces pre-existing iron-bearing minerals with the release of iron into the pore-water. Under oxidizing, alkaline conditions the iron precipitates as haematite or precursor oxides which converts to haematite in time. This phenomenon was noticed from the association of the haematitic iron oxide stains with the early diagenetic dolomite (Plate 3.7D). Calcite and ferroan calcite precipitated later in the diagenetic sequence seem to be free from this haematitic staining.

Regarding the timing of the iron oxide formation, both microscopic and SEM studies reveal its duration over a long period of time. The thin sections study indicates the staining of the clay film surrounding the detritals as well as most of the interstitial matrix. Both replacement and authigenic clays are stained except for authigenic kaolinite which remains unstained. Also the iron oxide film coats both the detrital and its authigenic phase. The SEM study reveals that sometimes the detrital grain is coated with mixed size of clay platelets arranged parallel to the grain surfaces (Plate 3.7E,F), which is analogous the mechanically infiltrated clay described by Walker (1976) and Walker *et al*. (1978). However, the origin of this coating is not the matter of discussion in this work. The EDAX analysis indicates an elemental composition of Si, K, Al, Fe with very small peak of Mg, this might be an indication of the staining of the clay film. Also the EDAX analyses of the authigenic clays (apart from kaolinite) indicates the presence of Fe peaks associated with haematitic staining.

All the above criteria suggest that the duration of the formation of the iron oxide seems to happen over a long period of time, which extends from the time of deposition, through the early stage of diagenesis and continuing after the formation of the early diagenetic mineral suite.

3.5.2 Dissolution

The detrital silicate grains underwent different degrees of alteration due to their reaction with the interstitial pore water with which they were not in equilibrium. This alteration process includes the dissolution and the *in situ* replacement by clay. The degree of alteration depends on the fundamental principles of mineral stability (Keller, 1969) in which minerals are stable only in their formation environment. The lowest members of Bowen's reaction series (olivine, pyroxene, amphibole and ca-plagioclase) tend to be the most unstable phase in the new sedimentary (or depositional) environment.

Dissolution which is a crucial diagenetic feature in these sandstones includes not only the detrital grains but also some of the authigenic minerals and carbonate cement as well. Dissolution is important for the following reasons: 1) As the dissolution takes place by hydrolysis (Walker, 1976; Walker *et al.*, 1978 and Turner, 1980), it supplies a vital source of different ions to the pore water including; K, Na, Al, Si, Ca, Mg and Fe. Most of these ions are precipitated later as authigenic minerals. 2) It provides a fundamental source of secondary porosity in the form of dissolution voids. 3) Dissolution increases the mineralogical maturity of the sediments as a consequence of increasing the quartz/feldspar ratio due to the abundance of feldspar dissolution. 4) Incomplete dissolution

and the clay replacement of the silicate mineral grains increase the clay-size fraction and so decrease the textural maturity (Folk, 1951).

The study of the Sherwood Sandstone Group shows that feldspar is the most common silicate mineral to suffer dissolution but both calcite and dolomite cement are extensively affected. The presence of relicts of feldspar, carbonate and biotite indicates their former existence and dissolution voids are picked out in thin section by dyed araldite resin. The complete absence of pyroxene and amphibole may indicate their extensive dissolution but it is unlikely that they were ever abundant in these sediments.

The feldspars suffer various degrees of intrastratal dissolution. As plagioclase is more chemically unstable than potassium feldspar, it is extensively dissolved and this may be reflected by its restricted abundance. However, K-feldspar has also been affected by this dissolution (Waugh, 1978). SEM, thin section and pore cast studies have been used to identify the different dissolution effects. Dissolution textures can be seen etching the periphery of authigenic rim cement (Plate 3.8A,B) and sometimes continue inward to the detrital core along the cleavage plane as indicated by the SEM study (Plate 3.8C,D) and resin pore cast (Plate 3.8E,F). Dissolution may affect the outer portions of feldspar grains (Plate 3.9A) thus affecting the textural maturity of the rock by decreasing the size of the dissolved grain. Extensive and continuous dissolution voids are also detected, starting from the authigenic overgrowth toward the detrital core with only remnants to indicate the former presence of minerals (Plate 3.9B). Commonly, the dissolution hollowed out the detrital feldspar core leaving only relicts of unaffected

authigenic rim (Plate 3.9C). Also dissolution can be seen to have followed previously formed microfracture (Plate 3.9D). This could be an indication of the extent of the dissolution process after mechanical compaction.

The dissolution effect on carbonate is very considerable in producing large amounts of the secondary dissolution pores. The dissolution affects the carbonate present as cementing material which is represented here mainly by calcite and ferroan calcite (Plate 3.9E,F), as well as the replacive dolomite (Plate 3.10A).

Detrital rock fragments are also affected by dissolution. Selective dissolution of unstable crystals in these sometimes produces relicts of finer grain size that were not present in the original rock (Plate 3.10B).

Dissolution is sometimes so extensive that no remnants of the original material were left as a clue to indicate its previous presence. This type of secondary pore can sometimes be detected by their larger size than the surrounding detrital grains (Plate 3.10C). These oversized pores (Schmidt and McDonald, 1979b) are quite common in these sandstones, and the original pore filling was more likely to have been carbonate (Pittman, 1979) than any detrital component. Completely dissolved grains and areas of cement can commonly be identified by the presence of relict iron oxide coatings (Plate 3.10D). This selective dissolution is due to the chemical stability of this post depositional film in the interstitial groundwater (Walker et al., 1978).

The previous description of the different dissolution features may indicate the duration of this process which started early in the

diagenesis and before the formation of the authigenic mineral sutie, and continued even after the late carbonate precipitation. The dissolution process could be still taking place at the present time at least for carbonate and feldspar as indicated by the chemistry of the groundwater (Chapter Five).

3.5.3 Clay Replacement

The clay replacement identified as the *in situ* replacement of the silicate grains by clay is as important as dissolution in changing the texture, mineralogy and the chemistry of the sediments. The alteration of silicates by means of clay replacement includes not only the individual minerals but also the rock fragments, which are disaggregated due to selective replacement of the more unstable mineral (Walker *et al.*, 1978). The replacement clay, which is considered authigenic (Wilson and Pittman, 1977) also affects the chemistry of sediments. These chemical changes result from the conversion of silicate minerals into clay and are associated with the release of ions into interstitial solutions. These may be removed in solution and under appropriate conditions may precipitate as other authigenic minerals (Walker *et al.*, 1978).

Feldspar is the most common silicate mineral to undergo this type of alteration. However, clay replacement is generally not as common as dissolution in these Triassic sandstones. The replacement clay occurs either irregularly, along cleavage or any plane of weakness, peripherally or sometimes completely replacing the original grains (Plate 3.10E,F and 3.11A,B). Sometimes the replacement is very extensive, leaving little evidence of the host grain which, due to the soft nature of the clay, is squeezed between the rigid detrital grains

(Plate 3.11C,D) affecting its hydrological character and especially permeability. This phenomenon may indicate that clay replacement was early in the diagenetic sequence and before burial compaction. Unfortunately, this clay replacement cannot be identified mineralogically under the ordinary microscope although the replacement features are more obvious than SEM.

In SEM studies feldspar is sometimes shown to be partially replaced by kaolinite associated with dissolution (Plate 3.11E,F) and sometimes replaced by kaolinite and/or illite (Plate 3.12A) or illite only (Plate 3.12B). Also with the SEM completely replaced detrital grains are sometimes seen. These consist of curled up plates (Plate 3.12C,D) in which EDAX analysis reveals a composition of Si, Al, K, Ca, Mg and Fe which may indicate a mixed layer illite-smectite possibly stained by iron oxide.

Occasionally dissolution and clay replacement of detrital grains are clearly associated and can be detected by both thin section and SEM study (Plate 3.12E,F). Thin section studies show that replacement clays are usually stained by iron oxides.

3.5.4 Authigenic Minerals

3.5.4.1 Quartz

Authigenic quartz is not a very common constituent in the authigenic mineral suite of the Triassic red sandstone under consideration, comprising usually minor amount. It does not therefore substantially affect the hydrogeological characters of these rocks but its formation in the early stages of diagenesis may have prevented extensive compaction during later burial (Plate 3.13A).

Secondary quartz is precipitated as optically continuous overgrowth on detrital quartz cores. For polycrystalline grains, each unit possesses its own overgrowth with the same intensity of undulatory extinction transmitted from the detrital core into the overgrowth (Plate 3.1F). The boundary between the detrital core and its authigenic rim sometimes can be identified by the presence of a hematitic clay film (Plate 3.13B) but in most cases overgrowths are not easily identified under the ordinary microscope. In many cases dust lines are not present on detrital grain surfaces and overgrowths can only be identified by the occurrence of euhedral crystal faces.

SEM study of the authigenic quartz indicates the presence of many features described by Waugh (1970a,b) and Pittman (1972). The overgrowths start with the precipitation of initial prismatic or rhombohedral crystals crystallographically oriented over the detrital core (Plate 3.13C,D). Sometimes these incipient crystals merge forming incomplete crystal faces (Plate 3.13E,F) resembling those described by Pittman (1972). Holes on the crystal surfaces could be due to the merging of irregular overgrowths. Sometimes these initial projections grow and start to merge with different crystallographic direction which may indicate polycrystalline detrital core on which these overgrowths were developed (Plate 3.14A,B). The growth of these inital crystals into a single crystal with prismatic termination is only rarely seen (Plate 3.14C).

Calcite and quartz cement commonly coexist in sandstone and may show replacement evidence which can be explained by the pH-solubility curves of quartz, calcite and amorphous silica (Blatt et al., 1980). However, in these sandstones the calcite is always found to replace quartz while the opposite phenomenon has never been detected (Plate

3.14D). As a result of this reaction the quartz margins are seen to be corroded whenever in contact with calcite cement. This relationship helps in predicting the sequence of diagenetic events, indicating that quartz overgrowth always pre-dates the formation of clacite.

The sources of the secondary silica are numerous and have been extensively discussed (Towe, 1962; Phillip et al., 1963; Füchtbauer, 1967; Sippel, 1968; Waugh, 1970b; Hower et al., 1976; Sibley and Blatt, 1976 and Hawkins, 1978). These different sources include: (1) pressure solution, (2) alteration of the silicate grains either by dissolution or by clay replacement, (3) clay diagenesis including the conversion of smectite to mixed layer I/S or pure illite, (4) the solution of siliceous dusts produced during aeolian abrasion of detrital quartz grains, (5) fresh surface or river water, (6) biochemical origin; dissolution of diatoms and radiolaria which are restricted to marine sediments, (7) the volcanic activity and the thermal springs, and (8) the replacement of the silica bearing minerals by carbonate. Many of these sources are clearly not applicable in the present study.

The precipitation of secondary quartz in these Triassic sandstones occurred soon after deposition and at shallow depth before any burial compaction took place. Fluvial or surface waters could, therefore, be an important source of silica. This type of water may contain 13 ppm dissolved silica which is greater than the solubility of quartz (6 ppm only) and sufficient to provide the source of quartz cement (Friedman, 1954). Together with this important source of silica, the dissolution of silicate mineral grains was probably important. Clay replacement and especially the replacement of feldspar

by kaolinite may also have provided silica (Hawkins, 1978). The common important source of silica, pressure solution, which sometimes supplies about one-third of the secondary quartz (Sibley and Blatt, 1976), is unlikely to have been important in this case because there is no evidence of deep burial or great compaction.

3.5.4.2 K-feldspar

Authigenic K-feldspar is a common minor constituent in the Sherwood Sandstone Group and in British Permo-Triassic sandstone in general where it forms not more than 4% of the total mineralogical composition (Waugh, 1978).

On the basis of the EDAX spot analyses most samples indicate the presence of only potassium, aluminium and silica. This result is in agreement with the results of Waugh (1978) on the British Permo-Triassic and Ali (1982) on the Triassic of Central England. The K-feldspar overgrowths are sometimes coarse enough to be recognized in thin section and are present on detrital cores of orthoclase, perthite, microcline and plagioclase. Complete optical continuity between host and overgrowth is common (Plate 3.14E) but in some cases there is a lack of optical continuity between the overgrowth and the host grain (Plate 3.14F). The lack of optical continuity could be either as a result of the compositional and/or structure differences. Ali and Turner (1982) noted that the authigenic K-feldspar is usually sanidine whilst the detrital grains are usually orthoclase. Reworked feldspar overgrowthshave also been detected in these sandstones (Plate 3.15A). The authigenic potassium feldspar is also present as pore filling crystal with no indication of any detrital core present (Plate 3.15B,E,F).

The SEM study of authigenic K-feldspar reflects its occurrence in two different habits. The first is represented by pseudorhombic crystals which are morphologically called adularia (Baskin, 1956) and the other habit comprises tabular prismatic crystals up to 20 μm in length (Plate 3.15C,D). These types of crystal forms were described by Stablein and Dapples (1977). Both authigenic crystal forms were present either as overgrowth on detrital core or as discrete crystals as part of the interstitial matrix (Plate 3.15E,F).

Different stages of the progressive growth of authigenic K-feldspar crystals have been detected in these Triassic sandstones and are similar to those described by Waugh (1978). Rhombohedral crystals were crystallographically oriented over the surface of the detrital grain and further growth resulted in increasing their number (Plate 3.16A,B). As the growth proceeded merging, stacking and overlapping of the rhombs resulted in the complete enclosure of the detrital core (Plate 3.16C,D). Geochemical and optical determinations indicate that this authigenic feldspar is potassiun intermediate sanidine for the Permo-Triassic sandstone (Waugh, 1978) and potassiun low sanidine in the Triassic of Central England (Ali and Turner, 1982).

The surfaces of authigenic K-feldspars are sometimes covered with an authigenic clay mineral which is probably illite (Plate 3.16E,F) as indicated from the EDAX spot analyses which show the presence of Si, Al, K and Fe. This authigenic clay formation is usually associated with dissolution of the K-feldspar. This association may indicate that authigenic illite post-dated the K-feldspar overgrowth.

Occasionally authigenic feldspars as well as their detrital cores

show partial or complete replacement by carbonate including both dolomite and calcite (Plate 3.5C,D,E). This indicates that potassium feldspar overgrowth precedes carbonate precipitation. Also, sometimes both the detrital feldspar and its authigenic rim are seen to be fractured with no indication of any welding of this fracture by carbonate cement (Plate 3.9 D). This could be an indication about the early diagenetic precipitation of K-feldspar preceded burial compaction which caused bending of ductile minerals and fracturing of non-ductile ones.

Dissolution is one of the most common features affecting both detrital and authigenic feldspar. Dissolution of the detrital core without any effect on the overgrowth indicates that dissolution occurred before authigenic precipitation. On the other hand the presence of extensive dissolution textures from the authigenic periphery inward indicates widespread dissolution after authigenic K-feldspar formation (Section 3.5.2). This dissolution could be still happening today as indicated from the mineral stability diagrams, which show that the present groundwater is unstable with respect to K-feldspar (Chapter Five).

3.5.4.3 Authigenic clays

The identification of clay minerals is based on X-ray diffraction analysis of < 2 μm oriented mounts which were prepared from the core samples as well as SEM and EDAX analyses. The X-ray diffraction results indicate the presence of kaolinite, mixed layer illite-smectite (I/S) and mica, together with smectite and chlorite both of restricted abundance and amount (Figure 3.4). Kaolinite is the most common and abundant authigenic clay mineral in the Sherwood

Sandstone Group, both in the Lenton and Nottingham Castle Formations. Mixed layer (I/S) clay is the second in abundance whilst illite is the least abundant. Detailed systematic XRD analysis of the whole depth ($\sim$195 m) of borehole A14 indicates that illite is the most abundant clay in the Permian sediments. The chlorite present is more likely to be of detrital origin as indicated from thin sections where it occurs in rock fragments and as inclusions in quartz (Plate 3.1D). The SEM study reveals no evidence of authigenic chlorite. Smectite is only detected in a very few samples in borehole A11. The presence of smectite and mixed layer clay (I/S) supports the results from the textural analyses that these sediments have not suffered deep burial.

Kaolinite is the most common and important authigenic clay mineral present. Its importance comes from its abundance also from the fact that it is well developed and can be easily recognized in both thin section and SEM. This provides an opportunity to develop a diagenetic sequence on the basis of different textural relationships.

The XRD traces reflect the high crystallinity of the kaolinite as the 001 reflection at about 7 A^{o} is very sharp (Figure 3.4). The kaolinite is developed as pore filling pseudohexagonal books which plug pore throats decreasing both porosity and permeability (Plate 3.17A,B,C). Its effect on permeability was also detected by decreasing the effective pore radius (Plate 3.17D,E). The SEM study reveals stacked pseudohexagonal plates which form the characteristic book shape as the most common habit (Plate 3.17C,F). However, vermicular shape (Plate 3.18A,B) as well as a rose-like shape were also detected (Plate 3.18C,D). The crystal size of the kaolinite seems to vary widely. They ranged between 2 to about 60 µm with a modal size of 10 µm. The kaolinite often shows intimate relationships with carbonate

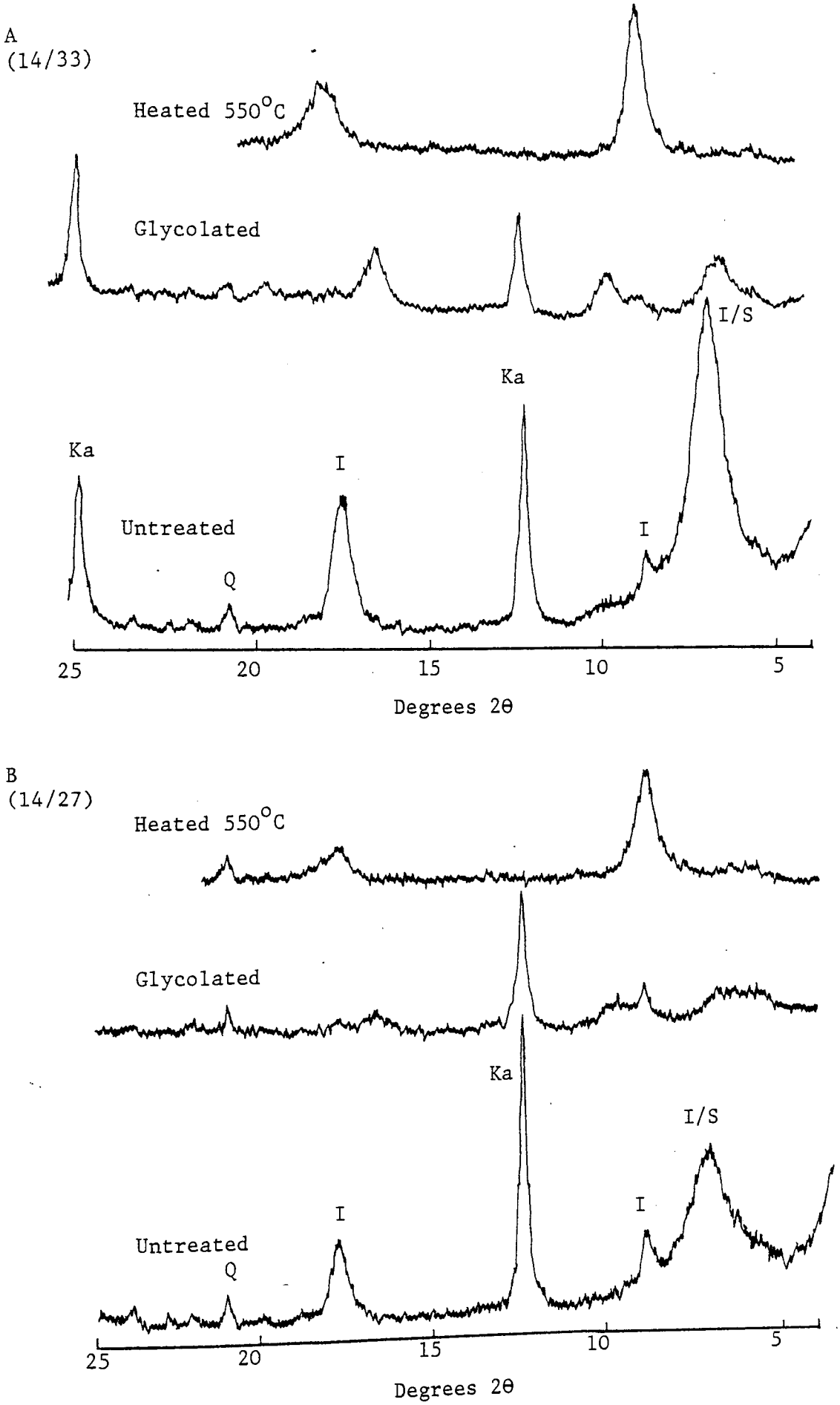

Figure 3.4 X-ray diffraction patterns of the clay fractions in the Sherwood Sandstone Group, using Ni filtered Cu Kα radiation. Ka = kaolinite, I = illite, I/S = mixed layer illite-smectite, Q = quartz.

as discuss in the following section (3.5.5).

The mixed layer illite-smectite can be classified according to Reynolds and Hower (1970) as interstratified I/S ordered with smectite ratio between 20-35%. Very rarely found are I/S clays with less than 20% of expandable layers. The 10 A^{o} reflection characterizing illite is sometimes seen to be very sharp indicating a high crystallinity index which is probably an indication of the presence of detrital mica.

The SEM study of these clay minerals although very important in reflecting their authigenic origin does not provide conclusive evidence of the different clay species present. This could be due to the lower percentage of the expandable layers making I/S clay of similar appearance to illite. The presence of these clays as pore lining and its absence at the grain contacts demonstrate their diagenetic origin (Plate 3.18E). Although volumetrically not very important it has a significant effect on the permeability because it commonly bridges pore throats (Plate 3.18F). The illite and I/S clays are present in different habits. They occur as flake-like platelets developed normal to the grain surface (Plate 3.16E,F). These platy crystals are occasionally found forming the very distinctive boxwork texture characteristic of illite. (Plate 3.19A,B.C.D) They rarely display acicular habit (Plate 3.14A) which is usually developed on authigenic quartz.

Very commonly, these flaky crystals display some sort of wavyness or curly appearance (Plate 3.14A, 3.19C,D,E,F, 3.20A,B,C). This wavy habit could be due to the presence of expandable layers, and this is supported by the EDAX spot analysis of almost all of them which

indicate the presence of Si, Al, K, Mg, Ca and Fe. Another habit for this clay was recorded where the flakes are characterized by a flame-like shape (Plate 3.20D,E.F).

3.5.4.4 Carbonate

Carbonate minerals are one of the most common diagenetic features of these Triassic sandstones and reaches up to ∿14% by weight of the composition of the Sherwood sandstones (Table 3.1). Staining by potassium ferricyanide and alizarin red-S indicates the presence of dolomite, ferroan calcite and non-ferroan calcite, with the abundance of dolomite increasing towards the Lenton Sandstone Formation. The effect of these cementing materials in decreasing the porosity and permeability of the reservoir rocks was considerable. This happened either by filling the intergranular pores (Plate 3.14D, 3.21A,B), cementation of dissolution pores and by sealing off permeability temporarily until later changes in ground water chemistry favoured the dissolution of these authigenic carbonates (Plate 3.21C,D). The role of carbonate dissolution in producing secondary porosity is very considerable. This is clearly observed in borehole A3 where there are abundant over-sized dissolution pores up to more than several centimetres in size and giving rise to a very friable sandstone. These dissolution vugs were observed clearly in hand specimens as well as thin sections (Chapter 4).

Dolomite is the earliest authigenic carbonate present occurring as single idiomorphic rhombic crystals or clusters of equidimentional crystals. These normally have straight contact between each other (Plate 3.21A,B,E,F), fill interstitial pores, and are commonly zoned (Plate 3.22A). One of the very common forms of dolomite are

ghosts in which evidence of the original material, such as the iron oxide grain coating (Plate 3.22B), is still preserved. This may indicate that this authigenic dolomite could have formed by the step-by-step dissolution and replacement of the original grain whatever this was. The water must be in a delicate state of balance so that dissolution and precipitation could occur virtually simultaneously (Blatt et al.,1980). The replacement of the detrital and authigenic K-feldspar by dolomite was also detected, indicating that at least some dolomitization post-dated the formation of authigenic K-feldspar (Plate 3.5E).

Calcite and ferroan calcite are both as common as dolomite and more abundant in the Nottingham Castle Formation. They occur mainly as coarsely crystalline sparry crystals filling the intergranular pores. They also replace pre-existing detrital and/or authigenic minerals, such as quartz, feldspar and dolomite indicating that they post-date these minerals (Plate 3.5C,D, 3.14D). Calcite and ferroan calcite are frequently found as disseminated patches up to 4.5 mm across. They coexist together as coarse crystals up to 60 μm, often with a ferroan calcite core (Plate 3.22C).

These carbonate cements have been affected by large scale dissolution creating a considerable percentage of secondary porosity. The pore water at the time of dissolution was undersaturated with respect to carbonate and more acidic. Because of the low solubility of the calcium carbonate in most natural water, it can be presumed that a very large volume of water flushed through the rock (Blatt et al., 1980).

3.5.5 Authigenic Minerals : Paragenetic Sequence Relationships

The SEM, EDAX spot analyses and the thin section study were used to build up a picture of the authigenic mineral sequence from their textural relationships. Quartz and feldspar are shown to be the earliest diagenetic minerals precipitated in these sandstones. The replacement of both detrital and authigenic K-feldspar by dolomite (Plate 3.5E) indicates that dolomite post-dated K-feldspar.

Kaolinite which is one of the most abundant authigenic minerals and has a great effect on the hydrogeological characteristics, is shown to have a complicated history. Relicts of dolomite occur within a kaolinitic matrix (Plate 3.22D) and sometimes well developed kaolinite apparently replaces dolomite (Plate 3.22E). The kaolinite relationships extend to include calcite and ferroan calcite as well, where kaolinite is shown to pre-date calcite and ferroan calcite as indicated from the presence of relics of authigenic kaolinite as inclusions in the carbonate (Plate 3.22F, 3.23A,B). Also the SEM study indicates the formation of kaolinite penecontemporaneously and/or after the calcite and potassium feldspar precipitation (Plate 3.23C,D,E,F).

The replacement of dolomite by calcite was also detected from the preservation of the rhombic crystal form of dolomite (Plate 23A,B), a feature indicating that dolomite is the earliest carbonate mineral formed.

The relation of the other authigenic clays (illite and I/S) and their position in the diagenetic sequence is not easy to determine. However, some textural relationships were detected, including the development of acicular illite on authigenic quartz (Plate 3.14A,B) indicating that illite post-dated quartz. Also the development of authigenic curled

clay flakes on authigenic feldspar surface indicates that K-feldspar formation preceded clays (Plate 3.14A,B). While calcite can be shown to have precipitated after the authigenic illite and the mixed layer (I/S) clay (Plate 3.19C,D). The relation of these authigenic clays (I and I/S) with the other diagenetic minerals is not clear but it seems likely that they formed after quartz and feldspar authigenesis and prior to calcite cementation.

The above relations may indicate that kaolinite is the latest authigenic mineral precipitated in secondary pore spaces. However, its precipitation started relatively early in diagenesis and may have continued for some time. The mineral stability diagrams (Chapter 5) confirm this conclusion, as the formation water is saturated with respect to kaolinite which means that this mineral could be still formed up till now.

3.6 POROSITY AS A FUNCTION OF DIAGENETIC PROCESSES

Diagenetic processes have a crucial effect on the hydrogeological characteristics of sediments. They cause the destruction of primary intergranular porosity and permeability by authigenesis and cementation, and also create secondary porosity by the dissolution of cements and detrital grains. The reduction of primary porosity takes place mainly in the early stages of burial diagenesis, whilst the creation of secondary porosity is more common in the later stages of diagenesis (Hayes, 1979). However, both reduction and enhancement of porosity started soon after deposition.

The intergranular primary porosity of well-sorted sands when initially deposited may reach 42.4% (Beard and Weyl, 1973), and sometimes more

than 50% for beach and aeolian sands which are loosely packed and well-sorted (Pryor, 1973). However, the water reservoir sandstones of the Sherwood Sandstone Group in this study have an average porosity of about 25% with a maximum of ∿ 32% recorded in borehole A3. So diagenetic processes must have had an important effect in destroying the primary porosity in these sandstones especially in view of the fact that much of the existing porosity is of secondary origin.

The porosity reducing process can be classified according to Hayes (1979) into physical (or mechanical), chemical and/or a combination of both chemical and mechanical. In these sandstones chemical processes, including the precipitation of authigenic minerals (cement), as well as clay replacement were the most crucial factors in destroying primary porosity. These authigenic minerals include quartz, K-feldspar, clay minerals (kaolinite, illite, mixed layer clays I/S), and carbonate (dolomite, calcite and ferroan calcite). These cementing materials precipitated as overgrowths on detrital cores (quartz and feldspar) or pore fillings (kaolinite, K-feldspar and carbonate) and also as pore lining (illite and illite-smectite). The effect of authigenic minerals in destroying the secondary porosity was also detected from the presence of dolomite ghosts which indicate the dissolution of the original grain with simultaneous dolomite replacement (Plate 3.22B). Also the precipitation of kaolinite, in the later diagenetic process, filling the interstitial voids which were probably of secondary origin. The clay replacement of the detrital grains also has some effect in reducing porosity, as the resulting fine clays show enormous increase in the size, more than the original detrital. This effect is limited in these sandstones under study (section 3.5.3), although when present has a great effect on permeability as well. Feldspars as

well as rock fragments are most common detritals undergo this alteration. Sometimes these replacement clays squeezed between the rigid framework grains (Plate 3.11C,D) decreasing both porosity and permeability as a result of compaction. The biotite is also shown to be affected by this combined chemical and physical process where they oxidized into hematitic iron oxide followed by mechanical compaction causing their bending (Plate 3.7C) and indicating the early replacement process succeeding the burial compaction.

The physical or mechanical processes which include compaction by burial and mechanical infiltration of clays were not important in the sandstones. Compaction results in bending of the ductile grains, fracturing of brittle ones and squeezing of the soft grains between the framework components causing the reduction of the intergranular porosity. This compaction had a very small role in these sandstones as detected from the thin sections study which could be due to the early precipitation of the rigid cementing materials (quartz, K-feldspar and carbonate) preventing physical compaction from extensive effect on the sediment. However, it seems likely that these sandstones have not undergone deep burial or great stress as indicated from the textural analyses and the clay mineralogy.

The other physical process which may reduce the primary porosity is the mechanical infiltration of clays into sediments which were free from clays when initially deposited (Walker, 1976; Walker et al., 1978). This mechanically infiltrated clay platelets deposited on the detrital grain surface decrease the textural maturity and consequently decrease the primary porosity. This type of matrix is not common in these sandstones under consideration, or even in the older Permian sandstone studied by Waugh (1978).

The amount of secondary pososity created during diagenesis is very considerable. Very recently secondary porosity has been given much attention because of its common occurrence and volumetric importance (Hayes et al., 1976; Lindquist, 1976; Stanton and McBride, 1976; Schmidt et al., 1977; Walker et al., 1978; Pittman, 1979; and Schmidt and McDonald, 1979b).

Regarding the timing of the enhancement of this secondary pososity, Schmidt and McDonald (1979a) conclude that this can happen at any stage of the diagenetic sequence and anywhere in the sedimentary column: (1) in the environment of deposition before any effective burial (eodiagenesis), (2) at any depth of burial above the metamorphic zone (mesodiagenesis), (3) during exposure following the period of burial (telodiagenesis).

The classification of secondary sandstone porosity has been dealt with in the last decade by Shenhav (1971), Pittman (1979) and Schmidt and McDonald (1979b). Shenhav (1971) defined four different types of porosity; intergranular, intercrystalline, intermediate and intra-crystalline. His classification depends on the mineralogy of the sediments and the pore texture. Pittman (1979) also identified four types of sandstone porosity including: intergranular, dissolution, fracture and microporosity. Schmidt and McDonald (1979b) point out that secondary porosity can be classified genetically (depending on the origin of the pores) or descriptively (depending on the pore texture). The genetic classification identifies the following types of porosity created by (1) fracturing, (2) shrinkage, (3) dissolution of detrital components, (4) dissolution of authigenic minerals (cement), (5) dissolution of authigenic replacive minerals, (6) hybrid origin. The descriptive or textural classification identifies the following

types, (1) intergranular pores, (2) oversized pores, (3) moldic pores, (4) intra-constituent pore, (5) fracture.

In the sandstones in this study the different pore types were identified mainly by the examination of impregnated thin sections together with the study of a few pore casts by means of SEM. The SEM study reveals that the pore spaces are very thin tabular or sheet like and highly interconnected and characterized by irregular outlines (Plate 3.24A,B). Also the pore cast resin study helped in identifying the micropores (< 0.5 μm) which resulted from dissolution, especially along feldspar cleavage planes (Plate 3.8C,D,E,F) or were associated with the authigenic platy clays.

The genetic classification of the secondary sandstone porosity (Schmidt and McDonald, 1979b) has been followed in identifying the different porosity type. The following types were recorded: (1) dissolution pores, (2) fractures, (3) shrinkage pores, (4) hybrid pores. Dissolution pores are the most common type.

(1) Dissolution pores include the pores resulting from the dissolution of detrital components and authigenic minerals, including overgrowths, pore fillings and replacive material. The most important form of these dissolution pores are oversized pores which are very common on both a micro and macroscale.

(2) Fracture porosity which includes grain fracture and rock fracture was a minor source of secondary porosity in these rocks. Rock fracturing is discussed in Chapter 4. The role of grain fracturing in creating secondary porosity is generally very poor in these rocks and results from the breakdown of the ductile grains due to burial.

As the effect of compaction in these sandstones is very limited, partly as a result of the early cementation, the grain fracture detected is very minor and is always unwelded by cement indicating that it post-dates cementation.

(3) Shrinkage porosity is rarely detected in these sandstones but it occurs as a result of the dolomitization of detrital carbonate fragments (Plate 3.24C).

(4) Hybrid porosity results from a combination of primary and secondary porosity or more than one type of the secondary porosity. Hybrid pores are quite common where it is very abundant in the dissolution porosity, resulting from dissolution of both detrital and its authigenic phase (Plate 3.9B). Also combination of fracture and dissolution pores (Plate 3.9D). These oversized pores could be as well hybrid pores (Plate 3.24D,E).

From the previous details, it seems that the porosity of the Sherwood Sandstone Group is a combination of both primary and secondary porosity. These may often be of equal importance to each or the secondary porosity much more common especially in the abundance of oversized pores. Dissolution pores of different types are the most common type of secondary porosity, and some of these could have formed in the present ground water regime (Chapter 5).

3.7 DISCUSSION

The diagenetic history of the Sherwood Sandstone Group can be classified into four stages depending upon the physical and/or chemical processes prevailing and their associated effect on destruction or enhancement of porosity at each stage. The Schmidt and McDonald (1979a) nomenclature

for diagenetic regimes is used here: (1) Stage one (eodiagenesis), (2) Stage two (mechanical/compaction or immature mesodiagenesis), (3) Stage three (early mature mesodiagenesis), (4) Stage four (late mature mesodiagenesis) Figure 3.5.

Stage "one" or the eodiagenetic stage comprises the early diagenetic changes which take place in the environment of deposition before any burial affects. Chemical processes govern dissolution and replacement as well as the precipitation of the authigenic cementing material. The net result of this stage is the destruction of the primary porosity although secondary porosity may be created in this stage.

Dissolution as well as clay replacement of the detrital components are very common diagenetic features assumed to have taken place very early in diagenesis. They both supply a vital source of ions to the interstitial pore water including: K, Na, Al, Si, Ca, Mg and Fe. These ions were used later in the formation of authigenic quartz, K-feldspar, kaolinite, dolomite, ferroan calcite and finally calcite. The other clays; illite, mixed layer illite-smectite and montmorillonite were precipitated after authigenic quartz and K-feldspar and are probably a product of authigenesis and clay replacement in the shallow burial environment. The formation of secondary quartz is controlled mainly by the amount of dissolved silica as its solubility was not affected by pH below 9. The formation of this authigenic quartz is assumed to be very early in the diagenetic sequence, at shallow depths, the pore water at that time should have more than 6 ppm dissolved silica.

The precipitation of K-feldspar as well as the clay minerals governed by the chemistry of the pore water and the thermodynamics of the minerals in the K_2O-Na_2O-Al_2O_3-SiO_2-H_2O system (Garrels and Christ,

1965; Hess, 1966; Helgeson et al., 1969 &1978) which will be dealt with in detail in Chapter 5. The precipitation of K-feldspar required high $(\frac{K^+}{H^+})$ and/or high (SiO_2). As K-feldspar was followed by either kaolinite, illite or montmorillonite, this indicates decrease of the silica or potassium dissolved in the pore water (Hess, 1966).

The formation of carbonate is sensitive to the pH of the interstitial water in contrast to quartz or silica precipitation. Early in the eodiagenetic stage, the dolomite precipitated, where the interstitial water was saturated with respect to dolomite and with high Mg/Ca ratio, and/or low salinity (Folk and Land, 1975). The source of the Ca and Mg in the water could be the dissolution of the pyroxene, amphibole and calcic plagioclase, where these minerals are shown to be completely absent from these rocks. Later and toward the end of the eodiagenetic period, the interstitial water was saturated with respect to calcite which favoured its precipitation. The presence of ferroan calcite cores may indicate that the interstitial water was mildly reducing at this time and more oxidizing later.

The red colouration of the sediments took place early in the diagenesis. The colouration took place over considerable time as indicated from hematitic film around both detrital and some authigenic phases. These red hematitic pigments precipitated as ferric oxyhydroxides from oxidizing alkaline interstitial pore water (Garrels and Christ, 1965; Whittemore and Langmuir, 1975). The evidence of the formation of this hematitic iron oxide before mechanical compaction has also been detected from the even distribution of the hematite along bended oxidized biotite flakes.

Dissolution of detrital framework grains is very common in this stage

of diagenesis and gives rise to a considerable amount of secondary porosity. However, clay replacement and authigenic cementing materials compete with this dissolution by reducing the primary porosity. The net result of this early diagenetic phase is porosity reduction.

Stage "two" or mechanical compaction corresponds to the immature stage of the mesodiagenesis. This physical process which results from the burial of the sediments affects both porosity and permeability. Mechanical compaction in these rocks is detected from bending of the ductile grains, fracturing of the brittle ones and squeezing of the soft clays. Replacement clay squeezed between the rigid detrital framework is the most common feature of this stage, indicating that the clay replacement took place earlier than this mechanical compaction. However, the presence of unaffected clay replacements by this compaction may indicate that replacement took palce over long period of time as long as the mineral is not unstable in the surrounding environment. The final result of this stage is reduction of porosity and permeability but this was of only minor importance in the sandstones in this study.

Stage "three" corresponds to the early mature stage of mesodiagenesis. In this stage the enhancement of secondary porosity is the most important process. Where the dissolution of the carbonate is the main source of secondary pores and any early diagenetic minerals, as most of the unstable detritals supposed to be dissolved in the early stages of diagenesis. As the carbonate is sensitive to the pH of the environment, the interstital water at that time should be more acidic and unsaturated with respect to calcite, and so favouring its dissolution and giving rise to the oversized pores or vugs. The result of this diagenetic stage is creating the most considerable part of the secondary porosity.

Stage "four" which could be taking place up to the present time. In this stage porosity and permeability are reduced because of the precipitation of another generation of authigenic minerals. The second generation of kaolinite is the most important authigenic mineral precipitated in this stage and the present ground water conditions favour its formation in recent times (Chapter 5). The Al^{3+} needed for the precipitation of this kaolinite could be supplied from the dissolution of the early authigenic K-feldspar during stage "three". The dissolution of K-feldspar could also be taking place at the present time because it is unstable in the present ground water conditions. Carbonates, including both dolomite and calcite, are also undergoing dissolution within the present groundwater regime.

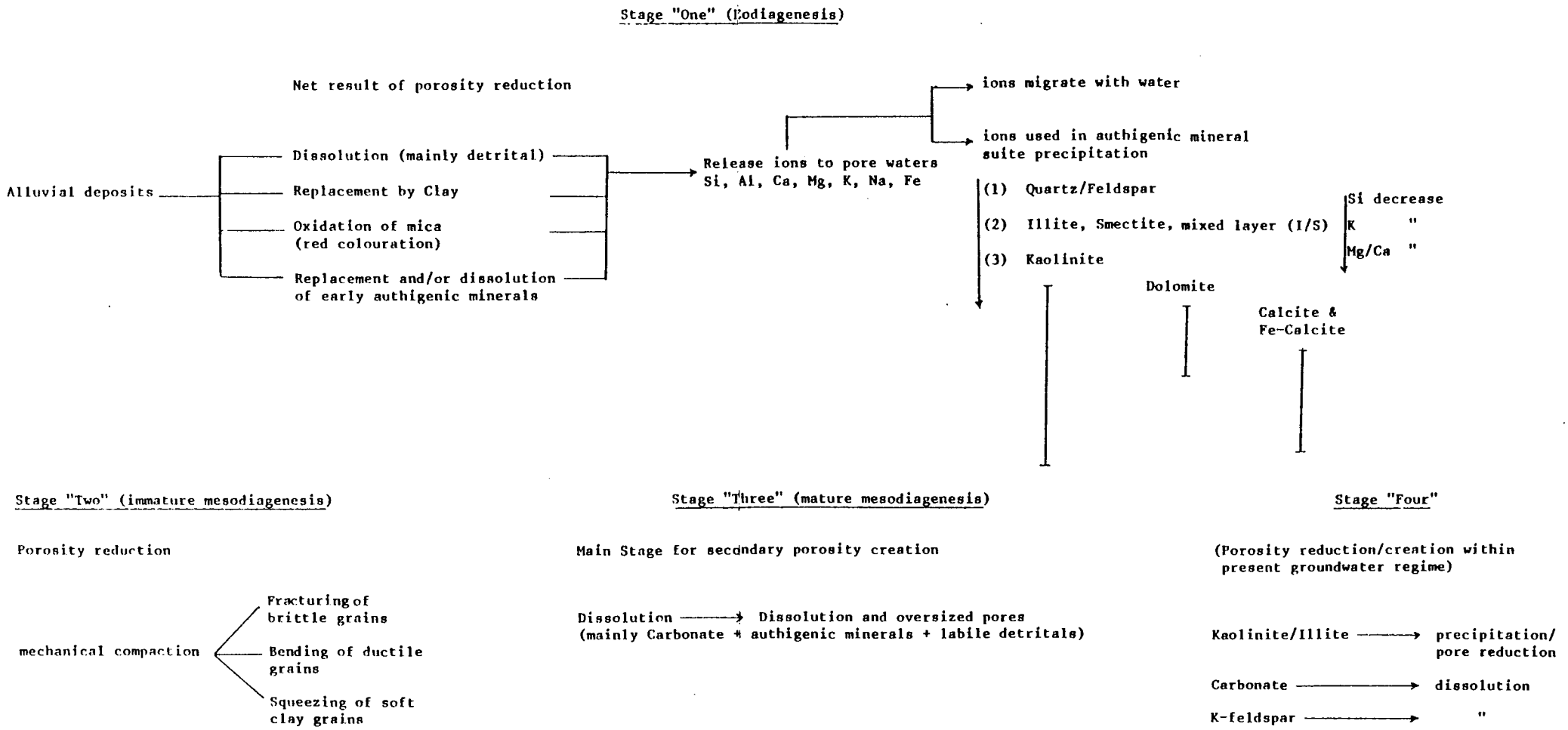

Figure 3.5 Schematic diagram of the diagenetic changes in the Sherwood Sandstone Group of north Nottinghamshire

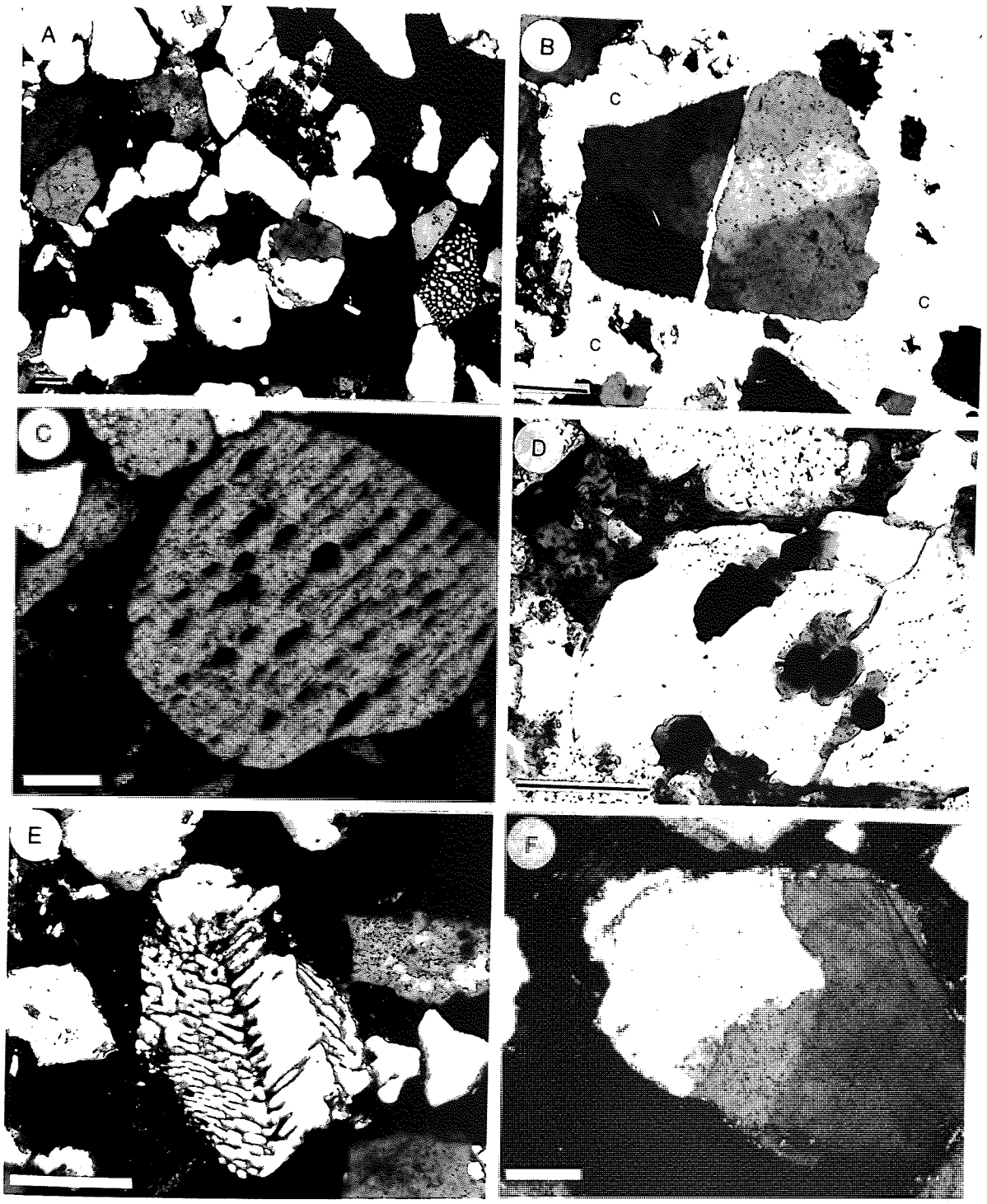

Plate 3.1 Thin section photomicrographs of detrital quartz types.

A. Different types of detrital quartz including water clear non-undulatory monocrystalline, undulatory monocrystalline and quartz in graphic intergrowth with K-feldspar, XN, BH A18/4 (33.5m)
B. Undulatory monocrystalline quartz shown to be split by calcite cement (c), XN, BH A18/4 (33.5m)
C. Monocrystalline quartz with abundant vacuoles, XN, BH A14/25 (134.6m)
D. Quartz with vermicular chlorite inclusions, XN, BH A11/9 (52m)
E. Intergrowth of quartz and K-feldspar forming myrmykitic texture, XN, BH A14(171.3m)
F. Polycrystalline quartz with overgrowth in optical continuity, together with haematitic clayey film separating the two phases, XN, BH A14/36 (92.2m)

Scale bar = 150 μm

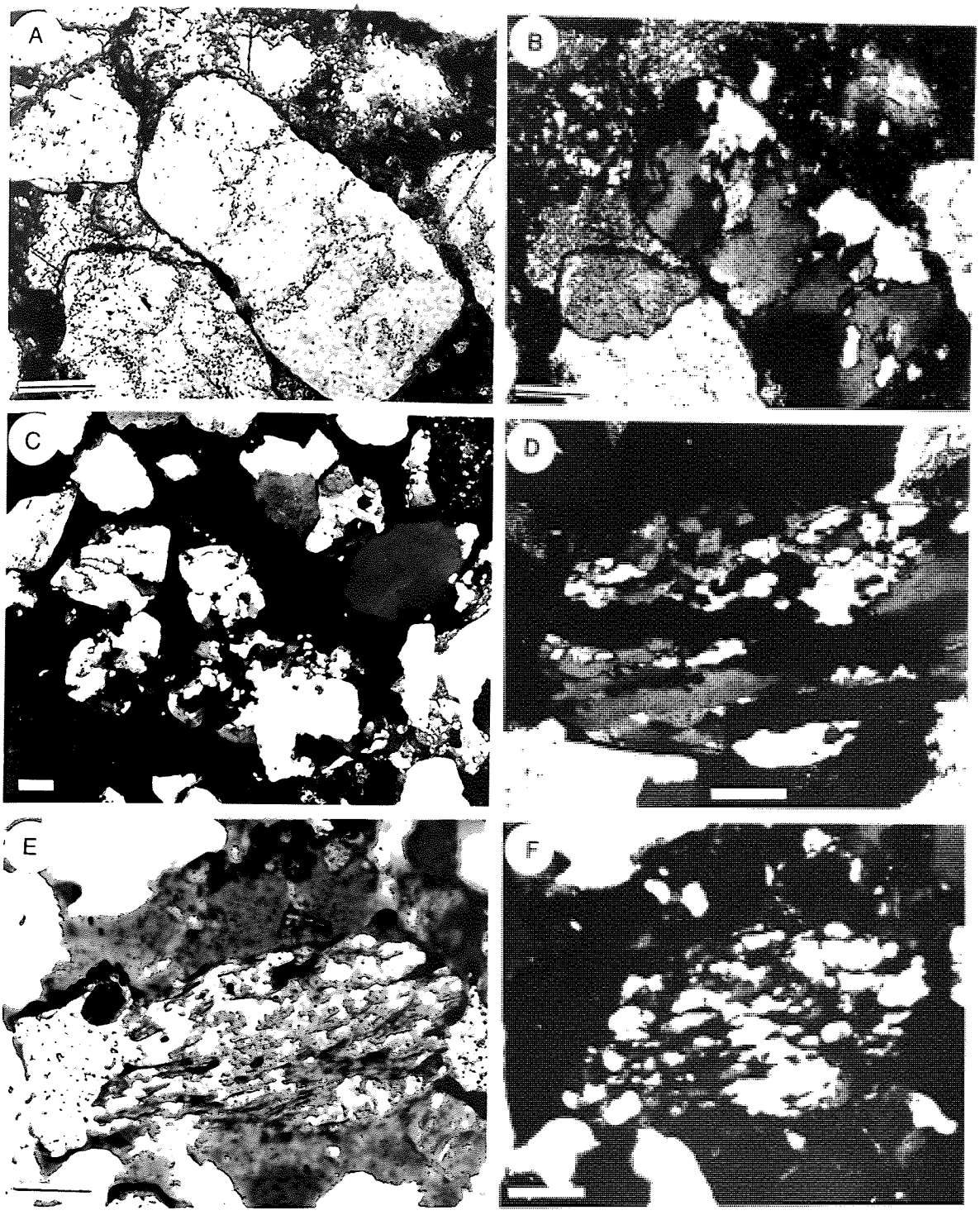

Plate 3.2 Thin section photomicrographs of detrital quartz types

A. Polycrystalline quartz with the internal crystal units defined by dust lines, PPL, BH A18/1 (4.7m)
B. A in crossed nicols
C. Monocrystalline non-undulatory quartz and polycrystalline quartz grains with sutured, granulated and polygonal cyrstal-crystal boundaries, XN, BH A18/2 (15m)
D. Polycrystalline quartz grain showing sutured and polygonal inter-crystal boundaries with the elongation of the crystal units, XN, BH A18/2 (15m)
E. Polycrystalline quartz with elongated crystal units and straight crystal boundaries associated with flaky mica inclusions in mica schist rock fragments, PPL, BH A18/2 (15m)
F. E in crossed nicols

Scale bar =150μm

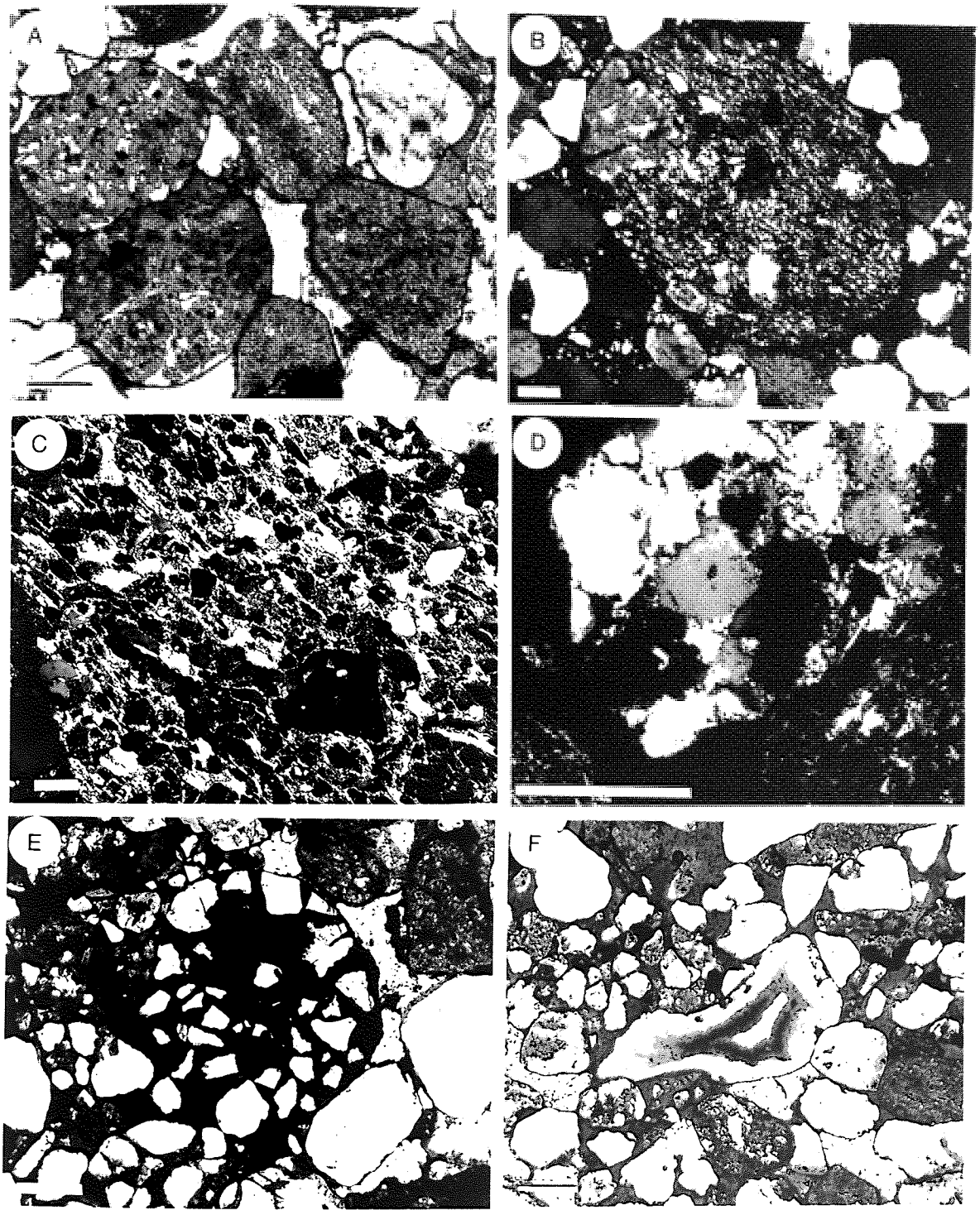

Plate 3.3 Thin section photomicrographs of different types of rock fragments

A. Different types of volcanic rock fragments including trachytic and microcrystalline texture, most of them shown to be stained with haematitic iron oxide, PPL, BH A18/13 (135m)
B. Volcanic rock fragment shows the porphyritic texture, XN, BH A18/1
C. Part of pyroclastic rock fragment, PPL, BH A18/1 (4.7m)
D. Sandstone rock fragment, XN, BH A18/2 (15m)
E. Haematitic quartz sandstone rock fragment, PPL, BH A18/13 (135m)
F. Rock fragment of chalcedony, PPL, BH A18/2 (15m)

Scale bar = 300 μm

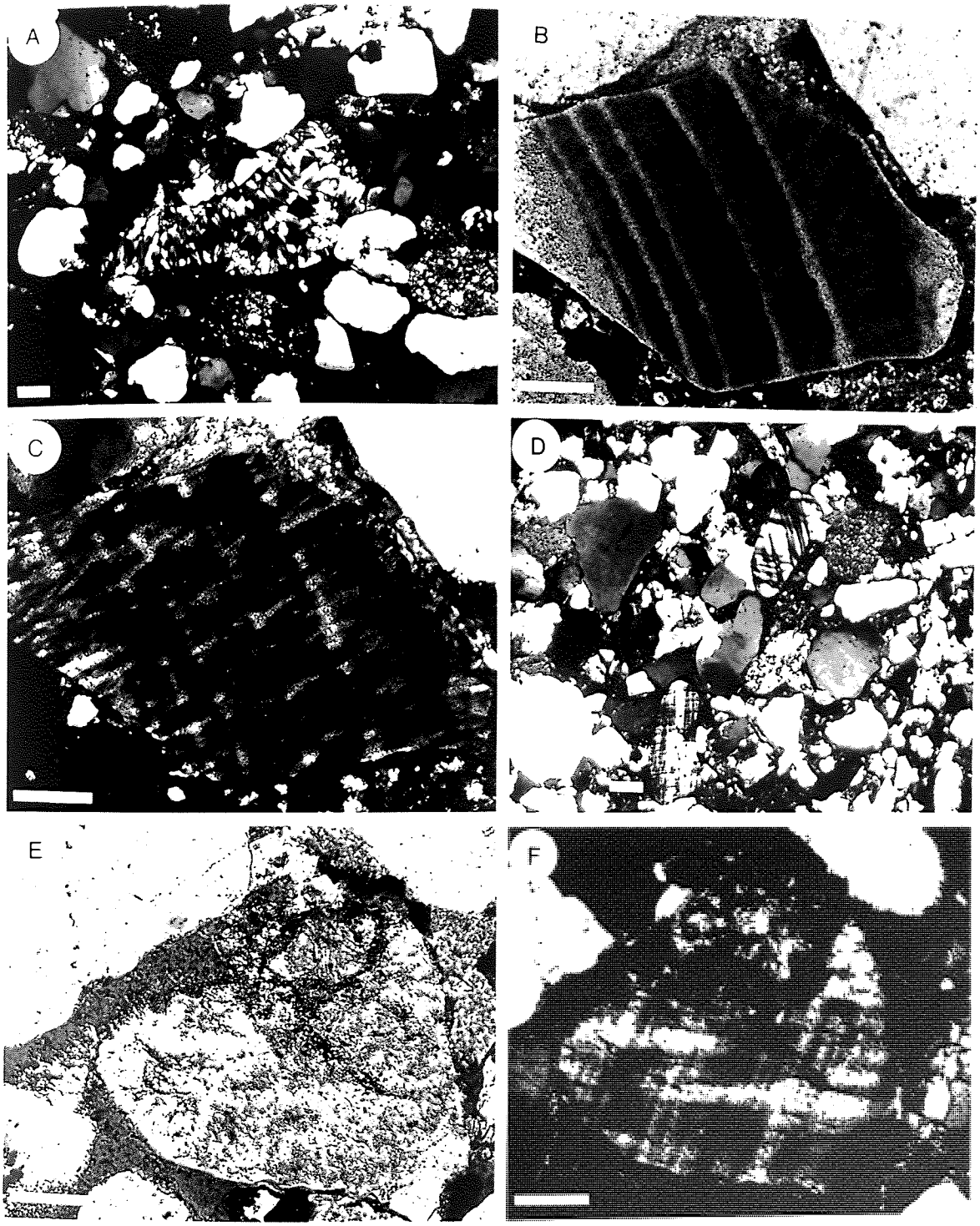

Plate 3.4 Thin Section photomicrographs of rock fragments and detrital feldspar types

A. Chalcedony rock fragment characterized by an alternative light and dark fibrous texture, XN, BH A18/12 (133m)
B. Detrital antipethite shown to be highly altered by vacuolization, PPL, BH A18/1 (4.7m)
C. B in crossed nicols
D. Fresh microcline grains show well-rounded outline and poly twinning, XN, BH A14/7 (187.7m)
E. Microcline grain shows partial dissolution and clay replacement, PPL, BH A18/2 (15m)
F. E in crossed nicols

Scale bar = 150 μm

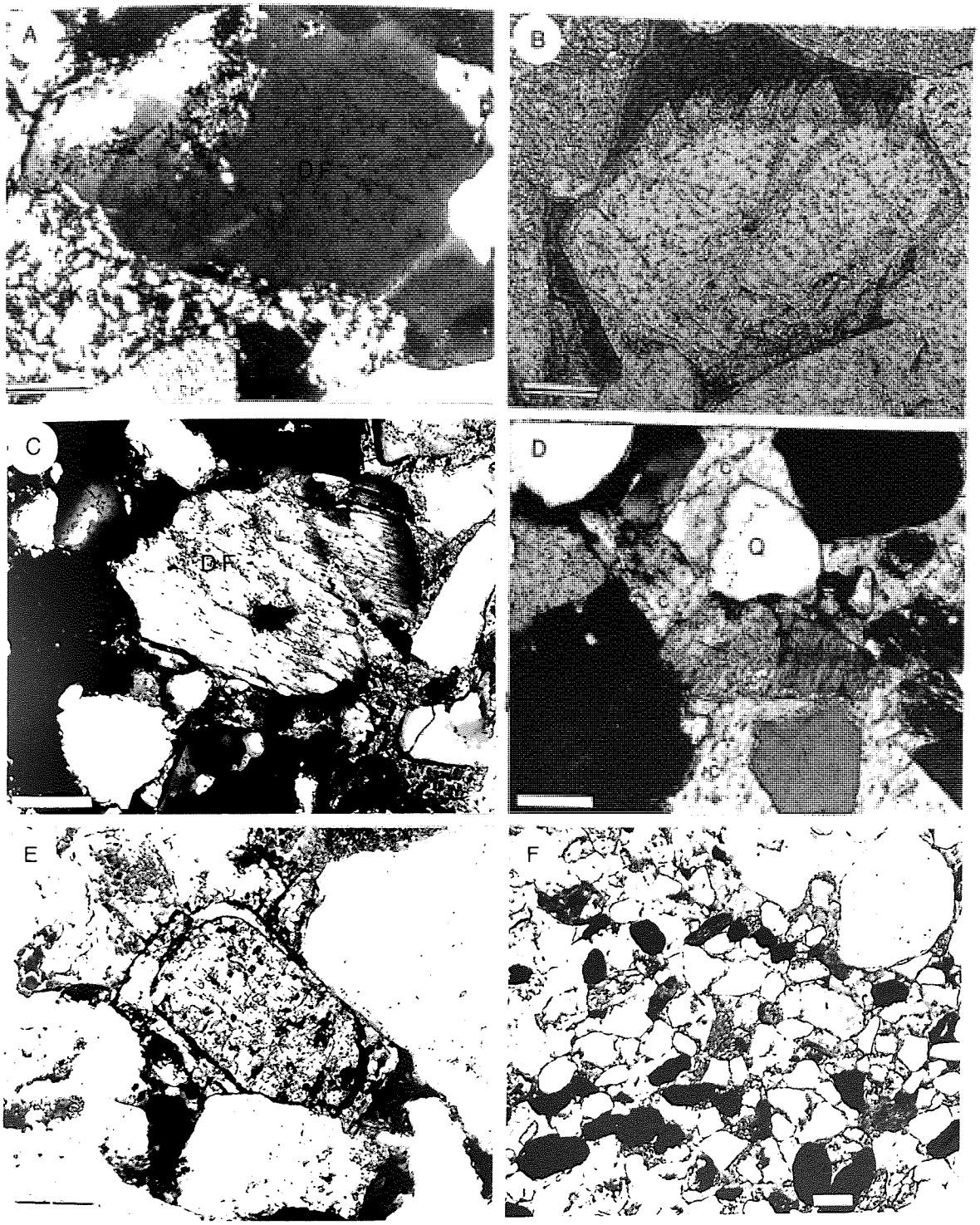

Plate 3.5 Thin section photomicrographs of detrital feldspars

A. Detrital feldspar (DF) shown to be partially altered to kaolinite together with authigenic kaolinite (Ka) filling the pore spaces, XN, BH A11/12 (15m)
B. Authigenic K-feldspar overgrowth shows evidence of dissolution with the development of the hacksaw termination, PPL, BH A18/3 (19.5m)
C. Detrital feldspar (DF) shown to be partially replace by Fe-Calcite (FC), XN, BH A11/6 (102.6m)
D. Partial replacement of both feldspar (F) and quartz (Q) by calcite (C), XN, BH A11/4 (33.5m)
E. Complete replacement of probably detrital feldspar grain and its overgrowth by dolomite, PPL, BH A11/6 (102.6m)
F. Opaque iron oxide grains concentrated in lamina, PPL, BH A14/9 (185.4m)

Scale bar = 150 μm

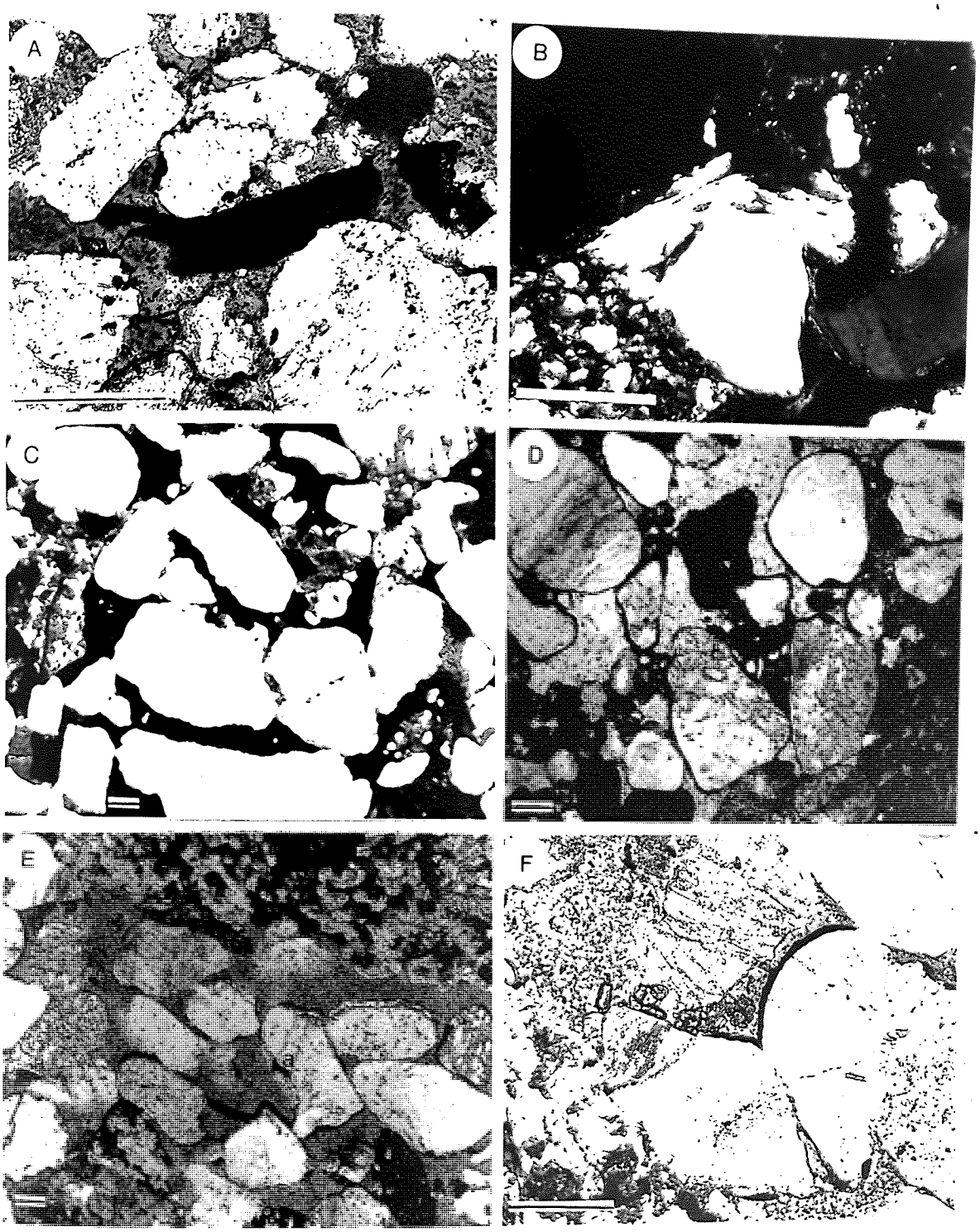

Plate 3.6 Thin section photomicrographs of the haematitic clay coatings

A. Almost complete replacement of biotite flake by haematite, PPL, BH A14/25
B. Partially oxidized biotite with the concentration of haematite in area kinked due to compaction, XN, BH A14/25 (134.6m)
C. Haematitic iron oxide stained the interstitial matrix which fills the pore spaces and consequently affects the hydraulic properties of the rock, PPL, BH A11/1 (13.5m)
D. Haematitic clay oxide films (dark rim) covering detrital grains with uneven thickness and sometimes absent at grain contacts, PPL, BH A18/13
E. Haematitic iron oxide shown to be almost rare in the highly porous and permeable rock, where it fills pits on the detrital grain surfaces (a) or forms continuous films absent at grain contacts (b) half crossed nicols, BH A14/42 (81.2m)
F. Haematitic clay coatings shown to be absent at grain contacts indicating its post-depositional origin, PPL, BH A14/42

Scale bar = 200 μm

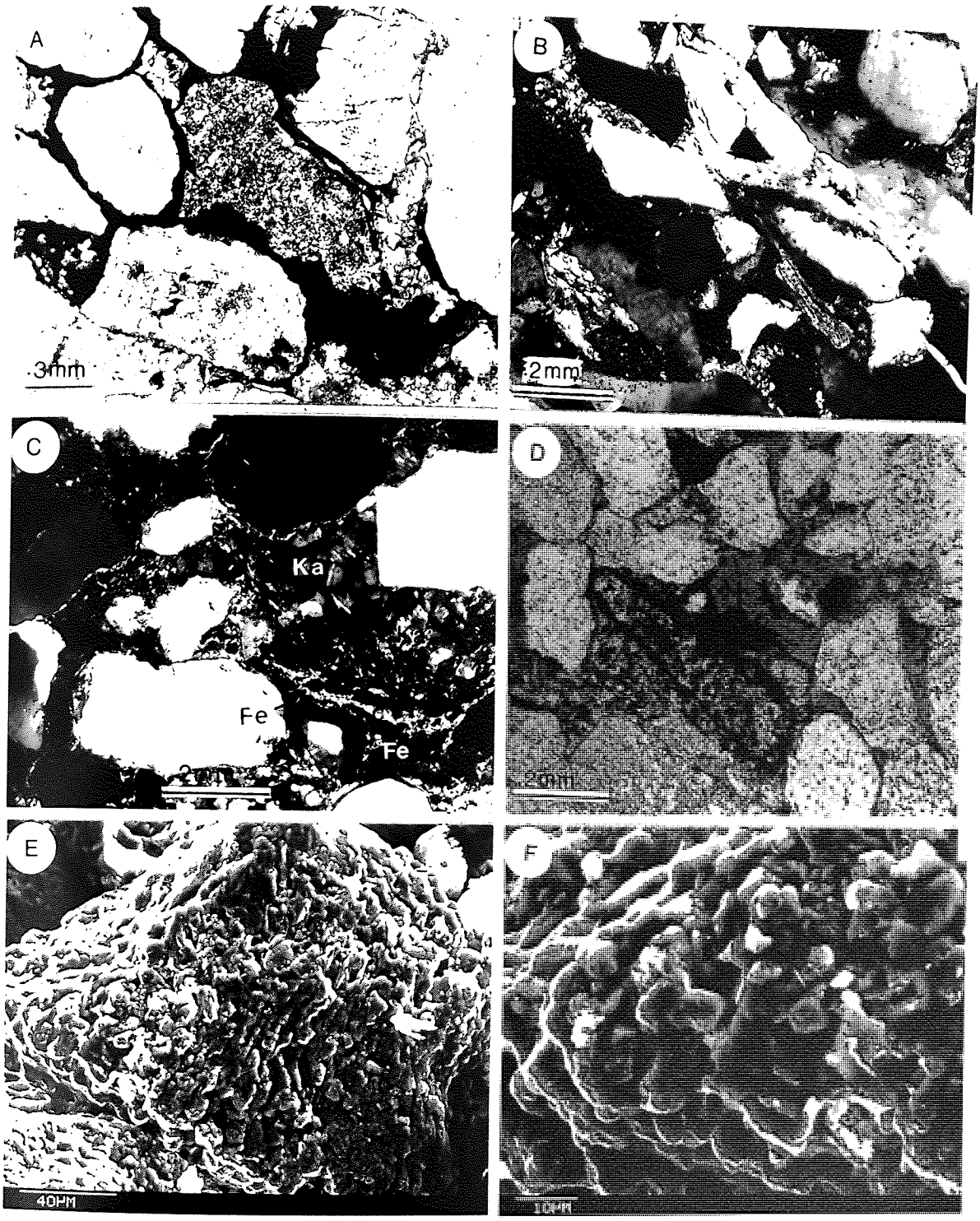

Plate 3.7 The haematitic clay coatings and the mechanically infiltrated clay

A. Interstitial haematitic pore fillings and linings greatly affect the hydraulic properties of the rock, PPL, BH A14/38 (89m)
B. Partially leached biotite flakes with the haematitic iron oxide concentrated along cleavage planes. Also compaction effect has been noticed from the bending of mica flakes, XN, BH A14/28 (130.35m)
C. Bended haematitic iron oxide lamina (Fe) associated with carbonate film (C), together with well-developed kaolinite (Ka) filled the pore spaces, XN, BH A14/29 (129.75m)
D. Association of haematitic iron oxide stains with the early diagenetic replacive dolomite, where dolomite probably replaced iron bearing silicate, PPL, BH A11/13 (59m)
E. Clay platelets oriented parallel to the grain surface, analogous to the mechanically infiltrated clay. SEM photomicrograph, BH A11/3 (22.7m)
F. Enlargement of the central left hand side part of E

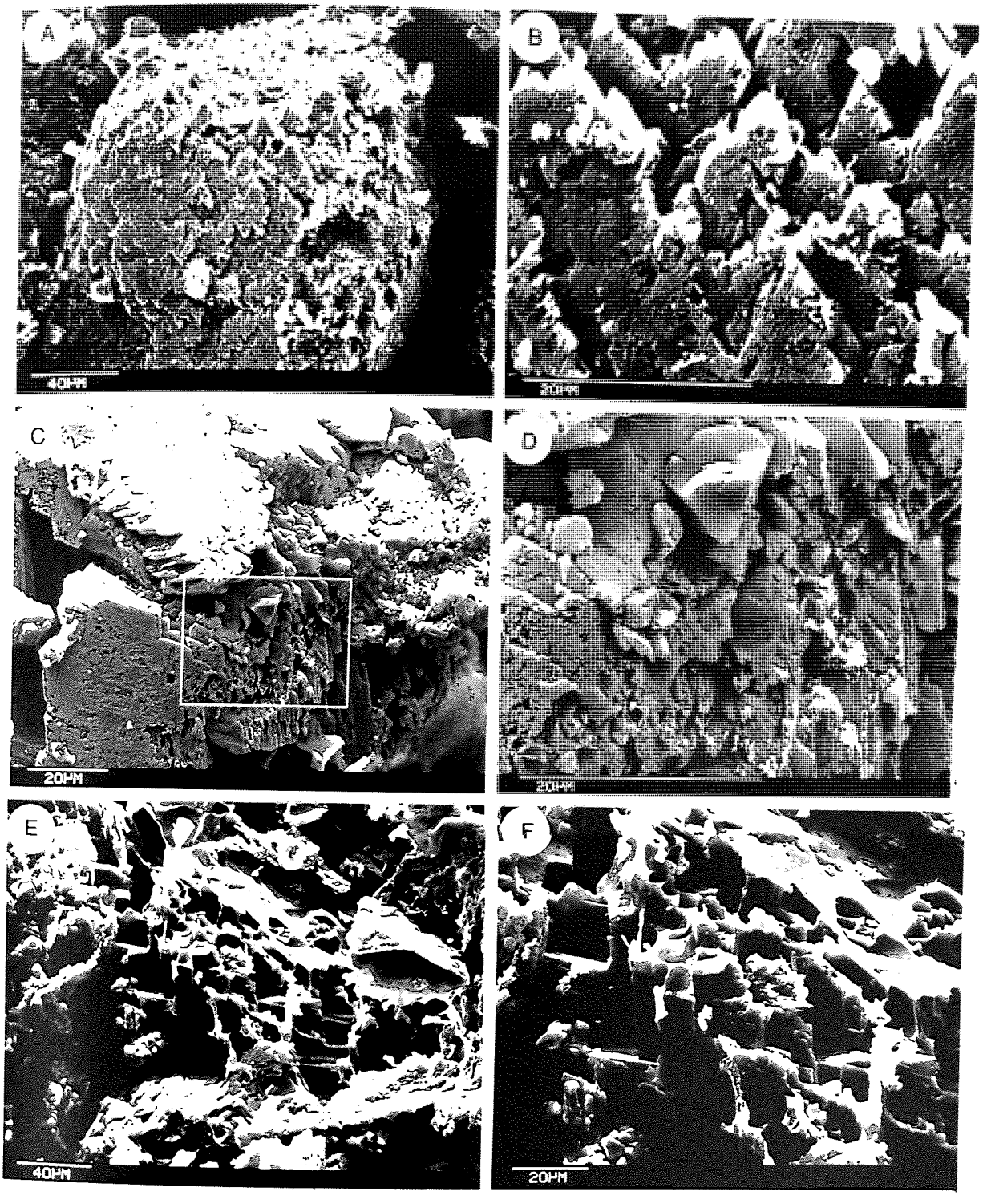

Plate 3.8 Dissolution features (All SEM photomicrographs)

A. K-feldspar grain showing v-shaped dissolution and hacksaw termination, BH All/3 (22.7m)
B. Enlargement of central area of A
C. K-feldspar overgrowth showing dissolution voids and needles, BH A18/2 (15m)
D. Enlargement of area outlined in C
E. Pore cast of secondary dissolution pores along cleavage planes of probably feldspar grain, BH A14/43 (78.8m)
F. Enlargement of central area of E

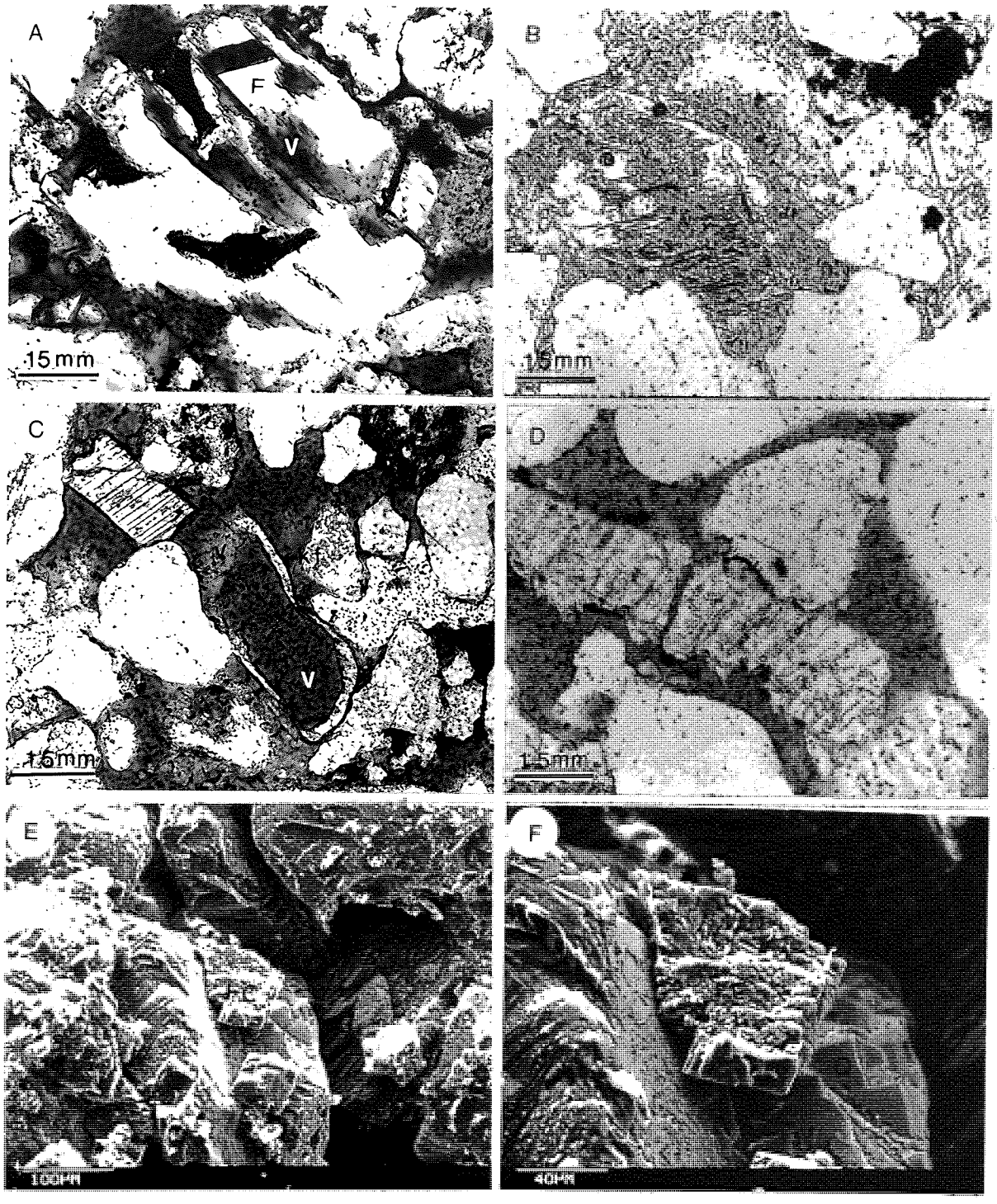

Plate 3.9 Dissolution features

A. Partially dissoluted feldspar grain (F), dissolution void (v) filled with araldite resin, thin section photomicrograph, PPL, BH A18/7 (104.5m)

B. Extensive and continuous dissolution affecting both detrital and authigenic feldspar and resulting in dissolution void (v), thin section photomicrograph, PPL, BH A18/2 (15m)

C. Dissolution effects, hollowed out the core (v) of probably feldspar grain and leaving only relicts of unaffected authigenic rim (kf), thin section photomicrograph, PPL, BH A14/25 (134.6m)

D. Dissolution along previously formed micro-fracture in feldspar grain, thin section photomicrograph, PPL, BH A18/2

E. Ferroan calcite cement (FC) affected by dissolution, SEM photomicrograph, BH A14/36 (92.2m)

F. Enlargement of central area of E

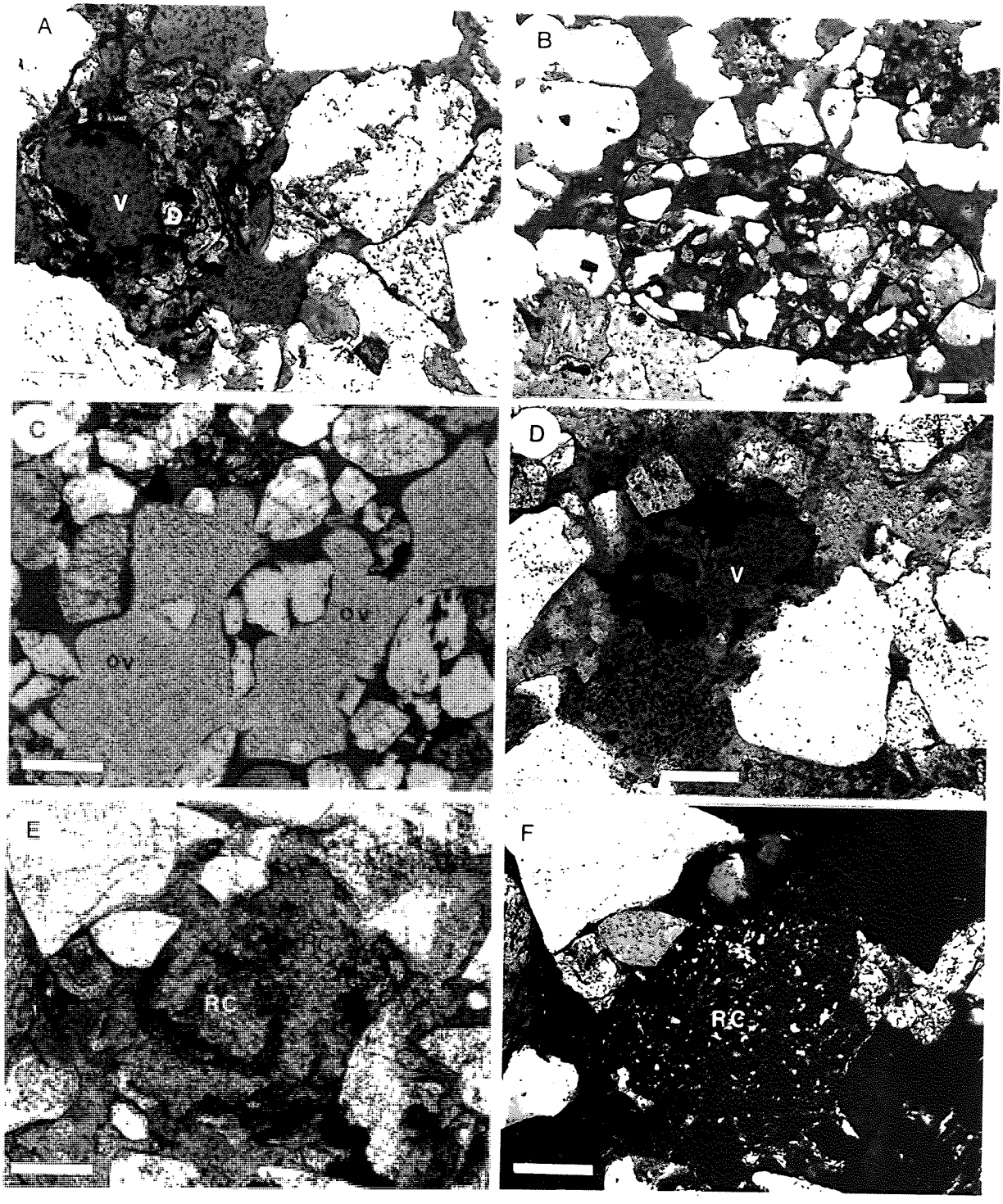

Plate 3.10 Dissolution and clay replacement features (All thin section photomicrographs)

A. Partial dissolution affecting replacive dolomite (D) and resulting in isolated dissolution void (V), PPL, BH A18/2 (15m)
B. Selective dissolution affecting detrital rock fragment (RF), PPL, BH A18/2
C. Oversized dissolution pores (OV), PPL, BH A14/32 (100.85m)
D. Extensive dissolution void (V) with remnants of the iron oxide coating, PPL, BH A14/25 (134.6m)
E. Detrital grain that has been replaced by clay (RC), PPL, BH A14/25
F. E in crossed nicols

Scale bar =150μm

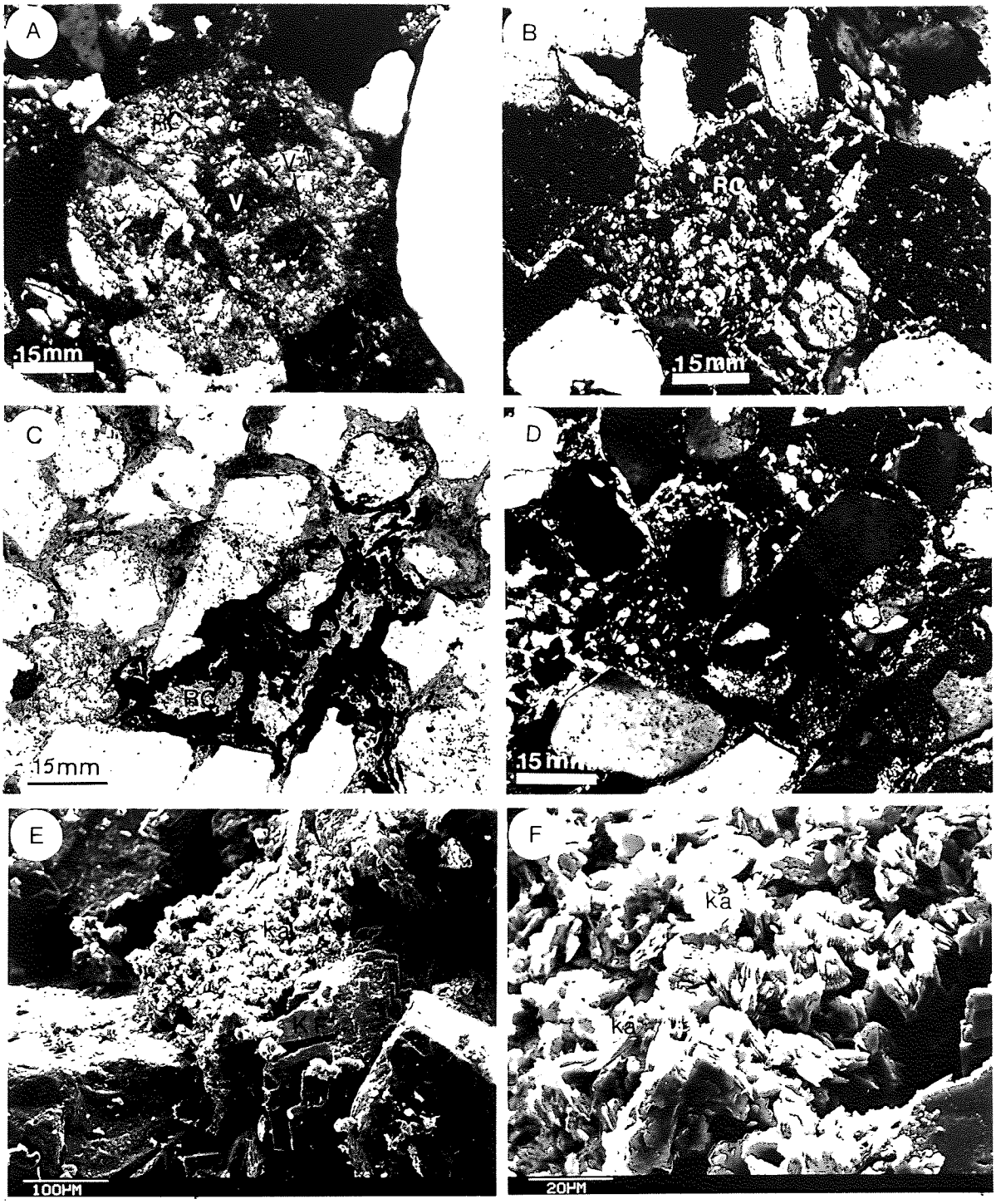

Plate 3.11 Clay replacement of silicate minerals

A. Detrital feldspar grain shown to be partially replaced by clay (RC) and partially dissolved, forming dissolution voids (V), XN, BH A18/13 (135 m)
B. Nearly complete replacement of a detrital silicate grain by clay (RC), thin section photomicrograph, PPL, BH A14/25 (134.6m)
C. Extensive replacement of a detrital silicate grain by clay (RC) and as a result of compaction the clay squeezed between the rigid framework grains decreasing both porosity and permeability, thin section photomicrograph, PPL, BH A18/6 (102.5m)
D. C in crossed nicols
E. K-feldspar grain and its overgrowth (KF) that has been partially dissoluted and partially replaced by kaolinite (Ka), SEM photomicrograph, BH A11/1 (13.5m)
F. Enlargement of central area of E

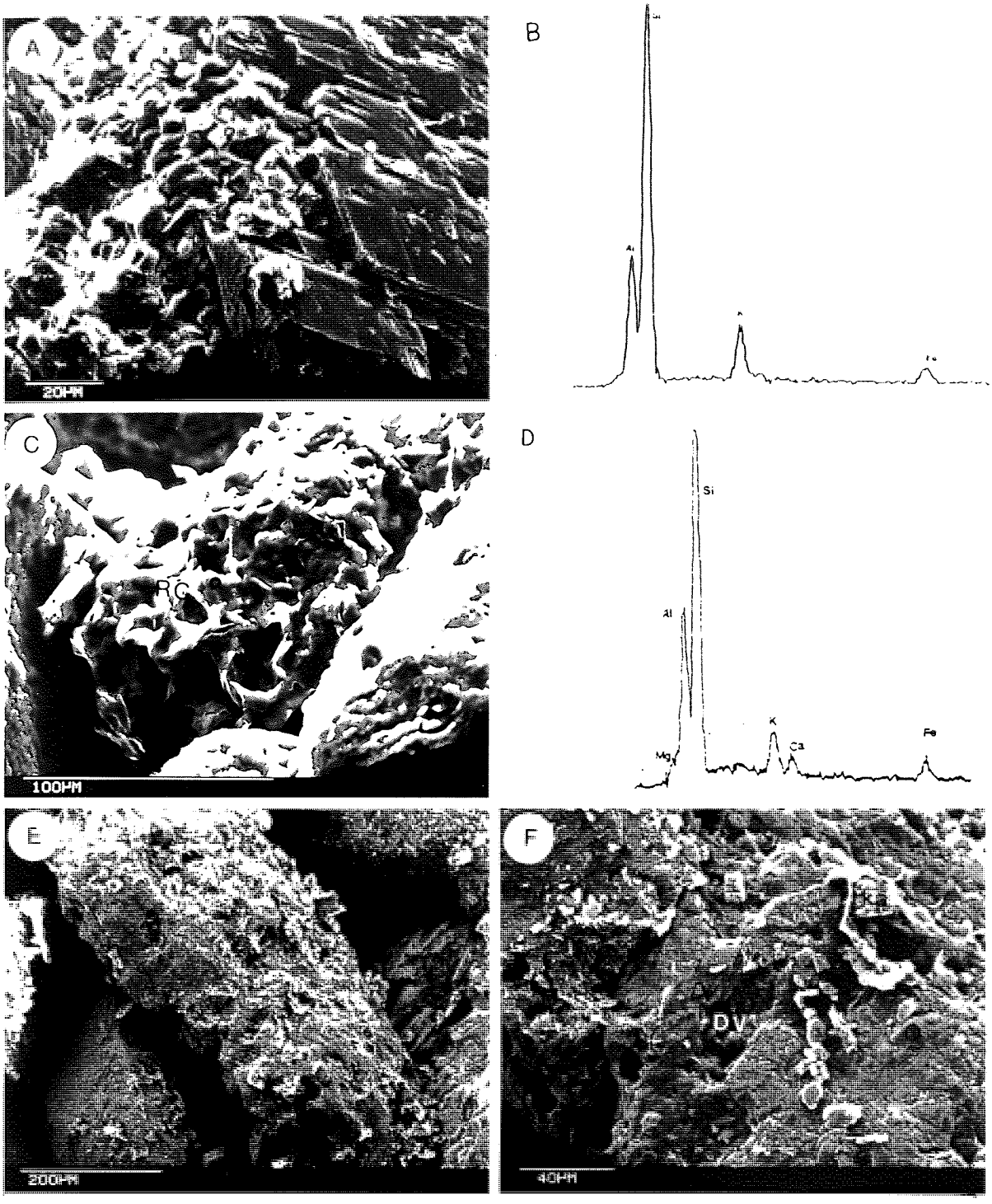

Plate 3.12 All SEM photomicrographs of clay replacement and dissolution

A. K-feldspar grains and their overgrowths (KF) shown to be partially replaced by kaolinite (Ka) and illite (I), BH A14/39 (85.3m)
B. EDAX spot analysis of the marked clay flake in A, indicating a composition of probably illite
C. Complete replacement of detrital grain by clay (RC), BH A11/3 (22.7m)
D. EDAX spot analysis of the marked flake in C, indicating a composition of probably mixed layer clay
E. Detrital grain that has been partially affected by dissolution (DV) and clay replacement (RC) together with the development of authigenic quartz (Q) and kaolinite (Ka) on its surface, BH A11/1 (13.5m)
F. Enlargement of central area in E

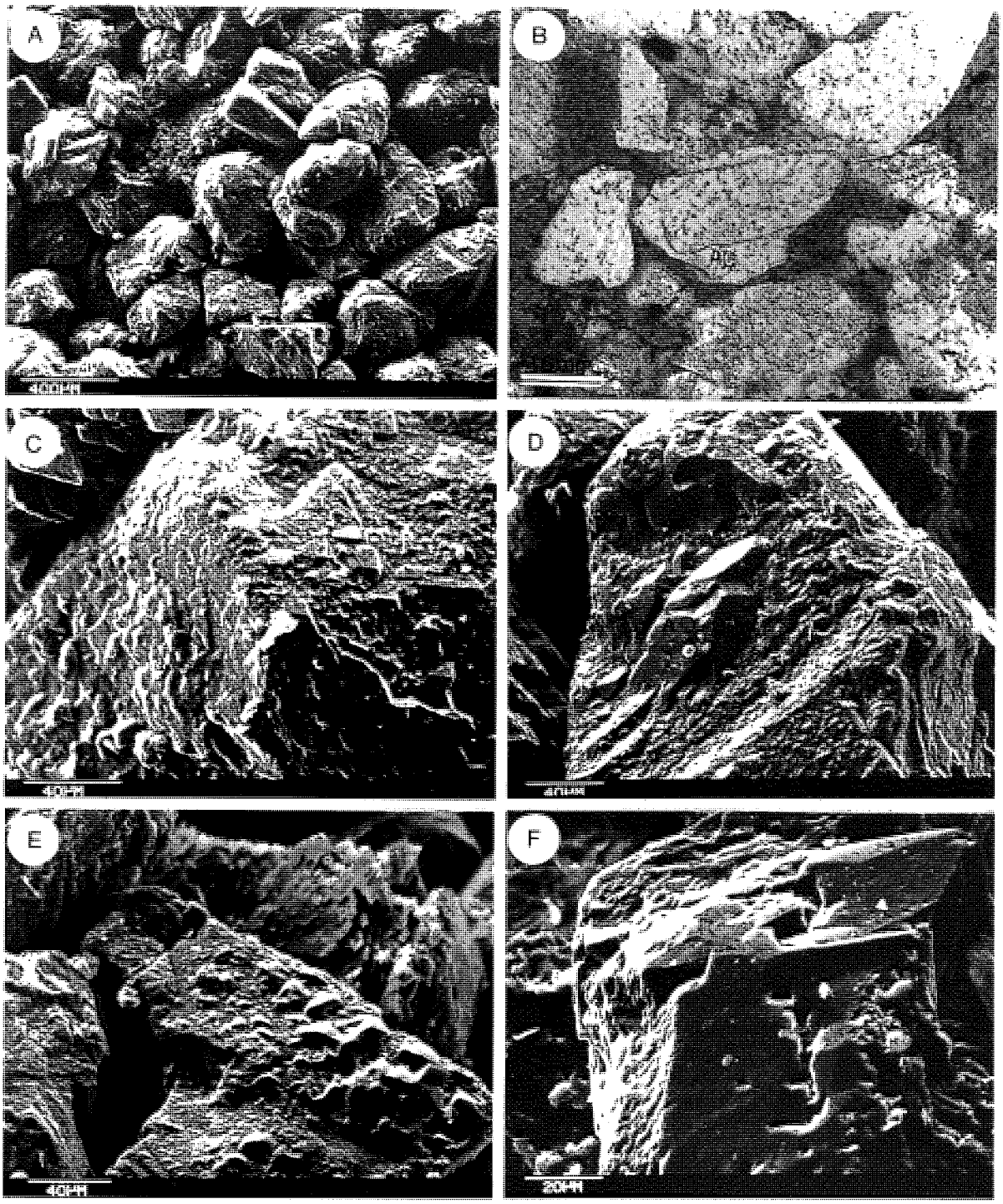

Plate 3.13 Authigenic quartz

A. Authigenic quartz and feldspar in the Sherwood Sandstone, and their minor effect on the hydraulic properties, SEM photomicrograph, BH A14/44
B. Haematitic clay coating defined the boundary between detrital and authigenic quartz, thin section photomicrograph, PPL, BH A14/25 (134.6m)
C. Incipient authigenic quartz crystals (AQ) developed on detrital quartz core, SEM photomicrograph, BH A14/44 (75.7m)
D. Merging and connection of rhombohedral crystals of authigenic quartz (AQ), SEM photomicrograph, BH A14/44
E. Merging of the incipient prismatic projections of authigenic quartz, SEM photomicrograph, BH A11/3 (22.7m)
F. Merging of irregular overgrowths resulted in the development of incomplete crystal faces (holes in the overgrowth surfaces), SEM photomicrograph, BH A14/39 (85.3m)

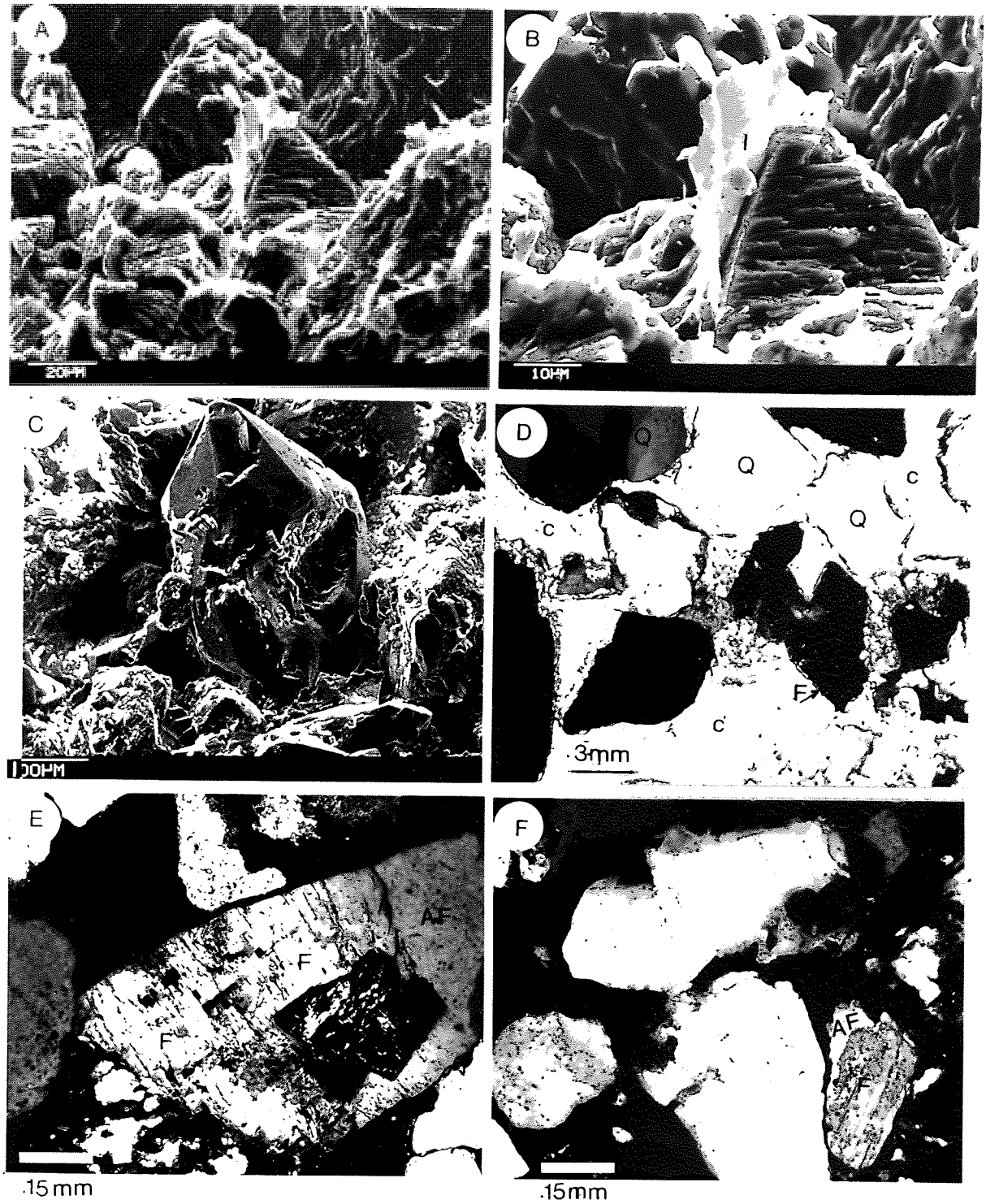

Plate 3.14 Authigenic quartz and feldspar

A. Different orientation of authigenic quartz (AQ) over a detrital polycrystalline quartz core. Authigenic acicular and flaky illite (I) shown to be developed following quartz and feldspar respectively, SEM photomicrograph, BH A14/27 (130.8m)
B. Enlargement of central area of A
C. Nearly complete quartz overgrowth showing the double pyramidal termination of prism faces, SEM photomicrograph, BH A14/44 (75.7m)
D. Quartz (Q) and feldspar (F) shown to be partially replaced by calcite cement (C), thin section photomicrpgraph, XN, BH A14/29 (129.75m)
E. Authigenic feldspar (AF) in optical continuity with its detrital core (DF), thin section photomicrograph, XN, BH A14/25 (134.6m)
F. Optical discontinuity between detrital feldspar core (DF) and its authigenic overgrowth (AF), thin section photomicrograph, XN, BH A14/9 (185.4m)

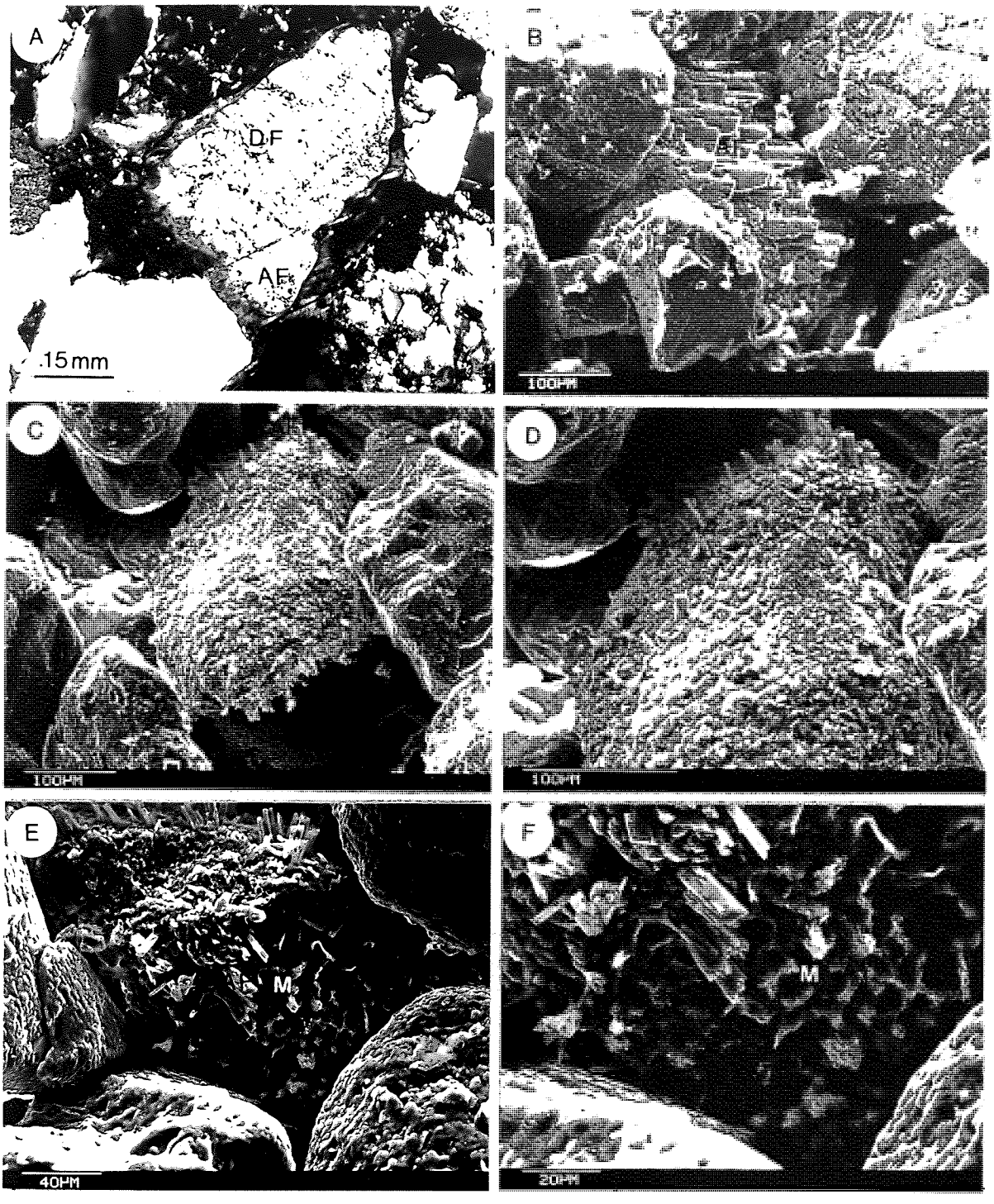

Plate 3.15 Authigenic K-feldspar

A. Reworked authigenic K-feldspar overgrowth (AF) in optical continuity with the detrital feldspar core (DF), thin section photomicrograph, XN, BH A14/37 (89.5m)
B. Authigenic K-feldspar (AF) filling the pore spaces, SEM photomicrograph, BH A14/36 (92.2m)
C. Tabular prismatic crystals of authigenic K-feldspar (AF) oriented perpendicular to the detrital grain surfaces, SEM photomicrograph, BH A11
D. Enlargement of central area of C, BH A11/3 (22.7m)
E. Rhombohedral and elongated tabular crystals of authigenic K-feldspar (AF) forming part of the interstitial matrix (M). EDAX spot analysis of the matrix indicate its composition of Si, Mn, Fe and Al, SEM photomicrograph, BH A11/9 (52m)
F. Enlargement of central area of E

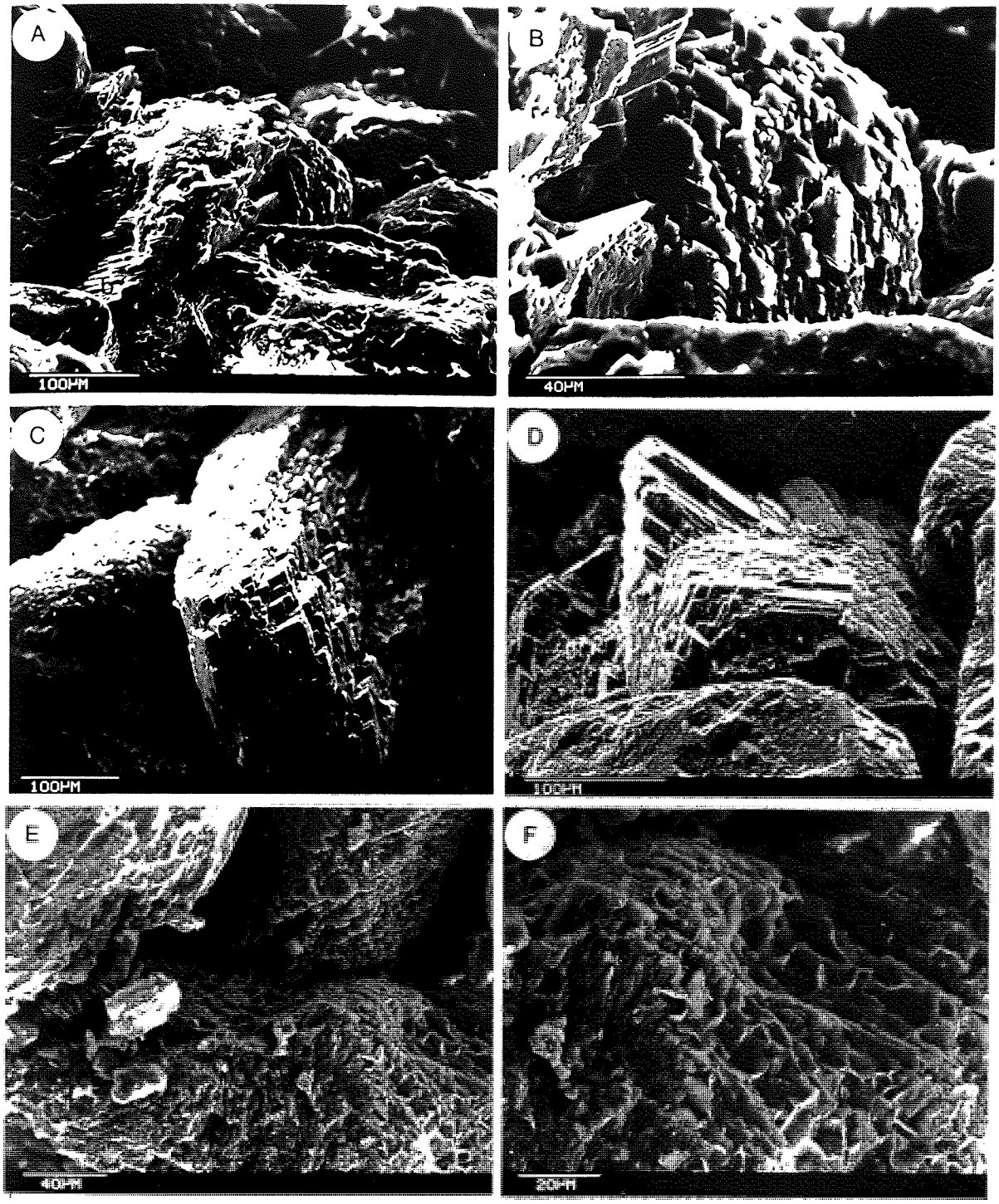

Plate 3.16 Authigenic K-feldspar and authigenic clay (All SEM photomicrographs)

A. Oriented rhombohedral crystals of authigenic K-feldspar over detrital grain surfaces (a), also complete blocking of pore spaces by authigenic K-feldspar was in area marked (b), BH A11/3 (22.7m)
B. Enlargement of area marked (a) in photomicrograph A
C. Authigenic K-feldspar covering completely the detrital core, BH A14/44
D. Merging and stacking of authigenic K-feldspar crystals resulting in complete enclosure of the detrital core, BH A14/44 (75.7m)
E. Development of authigenic illite (I) on dissoluted authigenic K-feldspar (AF), BH A11/3 (22.7m)
F. Enlargement of central area of E

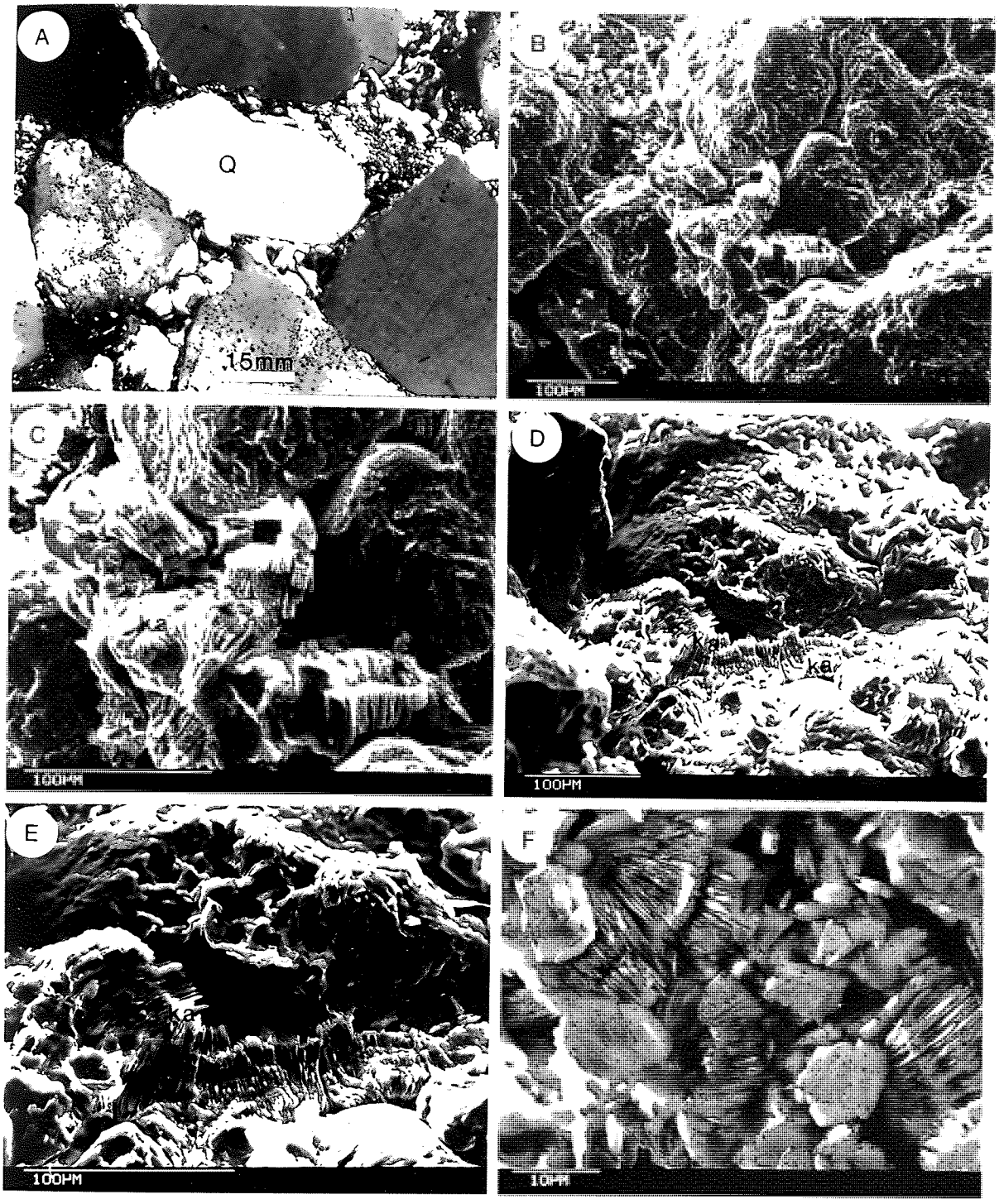

Plate 3.17 Authigenic kaolinite

A. Well-developed authigenic kaolinite filling the pore spaces and decreasing porosity and permeability, thin section photomicrograph, XN, BH A14/29 (129.75m)
B. Pseudohexagonal platy crystals of kaolinite (Ka) stacked together blocking pore spaces and pore throats and consequently affecting the hydraulic properties of the rock, SEM photomicrograph, BH A11/3
C. Enlargement of central area of B
D. Authigenic kaolinite (Ka) as pore lining decreasing the effective pore radius and consequently the rock permeability, SEM photomicrograph, BH A11/3 (22.7m)
E. Enlargement of central area of D
F. Pseudohexagonal platy crystals of kaolinite filling pore spaces, SEM photomicrograph, BH A14/36 (92.2m)

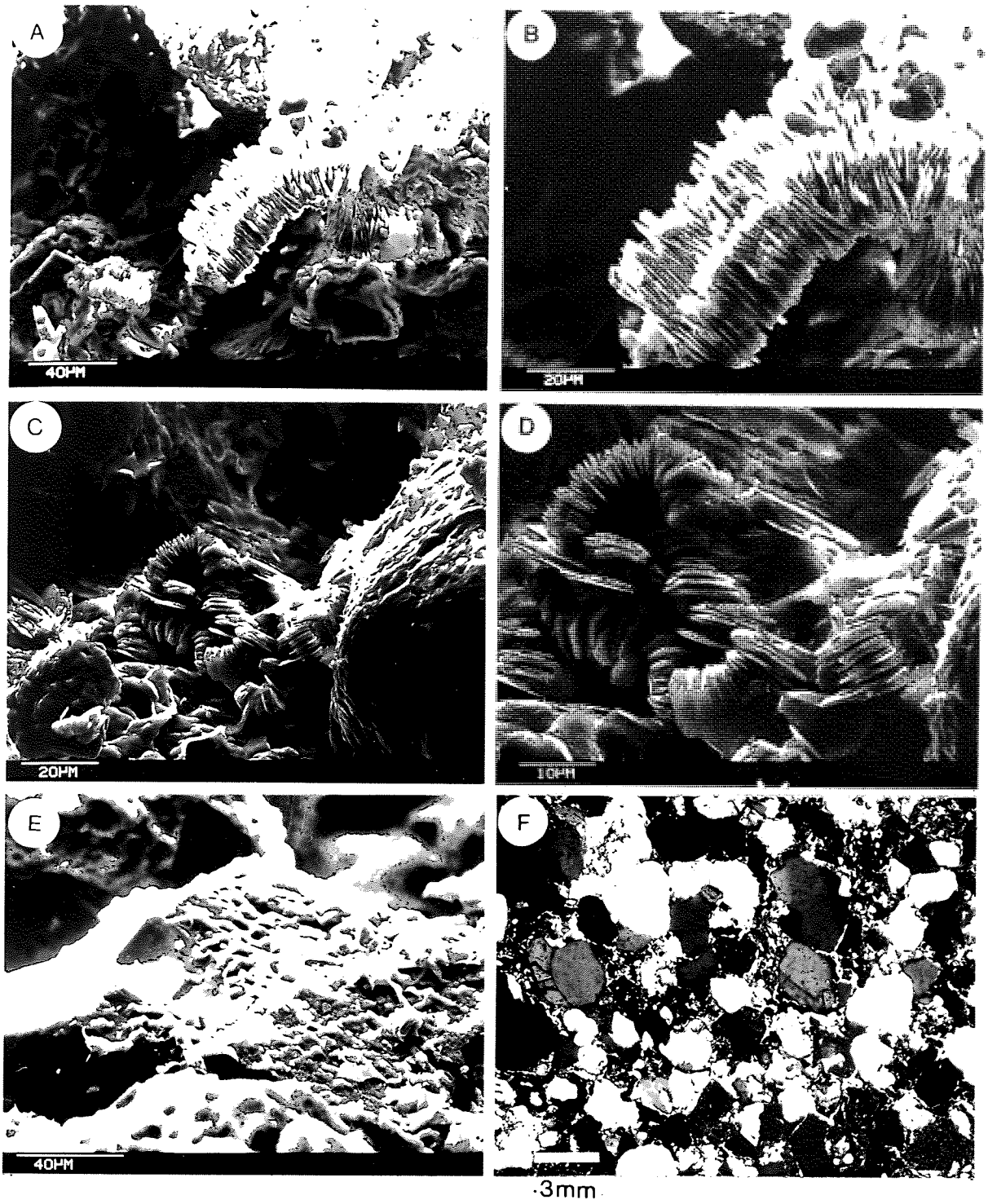

Plate 3.18 Authigenic clay

A. Well-developed vermicular kaolinite forming bridge by connecting the detrital grains, SEM photomicrograph, BH A14/36 (92.2m)
B. Enlargement of central area of A
C. Stacked pseudohexagonal platy crystals of kaolinite forming rose-like shape, SEM photomicrograph, BH A14/36
D. Enlargement of central area of C
E. Absence of authigenic clay at grain contacts, SEM photomicrograph, BH A14/27 (130.8m)
F. Authigenic clays present as pore linings, almost absent at grain contacts and also briding detrital framework grains, thin section photomicrograph, XN, BH A18/6 (102.5m)

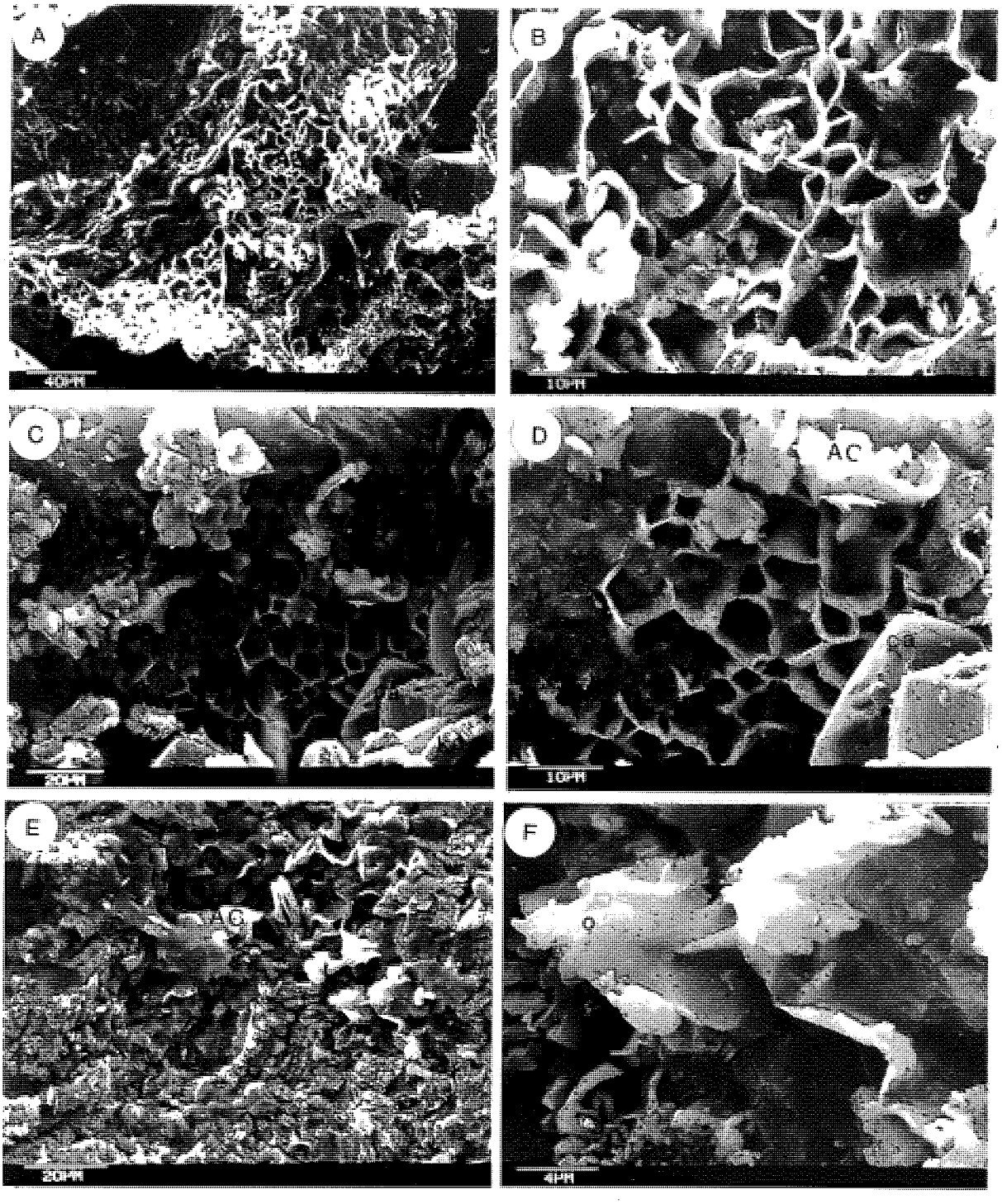

Plate 3.19 Authigenic clay (all SEM photomicrographs)

A. Authigenic clay (AC) covering the surfaces of detrital grain and characterized by the boxwork texture of illite (I), BH A11/3 (22.7m)
B. Enlargement of central left hand side area of A
C. Authigenic clay flakes which display the boxwork texture characterized illite (I) and sometimes a curly appearance (AC).(EDAX spot analysis indicatesthe presence of Ca, Mg, Si, Al and Fe) Authigenic kaolinite (Ka) and calcite (Ca) shown to be followed the authigenic clay, BH A11/3
D. Enlargement of central area of C
E. Authigenic clay (AC) flakes display the wavy appearance, BH A11/3
F. Enlargement of the central right hand side area of E. The EDAX spot analysis of marked flake indicates its composition of Si, Al, K and Fe elements

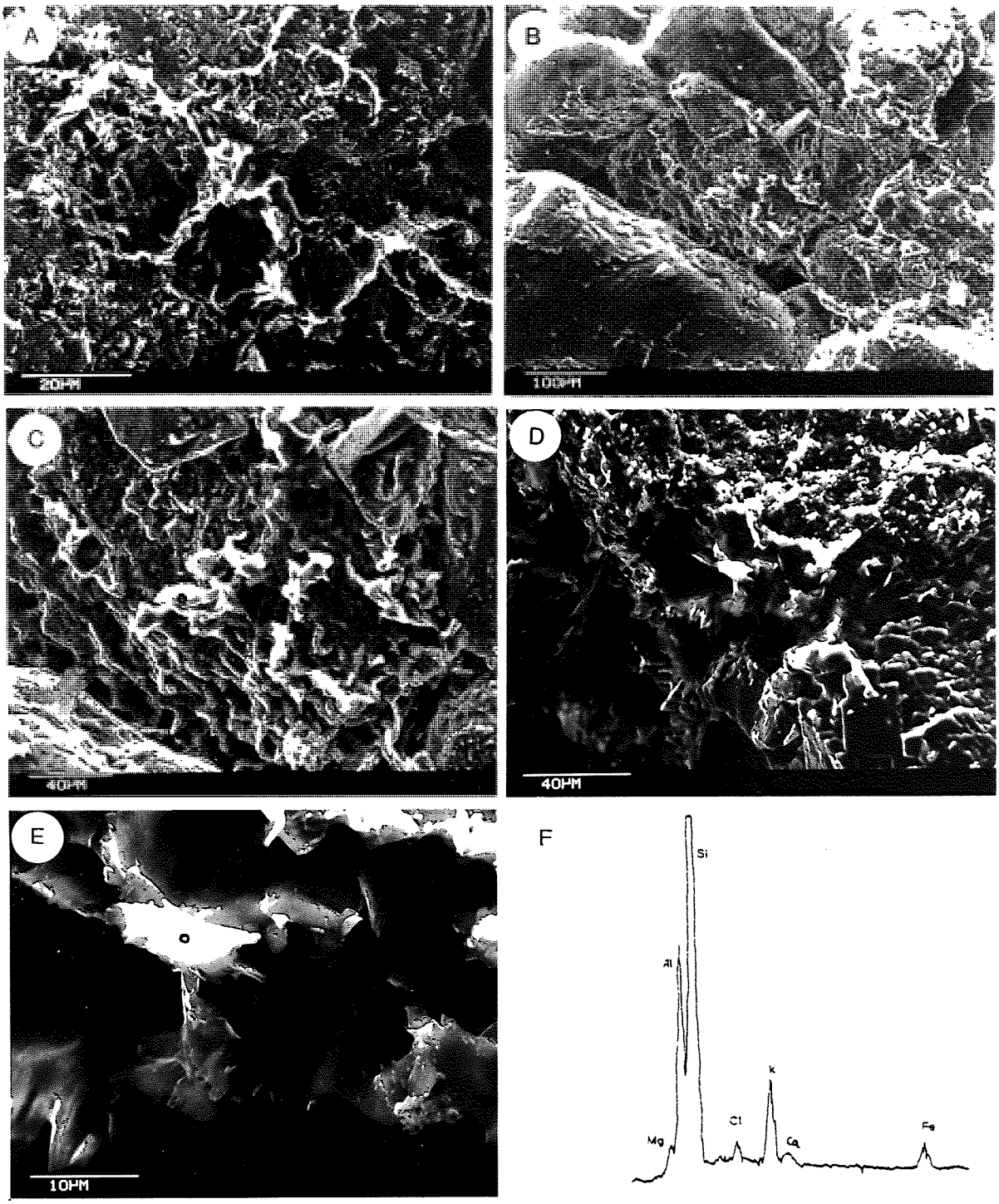

Plate 3.20 SEM photomicrographs for authigenic clay

A. Authigenic clay flakes display the curly appearance, developed on the surfaces of the detrital grains and bridging the framework grains, BH A11
B. Authigenic clays developed on the surfaces of the detrital grains where clay flakes display wavey or curly appearance, BH A11/3 (22.7m)
C. Enlargement of central area of B, and DEAX spot analysis of the marked flake indicate a composition similar to that in F.
D. Authigenic clay flakes characterized by wavey and sometimes flame-like appearance, BH A14/26 (133.2m)
E. Enlargement of central area of D
F. DEAX spot analysis of the marked flake in E where its composition may indicate mixed layer I/S clay

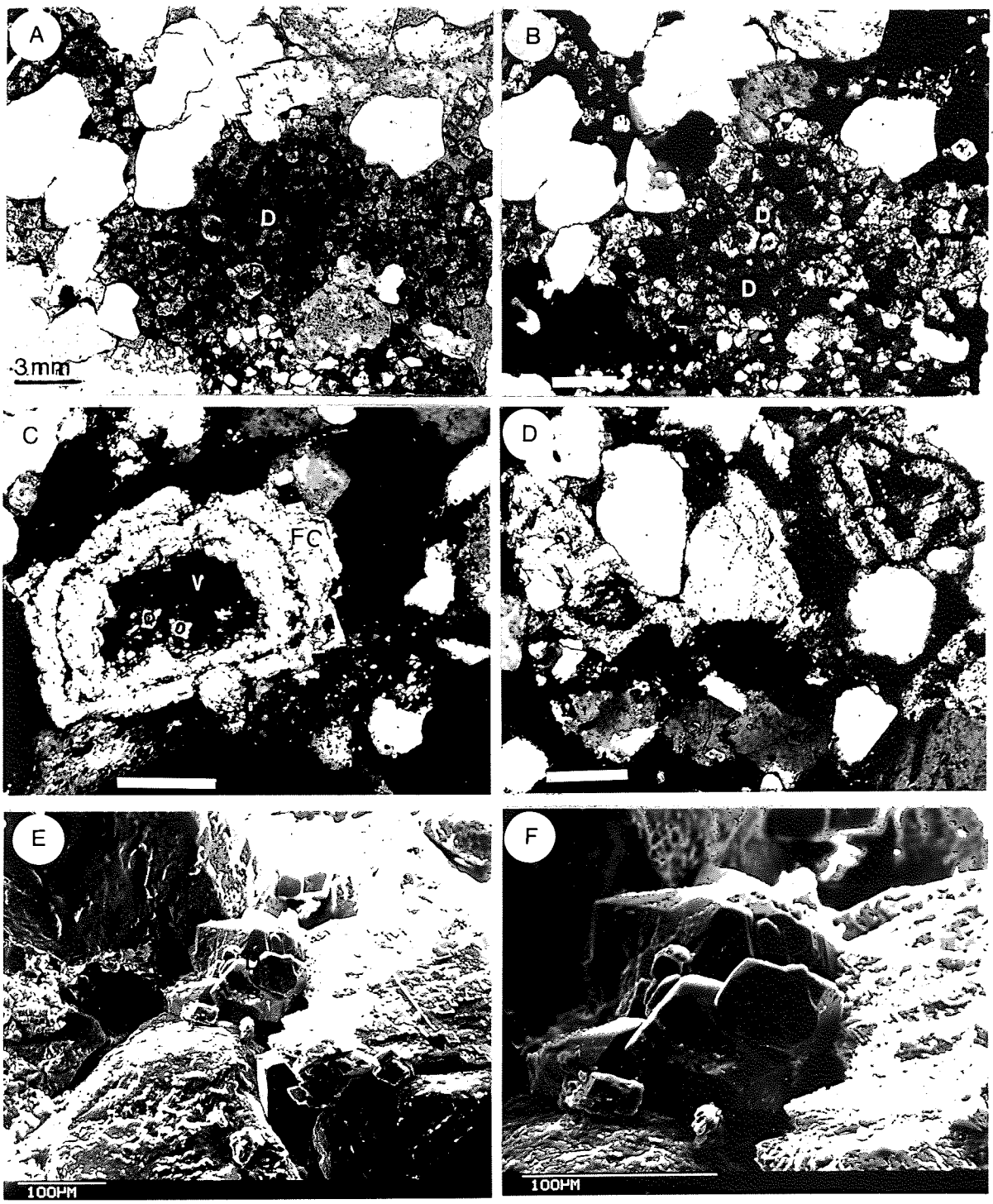

Plate 3.21 Carbonate cement

A. Clusters of zoned dolomite rhombs (D) stained with haematitic iron oxide, filling the pore spaces and drastically decreasing porosity and permeability of the rock, thin section photomicrograph, PPL, BH A18
B. A in crossed nicols, BH A18/3 (19.5m)
C. Ferroan calcite cement (FC) replaced previously dissolved grain with relicts of dolomite rhombs (D) and dissolution voids (V). This type of cement decreases the permeability by sealing off the dissolution pores, thin section photomicrograph, XN, BH A11/13 (59m)
D. Carbonate cement replaced previously dissolved detrital grain with the preservation of the haematitic clay oxide film (dark rim), thin section photomicrograph, XN, BH A11/13
E. Dolomite rhombs (D) well developed filling the pore spaces, SEM photomicrograph, BH A11/3 (22.7m)
F. Enlargement of central area of E

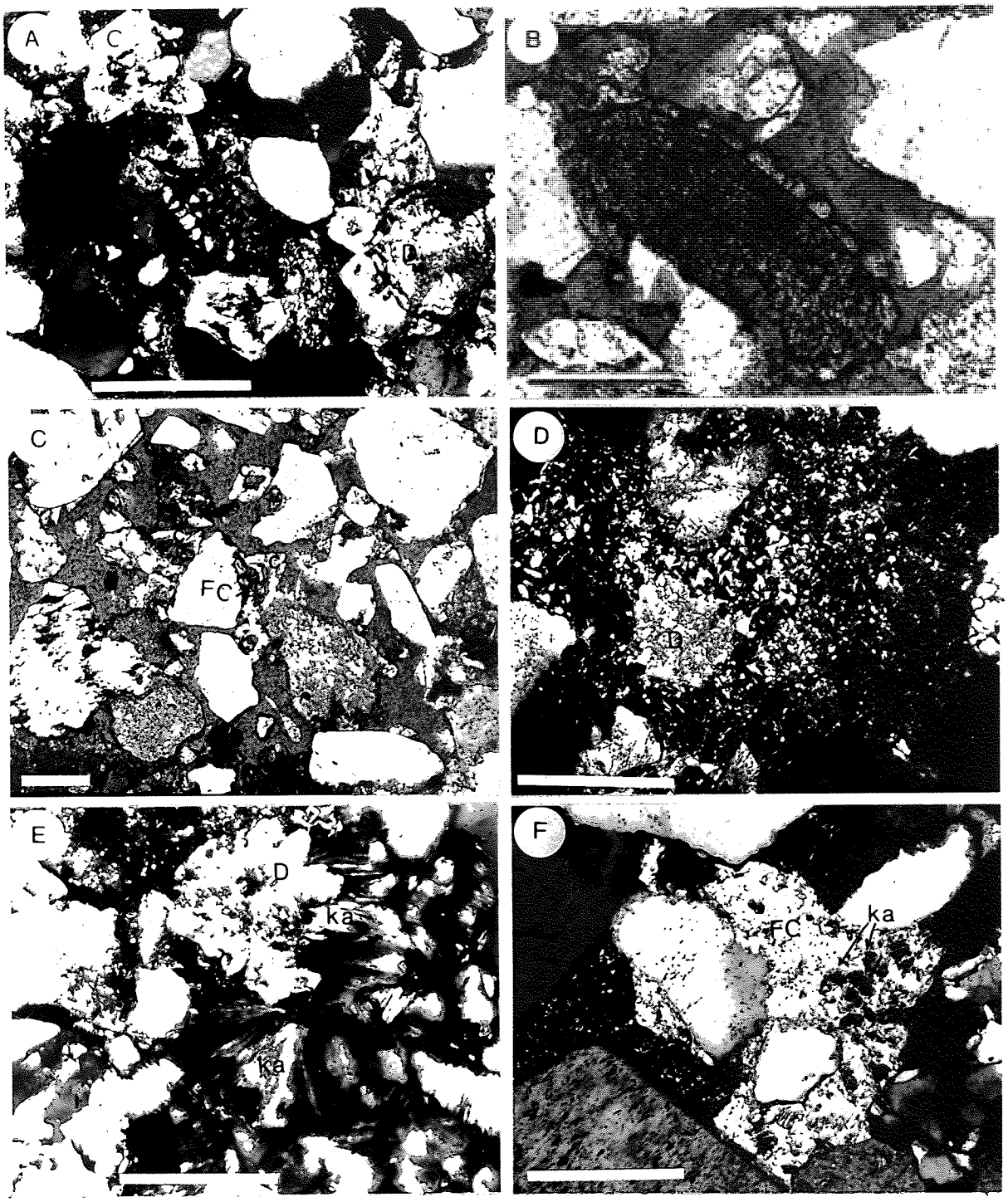

Plate 3.22 Carbonate cement and authigenic minerals sequence (All thin section photomicrographs)

A. Zoned dolomite cement (D), together with calcite (C) and ferroan calcite (FC) blocking the pore spaces, XN, BH A11/9 (52m)
B. Ghost grain of dolomite, PPL, BH A3/5 (18m)
C. Disseminated rhombs of calcite (C) with sometimes ferroan calcite core (FC), PPL, BH A18/2 (15m)
D. Relicts of dolomite (D) occurred within kaolinite matrix (Ka), XN, BH A14/30 (129.25m)
E. Well developed kaolinite crystals (Ka) shown to be eating the edges of previously formed dolomite (D), XN, BH A11/2 (15m)
F. Relicts of kaolinite (Ka) occurred within a ferroan calcite cement (FC), indicating the paragenetic sequence of these authigenic minerals, XN, BH A11/4 (29.5m)

Scale bar=.3mm

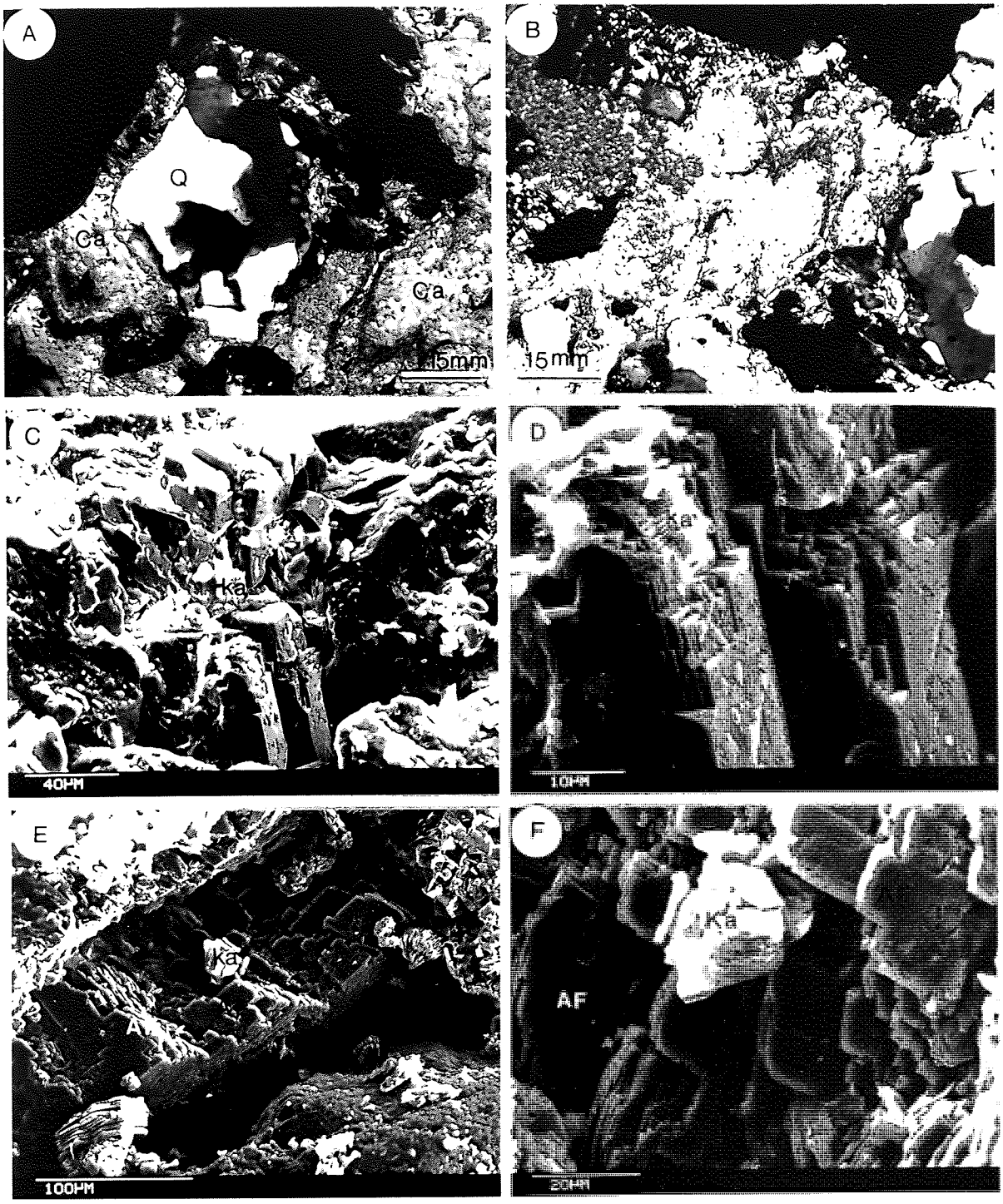

Plate 3.23 Paragenetic sequence of authigenic minerals

A. Relicts of well developed kaolinite (Ka) preserved within a replacive calcite cement (Ca), also calcite shown to be reacting with periphery of the quartz grain (Q), thin section photomicrograph, XN, BH A18/4
B. Calcite cement replaced probably dolomite as indicated from the preservation of the rhombic shape of the dolomite, thin section photomicrograph, XN, BH A18/4 (33.5m)
C. Authigenic kaolinite (Ka) precipitated penecontemporaneously or after calcite precipitation, SEM photomicrograph, BH A14/39 (85.3m)
D. Enlargement of central area of C
E. Authigenic feldspar (AF) shown to be followed by kaolinite (Ka), SEM photomicrograph, BH A11/1 (13.5m)
F. Enlargement of central area of E

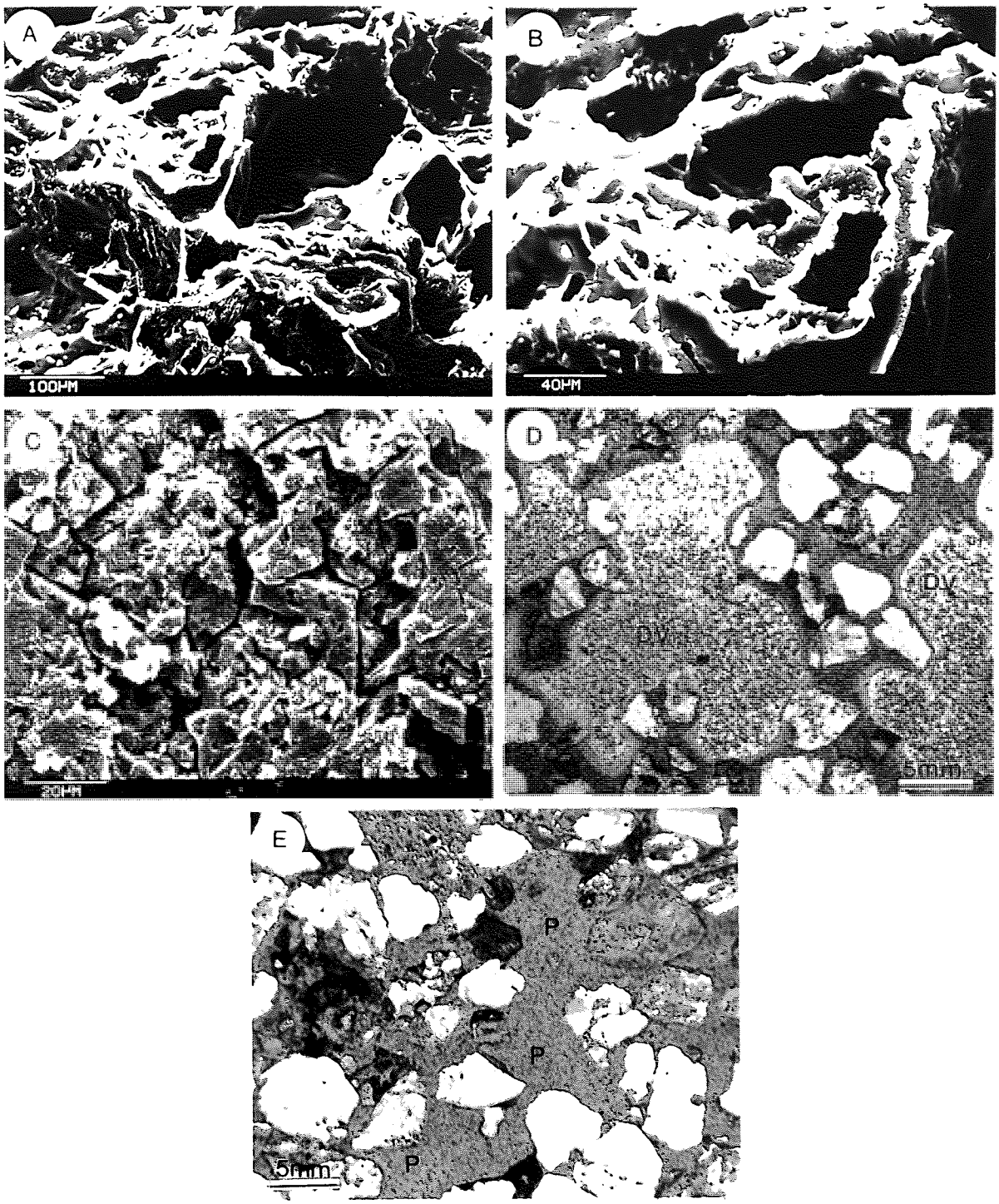

Plate 3.24 Different types of pores

A. Resin pore cast of highly interconnected, sheet like pore spaces in the Sherwood Sandstone, SEM photomicrograph, BH A14/43 (78.8m)
B. Enlargement of central area of A
C. Secondary shrinkage porosity in dolomite rock fragment, probably due to dolomitization, SEM photomicrograph, BH A18/1 (4.7m)
D. Over sized dissolution voids (DV), thin section photomicrograph, PPL, BH A14/35 (94.6m)
E. Interconnected pore spaces (P) more likely of dissolution origin, thin section photomicrograph, PPL, BH A14/38 (89m)

CHAPTER FOUR

POROSITY AND HYDRAULIC CONDUCTIVITY

4.1 INTRODUCTION

Porosity and permeability (more recently known as hydraulic conductivity) are the two most important factors controlling ground water movement. Both these aspects depend upon the nature of the interstices or voids between the solid fragments or framework components of the rock. A rock is called porous if it contains voids or pores between its framework components. The ratio of the volume of pore spaces to the total volume of the rock is called porosity (ϕ) and is usually expressed as a percentage:

$$\phi\ (\%) = \frac{\text{Volume of pore}}{\text{Total volume of sample}} \times 100 \qquad 4.1$$

Pores are created by different geological processes, and it is usual to distinguish primary and secondary porosity. The primary porosity results from voids which are left between the grains after deposition. Secondary porosity develops after the lithification of the rock and includes features such as fractures, fissures, joints and pores formed by dissolution of framework grains, authigenic minerals or pore-filling cements.

In this study the effect of secondary features cannot be neglected because they have an important influence on the hydraulic properties of the rocks. Both fractures and fissures are abundant in sandstone and associated mudstone beds and can be recognized from lithological and geophysical logs. Also solution voids are abundant mostly on a microscopic scale particularly in boreholes A11, A14 and A18 as

previously dealt with in Chapter Three. Macroscopic dissolution textures are also present notably in borehole A3 where openings and vugs are very common.

Permeability or hydraulic conductivity is defined as the ability of rock to transmit water under the influence of a pressure gradient. It is quantitatively expressed by the empirical relationship first recognized by the French hydrologist "Darcy" (1856), as the coefficient of permeability (K):

$$Q = - KA \frac{dh}{dl} \qquad 4.2$$

where Q is the flow rate, A is the cross-sectional area of flow and dh/dl is the hydraulic gradient. K is the permeability coefficient or hydraulic conductivity.

In this chapter the results of porosity and hydraulic conductivity studies using a variety of different methods will be presented. These methods include: a) water resaturation for measuring effective porosity, b) Hg-penetration method for the measurement of pore-size distribution, porosity and derivation of calculated permeability, c) a micro-photographic method of image analysis to measure pore-area, pore-shape and also to calculate porosity, and d) measurement of hydraulic conductivity using a falling head permeameter.

The study is based upon fifty samples collected from the four boreholes - A3, A11, A14 and A18 - within the Triassic red-bed aquifer and includes representatives of both Lenton Sandstone Formation and Nottingham Castle Formation of the Sherwood Sandstone Group. One sample from the Mercia Mudstone Group is also included.

The work reported in this chapter is designed to characterize the hydrological properties of the Sherwood Sandstone Group, and to reconcile the laboratory results with the results from the different geophysical logs. It is also an attempt to explain the effects of lithological (sedimentological and diagenetic) features upon the hydrogeological characteristics of this aquifer.

4.2 POROSITY

Porosity is one of the well-known physical characteristics of reservoir rocks or aquifers and one of the factors controlling the accumulation, migration and distribution of water, gas or oil in rocks. It is defined by the American Society for Testing and Materials (1961) as the ratio of the volume of voids of a given mass to the bulk volume of that mass. Those spaces which are not occupied by solid materials are known as pores, voids, pore-spaces or interstices. Those interstices or connected pore-spaces are of fundamental importance to the study of groundwater because they act as water conduits. According to their size, interstices may be classified as subcapillary, capillary and supercapillary. Subcapillary pores are so small that water is held within them mainly by adhesive forces, in capillary pores water is held mainly by surface tension. Supercapillary pores are larger than capillary ones.

Porosity can also be classified quantitatively into absolute (total or overall) and effective porosity. Absolute porosity is the measurement of the total volume of pore-spaces whilst the effective porosity is the volume of the connected pores only. Effective porosity is an indication of conductivity to fluid but not always a measure of it (Pirson, 1958).

Interconnected pores are saturated with ground water in the zone of saturation, and porosity in this case is a measure of the quantity of water contained per unit volume (Todd, 1959). But not all this quantity of water can be removed from a well by drainage or pumping. The amount of water which is free to drain from the rock by gravity is called specific yield, and is sometimes considered as effective porosity (Johnson, 1967). However, the definition of effective porosity by Todd (1980) is preferred in this work, which is the sum of the specific yield and specific retention, where specific retention is the part of water which is held to the solid material or retained against gravity (Meinzer, 1923):

Effective Porosity = Specific Yield + Specific Retention.

In this chapter we will deal mainly with the effective porosity although in moderate to high porosity rocks of the type under consideration there is little significant difference between effective and total porosity because almost all of the pores are interconnected. In low porosity rocks, however, the significant difference is high due to the restricted number of interconnected pores present.

4.2.1 Porosity Measurement and Results

There are a variety of methods for determining effective porosity. These include the determination of bulk volume and apparent grain volume; from which pore volume can be calculated and the direct measurement of the connected pore volume. In this study, the liquid resaturation method using deaerated distilled water as a displacing liquid has been used. The Hg injection method using Hg porosimeter was also used for pore-size distribution and porosity measurements.

Also a trial has been made for thin section porosity determination from seven representative samples using a simple method of image analysis.

The precision of the results depend on the method being used. However, the results of laboratory porosity measurements cannot be expected to correspond exactly with in situ conditions because of:

(1) Possible relaxation of cores due to release of over-burden and water pressure.

(2) The effect of hydraulic and mechanical processes in coring.

(3) Changes in clay minerals as a result of shrinking of some clays during the analysis, the conversion from one clay type to another, and the flushing of clay during the coring process. The high pressure in Hg injection method may also cause changes in the nature of pore-solids arrangement.

(4) The limitation of sampling which should be representative of the whole reservoir rock. This may not be so, especially when the reservoir rocks are very heterogeneous.

4.2.1.1 Liquid resaturation method

Fifty representative samples from the four boreholes were chosen and 1 inch (2.54 cm) diameter cores were cut perpendicular to the original core axes i.e. nearly parallel to the bedding planes. The surface of the samples were carefully cleaned by rinsing with water in order to prevent clays and cuttings from plugging the porous surfaces. The lengths of the cores ranged between 2.54 and 6.9 cm depending upon the nature of the sample.

The samples were oven-dried overnight at a temperature of 90-100°C. The dry, clean samples were then allowed to cool at room temperature in a desiccator containing dehydrated silica gel to remove any water vapour from the dry samples. These dry cores were used for measuring effective porosity as well as hydraulic conductivity.

The following procedure was used in determination of porosity:

(1) The clean, oven-dried cores were weighed in air separately to the nearest 0.0001 gm, (W).

(2) The weighed samples were then placed in the vacuum desiccator and the system evacuated for about 3-4 hours to less than 0.02 Torr.

(3) The desiccator was then isolated and deaerated distilled water was drawn slowly into the evacuated system. The cores were allowed to saturate by capillary action so that the air trapped in the pores was kept to a minimum.

(4) After the samples had been completely submerged they were allowed to soak under vacuum for about one hour or until there was no visible evidence of air bubbles. The pressure in the desiccator was then returned to atmospheric pressure at that time the samples were ready to be weighed.

(5) The saturated samples were individually weighed in air (Ws), making sure that the surfaces of the samples were wiped to remove any excess water. This wiping should be done either by hand or very carefully by cloth or paper because both cloth or paper may cause the desaturation of the sample.

(6) Each sample was then weighed whilst submerged in water and the net submerged weight calculated (Wm), using a suitable arrangement on the analytical balance to allow the sample to be suspended freely in the water. In this work a fine copper wire of known weight was used to suspend the sample freely in water. During this stage of the measurement care was taken to ensure that nothing disturbed the surface of the water.

(7) Samples were then returned to the desiccator immediately after weighing in order to keep them saturated for subsequent hydraulic conductivity measurement.

The liquid-resaturation method gives good results of high accuracy with rocks of moderate to high porosity and high permeability, but the results are not so accurate with low porosity and permeability rocks, largely due to the difficulty of complete resaturation. Incomplete resaturation results from either incomplete evacuation or the presence of a high proportion of micro-pores which can only be saturated under high pressure. Weighing errors may result from grain loss in cases of very friable samples or the incomplete removal of surface skins of water.

Calculation and results

Effective porosity and densities were calculated according to the following equations:

$$\phi_{sat} \ \% = \frac{Ws - W}{Ws - Wm} \times 100 \qquad 4.3$$

$$\rho_G = \frac{W}{W - Wm} \ gm/cm^3 \qquad 4.4$$

$$\rho_B = \frac{W}{Ws - Wm} \quad gm/cm^3 \qquad 4.5$$

$$\rho_S = \frac{Ws}{Ws - Wm} \quad " \qquad 4.6$$

where

ϕ_{sat} % = Effective porosity in percentage, measured by water-resaturation

ρ_G = Grain density (solid density)

ρ_B = Bulk dry density

ρ_S = Saturated density (wet density)

The details of the calculations are shown in Appendix 1 and the results tabulated in Table 4.1.

The results of the water-resaturation method indicate that the ϕ_{sat} of the Triassic sandstone under consideration is in the range of 17.76% to 32.45% with an overall average for the four boreholes (Av. ϕ_{sat}) equal to 25.63%. This range of results differs slightly from one borehole to another; in borehole A11 the values ranged between 17.76% - 27.96%, for borehole A14 this range was 21.49% - 28.64%, in borehole A18 the results varied between 18.40% - 28.49%, while in A3 this range was slightly higher than the other three boreholes - from 22.33% to 32.45%. The individual values are listed in Table 4.1. These results are comparable to those of Bow et al.(1970), for the Permo-Triassic aquifer of north-west England, which ranged between 12.3% to 30.3% and 19.0% to 28.3% for Bunter and Keuper Sandstone respectively. The results are also comparable to those of Williams et al. (1972) for Bunter Sandstone of Nottinghamshire, where interconnected porosity ranged between 20-32% for the different types of sandstone, with

Table 4.1 Porosity, density and hydraulic conductivity measurements of Sherwood Sandstone Group

Variables / Sample No	Depth (m)	Porosity ϕ_{Hg} %	Porosity ϕ_{sat} %	Porosity ϕ_{av} %	Deviation from average porosity Dev %	Pore radius Mr um	Density ρ_B	Density ρ_S	Density ρ_G	Hydraulic Conductivity Measured K_y (mm/sec)	Measured K_{in} (md)	Estimated K_{Hg} (mm/sec)	Estimated K_{in} (md)
Borehole A3													
3/1	6.4	30.13	30.71	30.42	0.95	16.22	1.34	2.14	2.65	2.0139×10^{-4}	2084.4	1.5859×10^{-2}	1641.4
2	8.5	27.21	32.45	29.83	8.78	15.73	1.75	2.07	2.58	3.6407×10^{-2}	3768.1	1.9128×10^{-2}	1979.7
3	14.3	25.61	26.10	25.86	0.95	9.17	1.95	2.21	2.64	7.6975×10^{-3}	796.7	6.9896×10^{-3}	723.4
4	15.5	28.24	29.93	29.09	2.91	30.11	1.84	2.14	2.62	1.1280×10^{-1}	11674.7	4.9273×10^{-2}	5099.8
5	18.0	25.90	26.35	26.13	0.86	26.02	1.83	2.09	2.48	5.8344×10^{-2}	6038.6	3.0795×10^{-2}	3187.3
6	23.2	28.18	28.97	28.58	1.38	14.44	1.87	2.16	2.64	1.0356×10^{-2}	1071.9	1.2857×10^{-2}	1330.7
7	25.3	23.95	24.72	24.34	1.58	11.84	1.99	2.24	2.64	9.5573×10^{-3}	989.2	6.7477×10^{-3}	698.4
13	57.9	28.80	29.76	29.28	1.64	16.22	1.85	2.15	2.64	2.222×10^{-2}	2299.7	1.4988×10^{-2}	1551.2
14	64.75	27.80	28.06	27.93	0.47	16.86	1.90	2.18	2.64	3.4266×10^{-2}	3546.5	1.4767×10^{-2}	1528.4
15	67	27.94	26.79	27.37	2.10	11.10	1.93	2.20	2.73	5.9873×10^{-3}	619.7	6.6087×10^{-3}	684.0
16	80.3	27.94	22.33	22.28	0.22	15.85	2.05	2.28	2.64	1.0656×10^{-2}	1102.9	1.0869×10^{-2}	1125.0
Borehole A11													
11/3	22.7	26.97	27.96	27.47	1.80	18.66	1.89	2.17	2.62	2.1458×10^{-2}	2221.0	1.5905×10^{-2}	1646.2
7	35	25.98	25.12	25.55	1.68	15.28	1.98	2.23	2.64	7.1815×10^{-3}	743.3	1.146×10^{-2}	1186.1
8	47	21.22	22.23	21.73	2.33	4.64	2.08	2.31	2.68	1.0724×10^{-3}	111.0	6.3637×10^{-4}	65.9
9	52	23.89	24.75	24.32	1.77	17.71	2.0	2.25	2.66	1.466×10^{-2}	1517.3	1.1864×10^{-2}	1228.0
10	54	25.23	24.82	25.03	0.82	14.64	2.01	2.26	2.68	8.1001×10^{-3}	838.5	8.7301×10^{-3}	903.6
11	57	17.34	19.82	18.58	6.67	1.85	2.16	2.36	2.69	1.3744×10^{-4}	14.2	8.0573×10^{-5}	8.3
13	59	22.87	25.60	24.24	5.97	10.33	1.99	2.25	2.68	1.1372×10^{-2}	1177.0	4.2046×10^{-3}	435.2
14	59.8	23.44	25.19	24.32	3.09	17.57	2.01	2.26	2.57	1.0734×10^{-2}	1111.0	1.2705×10^{-2}	1315.0
15	61	24.65	24.41	24.53	0.49	12.85	2.03	2.27	2.68	5.7903×10^{-3}	599.3	5.7879×10^{-3}	599.0
16	62.3	15.95	17.76	16.86	5.37	0.35	2.23	2.41	2.71	-	-	9.702×10^{-6}	1.0
17	63.5	15.54	18.27	16.91	8.07	0.16	2.15	2.33	2.63	1.4316×10^{-5}	1.48	7.292×10^{-6}	0.8
18	67	24.75	23.99	24.37	1.56	1.95	2.03	2.27	2.68	1.5238×10^{-3}	157.7	1.454×10^{-3}	150.5
Borehole A14													
14/49	65.1	28.98	26.6	27.79	4.28	7.27	1.97	2.24	2.69	1.4839×10^{-3}	153.6	2.0778×10^{-3}	215.1
44	75.7	27.51	28.64	28.08	2.01	21.96	1.39	2.17	2.64	1.2375×10^{-2}	1280.8	2.5492×10^{-2}	2638.5
43	78.8	22.39	23.07	22.73	1.50	21.96	2.07	2.29	2.67	2.5350×10^{-3}	262.4	1.9669×10^{-2}	2035.7
41	82.2	23.52	24.04	23.78	1.09	8.11	2.03	2.27	2.67	3.6838×10^{-4}	38.1	2.6806×10^{-3}	277.4
40	84.4	26.93	25.96	26.45	1.85	22.19	1.97	2.23	2.66	1.7802×10^{-2}	1842.5	2.2767×10^{-2}	2356.4
39	85.3	25.72	26.64	26.18	1.76	14.05	1.96	2.22	2.67	-	-	9.3385×10^{-3}	966.5
37	89.5	25.93	26.47	26.20	1.03	39.77	1.93	2.19	2.62	5.2943×10^{-2}	5479.6	6.9901×10^{-2}	7234.8
36	92.2	27.27	28.56	27.92	2.31	28.88	1.85	2.14	2.59	-	-	4.4148×10^{-2}	4569.3
35	94.6	23.79	24.70	24.25	1.88	22.67	2.02	2.27	2.68	1.1408×10^{-2}	1180.7	2.2353×10^{-2}	2313.6
34	96.0	26.20	28.04	27.12	3.39	20.67	1.90	2.18	2.64	1.6845×10^{-2}	1743.5	2.2444×10^{-2}	2323.0
33	98.4	26.66	24.81	25.74	3.59	21.73	2.01	2.26	2.77	4.7931×10^{-3}	496.1	2.315×10^{-2}	2396.0
32	100.85	24.05	25.10	24.58	2.14	19.16	1.96	2.21	2.62	3.6011×10^{-4}	3727.2	1.4502×10^{-2}	1501.0
28	130.35	24.14	21.65	22.90	5.44	6.39	2.08	2.30	2.65	1.2241×10^{-4}	12.7	1.0014×10^{-3}	103.6
27	130.8	27.31	27.33	27.42	0.33	20.87	1.92	2.19	2.64	1.1052×10^{-2}	1143.9	2.1685×10^{-2}	2244.4
26	133.2	22.84	21.49	22.17	3.05	34.0	2.09	2.31	2.67	1.6518×10^{-2}	1709.6	3.8795×10^{-2}	2808.2
25	134.65	25.96	28.33	27.14	4.4	20.67	1.84	2.18	2.64	1.9072×10^{-2}	1974.0	2.0613×10^{-2}	2133.4
24	171.3	27.37	26.93	27.15	0.81	10.44	1.94	2.21	2.66	-	-	5.3527×10^{-3}	554.0
23	171.8	26.34	26.97	26.66	1.81	9.09	1.95	2.22	2.68	7.9066×10^{-4}	81.8	3.6038×10^{-3}	373.0
16	179.65	25.39	27.40	26.40	3.81	14.05	1.95	2.22	2.68	-	-	9.3244×10^{-3}	965.1
Borehole A18													
18/4	33.5	26.56	26.87	26.72	0.58	26.35	1.92	2.19	2.63	3.0199×10^{-2}	3125.6	3.2443×10^{-2}	3357.8
6	102.5	25.46	28.49	26.98	5.62	21.96	1.90	2.18	2.65	4.4882×10^{-2}	4645.3	2.4673×10^{-2}	2553.7
7	104.5	29.64	29.18	29.42	0.80	20.27	1.87	2.16	2.64	2.8966×10^{-2}	2998.0	2.2628×10^{-2}	2342.0
8	109	23.41	24.34	23.88	1.95	7.75	2.02	2.26	2.67	7.3969×10^{-4}	76.6	1.7881×10^{-3}	185.1
10	114	16.98	18.40	17.69	4.01	3.63	2.16	2.34	2.54	1.7431×10^{-5}	1.80	2.6314×10^{-4}	27.2
11	118.5	21.67	25.97	23.82	9.03	1.6	1.98	2.24	2.67	3.2577×10^{-4}	33.5	2.0911×10^{-4}	21.6
13	135	23.23	24.73	23.98	3.13	11.98	2.02	2.26	2.58	3.7594×10^{-2}	3891.0	6.4168×10^{-3}	664.1
14	137	23.30	24.47	23.89	2.45	3.11	2.02	2.27	2.68	2.9153×10^{-4}	30.2	3.2112×10^{-3}	332.4

higher values recorded (33 to 36%) for shallow core samples.

The variation in ϕ_{sat} may be directly related to the changes of density which consequently reflect the lithological variation. For example, samples 18/10, 11/11, 11/16 and 11/17 which have the lowest ϕ_{sat} values in the two boreholes, have the highest ρ_S values of 2.34, 2.36, 2.41 and 2.33 gm/cm^3 respectively and consequently the highest ρ_B values: 2.16, 2.16, 2.23 and 2.15 gm/cm^3 respectively. These four samples are representative of the strata toward the base end of the Nottingham Castle Formation which consists of intercalation of mudstone, siltstone and fine sandstone with an abundance of red mud-flakes (intraformational conglomerate).

Advantage

One of the important advantages of the water resaturation method is the ability of repetition of the measurement, which reflects the accuracy of this method (Table 4.2). Table 4.2 shows data for six samples in which measurements were repeated and the arithmatic mean as well as the deviation % from the average value were calculated as a measure of the accuracy of the method. The values of deviation (d%) are obviously low except in sample number 14/28 which has 12.47% deviation. This sample is very fine sandstone with low hydraulic conductivity and this may account for this discrepancy. The results indicate that accuracy of this method is more dependent upon porosity and hydraulic conductivity of the measured sample since the efficiency of resaturation is very poor in the case of low permeability rocks.

Table 4.2 Replication of porosity measurements by the water resaturation method

Variables \ Sample No.	14/28	14/34	14/35	14/39	14/43	14/44
ϕ_1 %	24.35	28.03	24.94	26.65	23.5	28.9
ϕ_2 %	18.95	28.05	24.46	26.63	22.64	28.38
ϕ_{sat} %	21.65	28.04	24.70	26.64	23.07	28.64
Deviation from mean value d%	12.47	0.04	0.97	0.04	1.86	0.9
K_w (md)	12.7	1743.5	1180.7	966.5	262.4	1280.8

ϕ_1 first measurement ϕ_{sat} mean porosity value

ϕ_2 second measurement K_w hydraulic conductivity

4.2.1.2 Mercury porosimeter method

A mercury injection technique using Mercury Penetration Porosimeter model 900/901 series, of 50,000 psi (351 N/mm^2) pressure capacity has been used to determine pore-size distribution and porosity.

The theoretical basis of the mercury penetration method depends on the physical principle that non-wetting liquid forming a contact angle of more than 90^o with a given solid material will intrude the pores of the solid material only under sufficient pressure. The pressure required depends on the contact angle between the non-wetting liquid and the solids, and the surface tension of the liquid opposing its entrance into the small openings.

Assuming that the pores are circular in cross-section (i.e. have a cylindrical shape) the relation between pressure and pore radius is given by Washburn's (1921) pressure displacement equation:

$$P = \frac{-2\gamma CoS\ \theta}{r} \qquad 4.7$$

where P is the required pressure in psi, γ is the surface tension of the Hg (474 dyne/cm), θ is the contact angle between Hg and the solid material (chosen to be 140°) and r is the radius of the pore throat.* Because almost all of the pore spaces are of irregular shape, the size determined by this method are actually the sizes of pore throats (effective radius) or the narrow connections between large voids, assuming that they are cylindrical in shape.

The technique involves determination of the volume of mercury that may be forced into the interstices of the material to be examined under various pressures. Firstly, the system is evacuated to get rid of any gases or vapours so that the mercury is free to penetrate without additional impediment. The amount of mercury which penetrates the pores is proportional to the pore size and pressure applied.

The porosimeter consists of a pressure generator, means for determining the volume of the Hg intruded, a vacuum pump and vacuum indicator. A sample cell and reservoirs for the mercury and the pressure transmitting fluid complete the basic elements of the equipment.

The following is a brief description of the method used for determining the pore-size distribution and porosity in this study:

(1) For each sample to be studied thin slices were cut, of about 5 mm width, 3-4 mm thick and 10-15mm length. The size and the shape of the samples were the most suitable ones for both drying and the size of the cell. The sample slices were washed thoroughly and dried in an oven for about three days at a temperature of $100^{\circ}C$ to be sure that they were perfectly dry. The slices were

*details of derivation of equation 7 are shown in Appendix 2

then taken out of the oven only 30 minutes before running the experiment and transferred to a desiccator containing $CaCl_2$ so that the sample could cool to the room temperature in a dry atmosphere.

(2) The dry cool slices of sample were then placed into the sample cell of known weight and the complete cell weighed to the nearest 0.0001 gm in order to determine the sample weight (always 5-6 gm). The cell was then hung in the pressure chamber.

(3) The sample and the system were evacuated for at least two hours to a pressure of 20 μm Hg in order to remove any gases present and mercury allowed into the pressure vessel until it was full. Then sufficient air pressure was admitted into the chamber to permit the mercury outside the sample cell to drain out. The pressure vessel was evacuated again and the sample was then ready for testing.

(4) The pressure was gradually increased to atmospheric one and the volume of mercury penetrating the sample was measured by means of counts transferred into volume (Appendix 3).

(5) Higher pressures than atmospheric were applied with compressed air after filling the system with a pressure transmitting fluid.

(6) Mercury is slightly compressible as pressure increases and so correction was made by calculating the effect of pressure on the Hg compressibility by running a blank test (mercury only).

An important source of error in this method is the deviation from the assumed circular cross-section for the pore throats, which in almost

all cases are irregular. The effect will only be on the calculated radii and the shape of the pore-size distribution curve will not be appreciably different.

Also the angle chosen for the contact angle (θ, equation 4.7) between liquid (Hg) and solid surface is important because any deviation from the correct angle followed by error in the calculated pore radius will cause error in the calculated permeability. The just mentioned kind of error can be explained numerically by the relation given by Ritter and Drake (1945), where they assumed the contact angle θ equals 140°, and by the differentiation of equation 7 and elimination of P they got the following equation (equation 4.8):

$$\Delta r/r = -\Delta\theta \tan\theta \qquad 4.8$$

They found that the value of $\Delta r/r$ calculated for 1° deviation from the assumed 140° contact angle is only about 1.5%. In the case of a large deviation from the ideal contact angle, the effect is either magnification or reduction in the scale of pore-radius values, although the error may be considerable. For example, the calculated pore-radius at 100 psi for contact angles of 130°, 140° and 150° are 8.84, 10.55 and 11.92 A° respectively (assuming γ = 474 dyne/cm).

The experimental pore-size distribution data are presented in the form of cumulative pore-radius distribution curves, in which the pore volume (volume of penetrated Hg) is expressed in cubic centimetres (cc) of pore spaces per gram of oven-dried sample. The applied pressures in psi are also indicated (Figures 4.1 to 4.4). In deriving the pore-size distribution the surface tension of Hg was assumed to be 474 dyne/cm and the contact angle 140° for silicate (Price, 1977).

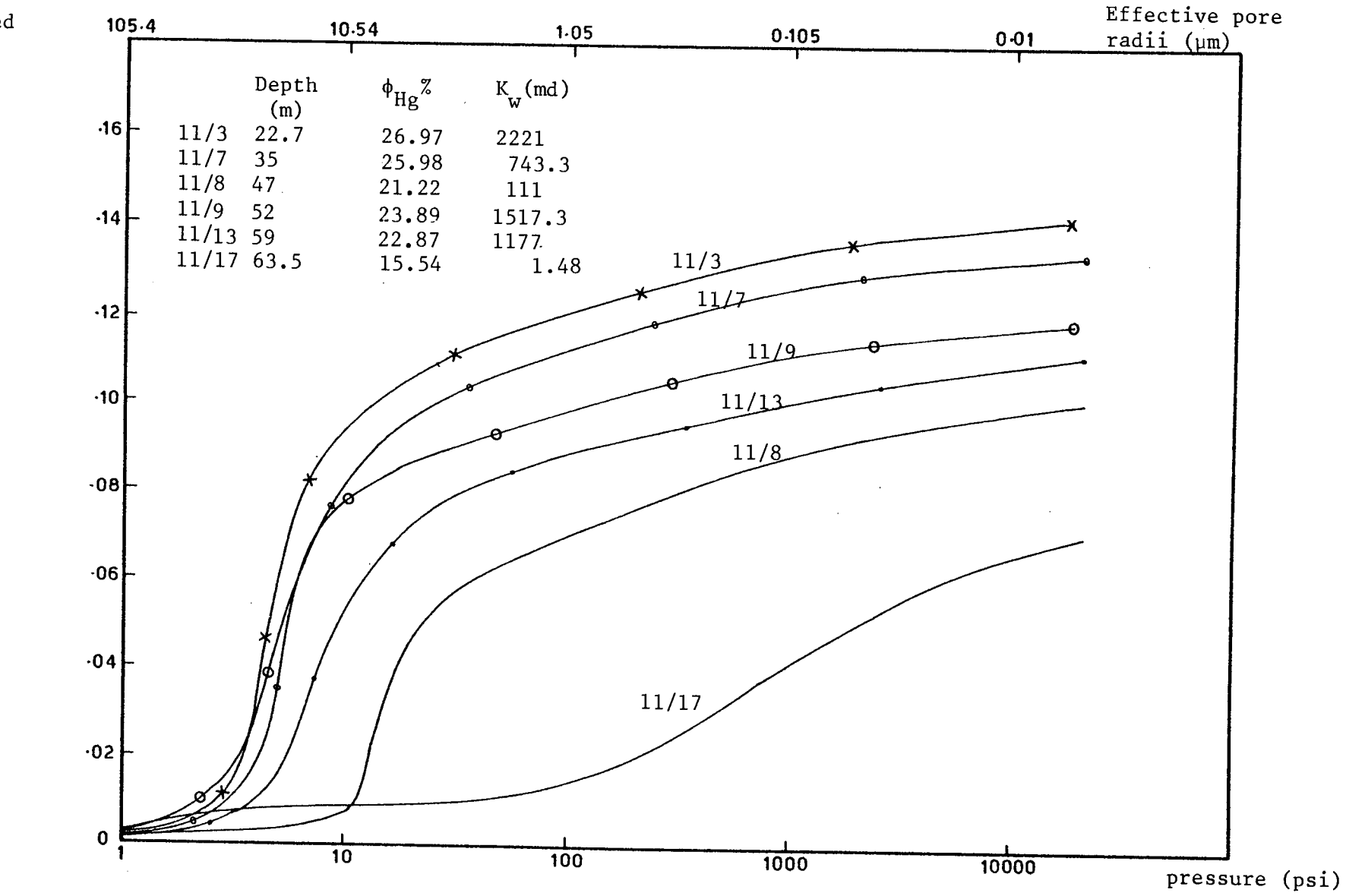

Figure 4.1 Pore-size distribution curves representing the Sherwood Sandstone Group of borehole A11

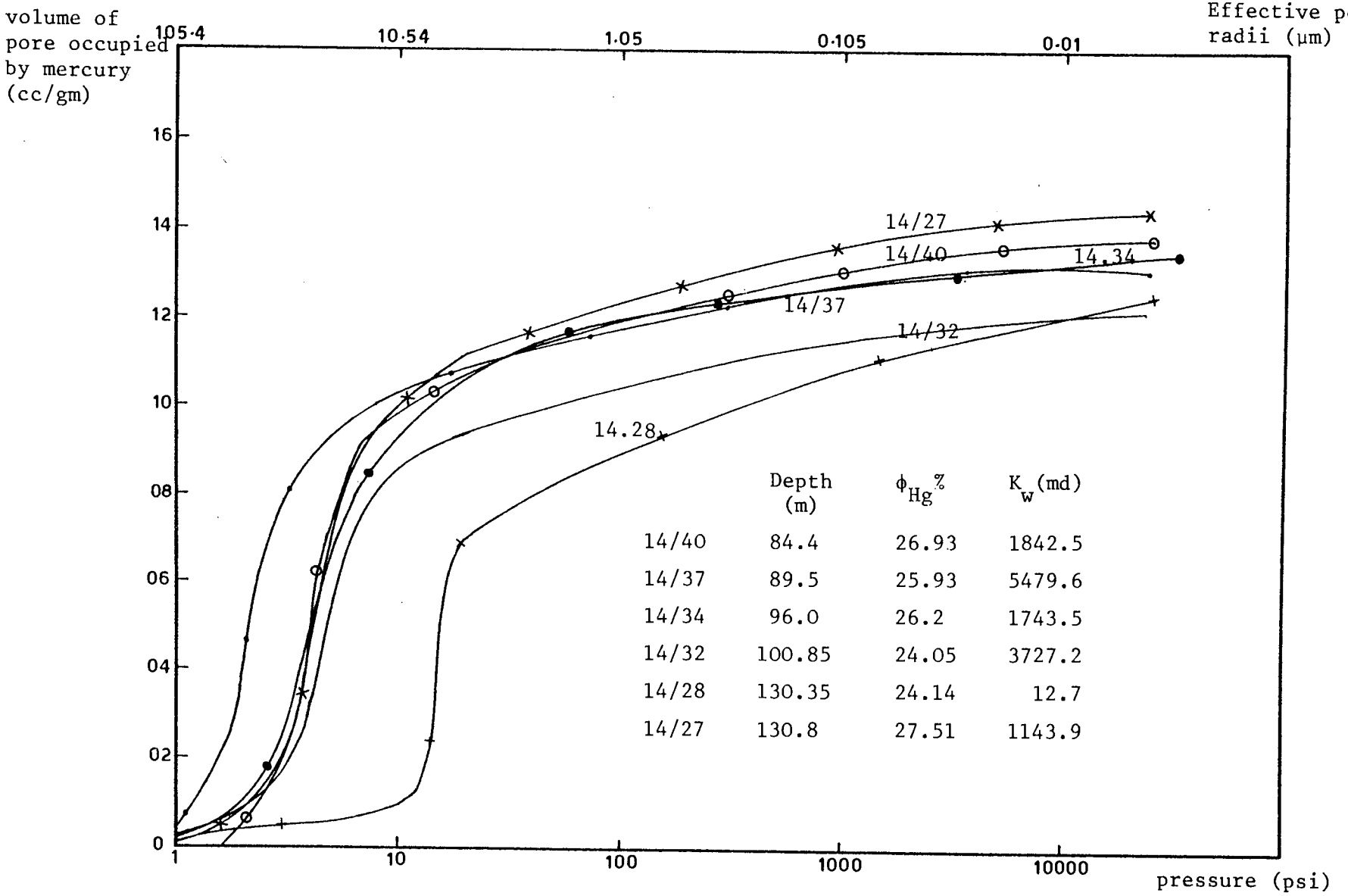

Figure 4.2 Pore-size distribution curves representing the Sherwood Sandstone Group of borehole A14

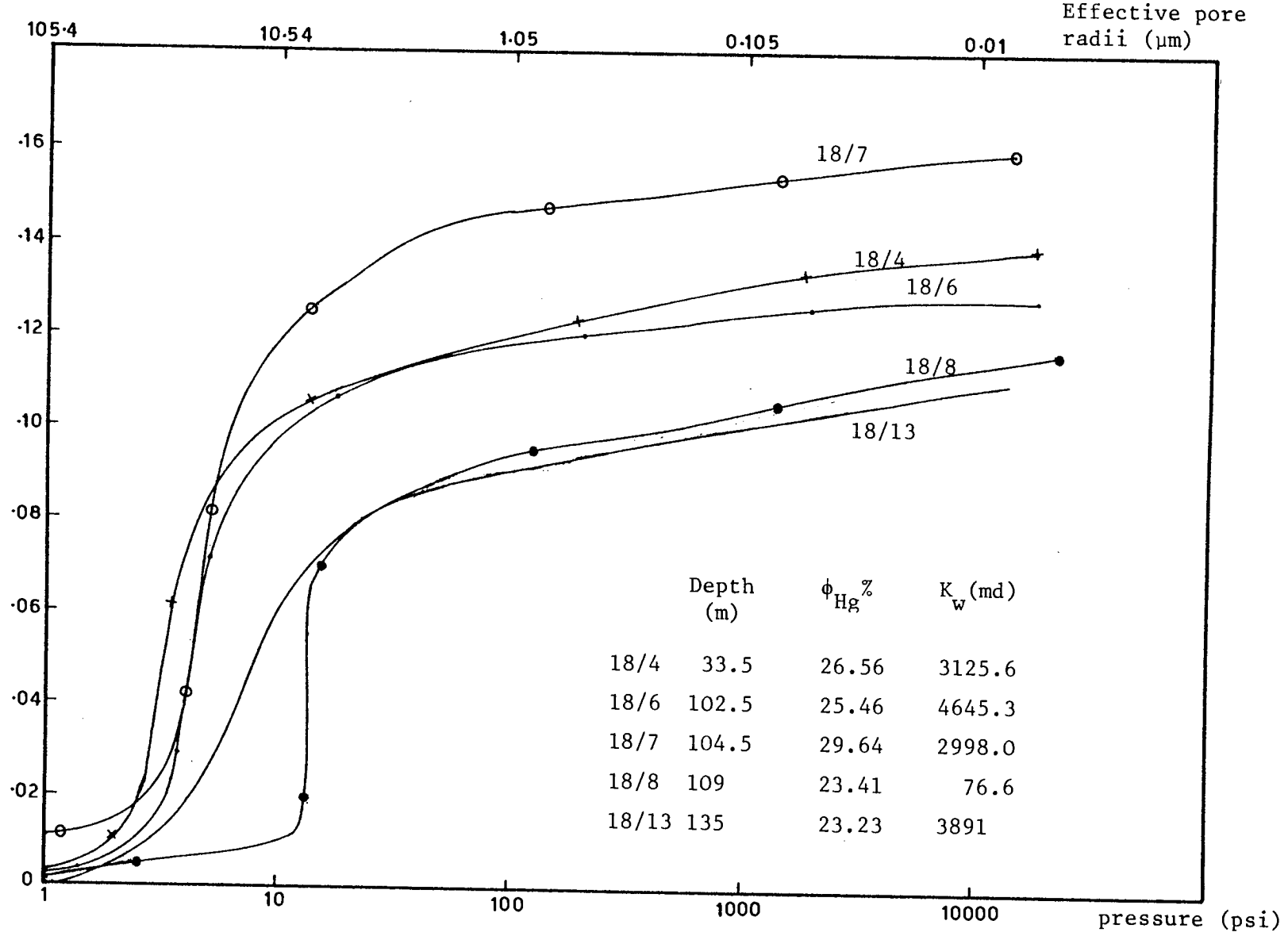

Figure 4.3 Pore-size distribution curves representing the Sherwood Sandstone Group of borehole A18

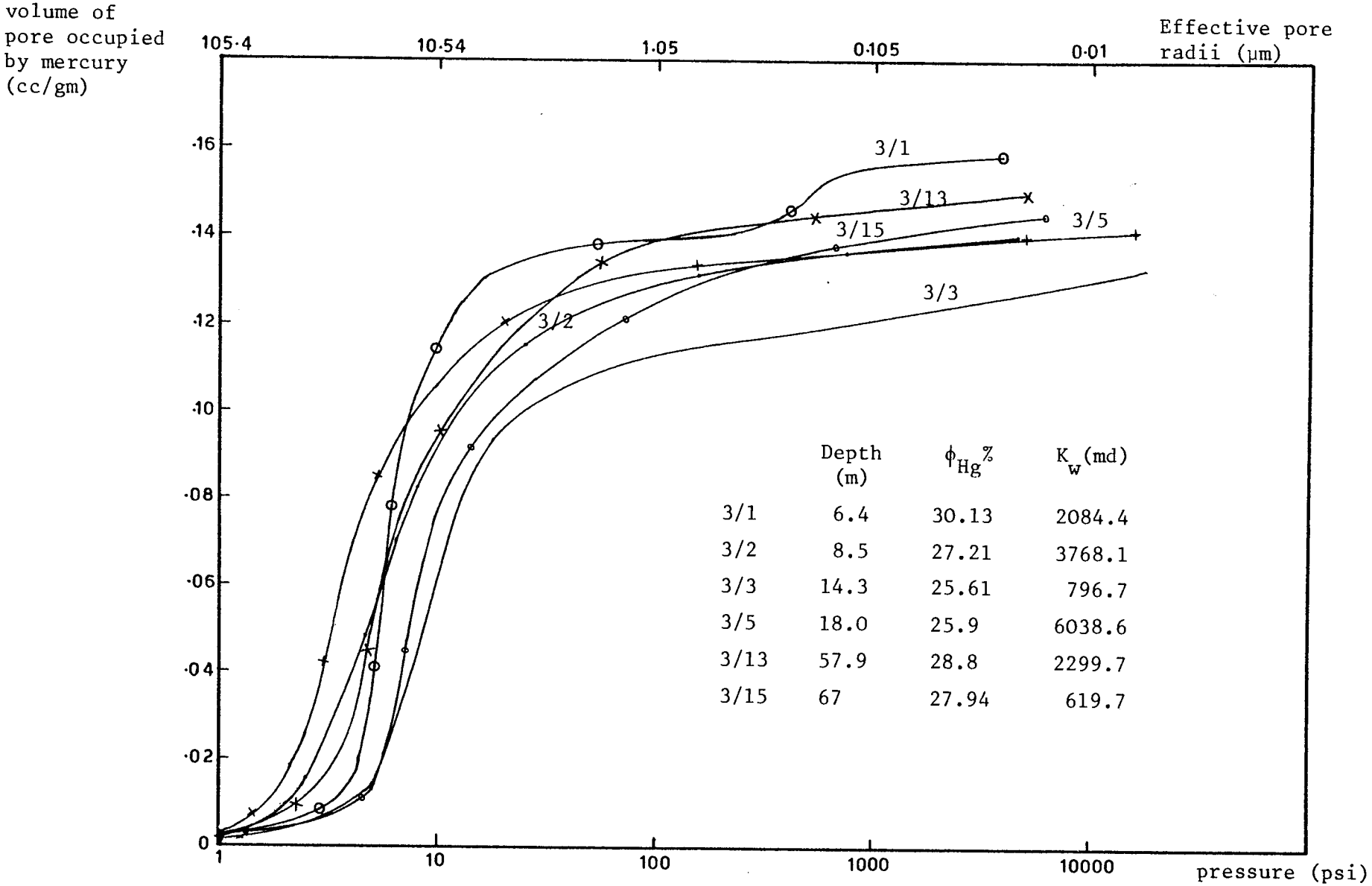

Figure 4.4 Pore-size distribution curves representing the Sherwood Sandstone Group of borehole A3

Porosity and hydraulic conductivity values were also calculated from the data (Table 4.1). The effective porosity measured using this method (ϕ_{Hg}) was calculated using the following equation (details in Appendix 3):

$$\phi_{Hg} = \frac{\Sigma E \times \rho_G}{(\Sigma E \times \rho_G) + 1} \qquad 4.9$$

where ΣE is the volume of pore spaces present in one gram of the sample (cc/gm), and ρ_G is the solid grain density in gm/cm^3.

Results

The results of effective porosity measured by mercury penetration method show an overall average porosity for the four boreholes (Av. ϕ_{Hg}) equal 24.85%, and the values range between 15.54% and 30.13%. This range of values differs slightly from one borehole to another depending upon the lithological and diagenetic features of the representative sample. For borehole A11 ϕ_{Hg} ranged between 15.54% - 26.97%, in A14 the range was from 22.39% - 28.98% and in A18 the range was slightly greater - from 16.98% - 29.64%. In A3 the values were generally higher than the other boreholes with ϕ_{Hg} ranging from 22.23% to 30.13%.

Representative pore-size distribution curves obtained from the fifty tested samples from the four boreholes are illustrated in Figures 4.1 to 4.4 and show that they have median pore sizes (Mr) ranging from 0.16 to 39.77 μm. Only six samples have Mr less than 4 μm (11/11, 16, 17 and 18, 18/10 and 11) and these represent the siltstones and mudstones intercalated with very fine sandstone beds toward the bottom end of the Sherwood Sandstone Group. Also the

results indicate that only 6% of the samples have Mr $>$ 30 μm, 26% having Mr between 30-20 μm, 40% with Mr 20-10 μm and 28% with Mr $<$ 10 μm.

4.2.1.3 Comparison of water resaturation and mercury penetration methods

The water resaturation method is an accurate method for the determination of porosity in highly permeable rocks but is less effective in rocks of low permeability because of the difficulty of obtaining complete vacuum and resaturation. The Hg penetration method is much more accurate in rocks with an abundance of micro-pores because the very high pressure available (50,000 psi) makes it easy for the non-wetting liquid (Hg) to penetrate the micro-pores. This is illustrated in sample A14/28 which is a very fine grained sandstone and has ϕ_{Hg} of 24.14% and ϕ_{sat} of 21.65%. Table 4.3 shows a comparison of the Hg porosimeter and water resaturation method.

The relation between ϕ_{Hg} and ϕ_{sat} is illustrated in Figure 4.5. This shows a marked correlation with a general tendency for ϕ_{sat} to be higher than ϕ_{Hg} with the overall average values being 25.63% and 24.85% respectively. The relationship between ϕ_{sat} and ϕ_{Hg} is best represented by a linear equation very close to the isotropy line (Y=X):

$$\phi_{sat} = 2.085 + 0.947\ \phi_{Hg} \qquad 4.10$$

The associated correlation coefficient is positively high (r = + 0.892) indicating that the correlation is significant at the 99.99 level. Comparison of the ϕ_{sat} and ϕ_{Hg} results show that there are differences although these may be expected because of the different methods of measurement (Manger, 1963). However, these differences are not uniform and it appears likely that variations in lithology and diagenesis

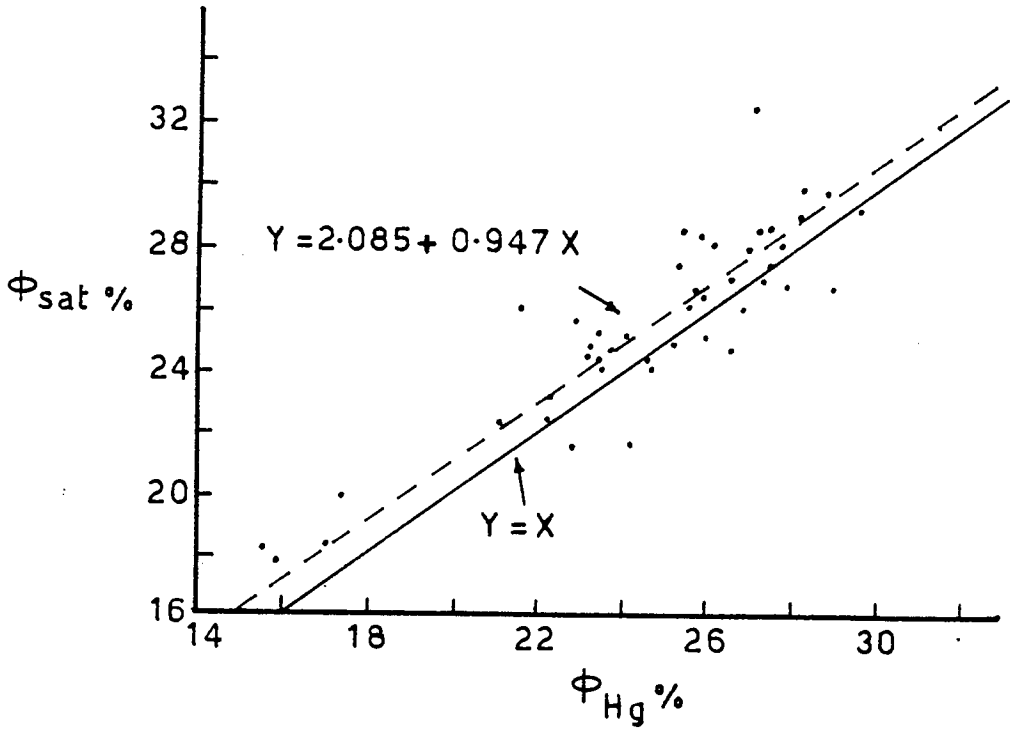

Figure 4.5 Comparison of porosity measured by water resaturation (ϕ_{sat}) and Hg injection (ϕ_{Hg})

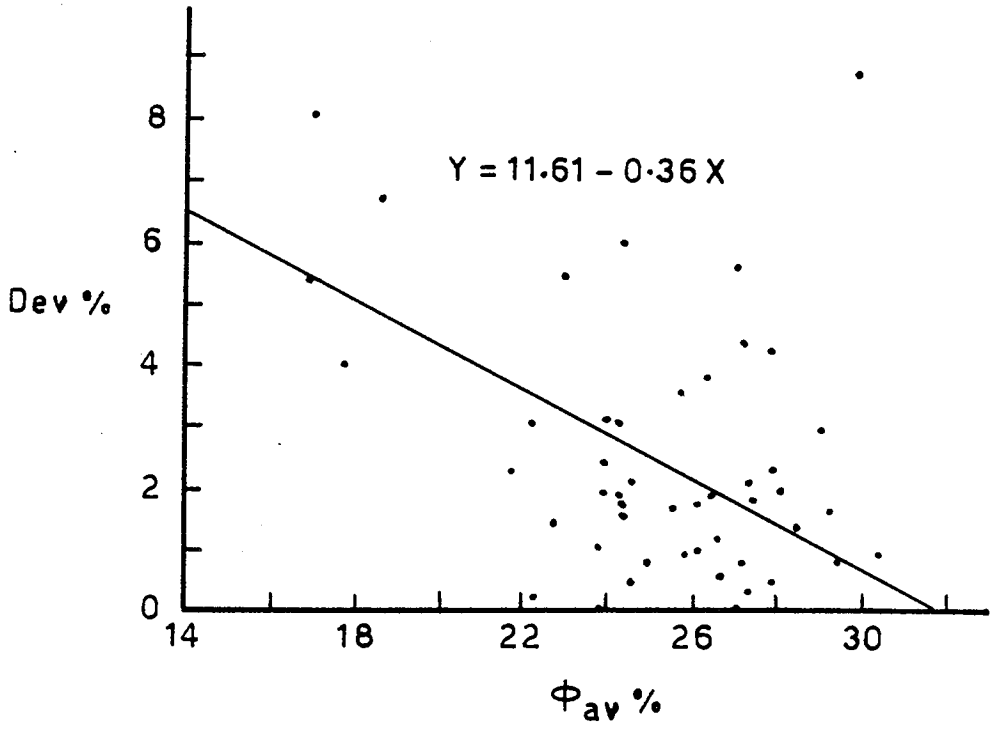

Figure 4.6 Relationship between porosity (ϕ_{av}) and deviation per cent from average porosity (Dev %)

Table 4.3 Advantages and disadvantages of water-resaturation and Hg-penetration methods

	Water Resaturation	Hg-penetration
1.	Quick, rapid, easy to design and operate. Economic.	Time consuming, expensive and not always available.
2.	Using water as a saturating liquid, near to the natural conditions in a water aquifer.	Using Hg as a saturating liquid.
3.	Errors result from the incomplete evacuation and resaturation especially when there is an abundance of micro-pores.	High accuracy in both evacuation and resaturation.
4.	Core sample of 2.5 cm diameter and 2.5 to 7.5 cm length usually used for this method. So it could be representative for the whole rock.	Very small sample relative to the sample used for water saturation e.g. chips of the sample 0.5 cm thick and about 5-7 gm weight. Not representative for heterogeneous samples (poorly sorted) especially the pebbly variety.
5.	Repetition is one of the advantages of this method with the possibility of using the same sample for hydraulic conductivity measurements. Although the repetition of wetting and redrying may affect, especially the clay mineral present.	Analysed sample cannot be used again for any kind of measurement. Also not easy to get a duplicate of the same sample exactly with the same characters. But it gives an idea about the distribution of the pore spaces in the sample.
6.	Weighing error associated with the errors arising from skin water and loss of friable grains.	The only weighing error present.
7.	Not very accurage in case of presence of high percentage of swelling clays (montmorillonite, and mixed layer clays).	More suitable than water resaturation in case of presence of swelling clays. However, the presence of clays under high vacuum may change the pore-size distribution with no effect upon the percentage of pore present.
8.	More accurate in case of medium-coarse sandstone with high permeability, on other hand less accuracy developed in case of fine grained sediments.	More reliable in case of fine grained sediments than any other method due to the high vacuum system available.

may exert some influence on the methods used.

It has been noticed from the results that the water resaturation method tends to minimize the bulk volume and consequently increase ϕ_{sat}. This could be one of the reasons why ϕ_{sat} is frequently higher than ϕ_{Hg}. However, the deviation is sometimes very high and this cannot be only attributed to differences in the method used. Examples showing such high deviations are: 3/2, 11/11, 13, 16 and 17, 14/16 and 25, 18/6 and 10 with the deviation per cent from average porosity (Dev %) ranging between $\pm$ 3.81% to $\pm$ 8.78%. Samples 11/11, 16 and 17 and 14/16 are very fine grained sandstone with a high percentage of the fine clay fraction reached up to 10.73% in the case of sample 14/16 (Table 3.1). Samples 3/2, 11/13 and 18/16 are slightly pebbly coarse grained sandstones. Sample 18/10 is a very fine grained sandstone with an abundance of mudstone flakes. The possible explanation of higher ϕ_{sat} than ϕ_{Hg} could be due to the presence of considerable amounts of clay (mainly kaolinite and mixed layer illite-smectite together with less abundant illite and very rarely detected smectite) which show initial large volume, slightly decrease on oven drying and show only a limited swelling on resaturation (Yong and Warkentin, 1966). This swelling does not occur in the case of the Hg penetration method . Also the increase of clay content or very fine fraction in sandstone increases the volume of water held on resaturation causing increase in the value of Ws (equation 4.3). consequently increasing ϕ_{sat}. Also the rearrangement of the clay particles, which may result because of high vacuum and pressure applied in the mercury penetration method, could cause not only porosity reduction (blocking the pore throats), but also change the pore size distribution (Diamond, 1970).

Samples which show the opposite result ($\phi_{Hg} > \phi_{sat}$) are seen in samples 14/26, 28, 33 and 49 and these can be divided into two categories. The first including 14/28 and 49 have maximum deviation from average porosity (Dev %) of $\pm$ 5.44% and 4.28% respectively. This could be due to incomplete resaturation or an abundance of micropores which could only be resaturated under high pressure. The second group includes 14/26 and 14/33 having deviations of 3.03% and 3.59% respectively and both are pebbly sandstone in which the Hg penetration specimens were pebble-free giving a higher value than expected.

One of the limitations of the Hg-penetration method is the impossibility of repetition of the measurement because of the retention of residual mercury in the sample. Furthermore duplicate measurements cannot be made because of the difficulty of finding samples of identical character. The water resaturation method has the advantage of the possibility of repetition with high accuracy of measurement except in the case of low permeability rocks. However, the water-resaturation technique is not very accurate if the examined sample has a high percentage of expandable clay (montmorillenite or mixed layer clay with high percentage of swelling layers). In the present study this is not considered an important problem because the samples contain abundant kaolinite and only a small proportion of swelling clays.

For medium-coarse grained sandstone with high ϕ and K both methods are equivalent and are equally effective unless a high percentage of swelling clay is present in which case the Hg-penetration method is recommended. Also the case of poorly sorted sandstone with considerable amounts of pebble the water resaturation is recommended, as the small size of the sample needed for the porosimeter technique will not be representative.

4.2.1.4 Petrographic determination of porosity: estimation from photomicrographs

The quantitative determination of different components in rocks (framework grains, pores, cement) by microscopic methods has been done for many years (Delesse, 1848). Point counters of various kinds have been used widely for this purpose, although they can be very inaccurate particularly because of operator error. The inaccuracy of this method for determining porosity is largely due to the submicroscopic pore spaces and the edge effects due to grain curvature in the normal thin section as discussed by Halley (1978).

In this work two methods have been used for calculating pore volume by microscopic methods. In each case photographs have been used in order to minimize the error arising from micro-pore spaces, which are easily overlooked under the microscope.

In the first method pore spaces, grains, cement and matrix percent were determined by means of simple manual measurements. Seven representative samples were chosen, and thin sections impregnated with green dyed resin (Araldite CYC 212) were prepared to provide contrast between void spaces and mineral grains. About 7-10 photographs were taken of each sample over an area of about 4 mm^2 in directions parallel and perpendicular to the bedding.

From these photographs, the percentage of voids (V%), grains (G%). cement (C%) and matrix (M%) were calculated manually (Table 4.4). Measurements were made of the intersection lengths of each component along linear traverses spaced equally along the two directions of each photograph. The result of this method represents length frequency which can be related to the area.

Table 4.4 Comparison between average laboratory porosity (ϕ_{av}) with that measured from photomicrographs

Sample No	ϕ_{av}	ϕ_{photo}	D_I%	V%	D_2%	G%	C%	M%
14/44	28.08	24.17	-13.92	29.52	+5.13	61.35	4.13	5.01
43	22.73	29.41	+29.39	33.16	+45.89	53.99	8.31	4.53
36	27.92	30.12	+7.88	31.16	+11.60	62.15	3.71	2.98
33	25.74	23.9	-7.15	25.43	-1.20	63.01	8.57	2.99
27	27.42	26.66	-2.77	30.11	+9.81	60.87	3.86	5.16
26	22.17	18.86	-14.93	18.54	-16.37	72.90	3.66	4.90
23	26.66	13.24	-50.34	22.70	-14.85	53.42	8.46	16.42

The second method used the same photographs and porosity was determined by means of measuring the pore space area with the Hewlett-Packard 9825A Desktop Computer and 9874A Digitizer. In this method the highly magnified photo is fixed onto the active area of the platen by means of magnets at each corner. The platen is a sheet of laminated glass with the X and Y conductors placed between the layers of glass. The top of the glass is lapped to provide uniform smoothness for the cursor vacuum feature. The area of each pore space is measured by tracing its boundary by means of a cursor by moving it around the edge of the close figure in clockwise direction. While digitizing, the XY coordinate of each point upon which the cursor moved recorded and transferred into area by means of the computer. The total area of pore spaces calculated from the integration of the separate areas of pore spaces. The area measurements are considered to represent volume according to Delesse's area-volume relationship (Galehouse, 1971). The results are represented in Table 4.4 in which ϕ_{photo}% is the porosity estimated from microscopic photos by digitizing.

The porosity calculated from photos by means of digitizing (ϕ_{photo}) and the volume of pores (V%) were compared to the laboratory porosity by calculating the maximum deviation of both from average porosity (ϕ_{av}); D_1 and D_2 respectively. The maximum deviation of ϕ_{photo} (%) from ϕ_{av} (D_1%) showed values ranging between -50.34 to +29.39%. Also the maximum deviation of V% from ϕ_{av} (D_2%) ranged from -14.85 to +45.89% (Table 4.4). For both values (ϕ_{photo}% and V%) the deviation from ϕ_{av} is high, where the highest negative values are samples 14/23 and 14/26, while the highest positive values represented by 14/36 and 14/43. Where 14/23 is very fine grained sandstone with Mr µm equal to 9.09 and the error is high due to the small size of the pores which led to great misleading in tracing the pores and consequently calculating porosity. For 14/26 also show high negative deviation where it is slightly pebbly sandstone. While the highest +ve deviation in samples 14/36 and 14/43 was due to the abundance of the dissolution vugs (over-sized pores) which formed a high percentage of the photos measured, giving rise to higher ϕ_{photo} and V% than it should have been.

This result could lead to a conclusion that measuring porosity by means of microscopic photos is inadequate and no one can rely on it as its deviation from laboratory porosity reaches up to 50%. This error could result from the abundance of micro-pores which are not easy to trace even with high magnification. The small area available to be covered by photographs may not be representative of the whole rock. Also the presence of over-sized pores increases the ϕ_{photo} above the actual porosity. Even with uniform pore-size distributions or well-sorted samples an operator error in tracing the pores increases as the area of pore decreases.

This method could be more effective in calculating the different types of pore present, i.e. primary and secondary pores or more specific, primary, dissolution, oversized, fractured.

4.2.2 Relation between Porosity and Deviation Percent from Average Porosity

This relationship which is illustrated in Figure 4.6 shows an inverse linear relation with correlation coefficient equal to -0.3554 and may be represented by the line:

$$Y = 11.613 - 0.364\ X \qquad 4.11$$

where Y is the Dev % and X is $\phi_{av}\%$. This negative correlation coefficient is significant at 98% level.

This negative correlation is consistent with the observed high difference between $\phi_{Hg}\%$ and $\phi_{sat}\%$ values in lower porosity rocks, whilst this difference decreases as porosity increases. This means that for practical purposes, the Hg penetration and water resaturation methods could be equally well-used for measuring high porosity rocks. However, in low porosity rocks the difference observed in the mercury penetration and water resaturation methods means that care should be taken in choosing the appropriate technique.

4.2.3 Density-Porosity Relationship

The relationship between porosity and saturation or wet density can be approximiated by the equation given by Nafe and Drake (1957):

$$\rho_S = \phi\, \partial + (1 - \phi)\, \rho_G \qquad 4.12$$

where δ is the water density (1.0 gm/cm^3), ρ_G is the grain density and ϕ is porosity represented here by ϕ_{sat}.

Nafe and Drake (1957) also found that despite the dependence of bulk density upon the particle grain density, the porosity-density relationship for a whole range of lithologies could be represented by nearly the same straight line in which ρ_G is considered to be 2.68 gm/cm^3. The equation 12 may then be written:

$$\rho_S = 1.0\ \phi + 2.68\ (1 - \phi)$$

Porosity-density relation results for the Bunter Sandstones studied by Barker and Worthington (1973) were represented by a straight line parallel to Nafe's line but somewhat off-set from it with ρ_G equal to 2.6 gm/cm^3.

In the sandstone studied in this work (Figure 4.7) almost all of the points are comparable to the Nafe line (ρ_G = 2.68 gm/cm^3) and another new line with ρ_G = 2.63 gm/cm^3. These results show slight deviation from Barker and Worthington (1973) results due to the lower value of ρ_G. However, the 50 points representing the porosity and ρ_S in this work show highly significant negative correlation ($r = -0.93$)(significant at 99.99 level) and define a relationship:

$$\rho_S = 2.74 + (-0.02\ \phi_{sat}) \qquad 4.13$$

4.3 HYDRAULIC CONDUCTIVITY

The permeability of a rock may be defined as its ability or capacity to transmit water (or fluid) through its interstices. This property is expressed now by the hydraulic conductivity (K), which has been given various names (effective permeability, coefficient of permeability,

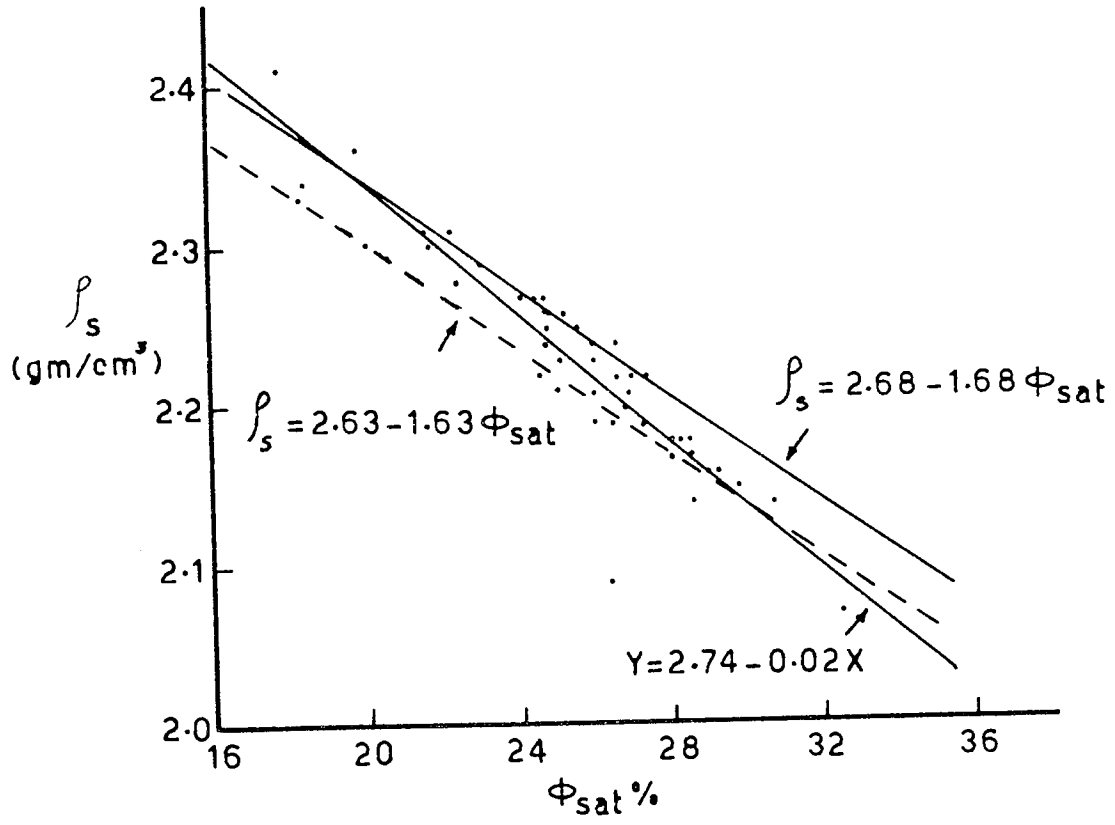

Figure 4.7 Relationship between porosity (ϕ_{sat}) and wet density (ρ_s)

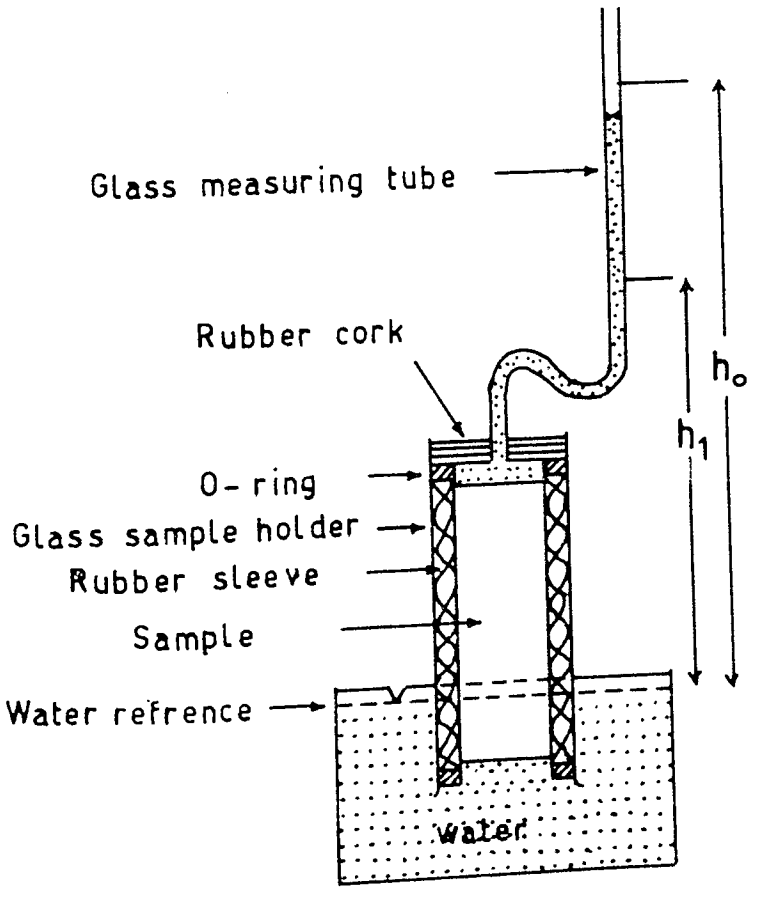

Figure 4.8 Falling head permeameter

intergranular permeability and seepage coefficient) is an important constant in the empirical flow equation pertaining to the property of both medium and fluid. If the property depends solely upon the structure and characteristic of the permeable media, regardless of the fluid properties, then the constant is called intrinsic permeability (K_{in}).

Hydraulic conductivity is defined according to Lohman et al. (1972) and Todd (1980) as the volume of ground water at the prevailing kinematic viscosity, transmitted in unit time through a cross-section of unit area under a unit hydraulic gradient measured at right angles to the direction of flow, and has the velocity unit (Length time^{-1}).

The part of the hydraulic conductivity (K) which is controlled by the rock (or media) properties only is called intrinsic permeability (K_{in}), previously known as absolute permeability (Ryder, 1948) and specific permeability (Todd, 1959). The relation between K and K_{in} is given by the following equation:

$$K = K_{in} \rho g/\mu \qquad 4.14$$

where μ is the dynamic viscosity of the fluid, ρ is the fluid density and g is the acceleration due to gravity. The intrinsic permeability has the unit of either area (L^2) or Darcy (petroleum engineering).

4.3.1 Hydraulic Conductivity Determination

The hydraulic conductivity can be determined by direct or indirect methods. The direct methods include the laboratory and field determination, whilst the indirect uses the calculation from formula (Eq. 4.14) or by dividing K_{in} (cm^2) by 1.02×10^{-5} to get K(cm/sec)

(Davis and De Wiest, 1966).

In the laboratory method for determining hydraulic conductivity (K), the permeameter is widely used. Either constant head or falling head permeameters may be used because they are simple to operate and inexpensive. However, the accuracy of this method with respect to the field determination is somewhat illusory. Removing the core from the subsurface changes all the confining forces and the rock matrix may expand causing change in pore radii. The degree of deviation from the actual values depends upon the depth of sample taken and its composition. Another important factor which contributes to this deviation is the difference in the pH of the water used in the laboratory from that flowing through the reservoir rocks. pH is the cause of the variations in the fluctuation properties of clays. When exposed to fresh water certain clays, especially montmorillonite, deflocculate and swell and sometimes either partially or fully plug pore throats (Pirson, 1958).

The field measurement of K includes many methods such as tracer tests, Auger Hole test, tube method and the slug method as well as the pumping test of wells which is the most reliable method because it is an in situ measurement and covers a sizeable part of the aquifer which is not disturbed.

Many attempts have been made to formulate a general equation for the determination of intrinsic permeability based on the relationship between K_{in} and rock properties such as, grain size and shape, porosity, packing, specific surface area and pore-size distribution. These attempts started in 1880 by Seelheim who introduced grain size into a relationship with permeability and found that the rate of fluid

flow is proportional to the square of the grain diameter. Many other authors (Hazen, 1893; Slichter, 1899; King, 1899; Terzaghi, 1925; Kozeny, 1927; Fancher et al., 1933; Fair and Hatch, 1933; Marshall, 1958 and Scheidegger, 1974) have calculated K_{in} from its relation with different media properties. However, these results are somewhat inaccurate because each equation only reflects the relation between K_{in} and one or two properties and takes no account of the various other properties which may influence K_{in}.

4.3.2 Laboratory Measurement of Hydraulic Conductivity

The hydraulic conductivity (K) was measured in this work using a falling head permeameter (Akroyd, 1957). The cores used previously for measuring effective porosity by means of water resaturation method were also used for measurement of K. The hydraulic conductivity measured here is considered to be the horizontal one because the core samples were drilled parallel to bedding planes.

The principle of the falling head permeameter method is to measure the time taken for a known volume of water with a given head to pass through a core sample of known length. The application of the following equation derived from Darcy's Law (Barker and Worthington, 1973), enables K to be determined:

$$K_w = \frac{\mu}{\mu_{20}} \cdot \frac{r_t^2}{r_s^2} \cdot \frac{L}{t} \cdot \text{Log}_e \left(\frac{h_0}{h_1}\right) \qquad 4.15$$

where μ, μ_{20} are the dynamic viscosity of distilled water at test temperature and 20°C respectively (poises), r_t is the radius of the tube (mm), r_s is the radius of the core sample (mm), L is the length of sample (mm), t is the time in seconds for water to fall from h_0

to h_1 and K_w is the hydraulic conductivity measured in mm/sec at 20°C.

4.3.2.1 Apparatus, procedure and results

The falling head permeameter constructed for this work (Figure 4.8) consists of:

(1) Two glass cylinders -the first is of small radius, and graduated while the second is of larger diameter used as core holder- connected together by fitted rubber cork.

(2) Rubber sleeves to fit the core sample inside to help prevent by-passing of water along the sides of the core.

(3) Two PVC O-rings (upper and lower) to prevent the core with its rubber sleeve from sliding along the sample holder.

(4) Water basin in which sample and holder should be immersed with a steady reference surface.

A total of 45 samples were tested using the preceeding method representing mainly the Sherwood Sandstone Group (44 samples) with only one sample from the Mercia Mudstone Group. Six measurements were made on each sample, three of them were done when sample reversed. An average of the time t (sec) was calculated and the temperature was recorded.

The disadvantage of this method arises from the small size of the sample to be examined in comparison with the size of the stratum from which the sample was taken and also the fact of the inevitable disturbance of the sample due to removing it from its natural environment. The advantage of this method arises from the possibility of obtaining a rapid assessment of the homogeneity of the aquifer.

The results of the horizontal hydraulic conductivity (K_w) are shown in Table 4.1. The values ranged from 1.43×10^{-5} mm/sec (1.48 md) to 1.13×10^{-1} mm/sec (11674.67 md), with an average value of 1.68×10^{-2} mm/sec (1743.67 md). For the Nottingham Castle Formation the K_w have values ranged between 1.22×10^{-4} mm/sec to 5.83×10^{-2} mm/sec with only one sample with a higher value of 1.13×10^{-1} mm/sec. These results are slightly lower than the Bunter sandstone at Nottinghamshire studied by Williams et al. (1972). The results are comparable to those from Bunter sandstones of South Lancashire and North Cheshire given by Bow et al. (1970) which ranged between 3×10^{-4} mm/sec to 3.5×10^{-2} mm/sec.

The results of the Lenton Sandstone Formation record lower values ranging between 1.43×10^{-5} mm/sec to 3.76×10^{-2} mm/sec. The lowest values correspond to the red mudstone and siltstone bands intercalated with the fine sandstone.

4.3.3 Indirect Determination of Hydraulic Conductivity : Calculation from Pore-Size Distribution

Many attempts have been made to calculate the intrinsic permeability from its relationship with other measurable properties of the rock. K_{in} has been calculated in this work by using the Marshall equation (1958), derived from the relation to both porosity and pore-size distribution. Marshall's assumption was that the rate of flow is controlled by the cross-sectional area of the pore throats connecting the interstices. As the pore throats are not uniform in size, the mean pore radius of them is calculated. If the mean radius of the pore throat in each n equal fractions of the total pore spaces is represented in decreasing order of size by r_1, r_2, r_3 ..... r_n mm, then K_{in} (mm^2) is given by equation:

$$K_{in} = \phi^2 \, n^{-2} \sum (2n - 1) \, r_n^2/8 \qquad 4.16$$

where ϕ^2 is the effective porosity in fraction and $\sum(2n - 1) \, r_n^2$ is the mean pore radius.

In this work, the fifty pore-size distribution curves obtained using the Hg penetration method have been used to calculate K_{in} (mm^2) which is converted into millidarcy (md). The results are given in Table 4.1. The hydraulic conductivity K_{Hg} at 20°C was determined by dividing K_{in} (mm^2) values by 1.02×10^{-8} (David and De Wiest, 1966), and represesented by K_{Hg} to distinguish it from the ones measured by falling-head permeameter (K_w)

The average hydraulic conductivity for the Sherwood Sandstone Group as estimated from the Hg porosimeter tests (K_{Hg}) is 1.47×10^{-2} mm/sec (1522 md) which is a bit lower than K_w. The values range from 7.29×10^{-6} mm/sec (0.75 md) to 6.99×10^{-2} mm/sec (7234.8 md).

4.3.4 Hydraulic Conductivity Results : Comparison between K_w and K_{Hg}

The hydraulic conductivity (K_w) measured by falling-head permeameter at 20°C ranges from 1.43×10^{-5} mm/sec (1.48 md) to 1.13×10^{-1} mm/sec (11674.67 md), with an average value of 1.68×10^{-2} mm/sec (1743.67 md). The range of results in the case of calculated hydraulic conductivity (K_{Hg}) at 20°C is 7.29×10^{-6} mm/sec (0.75 md) to 6.99×10^{-2} mm/sec (7234.8 md), with an average of 1.46×10^{-2} mm/sec.

The results indicate that average K_w is slightly higher than the average K_{Hg}. This difference is to be expected as a result of using different techniques and different saturation liquids. The wide range of hydraulic conductivity values recorded is due mainly to

grain size variation with mudstone and siltstone yielding the lowest values. The presence of mudstone flakes and pebbles in sandstones also reduce the hydraulic conductivity.

The bi-logarithmic distribution of K_w versus K_{Hg} (n = 45) shown in Figure 4.9 indicates that the points are clustered in two separate areas. The first group representing the higher values of K are tightly grouped near the isotropy line ($K_w = K_{Hg}$) whilst the second group with lower hydraulic conductivities are more widely scattered and K_Hg values are usually higher than K_w.

This difference in the estimated and measured values of hydraulic conductivity is clearly the result of the different experimental methods involved, in particular the use of different liquids (water and mercury) in the two methods. Another reason for the difference in K values could be the difficulty of obtaining complete vacuum and resaturation especially in fine grained rocks, which leads to lower K_w values than K_{Hg}. Also clay minerals, particularly swelling clays, would have the effect of reducing K_w relative to K_{Hg}. Another reason is the off-set of the actual pore-shape from the assumed one of circular cross-section, as the actual one seems to have tabular or sheet-like shape (Chapter 3).

The statistical study of the results shows that there is a marked positive correlation between K_w and K_{Hg} with a correlation coefficient of r = + 0.8802, which is highly significant (99.99% confidence level). This relation (Figure 4.9) can be represented by the line:

$$Y = 0.292 + 1.171\ X \qquad 4.17$$

where Y is $\log K_{Hg}$ and X is $\log K_w$. This line is very close to the

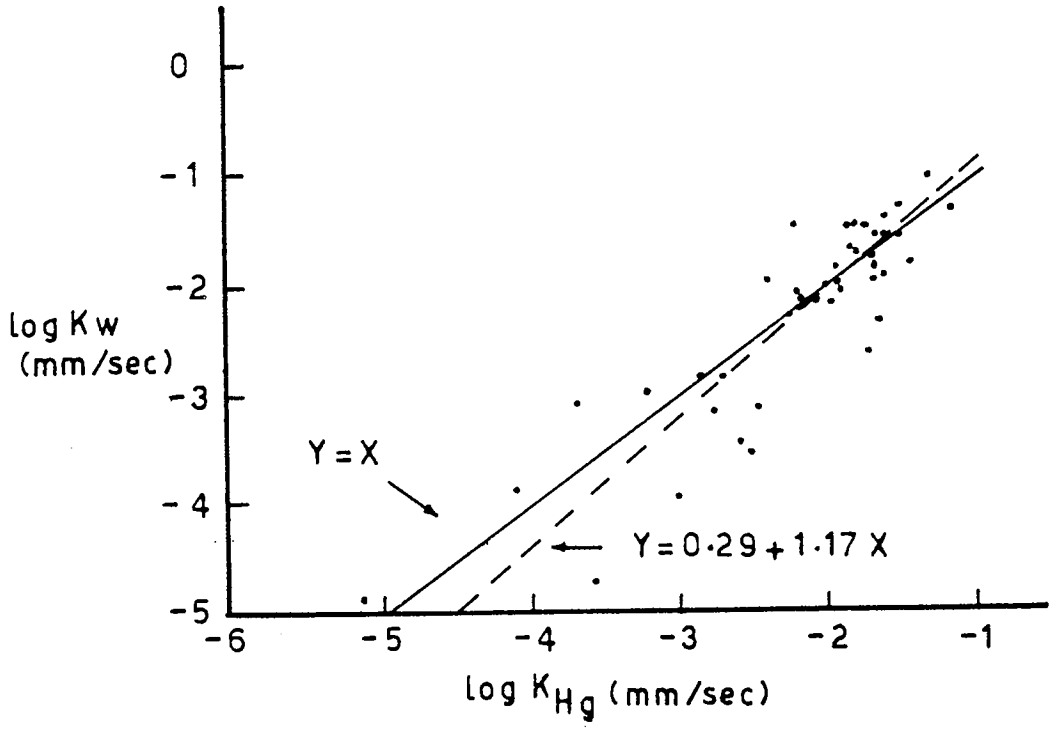

Figure 4.9 Comparison of measured hydraulic conductivity (K_w) with estimated values from pore-size distribution (K_{Hg})

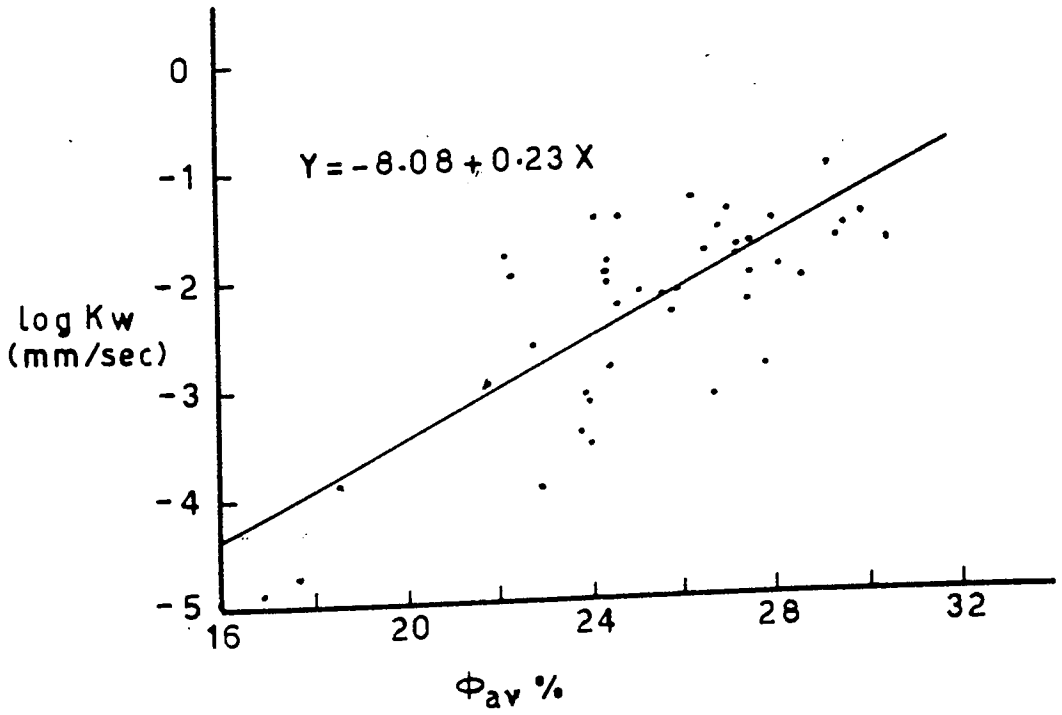

Figure 4.10 Relationship between porosity (ϕ_{av}) and hydraulic conductivity (K_w)

isotropy line at high values and shows greater off-set from Y = X line at the lower values. This result suggests that water resaturation and mercury porosimeter methods could be equally well-used for the determination of hydraulic conductivity in highly permeable rocks.

4.4 RELATIONSHIP BETWEEN HYDRAULIC CONDUCTIVITY-POROSITY AND PORE-SIZE DISTRIBUTION

Many factors exercise some control on porosity. These include grain size, sorting, amount of cement, intersticial matrix, shape of grains, fabric and diagenetic features; in particular authigenic pore-filling cements and dissolution. While the hydraulic conductivity in detrital rocks is chiefly affected by the radius of the pore throats, as well as the amount and type of clay mineral present where sandstone is practically impermeable if it contains 6-9% montmorillonite, but in the presence of kaolinite with up to 15% sandstone can remain quite permeable (Chilingarian and Wolf, 1975). The relationship between porosity and permeability and the different factors affecting them is not so easy to follow in porous sandstones because of their complex inter-relationship. The following are some of these relationships together with some examples.

There is a positive correlation between average effective porosity (ϕ_{av}) and hydraulic conductivity (K_w mm/sec), with a correlation coefficient of 0.7328. This relationship is shown in Figure 4.10) and the best fit line representing it is:

$$Y = -8.080 + 0.231\ X \qquad 4.18$$

where $Y = \text{Log } K_w$ and $X = \phi_{av}\%$.

Although it is apparent from this relationship that the higher values of hydraulic conductivity are associated with the more porous samples the correlation is not close enough to predict one from the other. This could be due to the presence of isolated dissolution pores resulting in low permeability. Also the sandstones with high clay content give rise to abundant micro porosity, small pore throats and consequently low permeability (Pittman, 1979).

The relationships between hydraulic conductivity (K_w and K_{Hg}) and the median pore radius of pore throats (Mr μm) are shown in Figures 4.11 and 4.12. In both cases there is highly significant positive correlation with r = 0.98 and 0.82 for Mr μm v. K_{Hg} and K_w respectively. The correlation is more significant in the case of Mr v. K_{Hg}, and this result is expected, as the pore radius calculated from P.S.D. is only an estimate based on the cylindrical pore throat model of the actual pore radius. The relationships can be represented by the following equations:

$$Y = 2.229 + 0.534\ X_1 \qquad 4.19$$

$$Y = 1.997 + 0.412\ X_2 \qquad 4.20$$

where Y = Log Mr m, X_1 = Log K_{Hg} and X_2 = Log K_w.

An important feature of the pore-size distribution curves is that some samples which end with the same ϕ_{Hg} have different pore-size distributions. The significance of this phenomenon is apparent when a comparison is made between hydraulic conductivity, type of diagenesis present, amount of interstitial clay present as well as the sorting of such samples. An example is given by samples 3/4 and 3/6 (Figure 4.13), where ϕ_{Hg} equals 28.24% and 28.14% respectively (ϕ_{av}% equals to 29.085 and 28.575). However, K_w equals to 1.13×10^{-1} mm/sec (11674.7 md) and 1.035×10^{-2} mm/sec (1071.9 md), and Mr equals to

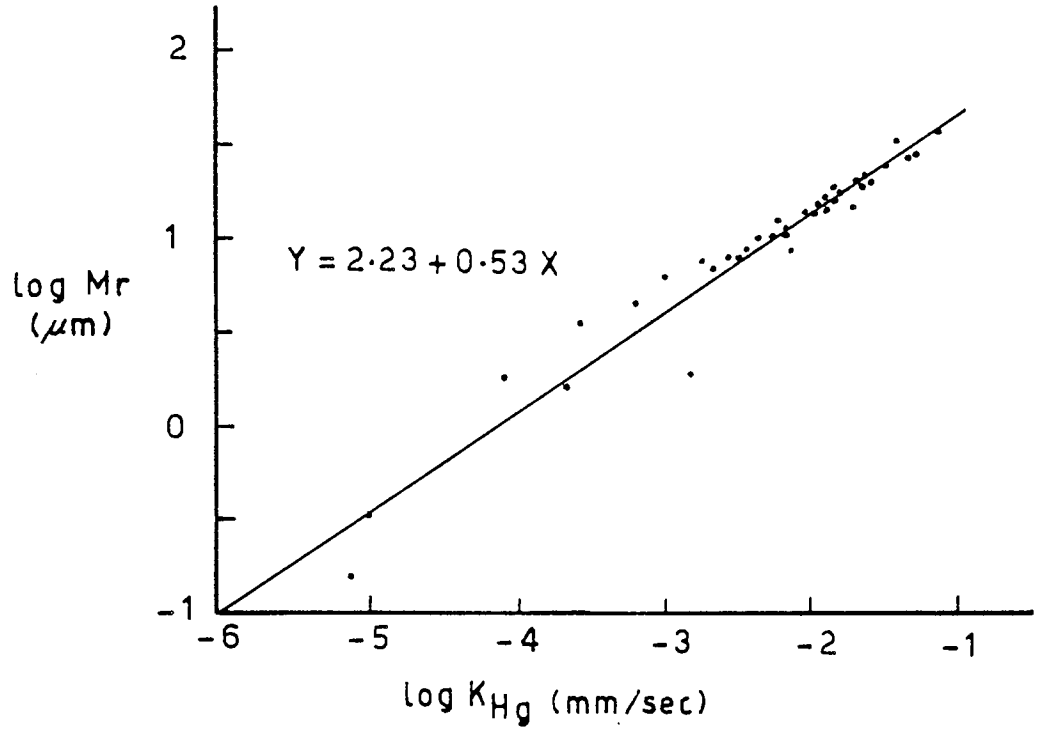

Figure 4.11 Relationship between calculated hydraulic conductivity (K_{Hg}) and median pore radius (Mr)

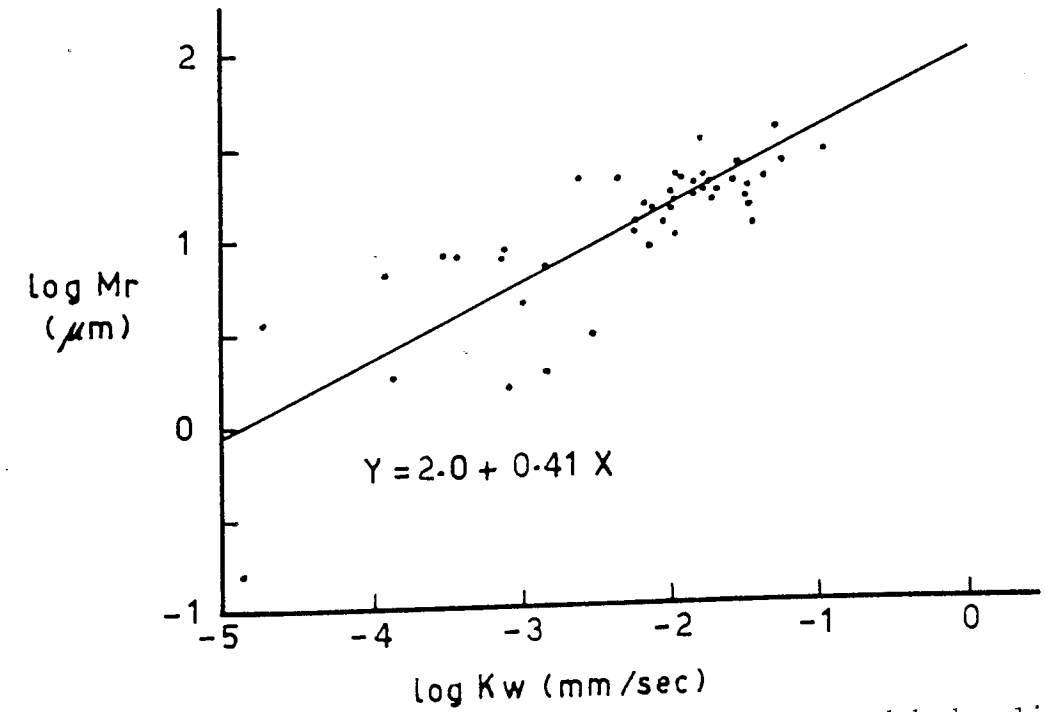

Figure 4.12 Relationship between measured hydraulic conductivity (K_w) and median pore radius (Mr)

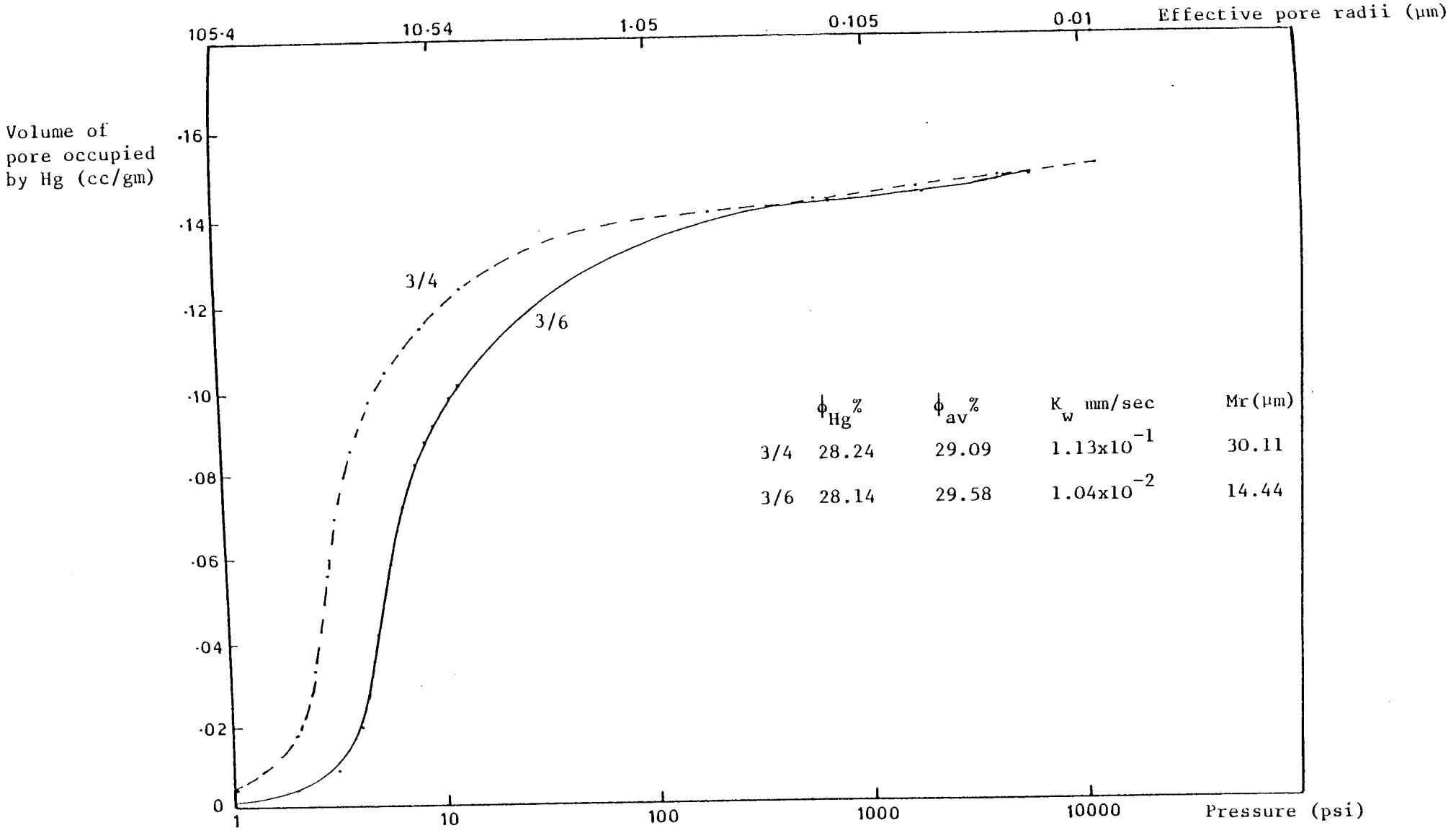

Figure 4.13 Relationships among porosity, hydraulic conductivity (K_w) and pore size distribution of samples 3/4 (dashed line) and 3/6 (solid line)

30.11 μm and 14.44 μm respectively. The microscopic study shows that 3/4 is coarser in grain size and more sorted than 3/6, while 3/6 has a higher clay content. Sample 3/4 has a higher carbonate cement (mainly dolomite) and an abundance of dissolution textures causing an increase in the secondary porosity and consequently the hydraulic conductivity. On the other hand, 3/6 is more tightly packed than 3/4, with an abundance of iron oxide clay films surrounding the grains. The lower K_w in 3/6 is thus thought to be due to the combination of these factors and the smaller Mr causing increase resistance to flow.

Another example is illustrated in Figure 4.14 where samples 14/23 and 14/33 are represented. These have nearly equal ϕ_{Hg} (26.34 and 26.66% respectively), while the K_w values are very different; 7.91×10^{-4} mm/sec (81.8 md) and 4.79×10^{-3} mm/sec (496.1 md). There is, in this case, a large difference in the value of median pore size: Mr equal to 9.09 μm (14/23) and 21.73 μm (14/33). This is readily explained according to the rock type, 14/23 is very fine sandstone with high clay content ($\sim$10%) as well as carbonate and hematitic clay films. These contribute to the blocking of pore throats and a decrease in the pore radius. Although 14/33 is a medium to coarse grained sandstone, a very high per cent of carbonate cement causes lower K values than expected.

Another feature shown by some samples is nearly equal K values, but different porosities, e.g. 14/26 and 14/40 (Figure 4.15). Here K_w is 1.65×10^{-2} mm/sec (1709.6 md) and 1.78×10^{-2} mm/sec (1842.5 md) respectively, while ϕ_{Hg} is 22.84% (14/26) and 26.93% (14/40), with Mr equal to 34 μm and 22.19 μm. Microscopic study shows that 14/40 is a moderately sorted, medium grained sandstone, while 14/26 is a

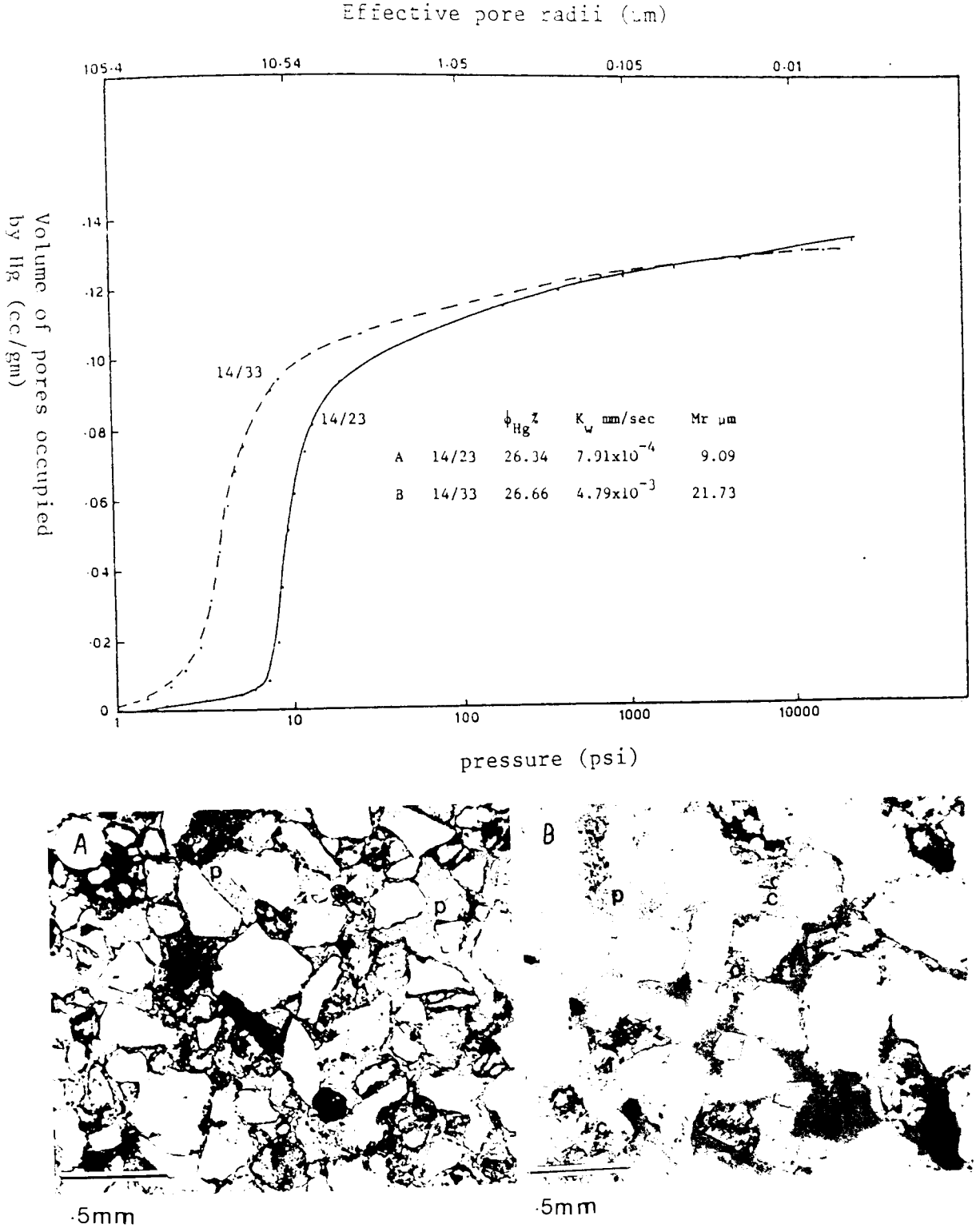

Figure 4.14 Pore size distribution curves and thin section photomicrographs for samples 14/23 (A, solid line) and 14/33 (B, dashed line). Notice the abundance of carbonate blocking the pore spaces and reducing permeability in B. Also the abundance of haematitic clay films and the smaller size of the pore spaces and grain size in A. C = carbonate, P = pore space

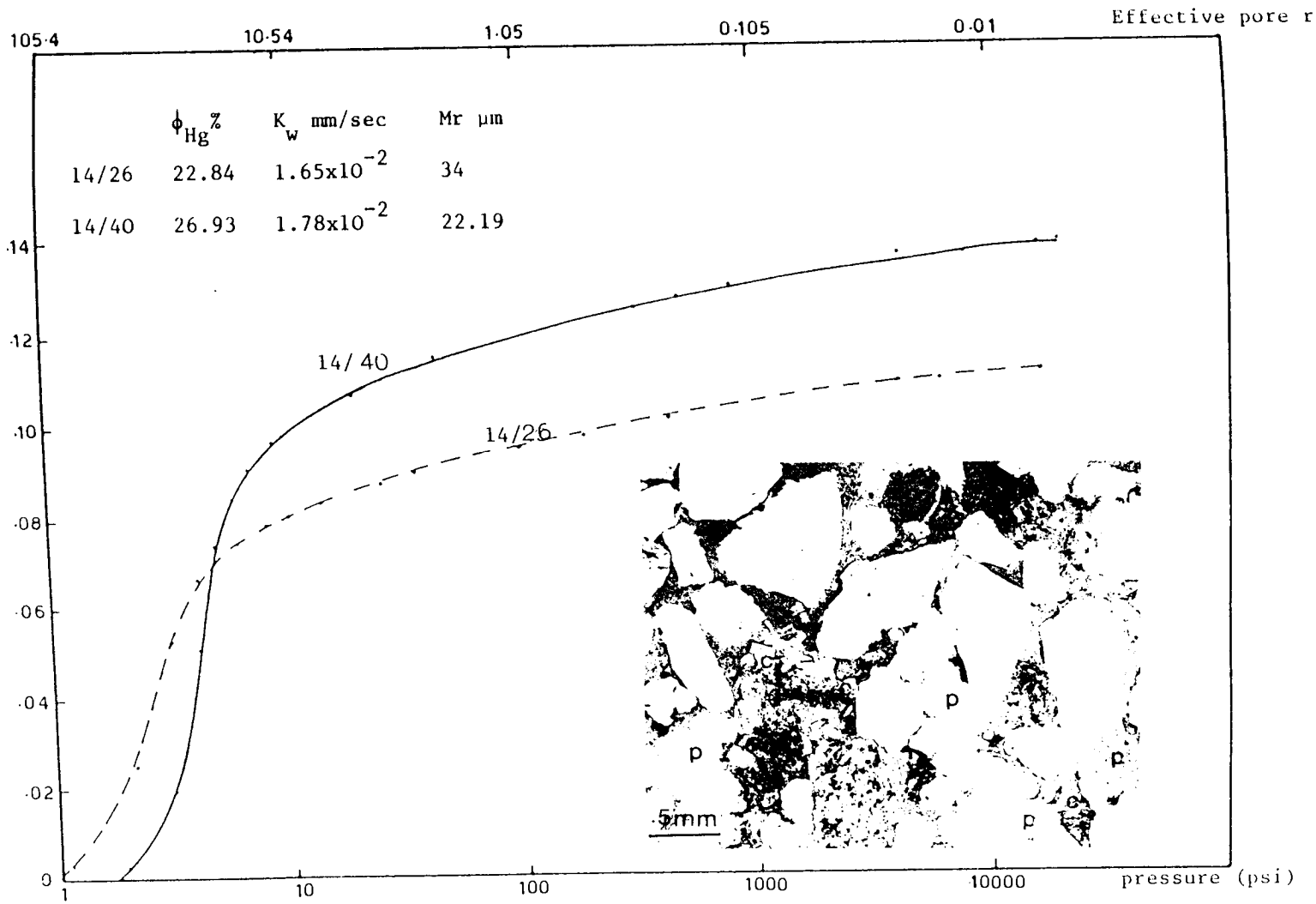

Figure 4.15 Pore size distribution curves, porosity and hydraulic conductivity of samples 14/26 (dashed line) and 14/40 (solid line), together with thin section photomicrograph of sample 14/26 showing the high carbonate content. C = carbonate, p = pore space

slightly pebbly sandstone with a higher percentage of carbonate (13.3%). Sample 14/40 also has a higher clay content (5.52%) than 14/26 (2.31%) and this may reflect the importance of authigenic minerals (especially clays) in reducing K values. Dissolution of authigenic carbonate in 14/26 may have resulted in higher porosity.

The just mentioned three examples indicate that pore-size distribution and Mr are a good indicator for hydraulic conductivity and this is in great agreement with the highly significant positive correlation of Mr v. K (Figures 4.11 and 4.12). Also the unclear relationship between porosity and hydraulic conductivity could be explained as a result of collection of factors, lithological and diagenetic ones. Diagenetic features are one of the most important factors, where development of authigenic minerals and pore filling cement have drastically affected permeability either by blocking the pore spaces or throats or by reducing the actual pore radius (Chapter Three) and in both cases affect K values. Also their effect on porosity is so important. The dissolution texture on the other hand has a very great effect in developing secondary porosity and consequently increasing hydraulic conductivity, if they are connected ones.

The factors affecting porosity of detrital rock are numerous, as mentioned before, the following are some examples to indicate the effect of some of these factors. Samples A14/23 and A14/27 have mean grain sizes (Mø) of 3.23 ø and 2.29 ø, and inclusive graphic standard deviations of (σ_I) of 0.76 and 1.05 respectively. According to Terzaghi (1925) and Trask (1931) the first sample might be expected to have a higher porosity than the other. However, the respective porosities are 26.66% and 27.42% indicating that coarser and more poorly sorted sandstone is slightly more porous. This may be due to

the higher percentage of interstitial clay present in 14/23 (∿10.7%) and an abundance of clay-oxide coating on almost all of the detrital grains. The most effective factor, not only on porosity but also to a great extent on permeability, is the median pore radius (Mr μm) which is equal to 9.09 and 20.87 μm respectively, and K_w equal to 7.91×10^{-4} mm/sec and 1.11×10^{-2} mm/sec (Figure 4.16).

Also packing density Pd% for the same samples are 54.93% (14/23) and 66.09% (14/27), and with reference to the number of contacts per grain, it is found that in sample 14/27 the floating and grains with one contact is higher than that of sample 14/23.

Samples 14/26 and 14/43 have Mϕ equal to 1.6ϕ and 1.7ϕ and σ_I are 0.68 and 0.99 respectively. The respectively average porosities (ϕ_{av}) are 22.17% and 22.73%. Both have a higher percentage of carbonate cement (13.3% and 14.3%) and both are slightly pebbly. In fact the samples are almost identical except that 14/26 is better sorted. But their hydraulic conductivity is different; K_w is equal to 1.65×10^{-2} mm/sec and 2.54×10^{-3} mm/sec for 14/26 and 14/43 respectively. This could be due to the pore-size distribution and the radius of the pore throats, where they have got Mr of 34.0 μm and 21.96 μm respectively (Figure 4.17).

4.5 RELATIONSHIP BETWEEN HYDRAULIC CONDUCTIVITY AND LITHOLOGY

In the hydraulic conductivities measured in the laboratory, fissured and fractured samples were avoided, which means that the K values represent that part of hydraulic conductivity affected by the inter-granular pore spaces only. These secondary fissures and fractures have a considerable effect on the hydraulic properties of the rocks.

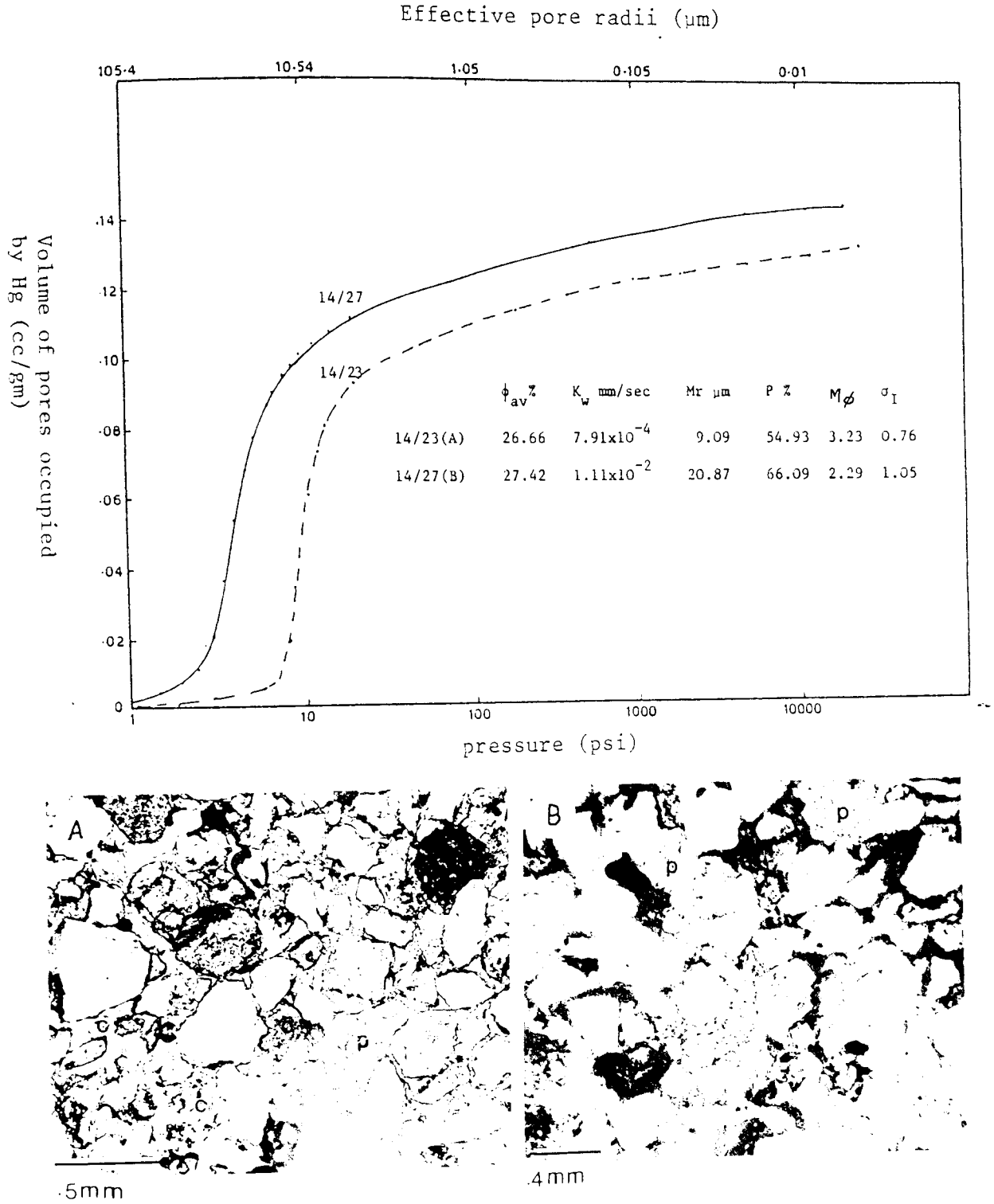

Figure 4.16 Comparison among porosity, hydraulic conductivity, pore size distribution and thin section photomicrographs of samples 14/23 (A, dashed line) and 14/27 (B, solid line) P = packing density, c = carbonate, p = pore space

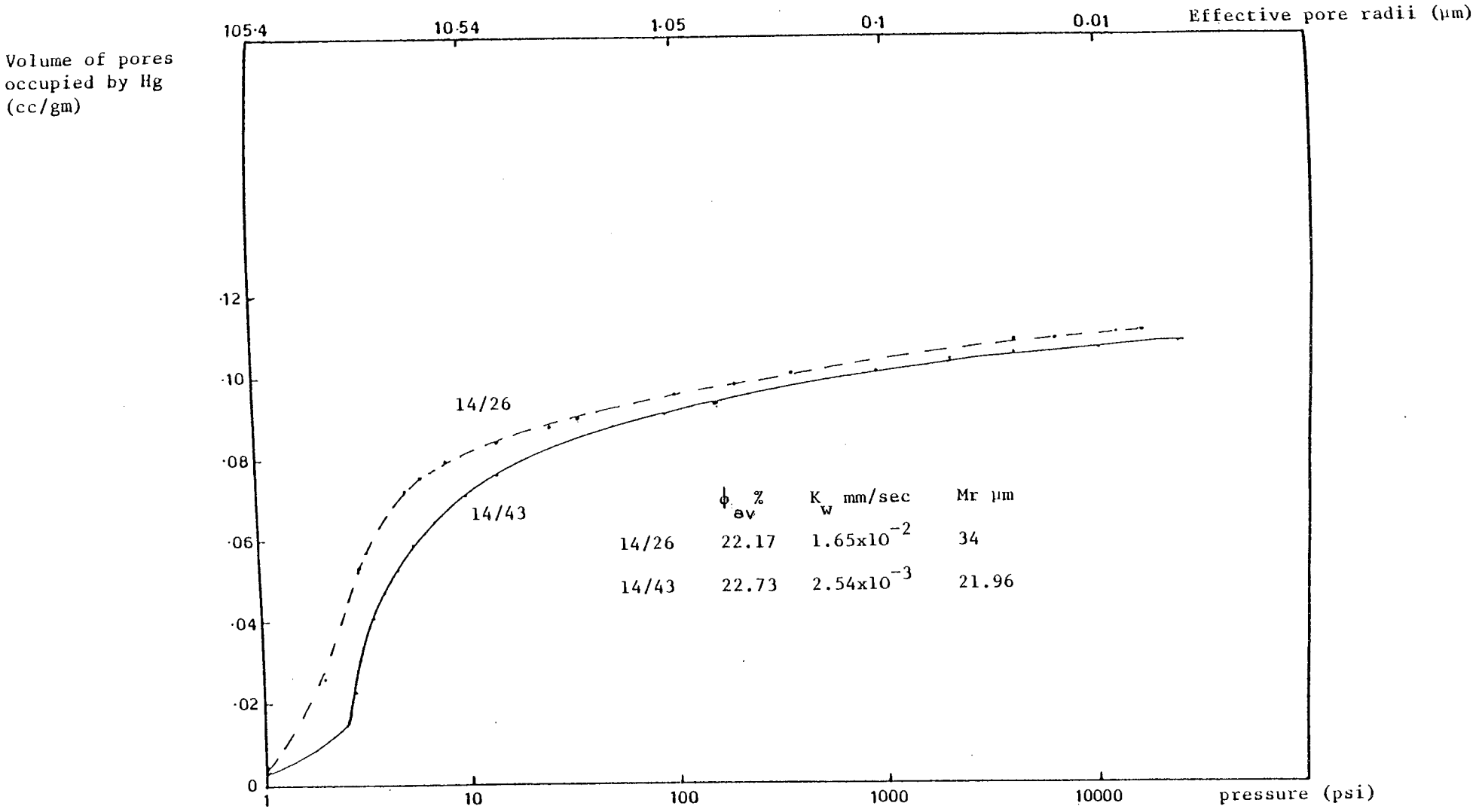

Figure 4.17 Relationships between porosity, hydraulic conductivity and pore size distribution of samples 14/26 (dashed line) and 14/43 (solid line)

This secondary feature was confirmed by both lithological and geophysical (caliper) logs as well as television logs as in the case of borehole A18 (Nottinghamshire Triassic Conjunctive Use Investigations, Report No. 5). Fractures occur in mudstone horizons of the transitional bed between Nottingham Castle and Lenton Sandstone Formations in all of the boreholes (Plate 4.1A) and in Clowick Formation (Keuper marl) represented in borehole A14 (Plate 4.1B). The fractures in these mudstones are mainly horizontal which may be effective for the possible movement of the water within it. This secondary fracture can be recognized from the caliper logs which show an increase in borehole diameter confirming the lithological features. In sandstone beds in both Nottingham Castle and Lenton Sandstone Formations, the fractures are abundant with horizontal, vertical and sometimes oblique ones. They are also sometimes abundant in borehole A3, in which some horizons look crumbly and broken or brecciated (Plate 4.1C). In this borehole, solution features are more abundant than anywhere else and the effect is microscopic as well as megascopic in the form of vugs (Plate 4.1D,E).

For the purpose of comparing the field pumping tests with the hydraulic characters from laboratory measurements, a rough estimation of transmissivity for BH A11, A14 and A18 gave values of 75, 172 and 195 m^2/day respectively. The field measurement of transmissivity at Epperstone, Nottinghamshire are 437 and 320 m^2/day for the observation points; old Epperstone Road (nearest to A18) and Goralstone (near to A14) respectively. This indicates that the field transmissivity is two to three times greater than laboratory data. The just mentioned lithological data is confirmed by this result, where fissuring and fracturing have great effects on the hydraulic characters of this water aquifer. This result is in agreement with Williams et al. (1972),

where they found that water moves through fissures four times greater as that by inter-granular flow at Edwinstowe, Nottinghamshire.

The hydraulic conductivities represented in this work as seen from Figures 4.18 to 4.21 show fluctuation in values from 1×10^{-5} to 1×10^{-1} mm/sec (low-high), with depth. This variation is controlled partly by lithological variation, where the lower values correspond to the mudstone beds toward the base of Nottingham Castle Formation. In the following each borehole will be dealt with separately.

For A14 the K_w values appear to fluctuate between 10^{-4} to 10^{-2} mm/sec, due to the abundance of mudstone beds separating Nottingham Castle Formation from Lenton Sandstone Formation in a transitional zone about 10 m thick. Also the thin mudstone layers throughout the Nottingham Castle Formation may possibly act as partial confining horizons (Figure 4.18). Secondary fractures do not appear to be abundant judging from the caliper log.

In A11 the K_w values also varied between 10^{-5} - 10^{-2} mm/sec also as a result of lithological variations. The secondary fractures have more effect than in A14 as noticed from the caliper log which record higher borehole diameter occasionally reaching 250 mm between 55 and 65 m depth, representing the transitional mudstone layers acting as a seal or impermeable bed (Figure 4.19).

For A18 the K_w values fluctuate between 10^{-5} to 10^{-2} mm/sec, where the values are highly decreased toward the mudstone transitional bed. In this borehole fissures and fractures have an effective rule upon the actual hydraulic properties as indicated from the television log (Nottinghamshire Triassic Conjunctive Use Investigations Report No. 5),

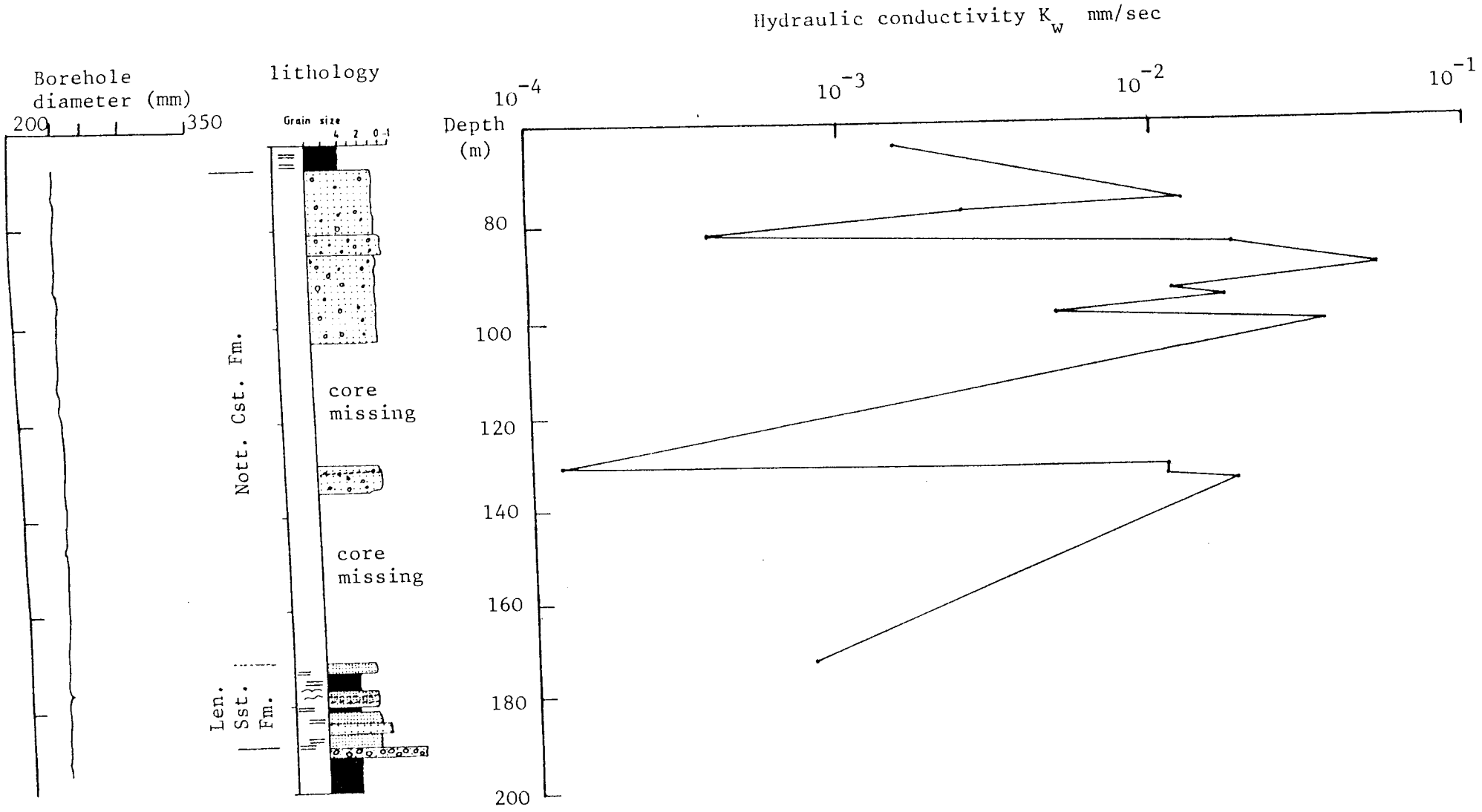

Figure 4.18 Caliper log, lithological and hydraulic conductivity variations with depth within the Sherwood Sandstone Group of BH A14

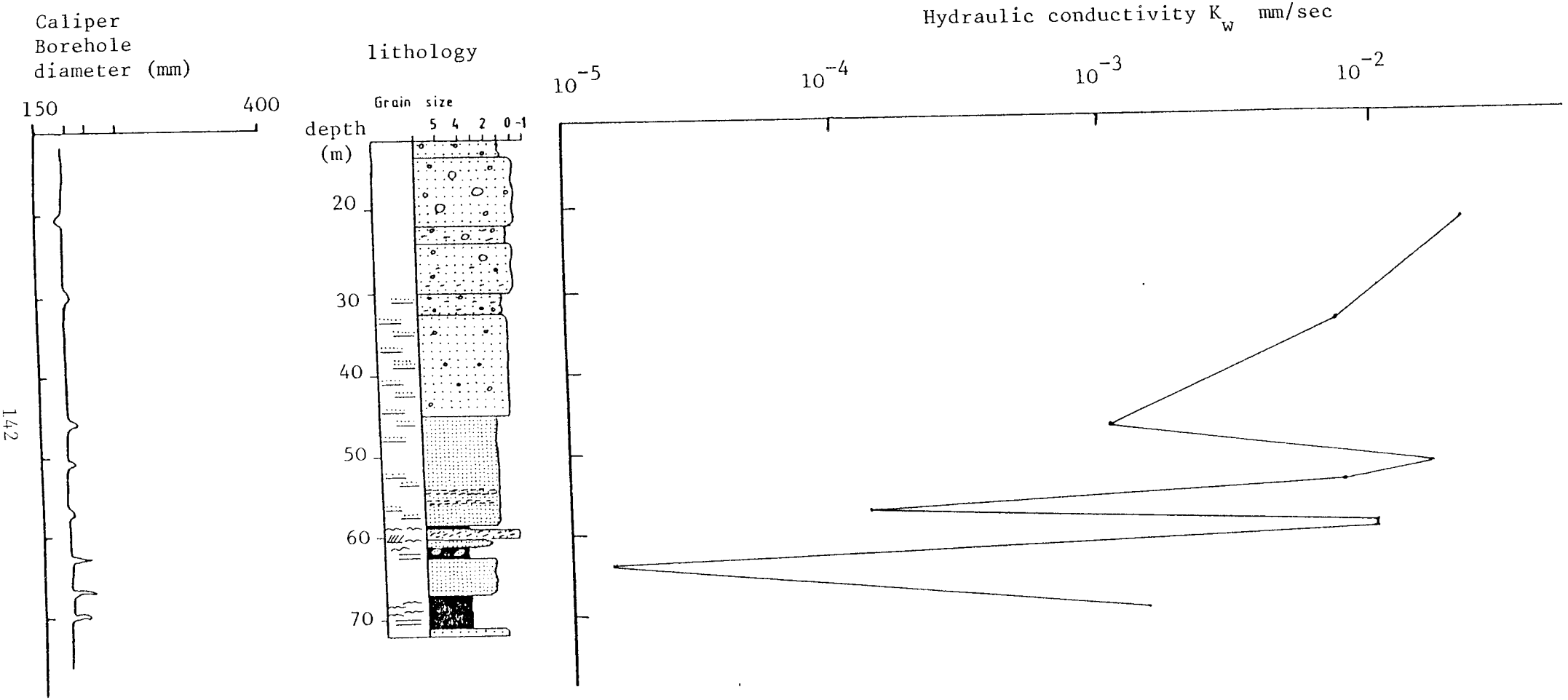

Figure 4.19 Caliper log, lithological and hydraulic conductivity variations with depth among the Sherwood Sandstone Group at BH A11

and from the caliper log (Figure 4.20) where the borehole diameter as a whole is higher than 200 μm, with occasional increase up to 275 mm at 29 m depth, and 250 μm at 45 m depth.

In borehole A3 although the K_w values show fluctuation with depth, the range of values - between 10^{-3} to 10^{-1} mm/sec - are higher than those of the other boreholes (Figure 4.21). These lower values tend to be due to an abundance of mudstone pebbles and flakes throughout the borehole (Plate 4.1F) and in particular toward the base of the borehole. In this borehole the high hydraulic conductivity values could be contributed to the abundance of dissolution features.

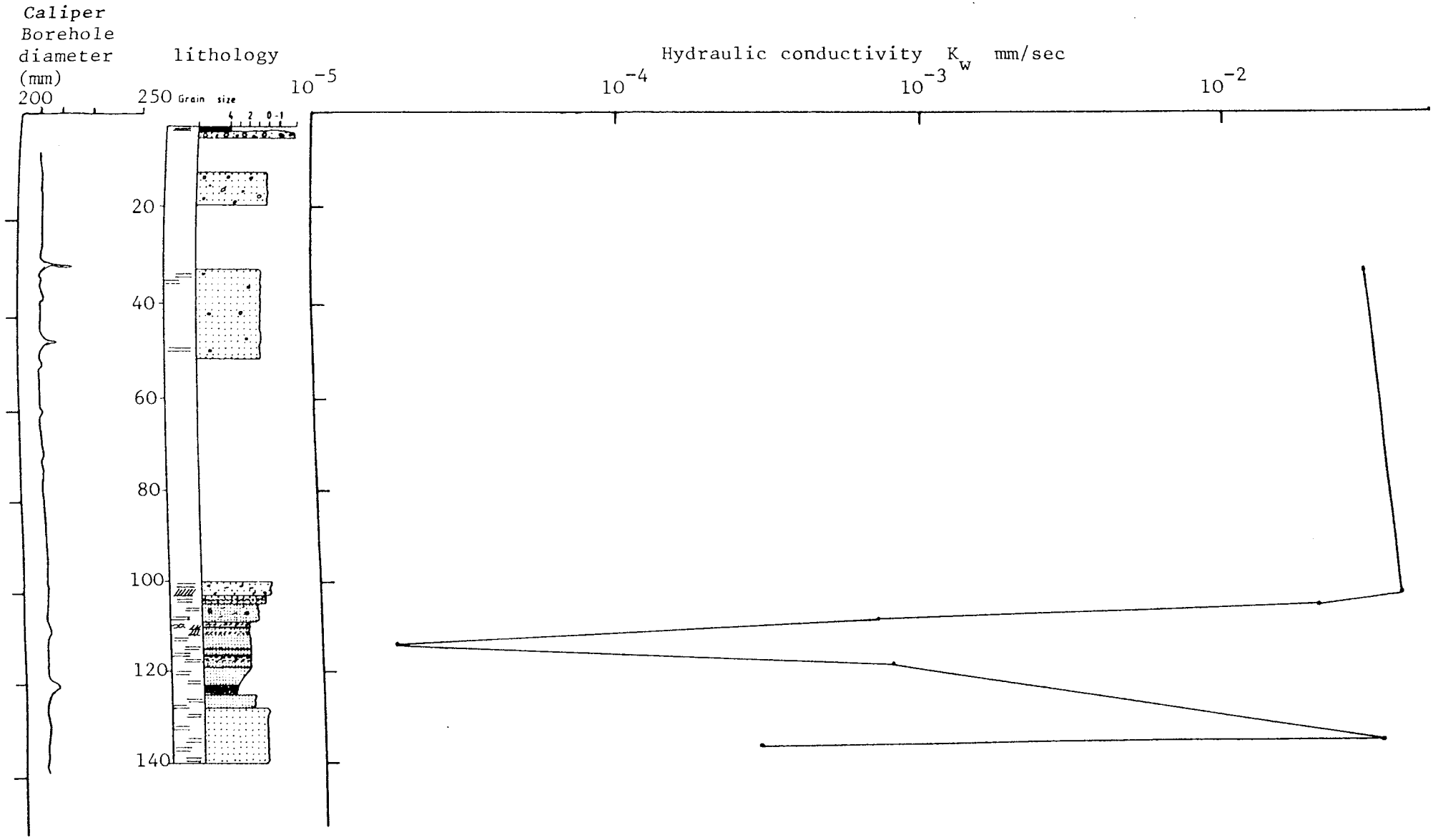

Figure 4.20 Caliper log, lithological and hydraulic conductivity variations with depth among the Sherwood Sandstone Group at BH A18

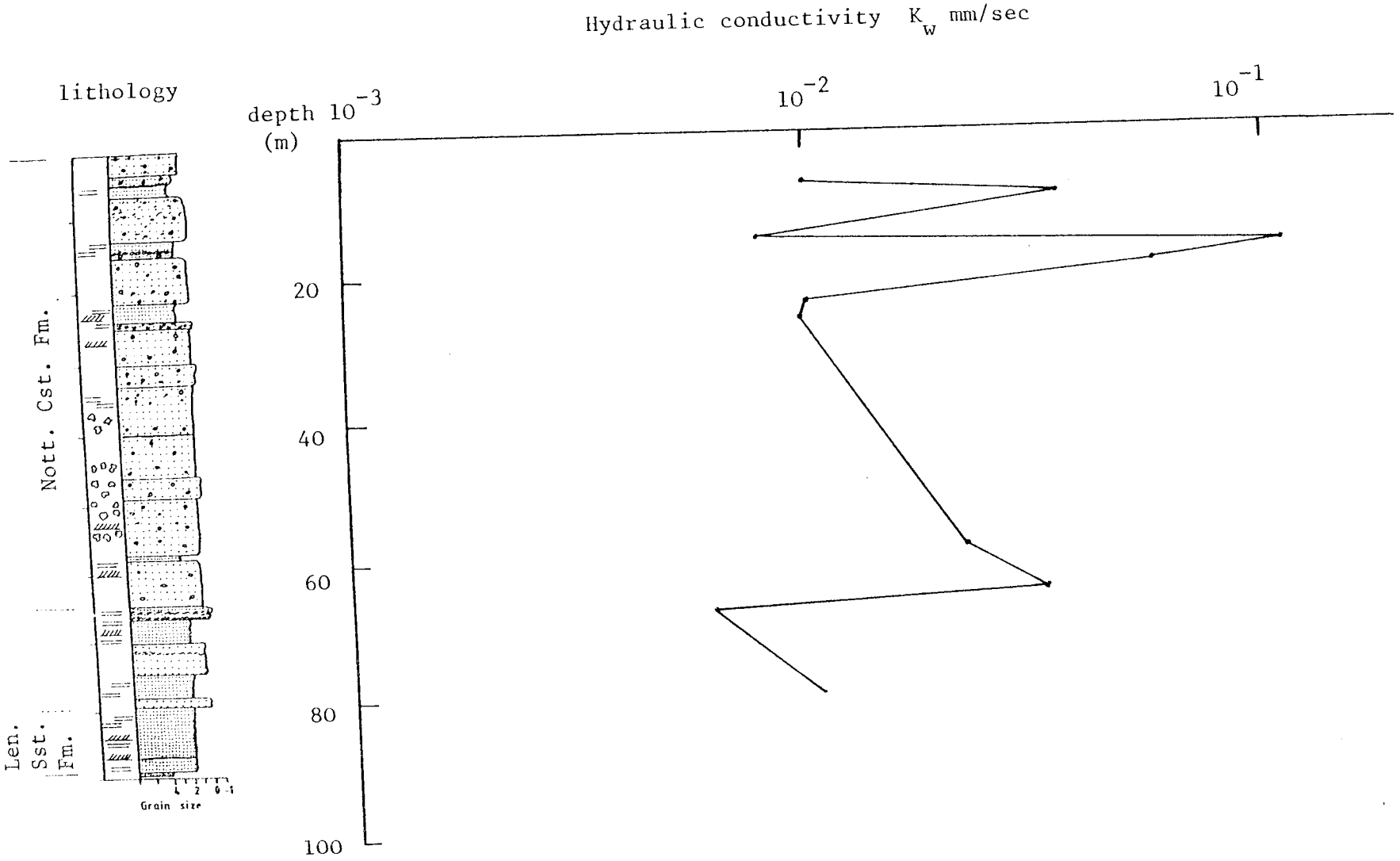

Figure 4.21 Lithological and hydraulic conductivity variations with depth among the Sherwood Sandstone Group at BH A3

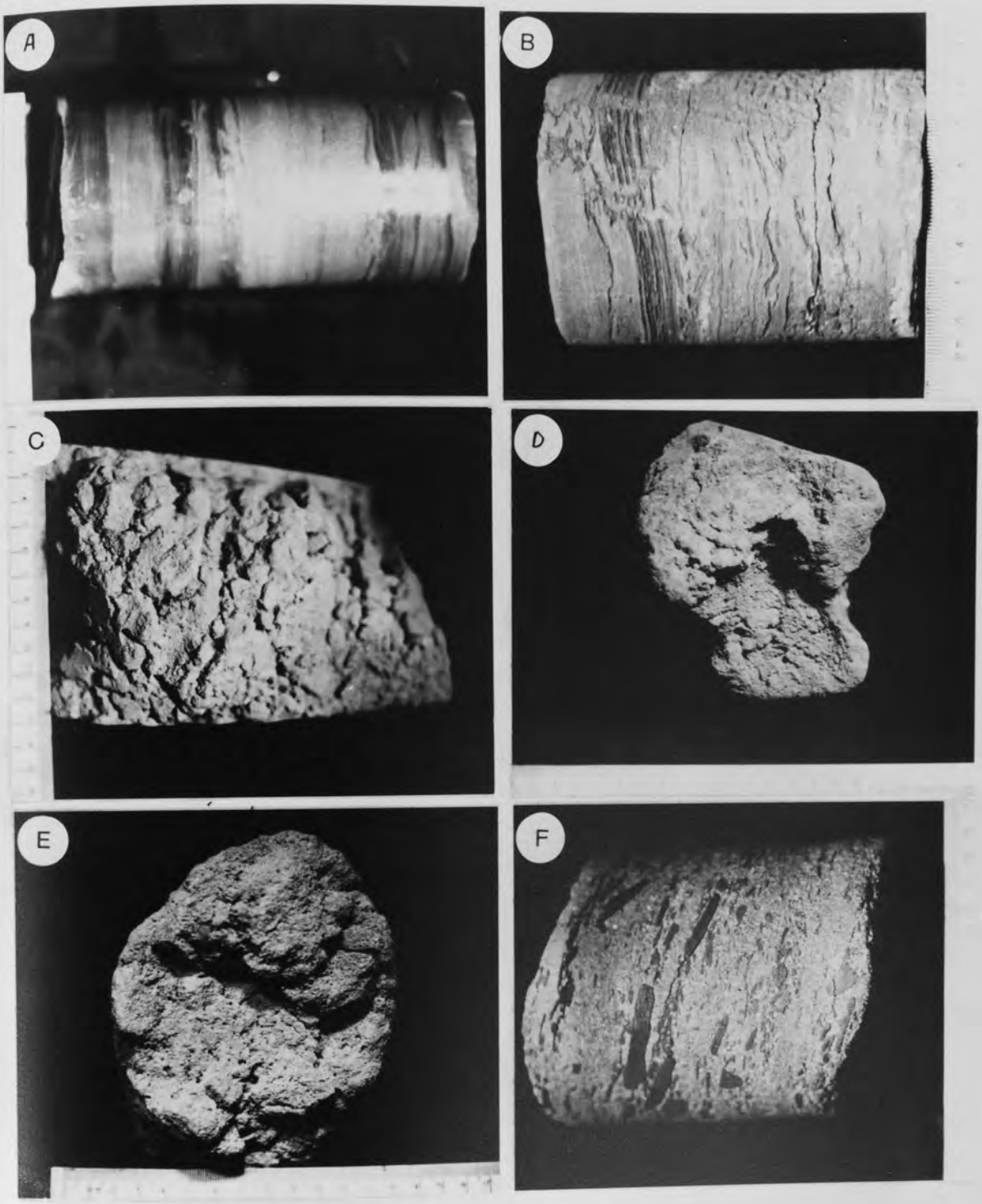

Plate 4.1

A. Horizontal fractures in mudstone horizons of the transitional unit between Nottingham Castle and Lenton Sandstone Formations, BH A14(71.7m)
B. Horizontal fractures in mudstone horizon of the Formation (Keuper marl), BH A14(178m)
C. Brecciated sandstone of Nottingham Castle formation at (51.5m) BH A3
D & E. Abundant megascopic dissolution voids in the sandstone of the Nottingham Castle Formation in BH A3(36.7& 64.8m)
F. Abundant mudstone flakes, slabs and pebbles in the sandstone of the Nottingham Castle Formation in BH A3(66m)

CHAPTER FIVE

GROUNDWATER CHEMISTRY

5.1 INTRODUCTION

The chemistry of Triassic groundwater has been given little attention in the past. Groundwater chemistry is important in affecting aquifer properties, chemistry of the rocks and also plays an important role in diagenetic processes.

Interstitial water, either groundwater or surface water is a very important medium for various chemical reactions related to aquifer alteration and diagenesis. These chemical reactions which include the removal of the unstable minerals either by dissolution and/or replacement, provide a vital source of elements for the groundwater. Some of these released ions may precipitate as authigenic minerals if the surrounding conditions are favourable, whilst the others may remain in solution and migrate with the groundwater. So the chemistry of the interstitial water is significantly affected by these diagenetic processes. As the alterations can take place at any time during the history of the sediments, and these processes probably are never truly terminated, so the chemistry of these interstitial pore waters can be considered to be constantly changing.

The processes governing the natural abundance of elements in groundwater and their migration within the aquifers are not fully understood at the present time. The first attempt to relate the hydrochemistry of Triassic aquifers to their geological environment was done by Edmunds and Morgan-Jones (1976) on the Triassic groundwaters of the Wolverhampton-East Shropshire area.

Diagenetic processes including both dissolution and replacement are considered to have a very important role on both porosity and intrinsic permeability. Dissolution is considered to be one of the most important processes responsible for creating secondary porosity in Triassic sandstones of the Nottinghamshire area (Chapter Three) with both framework components and cements having been affected. On the other hand, clay replacement, which is of only minor importance in the Nottinghamshire Triassic, is affective in decreasing the intrinsic permeability. However, both processes supply ions to the interstitial environment and a relationship between the chemistry of the water and the hydraulic properties of the rock could be predicted. The relationship between porosity, intrinsic permeability and water chemistry, as well as the origin of mineralization, has been studied before by Edmunds et al. (1973) on the Berkshire Chalk of England. Here they found that the highest mineralization is associated with the highest porosity and intrinsic permeability.

Chemical data for Triassic groundwater is scarce. However, the groundwater in the Bunter Sandstone (Sherwood Sandstone Group) in Nottinghamshire is dominated by calcium with magnesium and bicarbonate ions with total dissolved solids between 105-300 mg/l (Land, 1966). Edmunds and Morgan-Jones (1976) found that the waters in Bunter Pebble Beds and Upper Mottled Sandstones (Wildmoor Sandstone Formation) are considerably undersaturated with respect to calcite and dolomite with pH values $>7<8$ and +ve redox potential (Eh = +187 to +400 mV) in the Wolverhampton area.

The work done in this chapter is based upon: (1) The chemical analysis of 26 depth water samples collected from BH A11, A14 and A18. The

samples were analysed by atomic absorption spectrophotometry (AAS) for the elements: Ca, Mg, Na, K, Si, Al, Fe, Mn, Cr, Cu, V, Co and Zn. (2) Mineralogical analysis of suspended sediment in the aquifer. The water samples were filtered through 0.45 μm pore size filters and the fine fractions were mineralogically analysed by means of XRD to determine the clay minerals present associated with the groundwater. (3) Chemical analysis of the fine fractions by means of AAS. No discussion of these data is included here since no specific relationships were detected (Appendix 4).

One of the main aspects of this work has been to establish relationships between water chemistry and diagenetic processes which may be operating in the aquifer at the present time. The occurrence of minerals has been predicted on the basis of calculations from mineral stability diagrams and these compared with those actually present as seen from XRD, SEM and microscopic study. Also an approach to water mineralization and aquifer properties is discussed especially in relation to secondary porosity generation.

5.2 METHODOLOGY

5.2.1 Sampling and Field Work

The work done in this chapter is based upon the chemical analysis of 26 static groundwater samples collected during June 1981 from boreholes A11, A14 and A18. The depth water samples were taken at regular intervals of 10 m for BH A11 and 15 m for BH A14 and A18. The first sample in each borehole was taken just below the water level; for BH A11 and A18 the first sample was at 15 and 10 m depth and water level

was at 14.25 and 8.26 m depth respectively. In BH A14 the water level was at 5.74 m depth, but the first sample collected at 70 m depth because borehole casing extended to 70 m depth where the contact between Keuper Marl (Mercia Mudstone Group) and Bunter Sandstones occurs. The static water samples are considered to represent the interstitial water present at each depth (formation water). Dry and clean polyethylene bottles of half-litre volume were used for water collection after rinsing the bottle with the water being sampled. The bottle was then tightly sealed immediately after the field measurements, labeled and transferred to the laboratory for the rest of the analyses. The electric conductivity, pH and temperature measurements for each sample were done immediately after collecting the sample at the well head in the field. On the same day, the electric conductivity and pH were measured again at the laboratory, and the average of the sum of both readings was calculated. The results of these measurements as well as the sample depths are given in Table 5.1.

5.2.2 Sample Analysis

After the pH and specific conductivity measurements were done in the laboratory the water samples were filtered through 0.45 µm pore size filter using a millipore filter (model YY22 090 00). These fine fractions were used for subsequent mineral and chemical analyses, while filtered waters were analysed for the elements Ca, Mg, Na, K, Si, Al, Fe, Mn, Cr, Cu, V, Co and Zn using the atomic absorption spectrophotometer (Perkin-Elmer model 460). No chemical treatments were done on these water samples for the chemical analyses. Sometimes they had to be diluted with double distilled water to adjust the concentration of the elements to within the detection limits of the apparatus. All the

analyses were carried out within one week of the sample collection. The concentration of each element is expressed in ppm which is numerically equivalent to mg/l (up to the concentration of 700 mg/l) and the results are given in Table 5.1.

The fine sediment fractions obtained from the filtration of the water samples (using filters composed of pure biological mixtures of cellulose acetate and cellulose nitrate) were left to dry at room temperature. These fine fractions were used for qualitative mineral analysis by means of XRD, whenever the sample was quantitatively sufficient. Actually, only fourteen samples were suitable for XRD analysis. Co $K\alpha$, Ni filtered radiation was used between 2^{o} and 40^{o} 2 θ, to determine the clay minerals present associated with the water.

As the amount of the suspended materials in the water were quantitatively too small to be analysed, alternative fine fractions were prepared for chemical analyses. In this respect 17 representative rock samples were chosen from nearly the same depths as the collected water samples. For this purpose, the rock samples were disaggregated very carefully, sieved and the fine fractions (<38 μm) were collected for chemical analysis. These fine fractions were dissolved by the fusion method using a mixture of the rock sample and spectro flux in a furnace at 1000^{o}C for about 15 minutes. The mixture was then dissolved in 4% nitric acid and the samples analysed for the elements Ca, Mg, Na, K, Si, Al, Fe, Mn, Cr, Cu, Zn, Pb and Ni using AAS. The results are given in Appendix 4 as they have not been used for any discussion.

5.3 ANALYTICAL DATA

5.3.1 Specific Electrical Conductance

The electrical conductivity (EC) was used as an easy and rapid method to indicate the total dissolved solids. The conductance of groundwater increases with increasing salt content. As the conductance is a function of water temperature, the specific electrical conductance (SEC), measured in S/cm (Siemens/cm), at standard temperature (usually 25°C) is used especially for the purpose of comparison. As many natural waters have EC of less than one S/cm, it is convenient to refer to conductivity as µS/cm. The relationship between SEC (measured at 25°C and in the range 100 - 5000 µS/cm) and dissolved solids was shown by Richards (1954 in Todd, 1980) to be equivalent to 1 ppm dissolved solids/1.56 µS/cm.

The electrical conductance for each static water sample was measured in the field, by the well head, immediately after sample collection using a Harris Conductivity Meter C29960 14. The temperature of the water samples were also recorded at the site of collection to enable the conversion into specific electrical conductance. The EC readings were measured again on the same day using the same instrument in the laboratory to ensure the accuracy of the measurements. Both readings were nearly identical in all cases. These absolute values were converted into SEC at 25°C. The SEC for groundwater in the studied boreholes (Figure 5.1) shows more or less constant values ranged between 203 to 590 µS/cm which is roughly equivalent to a total amount of dissolved solids of 130 to 378 ppm.

BH A11 records the highest values, which fluctuate between ∿272 - 590

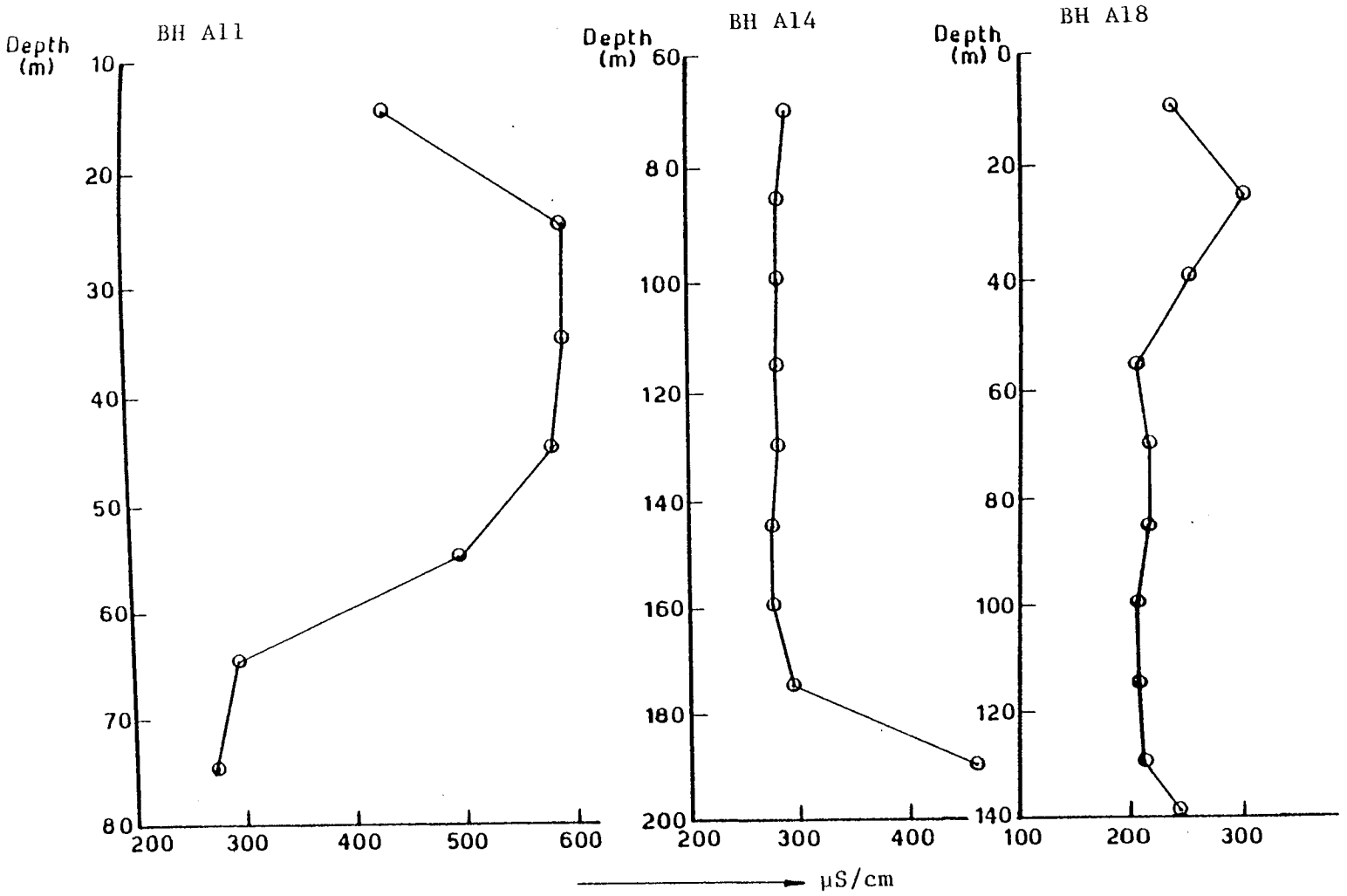

Figure 5.1 Specific electric conductivity in µS/cm (at 25°C) for Triassic groundwater of the Sherwood Sandstone Group

µS/cm and show a general decrease with depth (Figure 5.1). The highest conductivity values recorded for this borehole are between 25 - 45 m depth and represent the medium-coarse grained slightly pebbly sandstones of the Nottingham Castle Formation. These rocks also recorded the highest porosity and hydraulic conductivity values (Table 4.1) in BH A11 and the highest concentration of Ca, Mg and Na ions (Table 5.1). This suggests an association between high porosity/hydraulic conductivity and dissolution as a source of ions to the groundwater.

The SEC for BH A14 is nearly constant to about 160 m depth with values around 280 and 290 µS/cm indicating good quality water and reflecting the homogeneous lithology of the reservoir rocks (Chapter Two). Below 160 m depth, SEC shows an increase to a maximum value of 458.5 µS/cm at 190 m depth. This highly mineralised groundwater is associated with the conglomeratic bed which probably represents the Permian-Triassic boundary.

For BH A18, the SEC generally records low values ranged between 203 - 246 µS/cm indicating a low content of dissolved solids and consequently a good quality water. The SEC values are nearly constant throughout the borehole except towards the top (Figure 5.1) which recorded the highest SEC value of 291.6 µS/cm at about 25 m depth. The lowest dissolved solids recorded in this BH A18 could be due to dilution of formation water as a result of the abundance of secondary fissures and fractures recorded in this borehole.

5.3.2 pH Values

The pH, which is simply the negative logarithm of the hydrogen-ion concentration, was measured for all the groundwater samples at the site

of collection to give an idea about the acidity of the water. The pH readings were measured in the field using pH Meter model 101, special no 5761 Analytical Measurements. Calibration was performed using standard solution prepared from commercial buffer solution. The pH was measured again in the laboratory on the same day of collection, using Pye Model 291 pH Meter and using standard tablets for buffer solution. The average values of field and laboratory were calculated and are represented in Table 5.1.

The pH values ranged between 7.5 to 8.2 except for the first sample in BH A18 which recorded a higher pH value of 8.8. The pH values are more or less constant within each borehole. In BH A11 the values ranged between 7.5 and 8.2; values for BH A14 are between 7.6 and 7.8 and in BH A18 the values are between 7.9 and 8.2 with the exception of the higher value of 8.8 being recorded for the first sample.

Within the pH range of 7-8 bicarbonate is the dominant dissolved carbon species in the groundwater and reaches its maximum concentration at pH 8.2 where 97.9% of CO_2 present as HCO_3^- (Blatt et al., 1980 p. 347). Although the anion concentrations have not been determined in these groundwaters, the results of previous Triassic groundwater analyses in Nottinghamshire (Land, 1966) and in the Wolverhampton - East Shropshire area (Edmunds and Morgan-Jones, 1976) indicate the dominance of HCO_3^-. Using the pH values, temperature and HCO_3^- concentrations, Edmunds and Morgan-Jones (1976) calculated the saturation of the Triassic groundwater with respect to calcite and dolomite. They found that the Bunter Pebble Beds and the Upper Mottled Sandstones (Wildmoor Sandstone Formation) are undersaturated with respect to both calcite and dolomite. These results are consistent with the sandstones under study as indicated by the abundance of carbonate

dissolution textures and oversized pores.

5.3.3 Major Elements

5.3.3.1 Calcium and magnesium

Calcium is one of the major elements in the groundwater and one of the most common ions having a permissible limit in drinking water of 200 ppm. It was determined in these water samples with values up to 125 ppm and an overall average of 45.92 ppm. The concentration of Ca is highest in BH A11 and lowest in BH A18 (Table 5.1). The distribution of calcium in groundwater with depth is shown in Figures 5.2, 5.3 and 5.4. The variation compares very closely with the variation in specific electrical conductance (Figure 5.1). This feature reflects the important contribution which Ca^{2+} makes to the total amount of dissolved solids.

Magnesium concentration is more or less constant throughout the aquifer in each of the boreholes studied (Figures 5.2, 5.3 and 5.4) showing only small variation ranging from 16.6 to 39.5 ppm with an average of 26.11 ppm. In BH A11, Mg^{2+} reaches the highest values, ranging from 24.6 to 39.5 ppm, and shows a tendency to decrease with depth. For BH A18, the Mg^{2+} concentration is slightly lower than that of BH A11 ranging between 16.6 and 33 ppm and showing a slight fluctuation with depth. In BH A14 the concentration of Mg is much more stable than the other two boreholes ranging between 19.7 and 25.1 ppm.

The Mg/Ca ratio for the waters of BH A11 and A14 is lower than unity, while for BH A18 this ratio is > 1. Examination of the thin section corresponding to the respective water sample horizons it has been

noticed that in the BH A18 dolomite is the main carbonate cement present and shows extensive dissolution features. In BH A11 and A14 calcite and Fe-calcite were seen to be the most dominant carbonate minerals. This can be explained by the groundwater being undersaturated with respect to calcite and dolomite causing both minerals to react (Eq. 5.1, 5.2) with the interstitial water to reach an equilibrium. This would give rise to higher Mg^{2+} than Ca^{2+} in BH A18 where dolomite is the dominant mineral and higher Ca^{2+} than Mg in the others when calcite and Fe-calcite are the main carbonate cements.

$$CaCO_3 + CO_2 + H_2O \rightleftharpoons 2\ H\ CO_3^- + Ca^{2+} \qquad (5.1)$$

$$2(Ca,Mg)\ CO_3 + 2CO_2 + 2H_2O \rightleftharpoons 4\ H\ CO_3^- + 2Ca^{2+} + 2Mg^{2+} \qquad (5.2)$$

The reactions 5.1 and 5.2 (above) obviously result in the dissolution of carbonate minerals either on a micro- and macro-scale and give rise to the development of secondary pores in association with the release of Ca, Mg and HCO_3 ions to the groundwater.

5.3.3.2 Potassium and sodium

Although in the sedimentary rocks potassium is more abundant than sodium, natural waters in general have much lower concentration of K^+ as compared with Na^+. This is because K^+-bearing silicate minerals are relatively more resistant to chemical weathering than silicates containing Na^+. Also Na^+ ions tend to remain in the solution once they have been released from the silicate mineral structures, while K^+ ions tend to be fixed in solid authigenic products, especially clays.

The potassium content of natural waters is normally no more than

10-15 mg/l (Holden, 1970). In the Nottinghamshire Triassic groundwaters all the samples have K^+ contents less than 5 ppm except for the first sample in BH A18 which recorded a higher value of ∿10 ppm. The overall average for the three boreholes is 2.58 ppm.

Potassium concentration is more or less constant in the three boreholes showing a slight tendency to decrease with depth as is obvious from BH A11 and A18 (Figures 5.2 and 5.4). However, the values in BH A14 are much more constant than the others (Figure 2.3). For BH A11 K^+ ion concentration ranged between 1.02 to 4.96 ppm with the highest value recorded in the shallowest sample and with an overall tendency for K^+ to decrease with depth (Figure 5.2). In BH A18 the potassium concentration is nearly constant (1.53 - 2.03 ppm) except for the first sample which has 9.97 ppm K^+ content (Figure 5.4). While in BH A14 the K^+ concentration has the highest values ranging between 2.73 - 3.69 ppm with a tendency for the readings to be constant along the whole depth. The potassium content in the shallowest samples (BH A11, A18) record the highest values in the groundwater samples. These water samples are the nearest ones to the agricultural mantle. This is in accordance with Harth (1965) who found that the use of the fertilizers in areas of intense agriculture increases the concentration of potassium in groundwater.

Sodium content in these groundwaters is variable with a wide range of readings from 2.2 to 116.5 ppm and an average value of 34.52 ppm. The distribution of Na^+ in the groundwater with respect to depth shows no clear systematic variation as a whole (Figures 5.2, 5.3 and 5.4). In boreholes A11 and A18 the lowest concentration of Na^+ is associated with the transitional unit between the Nottingham Castle

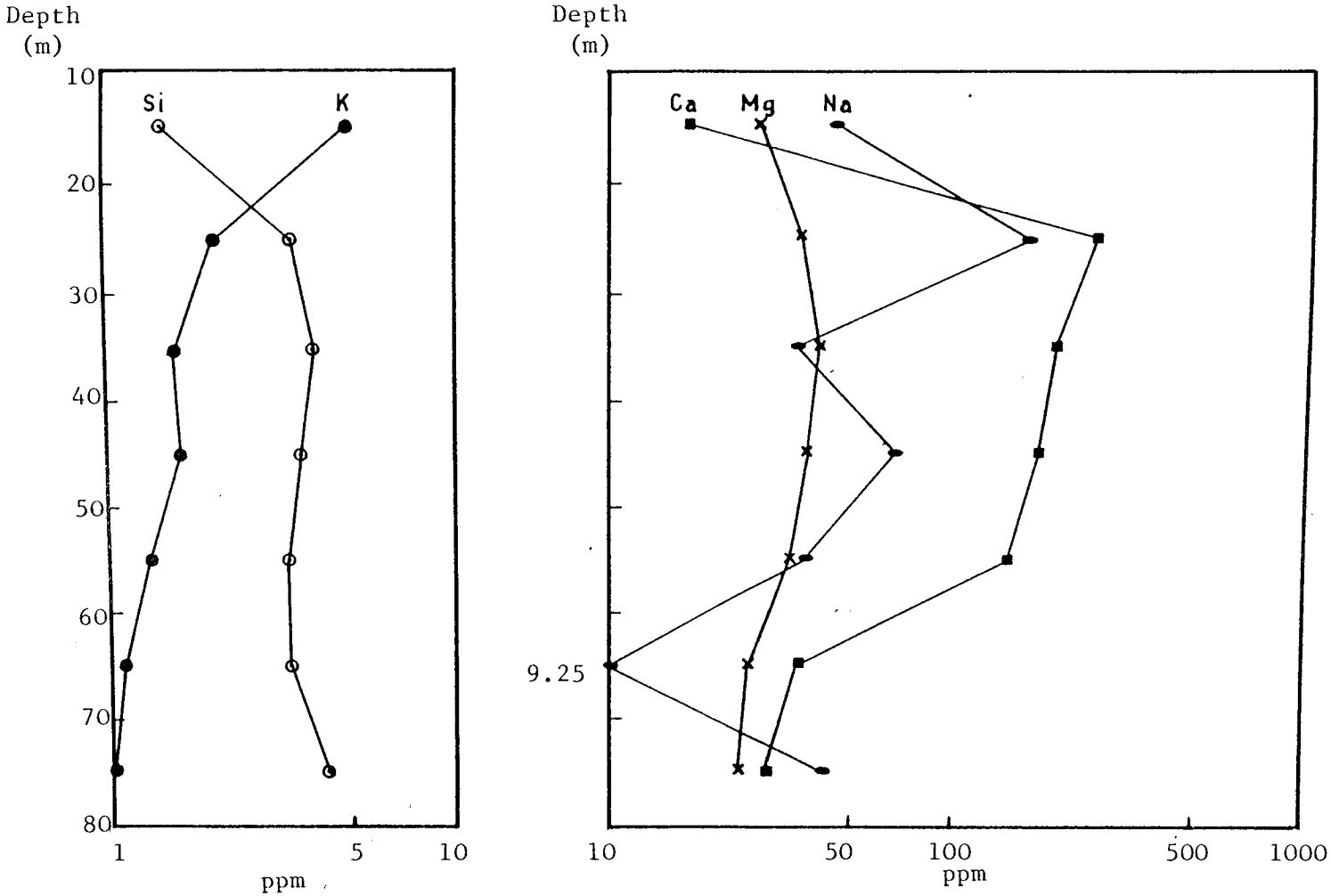

Figure 5.2 Concentrations of Calcium, Magnesium, Sodium, Potassium and Silicon in the Triassic Groundwater from Borehole A11

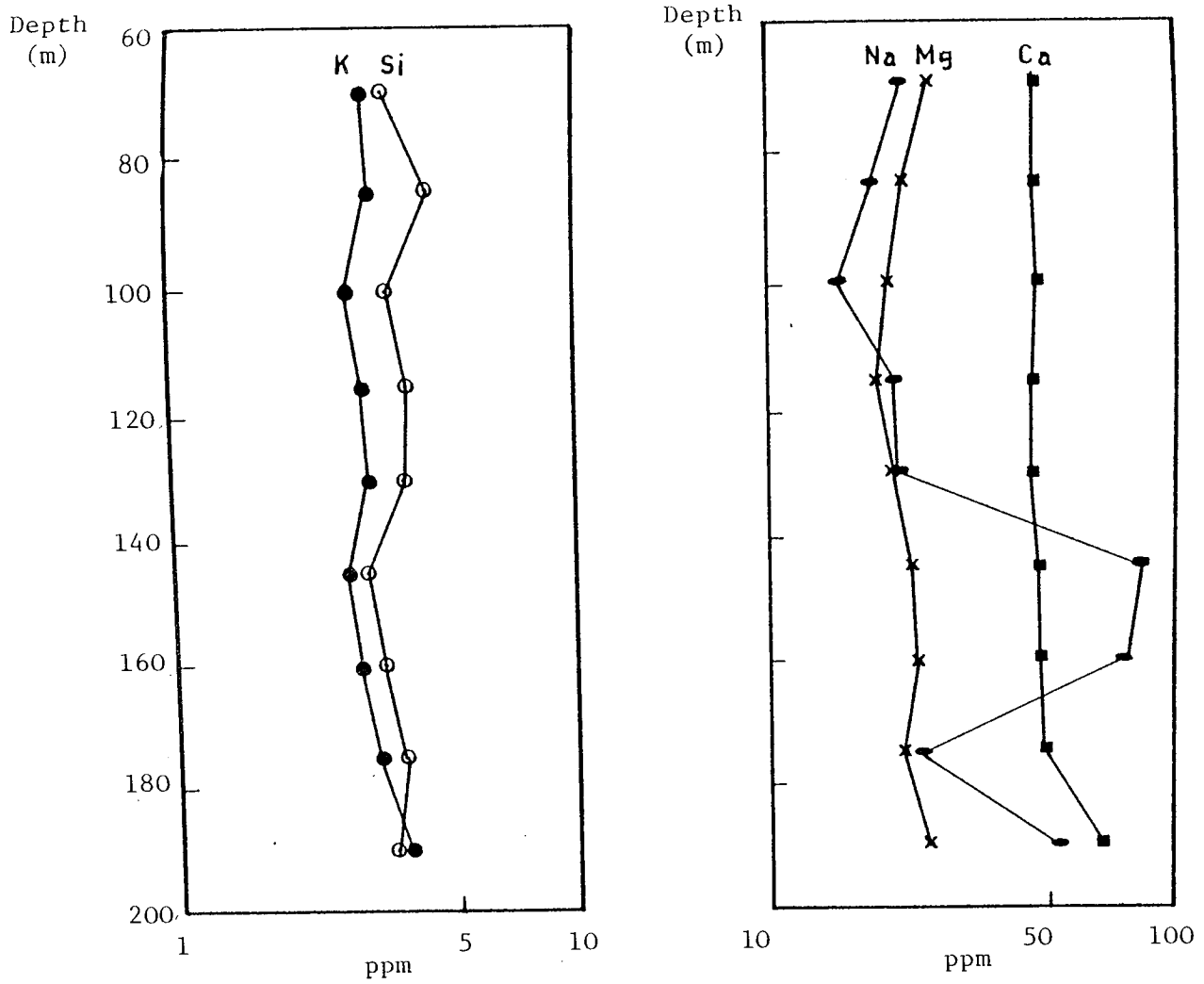

Figure 5.3 Distribution of Calcium, Magnesium, Sodium, Potassium and Silicon in the Triassic Groundwater from Borehole A14

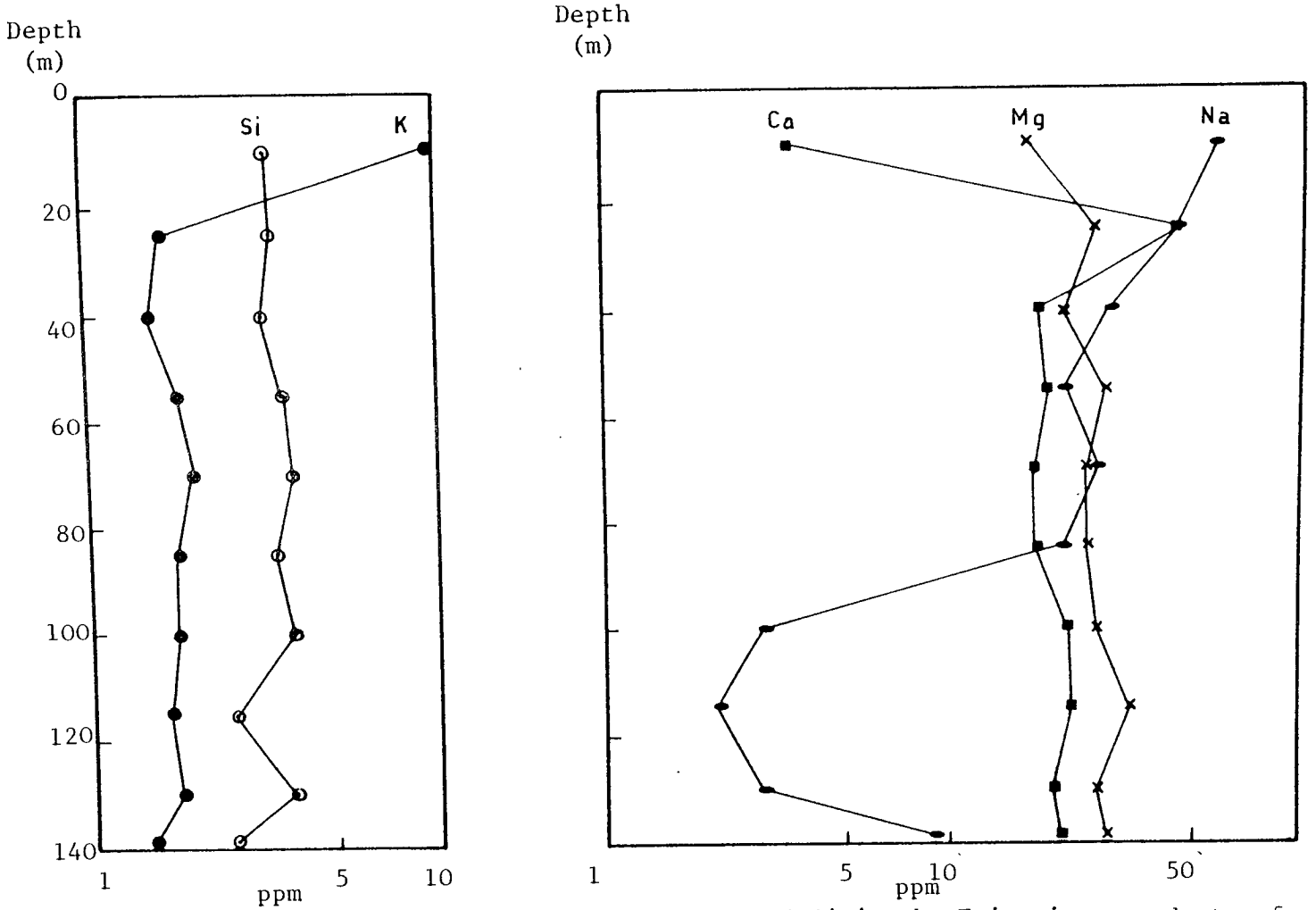

Figure 5.4 Concentrations of Ca, Mg, Na, K and Si in the Triassic groundwater from Borehole A18

Formation and the Lenton Sandstone Formation where there is an abundance of mudstone laminae e.g. sample No. 6 (BH A11), sample Nos. 23, 24 and 25 (BH A18) have the lowest Na^+ content (Table 5.1) and correspond to the transitional unit defined in the lithological logs (Figures 2.4 and 2.6). In BH A18 Ca^{2+} has the lowest concentration, and shows a reciprocal relationship with Na^+ ions (Figure 5.4) which may indicate cation-exchange between ground and interstitial clays. For BH A14 the sodium content ranged between 14.8 and 83.9 ppm and no definite relation with other elements could be seen except that the highest concentration of Na^+ corresponds to the lowest concentration of K^+ (Figure 5.5). Also Sample No. 15 which represents 175 m depth has a relatively low concentration of about 24 ppm, and corresponds to the transitional unit between the two formations comprising the Sherwood Sandstone Group.

5.3.4 Trace Elements

The concentration of trace elements in groundwaters results from the balance between geochemical abundance in the host rocks and the various physical and chemical controls within the aquifer. Generally sandstones have rather low concentrations of trace elements with respect to the other main lithological groups (Wedepohl, 1969). Some of the possible controls on trace element distribution in carbonate aquifers have been considered by Edmunds (1971, 1973). Also attempts have been made to define the natural trace element distributions and distinguish them from the input caused by environmental contamination in the Triassic sandstone groundwaters (Edmunds and Morgan-Jones, 1976).

All the groundwater samples under study were analysed for the following trace and minor elements (mainly heavy metal): Si, Al, Cd, Co, Cr, Cu,

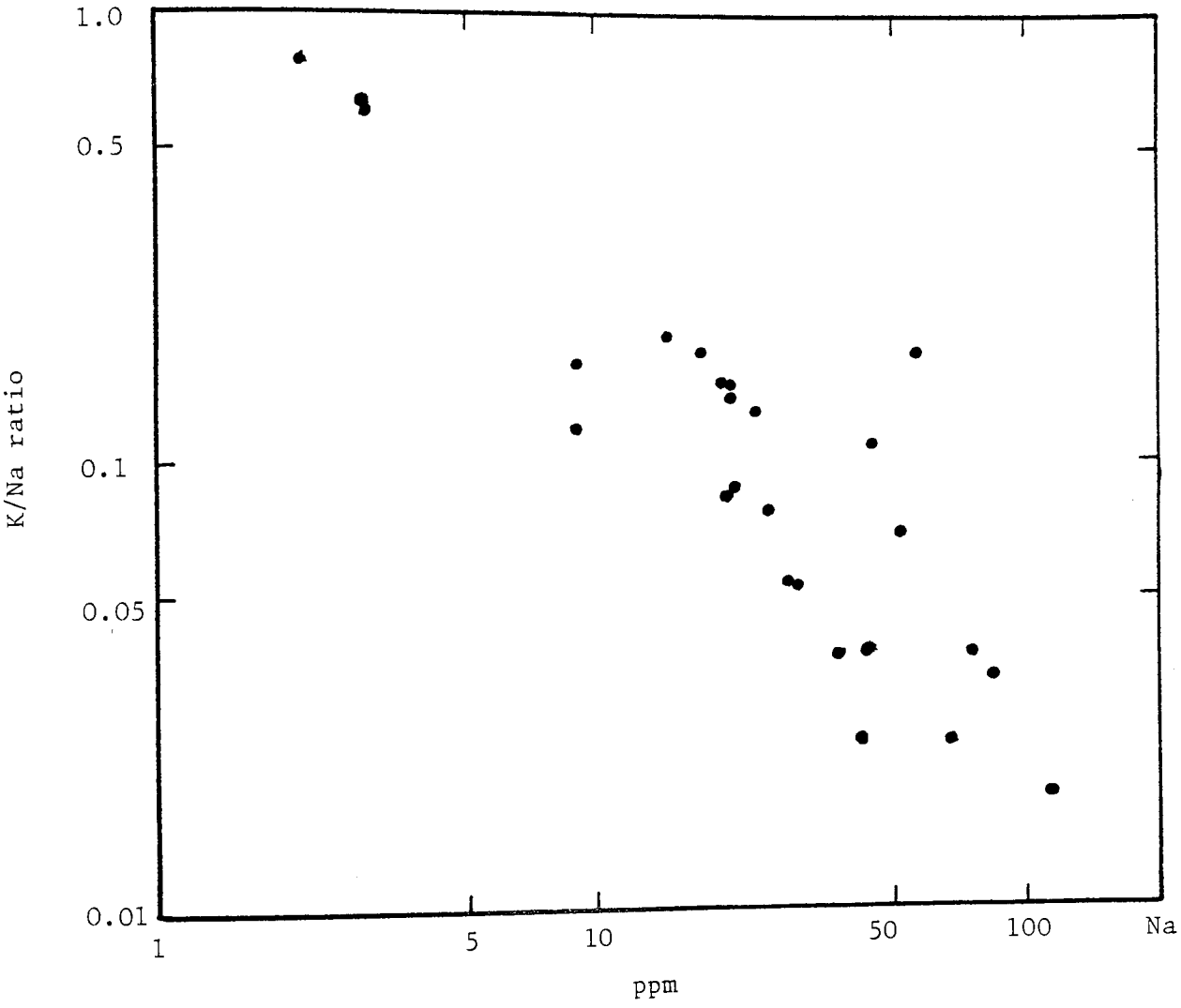

Figure 5.5 Plot of K/Na ratio against Na^+ concentration in the groundwater of the Sherwood Sandstone Group

Fe, Mn, Ni, Pb, V and Zn by means of the atomic absorption spectrophotometer. The values of each element in ppm are given in Table 5.1. These values refer to the concentration of the elements in the water itself since all samples were filtered through 0.45 μm millipore filters before the chemical analyses.

The distribution of silica in the studied groundwaters shows little regional variation with a range from 2.61 to 4.37 Si ppm (5.57 - 9.35 SiO_2 ppm) excluding the first sample in BH A11 which recorded $<$2.0 Si ppm. This silica concentration is within the preferable limit for drinking water. As the dissolution and/or alteration of the silica-bearing minerals is an obvious source of silica in these groundwaters the precipitation of authigenic clay minerals controls the silica concentration and the ultimate pH value in many groundwaters.

Iron concentration in groundwaters from BH A11 and A18 records lower values ($<$0.2 ppm) than the preferable limit for drinking. In BH A14, Fe shows slightly higher concentration, up to 0.57 ppm. This higher concentration of Fe could be due to the presence of some fraction below 0.45 μm which may exist in a colloidal form (Hem and Cropper, 1959). The abundance of this very fine fraction in BH A14 could be due to the presence of a large thickness of friable mudstone above the sandstone aquifer (Mercia Mudstone Group) as well as below the Sherwood Sandstone Group (represented by mudstone and siltstone of Permian age).

For the rest of the heavy metals detected in this work, almost all of the concentrations are less than the limit of detection of the AA instrument. The concentrations of Cu and Zn are less than the permissible limit for drinking water. No detailed conclusions can be

based on the trace element analyses. The distribution of twenty three minor and trace elements in Triassic groundwaters were investigated by Edmunds and Morgan-Jones (1976) for both natural and contaminated groundwaters. They found that the amount and nature of the impurities in the sandstone were the main control of trace element chemistry of the Triassic groundwater. The composition and reactivity of iron oxide cement is probably the most significant control of trace metal distribution. The natural trace metal levels are generally between 1 - 10 µg/l, where the high EH values of these groundwaters ensure the low concentration of the trace metals.

5.4 MINERAL ANALYSIS OF THE FINE RESIDUE

The fine fractions obtained from the filtration of the groundwater samples were used for mineral analysis by XRD. For each sample to be X-rayed a piece of the filter paper of 1.5 x 1.5 cm dimension was cut, and carefully fixed on the smooth surface of a wet ceramic disc. Each sample was treated with acetone to dissolve the filter paper, without affecting the orientation of the clay and the sample left to dry at room temperature. The dried fine fractions were analysed by XRD using Co Kα radiation between 2^{o} and 40^{o} 2θ. The samples were saturated with ethylene glycol for about 2 - 4 hours at $80^{o}C$. The glycolated samples were X-rayed under the same conditions as the first run to characterise the smectite if present. Finally, the samples were heated up to $550^{o}C$ for one hour and re-run after cooling in order to decompose any kaolinite that might be present.

Fourteen samples representing the three boreholes were prepared in this way and the clay minerals identified included kaolinite, illite

together with a restricted amount of montmorillonite (Figure 5.6). Quartz, feldspar and carbonate were also detected. Koalinite is characterised by the $\sim$7.15 A^{o} and 3.58 A^{o} reflections. The (001) shows sharp reflections indicating the well-crystallised nature of the kaolinite present (Figure 5.6). This was also observed very clearly from microscopic and SEM studies (Chapter Three). Illite is also present with the main reflections at 10.1 A^{o} and 5.09 A^{o} usually showing broad peaks. In a few cases the illite shows sharp peaks indicating higher crystallinity and in this case is probably of detrital rather than authigenic origin. The only other clay mineral present is montmorillonite characterised by a main reflection at $\sim$15 A^{o} which expands to 17 A^{o} on glycolation and collapses after heating to 10 A^{o}. Whereas illite and kaolinite are present in all the studied samples montmorillonite was seen in only one sample from borehole All.

5.5 WATER CHEMISTRY AND MINERAL STABILITY

Weathering or alteration of the aluminosilicate minerals is a slow and complicated reaction in which the overall effect is the removal of cations and part of the silica while Al and the remaining silica are transformed into secondary clay minerals. The nature of the clay minerals formed depends upon the environmental surroundings; kaolinite is more likely formed in acidic environments, while montmorillonite is more likely to form in alkaline solutions containing alkali earth metals and deficit of K^{+} ions. Illite is formed in the abundance of K ions in alkaline weathering conditions (Krauskopf, 1979).

In these Triassic sandstones the dissolution of the framework silicate

A

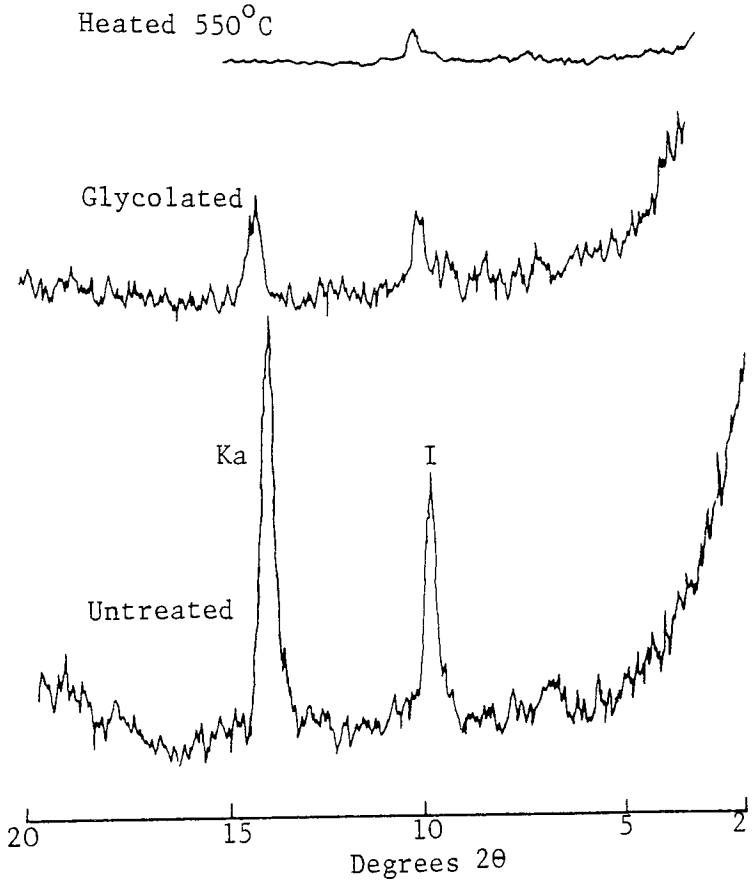

B

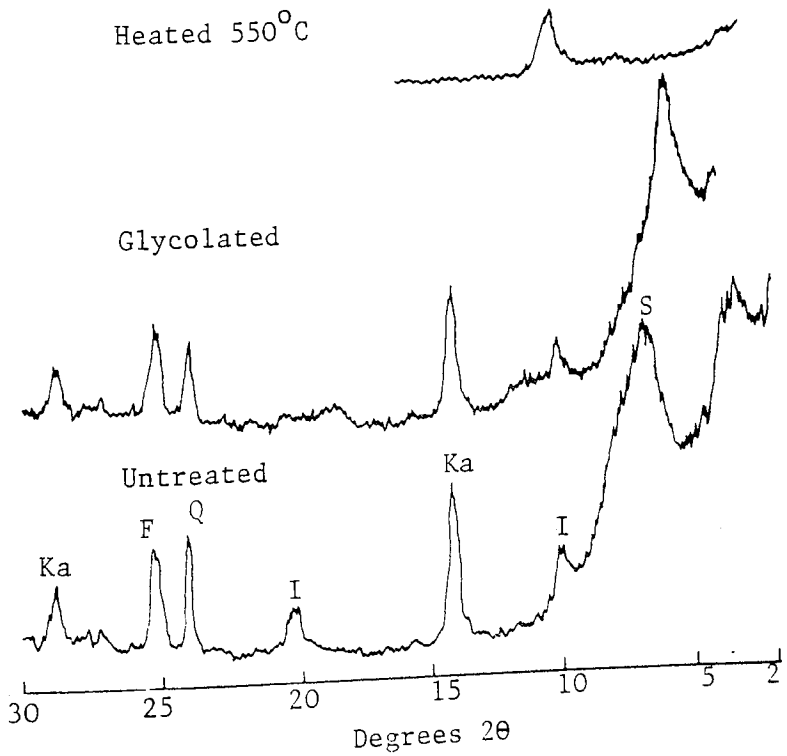

Figure 5.6 X-ray diffraction patterns of the fine fraction suspended in Triassic groundwater of the Sherwood Sandstone Group, from BH A14 (A) and BH A11 (B), using Ni filtered Co Kα radiation. (Ka = kaolinite, I = illite, S = smectite, Q = quartz and F = feldspar)

coupled with the process of clay replacement of the detrital grains provided Mg, Ca, Na, K, Al, Si and Fe ions to the interstitial water. These ions took part in the precipitation of authigenic minerals or cement. For predicting the possible minerals to be precipitated from groundwaters at the present time, the composition of the groundwater is plotted in theoretically calculated mineral stability diagrams for the systems K_2O-Na_2O-Al_2O_3-SiO_2-H_2O, and CaO-Al_2O_3-SiO_2-H_2O (Helgeson et al., 1969; Helgeson et al., 1978; Stanley and Benson, 1979).

The chemical data of the 26 groundwater samples were plotted in the stability field diagrams (Figures 5.7 - 5.10). The concentration of each cation in molality (m) was used instead of their activity and the assumption made that these waters are so dilute that molality is equivalent to the activity, according to Henry's law when the solution approaches infinite dilution (Garrels and Christ, 1965):

$$\text{molality (m)} = \frac{\text{ppm} \times 10^{-3}}{\text{gram formula weight}}$$

The groundwater data under study indicate that the kaolinite which is the main clay mineral should be stable in the present water condition. Illite is predicted to be stable from one diagram only under these groundwater conditions. Montmorillonite, mixed-layer illite-montmorillonite, K-feldspar, albite and K-mica are unstable, as the chemical compisition of the present groundwaters fall outside their stability field. So the dissolution or transformation of these minerals is to be expected at the present time (Equations 5.3 - 5.6). This phenomenon has already been observed, especially for K-feldspar which shows an extensive dissolution texture for both detrital and authigenic phase and also replacement by kaolinite and/or illite

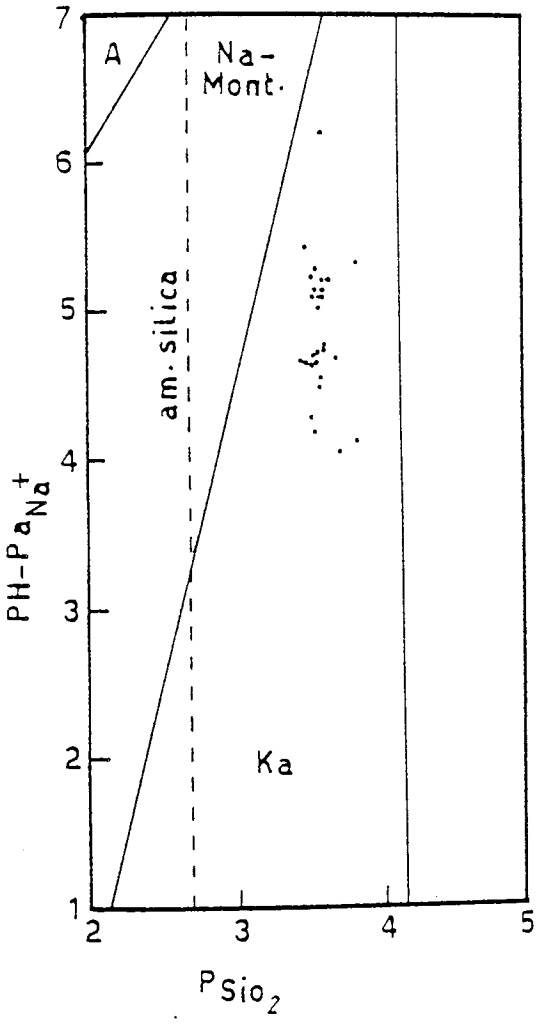

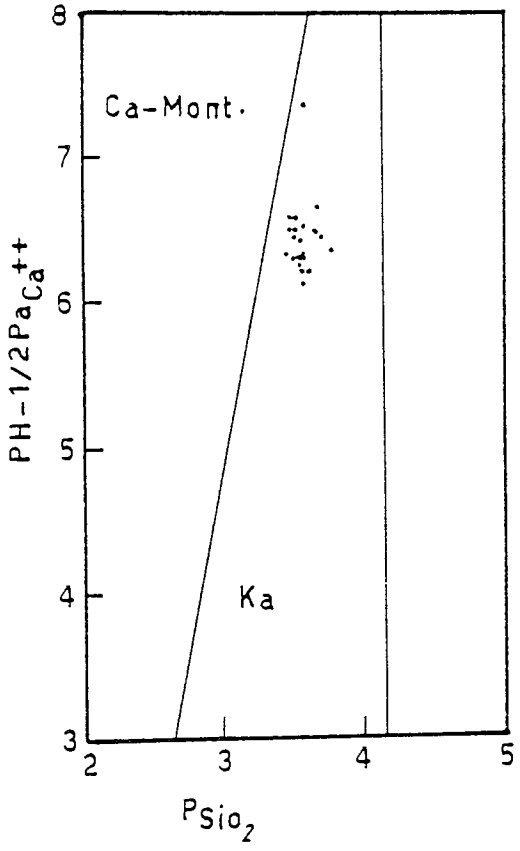

Figures 5.7 and 5.8 Plot of chemical composition of Triassic groundwater (from Sherwood Sandstone Group) on the stability field diagrams of Na and Ca silicate at 25°C and 1 atm. (after Helgeson et al, 1969). Ka = kaolinite, Mont = montmorillonite)

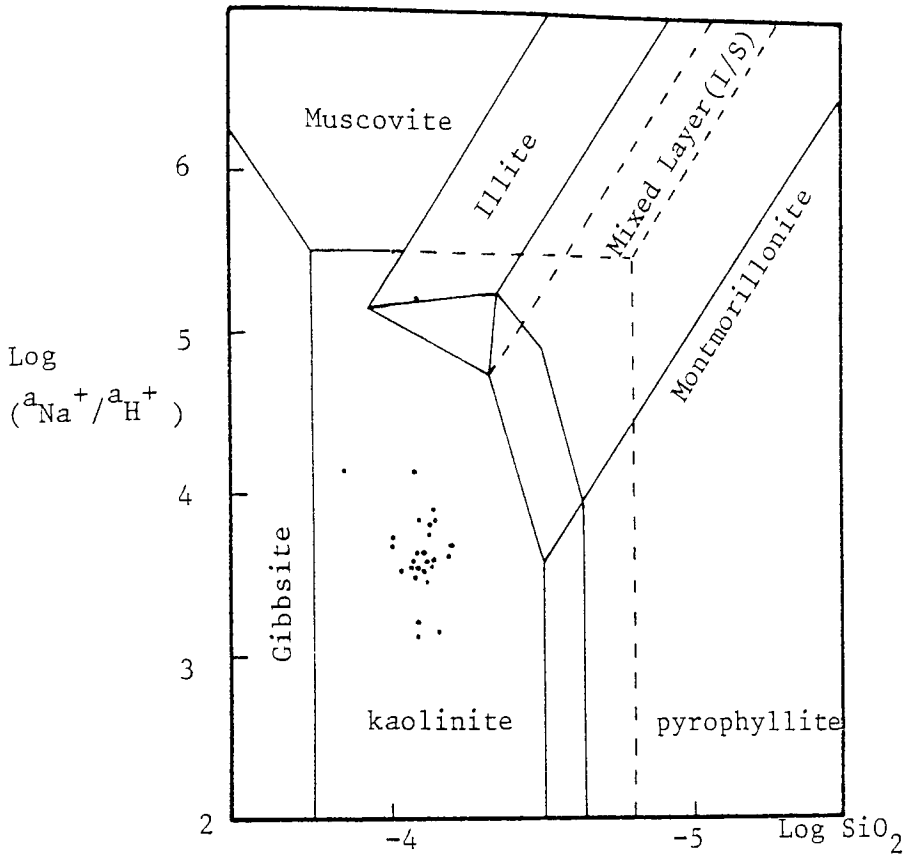

Figure 5.9 Plot of chemical composition of Triassic groundwater on the activity diagram for alumino silicate system showing the fields of clay minerals (after Stanley and Benson, 1979)

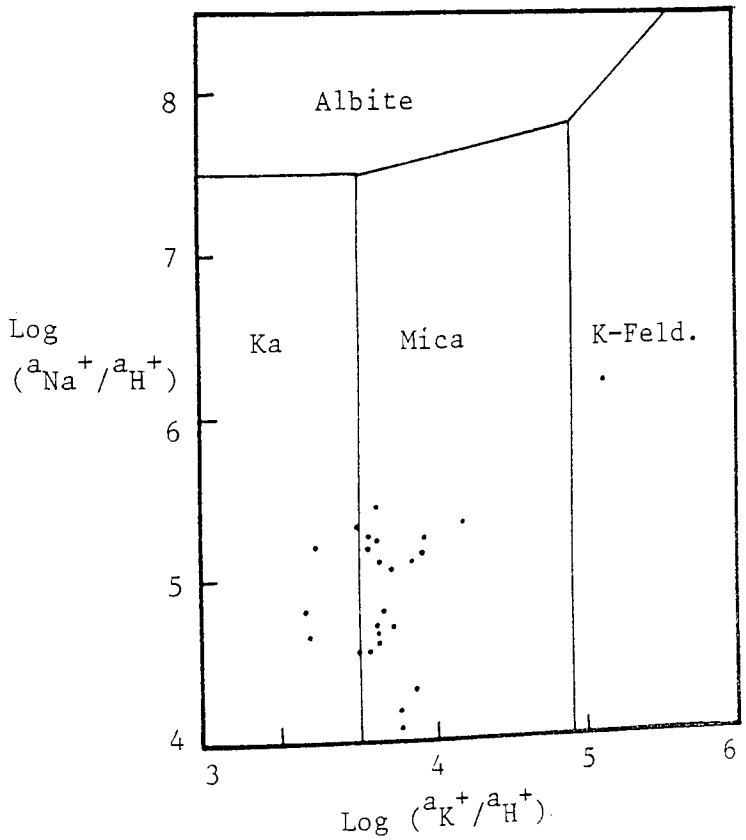

Figure 5.10 Plot of chemical composition of Triassic groundwater on the stability field diagram of the system K_2O-Na_2O-Al_2O_3-SiO_2-H_2O at 25°C and 1 atm. (after Helgeson et al., 1978)

(Equations 5.3 and 5.4 and Chapter Three).

$$2KAlSi_3O_8 + 2H^+ + H_2O$$

K-feldspar $\xrightarrow[\text{acid conditions}]{}$ $Al_2Si_2O_5(OH)_4 + 4SiO_2 + 2K^+$ (5.3)

kaolinite

$$3KAlSi_3O_8 + 12\,H_2O + 2H^+ \longrightarrow KAl_3Si_3O_{10}(OH)_2 + 2K^+ + 6H_4SiO_4$$

K-feldspar — alkaline conditions — K-mica

(5.4)

$$2NaAlSi_3O_8 + 2H^+ + H_2O$$

albite $\longrightarrow$ $Al_2Si_2O_5(OH)_4 + 4SiO_2 + 2NA^+$ (5.5)

kaolinite

$$2KAl_3Si_3O_{10}(OH)_2 + 3H_2O + 2H^+$$

K-mica $\longrightarrow$ $3Al_2Si_2O_5(OH)_4 + 2K^+ + 3H_2O$ (5.6)

kaolinite

5.6 DISCUSSION

The concentration and composition of the groundwater is a function of the rates of water movement in the sediments coupled with the kinetics of mineral dissolution and/or alteration as well as authigenic mineral and cement precipitation. As the processes of dissolution, alteration and cement precipitation are the most important diagenetic features governed by the chemistry of both sediments and percolating water, the study of chemical composition of water coupled with the mineralogy and petrography of the surrounding sediments may help in predicting the diagenetic processes prevailing at the present time.

The chemical composition of the Triassic groundwaters under consideration show that all plots fall in the stability field of kaolinite mainly. Illite stability is shown to be represented only in one diagram. This raises the possibility that these minerals were precipitated within the present groundwaters. K-feldspar, albite, muscovite, montmorillonite, mixed-layer (I/S) clay and quartz are not in equilibrium with the present groundwater, a feature consistent with the dissolution, replacement and transformation textures observed in association with these minerals (Chapter Three). These minerals were almost certainly precipitated during Triassic diagenesis and their persistence in the present groundwater can be explained because the chemical reaction and transformation of one mineral to another at low temperature and pressure is very slow and takes a long time (sluggish kinetics). So both stable and unstable minerals can be observed together.

The Triassic groundwaters are undersaturated with respect to dolomite and calcite (Edmunds and Morgan-Jones, 1976). This fact is obviously reflected by the extensive dissolution features affecting the carbonate minerals (calcite, Fe-calcite and dolomite) indicated from thin section and SEM study of the core samples (Chapter Three). The different features observed from stages three and four (mature stages of mesodiagenesis) of the diagenetic sequence are in general agreement with the results of water chemistry. Where the second generation of kaolinite is the most important authigenic mineral precipitating in "stage four" of the diagenetic sequence as indicated from microscopic and SEM studies, then it is also the main stable mineral predicted by the present groundwater conditions. The carbonates which show extensive dissolution features prevailing during "stage three" are probably still

undergoing active dissolution as indicated by the groundwater chemistry which is undersaturated with respect to both dolomite and calcite. The rest of the mineral assemblages in these sedimentary rocks, although not stable under the present groundwater conditions, can be considered metastable because of the sluggish kinetics involved in mineral transformation under low temperature and pressure.

Table 5.1 Chemical Composition of Triassic Groundwaters from the Sherwood Sandstone Group in Nottinghamshire

Variables / Sample No		Depth (m)	pH	TC°	SEC µS/cm	Ca^{++} ←	Mg^{++}	Na^{++}	K^{+}	Cd	Co	Cr	Cu	Fe	Mn	Pb	Ni	Zn	Si	Al →	V
								ppm													
BH A11	1	15	8.05	10	430.4	17.07	27.08	45.14	4.96	<0.05	<0.5	<0.2	<0.2	<0.2	0.197	<1.0	<0.2	0.05	<2.0	<2.0	<2.0
	2	25	7.50	9.9	586.8	125.46	35.57	116.48	2.09	"	"	"	"	"	<0.1	"	"	0.052	3.41	"	"
	3	35	7.55	9.7	590	119.81	39.46	30.38	1.62	"	"	"	"	"	"	"	"	<0.05	4.02	"	"
	4	45	7.85	9.7	581.2	118.11	37.37	67.90	1.65	"	"	"	"	"	"	"	"	0.081	3.65	"	"
	5	55	7.60	9.7	494.5	104.78	34.27	37.02	1.35	"	"	"	"	"	"	"	"	<0.05	3.36	"	"
	6	65	8.20	9.9	293.4	35.56	25.68	9.25	1.10	"	"	"	"	"	"	"	"	"	3.37	"	"
	7	68.5	8.20	10.5	271.9	29.22	24.58	42.31	1.02	"	"	"	"	"	"	"	"	"	4.29	"	"
BH A14	8	70	7.6	11.8	287.6	46.41	25.13	21.38	3.02	"	"	"	"	"	"	"	"	"	3.36	"	"
	9	85	7.8	11.5	281.6	45.69	21.65	17.92	3.15	"	"	"	"	0.33	"	"	"	"	4.37	"	"
	10	100	7.7	11.6	282.4	46.05	19.70	14.82	2.80	"	"	"	"	0.23	"	"	"	"	3.47	"	"
	11	115	7.7	11.8	279.6	45.0	18.77	20.49	3.03	"	"	"	"	<0.2	"	"	"	"	3.84	"	"
	12	130	7.7	12	282.2	45.44	20.93	20.94	3.08	"	"	"	"	0.35	"	"	"	"	3.81	"	"
	13	145	7.7	12	278.1	46.63	22.67	83.92	2.73	"	"	"	"	0.27	"	"	"	"	3.05	"	"
	14	160	7.7	12.05	277.8	47.30	23.49	76.20	2.90	"	"	"	"	0.37	"	"	"	"	3.30	"	"
	15	175	7.7	12.05	294.1	48.15	21.85	24.13	3.18	"	"	"	"	0.57	"	"	"	"	3.72	"	"
	16	190	7.7	11.75	458.5	68.16	25.03	52.78	3.69	"	"	"	"	0.48	"	"	"	"	3.51	"	"
BH A18	17	10	8.8	10.7	228.2	3.42	16.59	57.44	9.97	"	"	"	"	<0.2	"	"	"	"	3.38	"	"
	18	25	7.9	10.7	291.6	43.47	25.38	44.40	1.70	"	"	"	"	"	"	"	"	"	3.51	"	"
	19	40	8.0	10.5	246.4	17.82	21.18	28.91	1.56	"	"	"	"	"	"	"	"	"	3.31	"	"
	20	55	8.15	10.7	203.0	19.11	27.48	21.40	1.85	"	"	"	"	"	"	"	"	"	3.69	"	"
	21	70	8.2	10.7	211.3	17.87	24.48	26.08	2.03	"	"	"	"	"	"	"	"	"	3.88	"	"
	22	85	8.20	10.6	211.9	18.10	25.08	21.16	1.80	"	"	"	"	"	"	"	"	"	3.47	"	"
	23	100	8.20	11.0	205.5	21.73	26.67	2.91	1.80	"	"	"	"	"	"	"	"	"	3.84	"	"
	24	115	8.10	11.1	205	22.30	33.03	2.17	1.70	"	"	"	"	"	"	"	"	"	2.63	"	"
	25	130	8.10	11.0	209.7	20.05	27.29	2.89	1.81	"	"	"	"	"	"	"	"	"	3.77	"	"
	26	138.5	8.10	11.1	243.2	21.28	28.52	9.14	1.53	"	"	"	"	"	"	"	"	"	2.61	"	"
Average						45.92	26.11	34.52	2.58												
Maximum permissible level						200	125	200		.01	none	.05	1.0	.3	.3	.1	none	15	4.68		

CHAPTER SIX

DISCUSSION

In the previous chapters lithology, mineralogy, diagenesis, grain textures and the hydrogeological characteristics of a variety of Triassic sandstone aquifer samples has been described together with the chemistry of the interstitial groundwater. In each chapter the properties of these rocks are described and the relation between some of the parameters were discussed wherever appropriate. The main purpose of this chapter is actually to discuss in more general terms the relationships between these properties and in particular to discuss the main controlling influences on porosity and hydraulic conductivity.

The different properties involved in this discussion are included in Table 6.1 and include, the samples depth in metres, the matrix and cement percentage, grain parameters, mean size ($Mz\phi$), inclusice graphic standard deviation (σ_I), graphic skewness (SK_I), consolidation factor ($C_f\%$), packing density (Pd%), packing proximity (Pp%), the average porosity ($\phi_{av}\%$), the hydraulic conductivity in millidarcy (K_w) and the mean pore radius calculated from the pore size distribution curves (Mr μm).

Porosity and hydraulic conductivity are the two most important properties of water aquifers. There are many factors which exercise some control upon porosity and permeability including grain size, sorting, matrix and cement content, packing, grain contact, pore diameter, type of clays present as well as the type of water in contact with these sediments. As far as we are concerned in this study, the sandstones have been subjected to and are still being affected by

Table 6.1 Matrix and cement content, grain size parameters, packing, grain contact, porosity and hydraulic conductivity measurements of Sherwood Sandstone Group from BH A14

Sample No	Depth (m)	Cement (%)	Matrix (%)	Mz (ø)	σ_I (ø)	SK_I	C_f (%)	Pd (%)	Pp (%)	ϕ_{av} (%)	K_w (md)	Mr (μm)
14/44	75.7	-	-	-	-	-	53.9	63.36	36.05	28.08	1280.8	21.96
43	78.8	14.34	5.08	1.72	0.99	+.33	51.49	53.58	14.29	22.73	262.4	21.96
40	84.4	5.39	5.52	2.0	0.98	+.26	-	-	-	26.45	1842.5	22.19
39	85.3	6.36	6.58	2.26	1.1	+.35	-	-	-	26.18	-	14.05
37	89.5	7.05	5.56	1.65	0.67	+.32	-	-	-	26.20	5479.6	39.77
36	92.2	-	-	-	-	-	55.09	53.75	29.53	27.92	-	28.88
35	94.2	13.19	4.88	1.95	0.68	+.45	-	-	-	24.25	1180.7	22.67
33	98.4	-	-	-	-	-	54.08	63.01	29.25	25.74	496.1	21.73
27	130.8	6.11	7.69	2.29	1.05	+.51	50.98	66.09	33.99	27.42	1143.9	20.87
26	133.2	13.31	2.31	1.59	0.68	+.29	49.74	71.82	22.32	22.17	1709.6	34.0
25	134.65	5.23	2.75	1.99	0.70	+.31	-	-	-	27.14	1974	20.67
23	171.8	5.25	10.09	3.23	0.76	+.32	52.77	54.93	23.52	26.66	81.8	9.09
16	179.65	12.46	10.73	3.01	0.94	+.30	-	-	-	26.40	-	14.05

Mzø = mean grain size
σ_I = inclusive graphic standard deviation
SK_I = inclusive graphic skewness

C_f = consolidation factor
Pd = packing density
Pp = packing proximity

ϕ_{av} = average porosity
K_w = hydraulic conductivity
Mr = mean pore radius

different diagenetic processes. The hydraulic properties are consequently expected to change during their geological history. Most of the present pore spaces are of secondary origin as discussed in Chapter Three and dissolution as well as clay replacement could still be taking place. So, because of the just mentioned factors, it is not uncommon to find variation in some of the expected relationships between both ϕ and K and the different physical grain properties. The following is a discussion of some of the principal relationships.

Although particle size has no direct influence upon porosity there may be a considerable indirect effect through the influence of size upon packing. As grain size decreases friction and adhesion become important due to the high surface area of the grain with respect to the volume. So, porosity increases as grain size decreases. In these sandstones under consideration there is a low positive correlation between mean size ($Mz\phi$) and porosity (ϕ_{av}) with r = +.533, which is significant at only 90% confidence level. This relationship which is shown in Figure 6.1 is represented by the line:

$$Mz\phi = -2.2 + .17\ \phi_{av}\% \qquad 6.1$$

This relationship is not significant enough to accurately predict one property from the other because so many other factors have an influence: the high matrix and cement content of these rocks decreases the porosity whilst the creation of dissolution pores increases it.

The abundance of mixed size grains together with the presence of a considerable amount of pore filling cement and matrix reduce the significance of packing on the sandstone properties. In the sandstones under study there is no significant relationship between porosity

(ϕ_{av}%) and packing density Pd%) (correlation coefficient r = -.23). In theory, however, the packing density is a measure of the porosity in a cement- and matrix-free sand. As the percentage of cement or matrix in these sandstones reaches up to 14% and this may cause the poor correlation between these two parameters.

On the other hand, the relationship between porosity and packing proximity (Pp) is significantly positive with correlation coefficient r = +0.82 (significant at 98% confidence level). This relation (Figure 6.2) is represented by the line:

$$Pp = -66.57 + 3.62\ \phi_{av}\% \qquad 6.2$$

Grain contact analyses included measurements of the numbers of contacts per grain and the type of contacts as well as calculation of the consolidation factor (C_f). These indicate that the sandstones have not been affected by great stress or appreciable burial. However, the study of the lithological logs indicates the presence of considerable fissure systems of great importance to the hydraulic characteristics of these rocks. These fissures are free from any mineralization indicating their formation later than the diagenetic mineralization of the rocks which occurred during the second stage of diagenesis (Chapter Three). The effects of compaction on individual grains were limited as a result of the precipitation of the authigenic mineral suite. So the overall effect of physical or mechanical compaction resulted in the very important fissure system which plays an important role in the hydraulic properties of the aquifer. Secondary fissures account for the fact that water flow through the aquifer is two to three times more than anticipated through intergranular flow alone (Chapter Four).

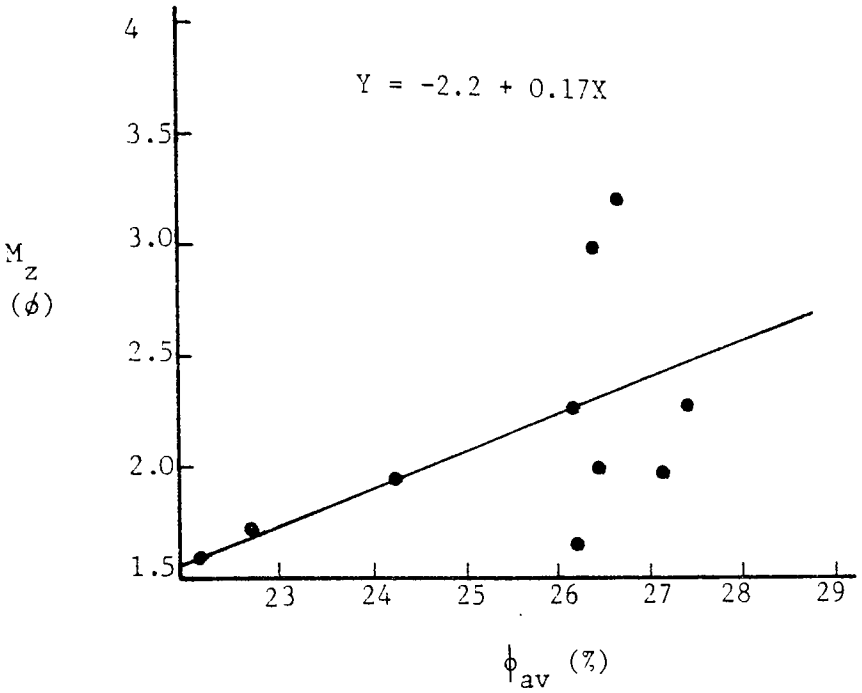

Fig 6.1 Relationship between average porosity (ϕ_{av}) and mean grain size ($M_z\phi$)

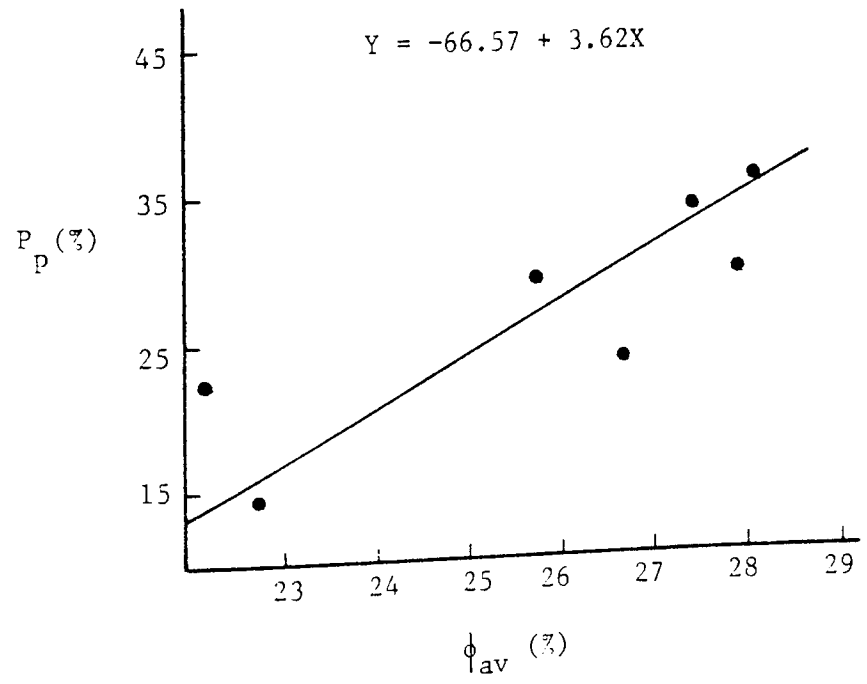

Fig 6.2 Relationship between average porosity (ϕ_{av}) and packing proximity (P_p)

The relation between grain contact represented by the consolidation factor $C_f\%$ and both porosity and permeability is not significant with the correlation coefficient (r) equal to +0.69 and -0.30 with porosity and hydraulic conductivity respectively.

The uniformity of the grain size is of fundamental importance to porosity. Well-sorted samples have the highest porosity and in general the finer grain size tends to be more uniform than the coarser varieties. However, low positive correlation coefficient was detected between ϕ_{av} and sorting σ_1 (r = +.23) which is not significant at all. This unexpected relationship could be due to the influence of the different diagenetic processes. For example, the incomplete dissolution and the selective dissolution of detrial grains gives rise to higher percentage of secondary porosity but at the same time decreases the textural maturity of the rock and this could be one of the reasons for the poor correlation.

No significant correlation was detected between ϕ_{av} and skewness (SK_1) (r = +.15).

The most significant relationship is between porosity (ϕ_{av}) and the cement content (Ct%), where the correlation coefficient (r) is equal to -0.83 (significant at 99.5% confidence level). This relation (Figure 6.3) is represented by the best fit line:

$$Ct\% = 69.96 - 2.39\ \phi_{av}\% \qquad 6.3$$

reflects the importance of these diagenetic cementing material upon the hydraulic characteristics of the aquifer.

The porosity shows weak positive correlation with matrix content (Mx%) with r = +.49 which is not very significant (80% confidence level).

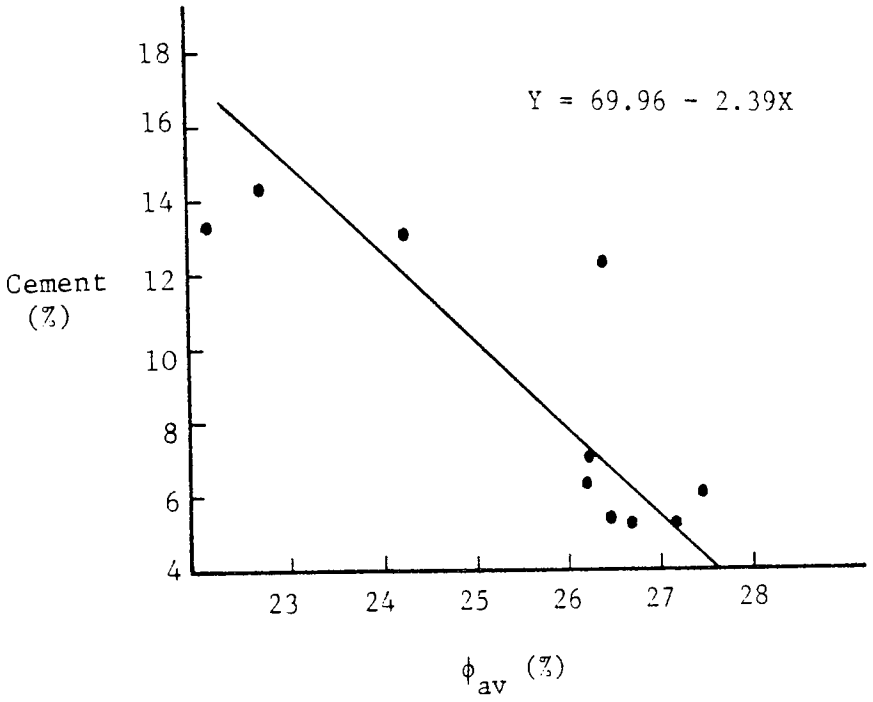

Fig 6.3 Relationship between average porosity (ϕ_{av}) and Carbonate cement content

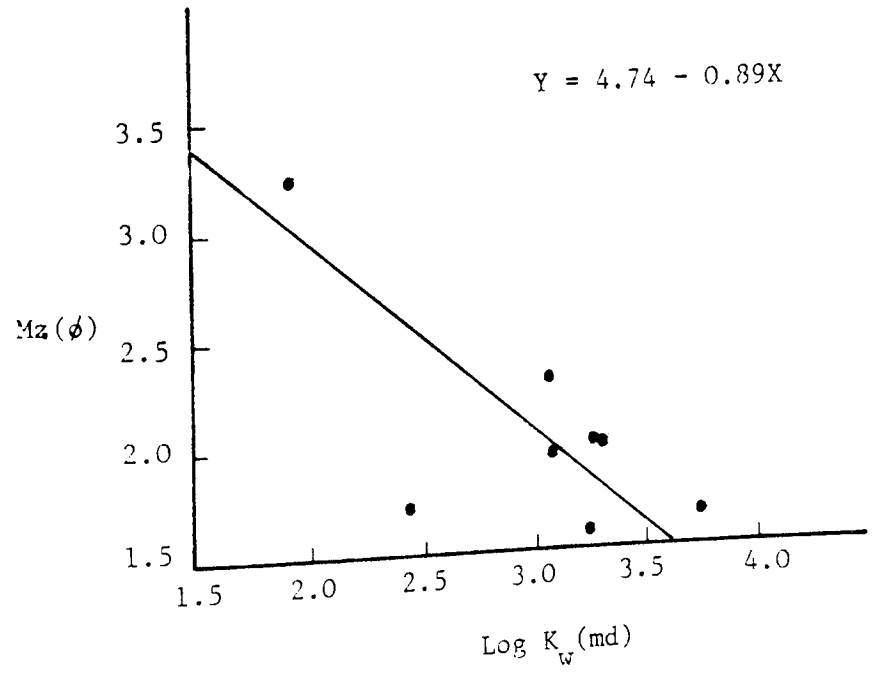

Fig 6.4 Relationship between measured hydraulic conductivity (K_w) and mean grain size (Mzϕ)

This relation although not very significant indicates that the higher the matrix percentage the higher the porosity tends to be. At first sight this relationship appears rather surprising. It could be due to partial and/or selective dissolution of the detritals together with clay replacement processes. This would then increase the amount of the fine fraction, decrease textural maturity, but create secondary porosity which, on the basis of textural observation, can be seen to be important in sandstones of this type. There is a highly significant relationship between hydraulic conductivity (Log K_w) and mean grain size (Mzϕ) (correlation coefficient r = -0.72), significant at 95% confidence level). This indicates that hydraulic conductivity increases as the grain size increases (Figure 6.4). Regarding the other grain size parameters, σ_I and SK_I, no significant relation was detected between them and K_w (correlation coefficient r = 0-.26 and -.03 for σ_I and SK_I respectively) indicating that sorting and skewness do not exercise any strong influence upon hydraulic conductivity.

Regarding the relationships between permeability, packing (pp and Pd) and grain contacts (C_f) only packing density (Pd) shows a significant correlation with r = +0.87. This correlation coefficient is significant at the 98% level. The relationship (Figure 6.5) can be represented by the line:

$$Pd = 19.4 + 15.61 \text{ Log } K_w \qquad 6.4$$

Correlation between Log K_w and Pp and C_f is not significant with r = 0.49 and -0.30 respectively.

Also no correlation was found between hydraulic conductivity (Log K_w) and cement (Ct%) with r = -.09. On the other hand the relation between matrix percentage (Mx%) and K_w is more significant with correlation

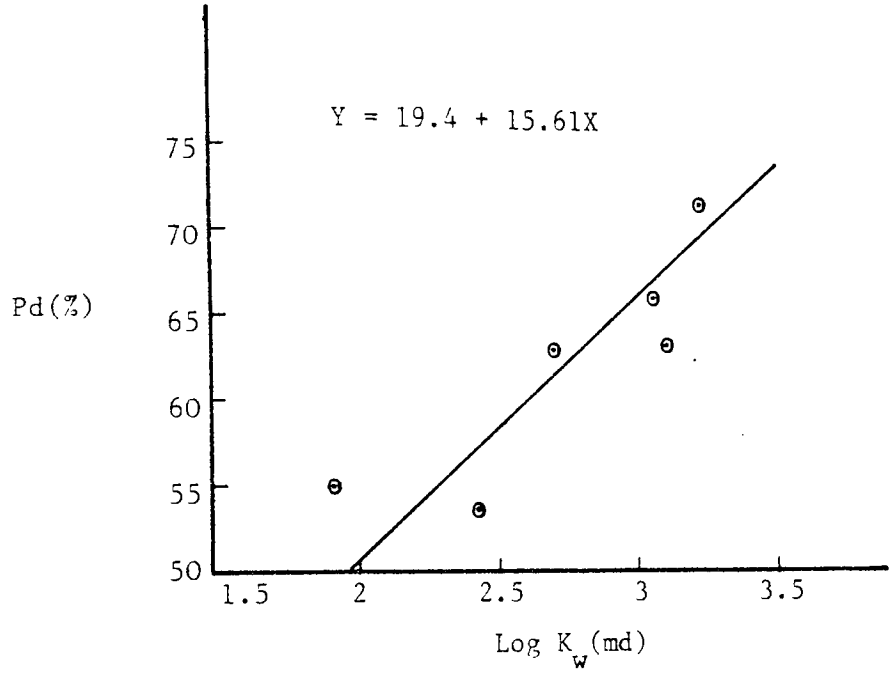

Fig 6.5 Relationship between measured hydraulic conductivity (K_w) and packing density (Pd)

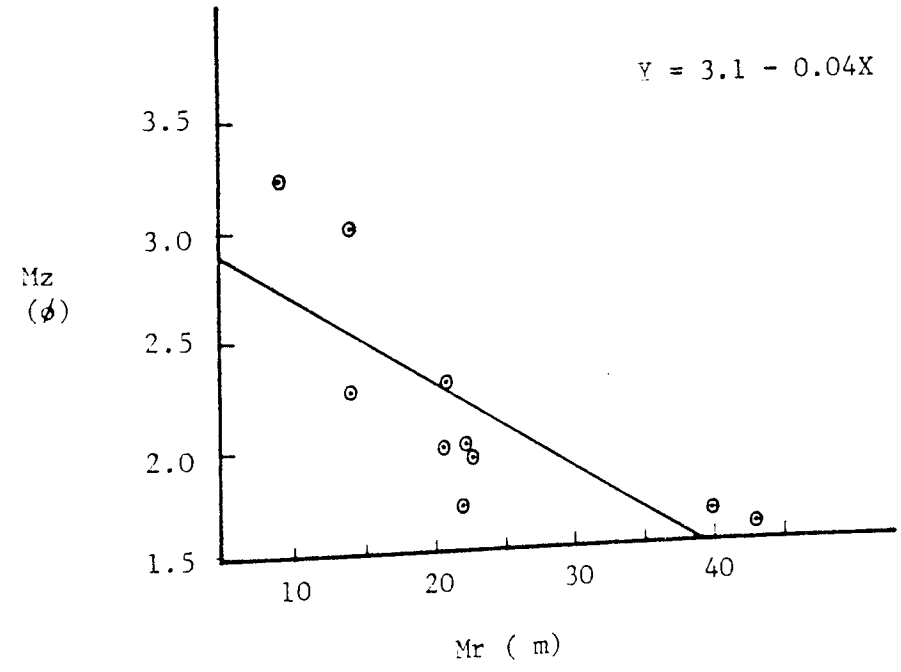

Fig 6.6 Relationship between median pore radius (Mr) and mean grain size (Mz)

coefficient r = -.61, being significant only at 90% confidence level.

The most significant relationships have been found between permeability and the median pore radius (Mr μm), which show high positive correlation coefficient with r = 0.98 and 0.82 for K_{Hg} and K_w respectively (Chapter Four, p. 120,121 , Figure 4.11, 12). Also highly significant correlation was detected between Mr μm and the mean grain size Mzϕ with r = -.79 (correlation coefficient significant at 99.5% confidence level). This relationship indicates that the finer the grain size the smaller the pore radius (Figure 6.6) a feature expected for inter-granular porosity.

There is no direct relationship between either porosity (ϕ) or hydraulic conductivity (K_w) and depth. This might be due to the small range of depth upon which these aquifer rocks are distributed (maximum depth 195 m in BH A14). On the other hand the feature is more likely related to lithology (Figures 4.18-21) because the lower values of K_w correspond to finer grained rocks (mudstone, siltstone), as well as to coarser rocks (pebbly sandstones) which contain an abundance of mudstone flakes. In general terms these results show the complex nature of the factors which control porosity and hydraulic conductivity in these sandstones. Simple physical relationships between grain size and porosity cannot be assumed. Porosity is reduced by authigenesis and cementation and created by secondary dissolution. Diagenetic processes also modify the original texture of the rock which further complicates the relationships. In future studies it seems important that hydrogeologists should make petrographic/diagenetic studies in order to properly elucidate the relationships between lithology, porosity and hydraulic conductivity.

The specific electrical conductance (SEC) which is a measure of the amount of dissolved solids in water indicates values ranging between 203 and 590 μS/cm which is equivalent to total amount of 130 to 378 ppm dissolved solids. The values of SEC indicate an association between high porosity/hydraulic conductivity and dissolution as a source of ions to the groundwater. This phenomenon was clearly observed in BH A11 where the highest ϕ and K_w values were recorded above 60 depth within the medium/coarse grained slightly pebbly sandstone of the Nottingham Castle Formation. Ground waters associated with these rocks (above 60 m depth) recorded the highest SEC as well as Ca^{++}, Mg^{++} and Na^{+} ion (Table 5.1). This may suggest an association between the high porosity/hydraulic conductivity and dissolution processes as a source of ions to the groundwater. On the other hand, the abundance of secondary fissures and fractures especially in BH A18 could result in the dilution of these groundwaters, either from surface water or river water (nearest to Dover Beck valley) causing the low values of SEC recorded in this borehole (203-246 μS/cm).

The results show that recent diagenetic processes (secondary dissolution) have some influence on the present groundwater chemistry.

CHAPTER SEVEN

CONCLUSIONS

This work on the properties of the Lower Triassic sandstone aquifer represented by the Sherwood Sandstone Group in North Nottinghamshire gives rise to a number of conclusions summarized in the following points:

1. The Nottingham Castle and Lenton Sandstone Formations comprise the Sherwood Sandstone Group in the area which has a maximum thickness of 120 m. The boundary between those two Formations is always gradational and a transitional unit of 2-14 m thick was distinguished towards the bottom of the Nottingham Castle Formation. The transitional unit comprises intercalations of sandstone, siltstone, mudstone and intraformational conglomerate (mud flake conglomerate). However, those two formations could not be readily distinguished, especially towards the north of the studied area (BH A3).

2. The Sherwood Sandstone Group forms a single water aquifer which can generally be classified as confined or unconfined. Truly unconfined conditions are probably not present, however, because of the presence of impermeable mudstone horizons which separate the permeable sandstone beds and give rise to partially confined conditions.

3. The Sherwood Sandstone Group comprises different rock types including conglomerate, pebbly sandstones, sandstones, siltstone and mudstone. The sandstones which are by far the dominant variety have been studied in detail. They are classified as sublitharenites and subfeldsarenite which are texturally immature to submature. These sandstones have

undergone some compaction but have not suffered deep burial or great stress as indicated from the textural and clay mineral analyses.

4. The sandstones have undergone numerous diagenetic changes and reached the mature stage of the mesodiagenetic regime. These changes included:

(a) The reddening of the sediments, which started early in the diagenetic sequence and continued for a long time after the formation of some of the authigenic minerals.

(b) Dissolution which is a crucial diagenetic feature affecting both detrital and authigenic components and providing a fundamental source of secondary porosity. The carbonate cements (dolomite, ferroan calcite and calcite) are extensively affected by dissolution giving rise to the obviously abundant over-sized pores on a micro- and macro-scale and producing large amounts of secondary dissolution pores. This dissolution process started early in diagenesis and before the formation of the authigenic mineral suite. It continued even after the burial compaction and could still be taking place at the present time at least for carbonate (both calcite and dolomite) and K-feldspar.

(c) Clay-replacement of the unstable detrital minerals, especially feldspar, occurs in these aquifer rocks but is generally not very common.

(d) Development of an authigenic mineral suite which includes in paragenetic sequence: quartz, K-felspar, kaolinite, dolomite, ferroan calcite, calcite and kaolinite. Authigenic illite and mixed layer (I/S) clay have no definite position in the diagenetic sequence but can be shown to post-date quartz and K-feldspar and pre-date carbonate

as indicated in the following paragenetic sequence:

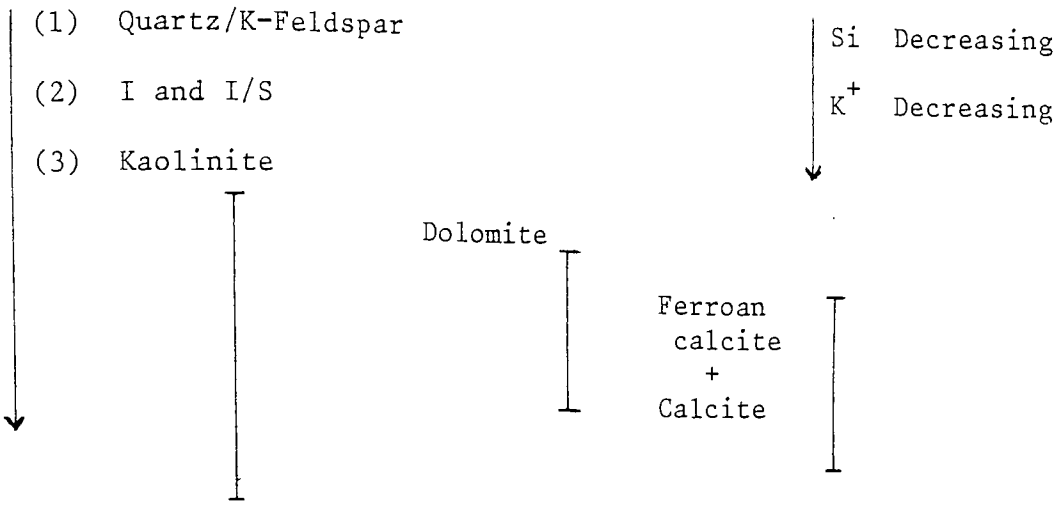

5. The precipitation of authigenic quartz in these sandstones took place soon after deposition at shallow depths before any burial compaction. Fluvial or surface waters could therefore be an important source of silica. Dissolution of silicate minerals and to a less extent clay replacement may also be considered as sources of silica.

6. X-ray diffraction, SEM with energy-dispersive analysis and petrographic studies indicate that kaolinite is the most abundant authigenic clay mineral in the Sherwood Sandstone Group. Mixed layer (I/S) clay is the second in abundance is the second in abundance and has a smectite ratio usually between 20-35% and very rarely less than 20%. Illite is the least abundant clay mineral but its abundance increases downwards towards the underlying Permian rocks. Smectite is very restricted in amount and abundance.

7. Carbonate minerals are the most common cementing materials in these sandstones and include: dolomite, ferroan calcite and calcite, with dolomite increasing towards the Lenton Sandstone Formation. The sequence of these carbonate minerals indicates the decrease of

Mg/Ca ratio and the Fe content in the groundwater during the period of their precipitation.

8. Diagenetic processes have had an important effect in destroying the primary porosity, especially in view of the fact that much of the existing porosity is of secondary origin as well as the high percentage of carbonate and clay minerals present. Also the effect of diagenesis on the permeability of these sandstones was to initially reduce it by blocking of pore throats or reduction of the effective pore diameter due to pore lining. Subsequent diagenesis, in particular dissolution, has been the main process in producing secondary porosity and increasing the permeability.

9. Different types of pores have been identified in the Sherwood Sandstones which are genetically classified as: a) dissolution, b) fractures, c) shrinkage, d) hydrid pores. Dissolution pores are the most common type.

10. The diagenetic history of the Sherwood sandstones was classified into four stages depending upon the physical and/or chemical processes prevailing and consequently their effect on the creation or destruction of the porosity during each stage.

(a) Stage "One" or the eodiagenetic stage included the changes which took place in the shallow depositional environment. Chemical processes controlled dissolution and replacement of the detrital components together with the precipitation of most of the authigenic mineral suite.

(b) Stage "Two" or mechanical compaction, corresponds to the immature stage of mesodiagenesis in which the physical processes resulting from

the burial of the sediments governed the diagenetic changes. The final result of these changes were the reduction of porosity and permeability. Secondary pores (fractures type) were created at this stage.

(c) Stage "Three" corresponds to the early mature stage of mesodiagenesis. Secondary porosity generation was the most effective process during this period with carbonate dissolution being the main source of secondary pores. The pore waters during this period were more acidic and undersaturated with respect to carbonate.

(d) Stage "Four" represents diagenesis in the present groundwater regime and could be still taking place at the present time. Porosity and permeability may be reduced as a result of the precipitation of kaolinite. On the other hand, the present water is under saturated with respect to carbonate, K-feldspar, mixed layer (I/S) clay and smectite, and these minerals may be presently being dissolved.

11. Turning to the hydraulic properties of these Triassic aquifers, the porosity measured by the water-resaturation method gave results (ϕ_{sat}) which ranged between 17.76% and 32.45% with an overall average (Av ϕ_{sat}) of 25.63%. This method gives good results of high accuracy with highly porous and permeable rocks. However, the results are not so effective for low porosity and permeability rocks mainly due to the difficulty in obtaining complete vacuum and consequently re-saturation.

12. The results of porosity measured by the Hg-injection method (ϕ_{Hg}) ranged between 15.54% and 30.13% with an overall average value (Av ϕ_{Hg}) of 24.85%. The median of the effective pore radius (Mr)

ranged between 0.16 to 39.77 μm, with only 10% less than 10 μm.

13. Porosity results for the Hg-penetration and water resaturation methods show a marked correlation with a tendancy for ϕ_{sat} to be higher than ϕ_{Hg}, with average values of both equal to 25.63% and 24.85% respectively. This relation is best represented by a linear equation (4.10), very close to the isotropy line, with highly positive

$$\phi_{sat} = 2.085 + 0.97\ \phi_{Hg} \qquad 4.10$$

correlation coefficient (r = +0.892) significant at the 99.99% level. The comparison of these two methods shows some differences which may be expected in view of the different techniques used and the different sources of errors associated with each method. However, it appears likely that variation in lithology and diagenesis may exert some influence on the method used, especially the pebbly nature of some sandstones, the abundance of mudstone flakes, and amount and types of clay mineral present.

14. The relationship between average laboratory porosity ϕ_{av} and deviation per cent from average porosity shows an inverse linear relation represented by equation 4.11, which has a negative correlation coefficient of r = -0.355 which is significant at the 98% level.

$$\text{Dev } \% = 11.613 - 0.364\ \phi_{av} \qquad 4.11$$

This negative correlation is in good agreement with the observed difference between the result of ϕ_{Hg} and ϕ_{sat} in rocks with low porosity and permeability. This difference decreases with increasing porosity. This result could lead to the recommendation that Hg penetration and water resaturation methods could be equally well-used

for highly porous rocks. In low porosity rocks care should be taken in choosing the appropriate method.

15. Petrographic determination of porosity using photomicrographs of thin sections were done either manually for the intersection lengths of the pore spaces (V%) or using a Digitizer for measuring pore area (ϕ_{photo}%). The results compared to the average laboratory porosity (ϕ_{av}) show a very high deviation per cent (D_1 and D_2) for ϕ_{photo} and V% respectively. D_1 ranged between -50.34 to +29.39% and D_2 ranged from -14.85 to +45.89%. This high deviation from average laboratory result could lead to the conclusion that measuring porosity by means of photomicrographs (or directly in impregnated thin sections) is generally inadequate and unreliable. However, the method was useful for estimating the amount of different types of pores present.

16. The saturation density and porosity show highly significant negative correlation (r = -0.93) significant at the 99.99% level and define a relationship

$$\rho_s = 2.74 + (-0.02\ \phi_{sat}) \qquad 4.13$$

17. The horizontal conductivity measured by falling head permeameter (K_w) gave values for the Sherwood Sandstone Group ranging between 1.43×10^{-5} mm/sec (1.48 md) and 1.13×10^{-1} mm/sec (1167.67 md) with an average of 1.68×10^{-2} mm/sec (1743.67 md). The estimated hydraulic conductivity from the pore-size distribution curves gave results (K_{Hg}) between 7.29×10^{-6} mm/sec (0.75 md) and 6.99×10^{-2} mm/sec (7234.8 md) with an average of 1.47×10^{-2} mm/sec (1522 md).

18. The comparison between K_w and K_{Hg} indicates that both have a wide range of values and this is mainly due to lithological variation;

impermeable siltstone and mudstone horizons yield the lowest values. Also K_w is slightly higher than K_{Hg}. The relationship between the two methods is represented by a linear equation (4.17) which shows a marked positive correlation (r = +0.88), highly significant at the 99.99% level.

$$\text{Log } K_{Hg} = 0.292 + 1.171 \text{ Log } K_w \qquad 4.17$$

This line is very close to the isotropy line at the higher hydraulic conductivity values where the points are tightly grouped. However, many points show great off set from Y = X line at the lower values. These differences in the measured and estimated values clearly resulted from: 1) the different experimental methods employed, particularly the use of different liquids (water and mercury), 2) the difficulty of obtaining complete vacuum and resaturation in the finer grained rocks, 3) the amount and kind of clay present, especially swelling clays, and 4) the off set of the actual pore shape from the assumed one of circular cross section. The actual pores are of tabular or sheet-like shape as indicated from pore-cast studies. Thus those two methods could be equally well-used for the measurement of hydraulic conductivity in highly permeable rocks.

19. The relationship between ϕ_{av} and K_w is represented by the line:

$$\text{Log } K_w = -8.08 + 0.231 \text{ Log } \phi_{av} \qquad 4.18$$

with a positive correlation coefficient of r = + 0.7328. It appears from this relationship that the higher values of K_w are associated with more highly porous rocks. However, the correlation is not close enough to predict one from the other.

The relationships of hydraulic conductivity (K_w and K_{Hg}) and the median pore radius (Mr μm) is represented by equations 4.19 and 4.20

$$Mr = 2.229 + 0.534 \text{ Log } K_{Hg} \qquad 4.19$$

$$Mr = 1.997 + 0.412 \text{ Log } K_w \qquad 4.20$$

where the two equations show highly significant positive correlation with r = 0.98 and 0.82 respectively. The above relationship together with the detailed study of some examples indicates that the size of the pore throat is the most effective factor controlling hydraulic conductivity values, and both pore-size distribution curves and Mr are good indicators of hydraulic conductivity.

20. Comparison of the hydraulic characters of these Lower Triassic aquifer rocks as measured in the laboratory with those measured from field pumping tests indicate that field transmissivity is two to three times greater than the laboratory data. This is consistent with the lithological data that fissuring and fracturing have great effects on the hydraulic properties of these aquifer rocks.

21. The chemistry of the groundwaters reveals that the water has pH values between 7.5 and 8.2, with the total amount of dissolved solids 130 to 378 ppm, and specific electrical conductance between 203 and 590 μS/cm. Calcium and sodium are most common ions in the groundwater with average values of 45.92 ppm and 34.52 ppm respectively. The groundwater is undersaturated with respect to dolomite, calcite, K-feldspar, albite, mixed layer (I/S) clay and montmorillonite. These authigenic minerals are not in equilibrium with the present groundwater, a feature consistent with the dissolution, replacement and transformation textures observed in SEM and thin section studies.

Only kaolinite and, to some extent, illite are stable under the present water conditions, as all plots fall in the stability field of these two minerals. This raises the possibility of the precipitation of these minerals under the present groundwater conditions.

Appendix 1 - Formula for calculating porosity from water resaturation method

1. W is the dry weight of the sample

2. W_s is the saturated weight of the sample

3. W_m is the net submerged weight of the sample

4. Volume of connected pores = volume of water in the sample (or saturating)

$$= \frac{W_s - W}{\text{water density}} = W_s - W \qquad (1)\ *$$

5. Bulk volume of sample = bulk volume buoyancy ÷ water density

$$= \frac{W_s - W_m}{\text{water density}} = W_s - W_m \qquad (2)\ *$$

6. Grain volume = grain volume buoyancy ÷ density of water

$$= \frac{W - W_m}{\text{density of water}} = W - W_m \qquad (3)\ *$$

7. Effective porosity $\phi_{sat}\ \% = \frac{W_s - W}{W_s - W_m} \times 100$

8. Grain density $\rho_G = \frac{W}{W - W_m}\ gm/cm^3$

Bulk grain density $\rho_B = \frac{W}{W_s - W_m}\ gm/cm^3$

Saturation density $\rho_S = \frac{W_s}{W_s - W_m}\ gm/cm^3$.

* In all equations above (1,2,3) we considered the density of water was equal to the unity at room temperature.

Appendix 2 - Derivation of Washburn Equation

Washburn (1921) has pointed out the fact that the surface tension opposes the entrance of non-wetting liquid into a small pore. This opposing force F_o is given by equation 1:

$$F_o = - 2 \Pi r \gamma \text{Cos } \theta \qquad (1)$$

This opposition can be overcome by the application of external force Fa

$$Fa = \Pi r^2 P \qquad (2)$$

where P is the applied external pressure.

At equilibrium

$$\Pi r^2 P = - 2 \Pi r \gamma \text{Cos } \theta$$

$$\therefore r = \frac{- 2 \gamma \text{Cox } \theta}{P} \qquad (3)$$

In deriving the pore-size distribution, the surface tension of Hg (γ) was assumed to be 474 dynes/cm (474×10^{-6} N/mm), and the contact angle between Hg and silicate mineral considered to be 140^o. Using these values equation 3 could be written simply as

$$r_{\mu m} = \frac{105.4}{P(psi)} \qquad (4)$$

From this relation it appears that under zero pressure, none of the liquid will penetrate through the pores.

Appendix 3 - Pore size distribution data and porosity calculation

Sample identification A14/27
Sample weight (W_s) 4.5218
Cell factor 0.00079 cc/count

A	B	C	E
Applied pressure (psi)	Penetration counter indication	Corrected counter indication (B-"Blank" result)	Volume of pores of certain diameter and larger C (Factor÷W_s) (cc/gm)
1.0	10	10	.00175
1.25	19	19	.00332
1.5	28	28	.00489
1.75	34	34	.00594
2	42	42	.00734
2.5	65	65	.01136
2.75	87	87	.01520
3.1	120	120	.02097
3.3	156	156	.02725
3.55	209	209	.03651
3.75	257	257	.04490
3.95	287	287	.05014
4.1	308	308	.05381
4.25	335	335	.05853
4.85	388	388	.06779
5.15	417	417	.07285
5.4	444	444	.07757
6.25	483	483	.08438
6.5	495	495	.08648
7.05	519	519	.09067
7.5	531	531	.09277
8	544	544	.09504
8.45	553	553	.09661
9.1	563	563	.09836
10.1	578	578	.10098
11	588	588	.10273
12	596	596	.10413
13	603	603	.10535
14	611	611	.10675
15	618	618	.10797
20	638	638	.11146
560	768	768	.13418
5000	817	813	.14204
8000	825	817	.14274
12000	834	820	.14326
16000	838	821	.14344
20000	845	824	.14396

$\Sigma E = 0.14396$ cc/gm
$\rho_G = 2.636$ gm/cm^3

$$\phi_{Hg} = \frac{\Sigma E \times \rho_G}{(\Sigma E \times \rho_G) + 1}$$

$\phi_{Hg} = 0.2751$ (27.51%)

Appendix 4 - Chemical Analyses of Fine Residues (< 0.38 μm)

Variables / Sample No.	Depth (m)	Equivalent Water Sample	Si ←	Al %	Ca	Mg	Fe	Na	K →	← Mn	Zn ppm	Cu	Cr	Pb	Ni →
BH A11															
1	14.8	1	22.01	12.68	1.39	2.16	1.94	0.088	2.17	243.5	57.8	810.6	< 0.2	< 1.0	< 0.5
2	22.8	2	19.04	12.24	2.73	2.79	1.70	0.080	1.72	250.8	62.8	353.7	"	"	"
3	35	3	21.51	11.41	1.99	1.92	1.95	0.095	2.35	202.7	71.2	373.8	"	"	"
4	54.7	5	17.41	8.31	5.66	4.41	2.22	0.074	1.42	461.74	78.2	412.2	"	"	"
5	63	6	28.79	6.60	0.95	2.47	4.65	0.124	2.19	203.2	81.6	126.0	"	"	"
6	67	7	33.06	7.12	3.70	4.01	1.97	0.086	1.86	334.1	155.0	763.9	"	"	"
BH A14															
7	84.4	9	26.88	11.84	0.04	1.09	1.71	0.074	3.97	148.1	137.2	398.1	"	"	"
8	130.2	12	25.23	10.09	2.39	3.00	2.06	0.141	3.84	202.0	84.5	998.4	"	"	"
9	130.8	12	28.93	10.27	0.69	1.55	2.48	0.663	4.47	157.5	106.9	378.8	"	"	"
10	175	15	32.69	5.69	1.05	1.79	2.76	0.079	3.35	174.9	74.6	47.5	"	"	"
11	190	16	23.61	13.96	0.96	1.54	6.02	0.066	2.03	201.5	60.7	147.1	"	"	"
BH A18															
12	15	17	27.75	9.06	3.41	3.22	2.04	0.084	3.00	409.5	74.0	787.9	"	"	"
13	33.5	18/19	23.04	8.88	3.70	2.85	1.68	0.114	2.08	328.1	62.3	2024.4	"	"	"
14	51.5	20	10.33	4.02	12.94	11.07	1.63	0.063	1.24	965.6	46.5	362.6	"	"	"
15	102.5	23	20.87	9.64	3.29	3.47	2.26	0.077	2.46	300.9	68.1	1490.4	"	"	"
16	114	24	30.67	8.63	2.72	3.10	2.13	0.081	3.9	180.1	60.3	156.0	"	"	"
17	135	26	22.03	11.84	2.09	1.98	3.39	0.065	2.00	240.6	75.0	823.8	"	"	"

REFERENCES

Akroyd, T.N.W., 1957. Laboratory Testing in Soil Engineering. Soil Mechanics Ltd. Lond., 233 p.

Ali, A.D., 1982. Triassic Stratigraphy and Sedimentology in Central England. Thesis, Univ. Aston in Birmingham.

Ali, A.D. and Turner P., 1982. Authigenic K-feldspar in the Bromsgrove Sandstone Formation (Triassic) of Central England. J. Sediment. Petrol., 52, 187-197.

American Petroleum Institute, 1961. Recommended practice for core-analysis procedure. R.P. No. 40, Dallas, Texas, 55 p.

Barker, R.D. and Worthington, P.F., 1973. Some hydrogeophysical properties of the Bunter Sandstone of northwest England. Geoexploration, 11, 151-170.

Baskin, Y., 1956. A study of authigenic feldspars. J. Geol., 64, 132-155.

Beard, D.C. and Weyl, P.K., 1973. Influence of texture on porosity and permeability of unconsolidated sand. Bull. Am. Assoc. Petrol. Geol., 57, 349-369.

Blatt, H. and Christie, J.M., 1963. Undulatory extinction in quartz of ingeous and metamorphic rocks and its significance in provenance studies of sedimentary rocks. J. Sediment. Petrol., 33, 559-579.

Blatt, H., Middleton, G. and Murray, R., 1980. Origin of Sedimentary Rocks. 2nd Ed., Prentice-Hall, New Jersey, 782 p.

Bow, C.J., Howell, F.T., Payne, C.J. and Thompson, P.J., 1969. The lowering of the water table in the Permo-Triassic rocks of South Lancashire. Water and Water Eng., 73, 461-463.

Bow, C.J., Howell, F.T. and Thompson, P.J., 1970. Permeability and porosity of unfissured samples of Bunter and Keuper sandstones of South Lancashire and North Cheshire. Water and Water Eng., 74, 464-466.

Carroll, D., 1970. Clay minerals: a guide to their X-ray identification. Spec. Pap. geol. Soc. Am., 126, 80 p.

Chilingarian, G.V. and Wolf, K.H., 1975. Compaction of Coarse-Grained Sediments. I. New York, Elsevier Pub. Co., 552 p.

Darcy, H., 1865. Les fontanes publiques de la villa de Dijon. V. Dalmont, Paris, 647 p.

Davis, S.N. and DeWiest, R.J.M., 1966. Hydrogeology. John Wiley and Sons, Inc., New York, 463 p.

Delesse, A., 1848. Procede mechanique pour determiner la composition des roches. Ann. des Mines, 13, 379-388.

De Rance, G.E., 1882. Report on the investigation of the circulation of underground waters in the permeable formations of England. Rep. Brit. Assoc. Adv. Sci, 8, 213-239.

Diamond, S., 1970. Pore size distribution in clays. Clays clay Miner., 18, 7-23.

Dickson, J.A.D., 1965. A modified staining technique for carbonates in thin section. Nature, 205, p 587.

Edmunds, W.M. 1971. Hydrogeochemistry of groundwaters in the Derbyshire dome with special reference to trace constituents. Rep. No. 71/7., Ins. Geol. Sci., 52 p.

Edmunds, W.M. 1973. Trace element variations across an oxidation-reduction barrier in a limestone aquifer. Proc. Symp. Hydrogeochemistry and Biogeochemistry, Tokyo 1970, 500-526.

Edmunds, W.M. Lovelock, P.E.R. and Garry, D.A., 1973. Interstitial water chemistry and aquifer properties in the upper and middle chalk of Berkshire, England. J. Hydrol., 19, 21-31.

Edmunds, W.M. and Morgan-Jones, M., 1976. Geochemistry of groundwaters in British Triassic sandstones: the Wolverhampton-East Shropshire area. Q. J. Eng. Geol., London, 9, 73-101.

Fair, G.M. and Hatch, L.P., 1933. Fundamental factors governing the streamline flow of water through sand. J. Am. Water Works Assoc., 25, 1551-1565.

Fancher, G.H., Lewis, J.A. and Barnes, K.B. 1933. Some physical characteristics of oil sands. Penn. State. Coll. Mineral Ind. Exp., Sta. Bull., 12, 66-167.

Fetter, C.W., 1980. Applied Hydrogeology. Bell & Howell Company. Columbus, Toronto, London & Sydney, 488 p.

Folk, R.L., 1951. Stages of textural maturity in sedimentary rocks. J. Sediment. Petrol., 21, 127-130.

Folk, R.L., 1954. The distinction between grain size and mineral composition in sedimentary nomenclature. J. Geol., 62, 344-359.

Folk, R.L., 1974. Petrology of Sedimentary Rocks. Austin, Texas, Hemphills, 182 p.

Folk, R.L., 1976. Reddening of desert sands: Simpson Desert, N.T., Australia. J. Sediment. Petrol., 46, 604-615.

Folk, R.L., Andrews, P.B. and Lewis, D.W., 1970. Detrital sedimentary rock classification and nomenclature for use in New Zealand. N.Z. J. Geol. Geophys., 13, 937-968.

Folk, R.L. and Land, L.S., 1975. Mg/Ca ratio and salinity: two controls over crystallization of dolomite. Bull. Am. Assoc. Petrol. Geol., 59, 60-68.

Folk, R.L. and Ward, W.C. 1957. A study in the significance of grain size parameters. J. Sediment. Petrol., 27, 3-26.

Friedman, M., 1954. Miocene orthoquartzite from New Jersey. J. Sediment. Petrol., 24, 235-241.

Füchtbauer, H., 1967. Influence of different types of diagenesis on sandstone porosity. 7th World Petroleum Congr. Proc., 2, 353-369.

Galehouse, J.S., 1971. Point counting. In: R.E. Carver (Ed.), Procedures in Sedimentary Petrology. John Wiley and Sons. New York, 385-407.

Garrels, R.M. and Christ, C.L., 1965. Solutions, Minerals and Equilibria. Harper and Row Pub., New York, 450 p.

Halley, R.B., 1978. Estimating pore and cement volumes in thin section. J. Sediment. Petrol., 48, 642-650.

Harth, H., 1965. Zum problem der anreicherung der gewässer mit kaliumsalzen und K Dt. gewässerk. Mitt. Sonderh. S. 4-7, Koblenz-Rhein.

Hawkins, P.J., 1978. Relationship between diagenesis, porosity reduction and oil emplacement in Late Carboniferous sandstone reservoirs, Bothamsail oilfield, E. Midlands. J. geol. Soc. London, 135, 7-24.

Hayes, J.B., 1979. Sandstone diagenesis - the hole truth. In: P.A. Scholle and P.R. Schluger (Eds.), 1979. Aspects of Diagenesis. Spec. Publ. Soc. Econ. Paleontol. Mineral., Tulsa, 26, 127-139.

Hayes, J.B., Harms, J.C. and Wilson, T.Jr., 1976. Contrasts between braided and meandering stream deposits, Beluga and Sterling Formations (Tertiary), Cook Inlet, Alaska. In: T.P. Miller (Ed.), Recent and ancient sedimentary environments in Alaska. Alaska Geol. Soc., J1-J27.

Hazen, A., 1893. Some physical properties of sands and gravels with special reference to their use in filtration. In: S.J. Pirson, 1958. Oil Reservoir Engineering, 2nd ed., New York, Toronto, London, 735 p.

Helgeson, H.C., Garrels, R.M. and MacKenzie, F.T., 1969. Evaluation of irreversible reactions in geochemical progress involving minerals and aqueous solutions. II, Applications. Geochim. Cosmochim. Acta., 33, 455-481.

Helgeson, H.C., Delany, J.M., Nesbitt, H.W. and Bird, D.K., 1978. Summary and critique of the thermodynamic properties of rock forming minerals. Am. J. Sci., 278A, 229 p.

Hem, J.D. and Cropper, W.H., 1959. Survey of ferrous-ferric chemical equilibria and redox potentials. U.S. Geol. Surv. Water Supply Pap., 1459-A, 31 p.

Hess, P.C., 1966. Phase equilibria of some minerals in the K_2O-Na_2O-Al_2O_3-SiO_2-H_2O system at 25°C and 1 atmosphere. Am. J. Sci., 264, 280-309

Holden, W.S., 1970. Water Treatment and Examination. Churchill, London, 513 p.

Howell, F.T., 1965. The significance of the ingress of saline waters into the Permo-Triassic aquifers of south Lancashire. Water and Water Eng., 69, 364-365.

Hower, J., Eslinger, E.V., Hower, M.E. and Perry, E.A., 1976. Mechanism of burial metamorphism of argillaceous sediments. 1: Mineralogic and chemical evidence. Bull. geol. Soc. Am., 87, 725-737.

Johnson, A.I., 1967. Specific yield - Compilation of specific yield for various materials. Water Supply Pap. U.S. Geol. Surv., No. 1662-D, 74 p.

Hubert, J.F. and Reed, A.A., 1978. Red-bed diagenesis in the East Berlin Formation, Newaric Group, Connecticut Valley. J. Sediment. Petrol., 48, 175-184.

Kahn, J.S., 1956. The analysis and distribution of the properties of packing in sand-size sediments. 1. On the measurement of packing in sandstones. J. Geol., 64, 385-395.

Keller, W.D., 1969. Chemistry in Introductory Geology. Bros. Pub., Columbia, Missouri, 108 p.

Kendal, P.E., 1921. The porosity of rocks and its influence upon the yield of wells and boreholes. Trans. Inst. Wat. Eng., 26, 28-43.

King, F.H., 1899. Principals and conditions of movements of ground water. U.S. Geol. Surv., 19th Ann. Rept., Part 2, 295 p.

Kozeny, J., 1927. Über Kapillare Leitung des Wassers im Boden, Sitzber. Akad. Wiss. Wien, Math. naturw. K., 136-2A, 271 p.

Krauskopf, K.B., 1979. Introduction to Geochemistry. McGraw-Hill, Kogakusha, Ltd., New York, 617 p.

Kunze, G.W., 1955. Ethylene glycol solvation technique used in X-ray diffraction. Clays clay Miner. In: W.O. Milligan (Ed.) Publication 395, Nat. Acad. Sci - Nat. Res. Count. Washington, 88-93.

Land, D.H., 1966. Hydrogeology of Bunter sandstone in Nottinghamshire. Water Supply Pap. Inst. Geol. Sci, Hydrogeol. Rep. No. 1, 24 p.

Lindquist, S., 1976. Leached porosity in overpressured sandstones - Frio Formation (Oligocene), south Texas. Bull. Am. Assoc. Petrol. Geol., 60, 1612-1613.

Lohman, S.W. et al. 1972. Definitions of selected ground-water terms - Revisions and conceptual refinements. U.S. Geol. Surv., Water Supply Pap., 1988.

Lovelock, P.E.R., 1977. Aquifer properties of Permo-Triassic sandstones in the United Kingdom. Bull. geol. Surv. G.B., 56, 1-51.

Manger, G.E., 1963. Porosity and bulk density of sedimentary rocks. Bull. U.S. Geol. Surv., No. 1144-E, 55 p.

Marshall, T.J., 1958. A relation between permeability and size distribution of pores. J. Soil Science, 9, 1-8.

Meinzer, O.E., 1923. Outline of groundwater hydrology, with definitions. U.S. Geol. Surv. Water Supply Pap. 494, 71 p.

Moore, C.C., 1904. The study of the volume composition of rocks and its importance to the geologist. Proc. Liverpool Geol. Soc., 9, 129-162.

Nafe, J.E. and Drake, C.L., 1957. Variation with depth in shallow and deep water marine sediments porosity, density and the velocities of compressional and shear waves. Geophysics, 22, 523-552.

Phillip, W., Drong, H.J., Flüchtbauer, H., Haddenhorst, H.G. and Jankowsky, W., 1963. The history of migration in the Grifhorn Trough (NW-Germany). 6th World Petroleum Congr. Proc., Sec. 1, Pap. 19, 457-481.

Pirson, S.J., 1958. Oil Reservoir Engineering. 2nd Ed., New York, Toronto, London, 735 p.

Pittman, E.D., 1972. Diagenesis of quartz in sandstones as revealed by scanning electron microscopy. J. Sediment. Petrol., 42, 507-519.

Pittman, E.D., 1979. Porosity, diagenesis and productive capability of sandstone reservoirs. In: Aspects of Diagenesis. Spec. Publ. Soc. Econ. Palaeontol. Mineral. Tulsa, 26, 159-173.

Pittman, E.D. and Duschatko, R.W., 1970. Use of pore casts and scanning electron microscope to study pore geometry. J. Sediment. Petrol., 40, 1153-1157.

Price, M., 1977. Specific yield determinations from a consolidated sandstone aquifer. J. Hydrol., 33, 147-156.

Pryor, W.A., 1973. Permeability and porosity variations in some Holocene sand bodies. Bull. Am. Assoc. Petrol. Geol., 57, 162-189.

Reynolds, R.C. and Hower, J., 1970. The nature of interlayering in mixed-layer illite-montmorillonite. Clays clay Miner., 18, 25-36.

Richards, L.A., 1954. Diagenesis and improvement of saline and alkali soils. In: D.K. Todd (Ed.), Groundwater Hydrology. 2nd Ed. John Wiley & Sons. New York, Toronto, 535 p.

Ritter, H.L. and Drake, D.L, 1945. Pore size distribution in porous materials. Industrial Engineering Chemistry. Anal. Ed., 17, 782-786.

Rittenhouse, G., 1973. Pore-space reduction in sandstones: controlling factors and some engineering implications. Off shore Technol. Conf. Am. Inst. Min., Metall. Pet. Eng., Pap., OTC 1806, I-683 - I-692.

Ryder, H.M., 1948. Permeability, absolute, effective measured. World Oil, 125, 173-177.

Scheidegger, A.E., 1974. The Physics of Flow through Porous Media. 3rd Ed., Univ. Toronto Press, 353 p.

Schmidt, V. and McDonald, D.A., 1979a. The role of secondary porosity in the course of sandstone diagenesis. In: P.A. Scholle and P.R. Schluger (Eds.), 1979. Aspects of Diagenesis. Spec. Publ. Soc. Econ. Palcontol. Mineral., Tulsa, 26, 127-207.

Schmidt, V. and McDonald, D.A, 1979b. Texture and recognition of secondary porosity in sandstone. In: P.A. Scholle and P.R. Schluger (Eds.), 1979. Aspects of diagenesis. Spec. Publ. Soc. Econ. Paleontol. Mineral., Tulsa, 26, 209-225.

Schmidt, V., McDonald, D.A. and Platt, R.L., 1977. Pore geometry and reservoir aspects of secondary porosity in sandstones. Bull. Can. Pet. Geol., 25, 271-290.

Severn Trent Water Authority, Nottingham Triassic conjunctive use investigation, 1976, Report Nos. 4, 5, 6.

Shenhave, H., 1971. Lower Cretaceous sandstone reservoirs, Israel: petrography, porosity, permeability. Bull. Am. Assoc. Petrol. Geol., 55, 2194-2224.

Sibley, D.F. and Blatt, H., 1976. Intergranular pressure solution and cementation of the Tuscarora orthoquartzite. J. Sediment. Petrol., 46, 881-896.

Sippel , R.F., 1968. Sandstone petrography, evidence from luminescence petrography. J. Sediment. Petrol., 38, 530-554.

Slichter, C.S., 1899. Theoretical investigation of the motions of groundwaters. U.S. Geol. Survey, 19th Ann. Rept., Part 2, 312 p.

Stablein, N.K. and Dapples, E.C., 1977. Feldspars of the Tunnel City Group (Cambrian), Western Wisconsin. J. Sediment. Petrol., 47, 1512-1538.

Stanley, K.O. and Benson, L.V., 1979. Early diagenesis of high plains Tertiary vitric and arkosic sandstone, Wyoming and Nebraska. Spec. Publ. Soc. Econ. Paleontol. Mineral., Tulsa, 26, 401-423.

Stanton, G.D. and McBride, E.F., 1976. Factors influencing porosity and permeability of lower Wilcox (Eocene) sandstone, Karnes county, Texas. Am. Assoc. Petroleum Geologists and Soc. Econ. Palaeontol. Mineral. Ann. Meeting Abs., 3, 118-119.

Swinnerton, H.H. 1948. The Permo-Trias. In: Guide to the Geology of the East Midlands. Univ. of Nottingham, 53-59.

Taylor, F.M., 1968. Permian and Triassic Formations. In: P.C. Sylvester-Bradley and T.D. Ford (Eds.), The Geology of the East Midlands. Leicester University Press, 149-173.

Taylor, J.M., 1950. Pore-space reduction in sandstones. Bull. Am. Assoc. Petrol. Geol., 34, 701-716.

Terzaghi, C., 1925. Principles of soil mechanics. Eng. News Record, 95, p 914.

Thein, M., 1966. A petrological study of the Upper Cambrian rocks in parts of Wisconsin and Minnesota. PhD Thesis, Northwestern University, Evanston, Illinois.

Thompson, D.B., 1970. Sedimentation of the Triassic (Scythian) red pebbly sandstones in the Cheshire Basin and its margins. Geol. J., 7,, 183-261.

Todd, D.K., 1959. Groundwater Hydrology. John Wiley & Sons, Inc., New York, London, 336 p.

Todd, D.K., 1980. Groundwater Hydrology. 2nd Ed., John Wiley & Sons. New York, Chichester, Toronto, 535 p.

Towe, K.M., 1962. Clay mineral diagenesis as a possible source of silica cement in sedimentary rocks. J. Sediment. Petrol., 32, 26-28.

Trask, P.H., 1931. Compaction of sediments. Bull. Am. Assoc. Petrol. Geol., 15, 271-276.

Turner, P., 1980. Continental Red Beds. Development in Sedimentology. No. 29, Elsevier, Amsterdam, 562 p.

Turner, P. and Archer, R., 1977. The role of biotite in the diagenesis of red beds from the Devonian of Northern Scotland. Sediment. Geol., 19, 241-251.

Walker, T.R., 1967. Formation of red beds in modern and ancient deserts. Geol. Soc. Am. Bull., 78, 353-368.

Walker, T.R., 1976. Diagenetic origin of continental red beds. In: H. Falke (Ed.), The Continental Permian in Central, West and South Europe. D. Reidel, Dordrecht-Holland, 240-282.

Walker, T.R., Ribbe, P.H. and Honea, R.M., 1967. Geochemistry of hornblende alteration in Pliocene red beds, Baja California, Mexico. Geol. Soc. Am. Bull., 78, 1055-1060.

Walker, T.R. Waugh, B. and Crone, A.J., 1978. Diagenesis in first-cycle desert alluvium of Cenozoic age, southwestern United States and northwestern Mexico. Geol. Soc. Am. Bull., 89, 19-32.

Warrington, G., Audley-Charles, M.G., Elliott, R.E., Evans, W.B., Ivimey-Cook, H.C. Kent, P.E., Robinson, P.L., Shotton, F.W., and Taylor, F.M., 1980. Triassic. Geol. Soc. Spec. Rep., No. 13, 78 p.

Washburns, E.W., 1921. Note on a method of determining the distribution of pore sizes in a porous material. Proceedings, National Academy of Sciences, 7, p 112.

Waugh, B., 1970a. Formation of quartz overgrowths in the Penrith Sandstone (Lower Permian) of northwest England as revealed by scanning electron microscopy. Sedimentology, 14, 309-320.

Waugh, B., 1970b. Petrography, provenance and silica diagenesis of the Penrith Sandstone (Lower Permian) of northwest England. J. Sediment. Petrol., 40, 1226-1240.

Waugh, B., 1978. Authigenic K-feldspar in British Permo-Triassic sandstones. J. geol. Soc. London, 135, 51-56.

Wedepohl, K.H., 1969. Handbook of Geochemistry. Vol. 1. Springer-Verlag, Berlin, 442 p.

Whittemore, D.O. and Langmuir, D., 1975. The solubility of ferric oxyhydroxides in natural waters. Groundwater, 13, 360-365.

Williams, B.P.J., Downing, R.A. and Lovelock, P.E.R., 1972. Aquifer properties of the Bunter sandstone in Nottinghamshire, England. 24th Sess. Int. Geol. Congr. Canada, Section 11, 169-176.

Wilson, M.D. and Pittman, E.D., 1977. Authigenic clays in Sandstones: Recognition and influence on reservoir properties and palaeo-environmental Analysis. J. Sediment. Petrol., 47, 3-31.

Yong, R.N. and Warkentin, B.P., 1966. Introduction to Soil Behavior. Collier-Macmillan Ltd., N.Y., 451 p.

Young, S.W., 1976. Petrographic texture of detrital polycrystalline quartz as an aid to interpreting crystalline source rocks. J. Sediment. Petrol., 46, 595-603.